This is to certify that the
thesis entitled

GLOBAL PRECISION ANALYSIS OF SU(2) x SU(2) x U(1) MODELS

presented by

Kai Ruven Schmitz

has been accepted towards fulfillment
of the requirements for the

M.S. degree in Physics and Astronomy

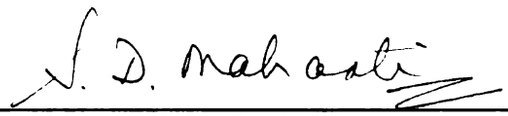

Major Professor's Signature

7/10/09

Date

GLOBAL PRECISION ANALYSIS OF $SU(2) \otimes SU(2) \otimes U(1)$ MODELS

By

Kai Ruven Schmitz

A THESIS

Submitted to
Michigan State University
in partial fulfillment of the requirements
for the degree of

MASTER OF SCIENCE

Physics and Astronomy

2009

ABSTRACT

GLOBAL PRECISION ANALYSIS OF $SU(2) \otimes SU(2) \otimes U(1)$ MODELS

By

Kai Ruven Schmitz

$G(221)$ models extend the electroweak gauge group of the Standard Model by an additional $SU(2)$ which results in the presence of three new heavy gauge bosons Z' and $W'^{\pm}$ with masses at the TeV scale. In this thesis a global fit analysis of the most prominent $G(221)$ models — the left-right (LR), leptophobic (LP), hadrophobic (HP) and fermiophobic (FP) models as well as the ununified (UU) and non-universal (NU) models — is presented. Utilizing a modified version of the Fortran plotting package GAPP the $G(221)$ models are fitted to a set of 37 electroweak observables including a multitude of Z pole observables, the mass and the width of the $W^{\pm}$ boson, the mass of the top quark and various low-energy observables. The experimental precision with which the electroweak observables have been measured allows to put strong bounds on the parameters of the $G(221)$ models and to constrain the masses of the Z' and the $W'^{\pm}$. As a confirmation of the power of the Standard Model the scale of the new physics in the $G(221)$ models is generally found to be very high. For each $G(221)$ model under study the most important observables that drive the minimization of χ^2 can be identified. Among the most relevant observables are the hadronic cross section in e^-e^+ annihilation and the weak vector charge of cesium-133. To illustrate which values of the $G(221)$ parameters are consistent with the experimental data plots of the parameter space are presented that indicate the viable regions at 95% CL. Likewise plots of the Z' and $W'^{\pm}$ masses demonstrate which masses of the new heavy gauge bosons are already ruled out by the data and which are still possible. In a closing remark the constraints from the ZW^+W^- vertex on the $G(221)$ parameters are considered. As it turns out the bounds on the ZW^+W^- coupling do not affect the results of the global fit analysis.

ACKNOWLEDGMENT

In last August I came to Michigan State to learn more about elementary particles and the fundamental forces of nature. I had not any attended lecture on high-energy physics in my luggage, just my thirst for knowledge and the perception that I would miss a great and intriguing field in physics if I did not take the opportunity and study particle physics at MSU. Now, almost one year later, I find myself becoming a high-energy physicist that is fascinated by the topics he is working on. All this would not have been possible without the help and support of many people that stood by my side in the last months. I would like to take this opportunity to express my gratitude to all of them.

In the first place, I wish to thank my advisor, Prof. Chien-Peng Yuan. When I first stepped into his office in last August looking for someone I could work for as a Research Assistant he offered me to join his group right away. Brimming with ideas and passionate about the projects he proposed to me, he made me sense from the very first what a blessing it would be to have him as my advisor. Since then he has proven to be an excellent guide on my way through the landscape of particle physics. Thanks to his mentoring I learned much more in the last year than I had ever dared to hope.

I would also like to thank Prof. Wayne Repko and Prof. Carl Schmidt who have made themselves available as members of my advisory committee. Not only do I appreciate their willingness to read my thesis and to be on my committee, I am also very thankful to them for the deep insight into Quantum Field Theory and Quantum Electrodynamics that I could gain in their classes. Had I not taken their courses I would not have been prepared for writing this thesis.

One of the pillars of this project was the Fortran package GAPP that has been written by Professor Jens Erler. I would like to express my deepest gratitude to Professor Erler for placing the newest version of the GAPP code at my disposal and

for helping me so patiently while I was making my first steps with GAPP. Without his support it would have taken me much longer to get started with my thesis.

My stay at Michigan State only became possible due to the cooperation program of the German National Merit Foundation with the MSU Physics Department. I deeply acknowledge the support that I received from both institutions. On the American side it was Prof. Wolfgang Bauer that helped making my year abroad a success. The driving forces on the German side were Dr. Astrid Irrgang, Dr. Inga Scharf, Dr. Julia Schuetze and Annette Schwarzenberg. My special thanks go to all of them.

Furthermore, I am especially grateful to Ken Hsieh who assisted me in carrying out this project in countless ways. He taught me so much about the Standard Model and electroweak physics in general, was always there for me when I needed assistance and never became tired of answering my questions. In the last months he was not only an excellent teacher and collaborator but became also a good friend. My thanks go out to Jianghao Yu who especially assisted me at the first stage of my project. Without his help I would not have been able to start working on this thesis. Over the last year he has become much more to me than just an office mate.

My Master studies would not have been the same without my friends that I made at MSU during the last months. I can consider myself fortunate that I met Kirstie Sieloff and Martin Schuetz. The adventures that we had will always be on my mind. I am also particularly thankful to Sarah Heim, Christine Sung and Martin Kell for all the good times we had together. Stefano Di Chiara, Mohammad Hussein and Baradhwaj Panayancheri-Coleppa made the office we worked in together to a pleasant place. I would like to thank them for creating such a nice atmosphere. Furthermore, my thanks go out to my friends in Old Europe that did not forget me while I was studying in the New World. I am looking forward to see you again soon.

Finally, my sincere gratitude goes to my parents, my brother and my sisters who supported me from home as best as they could and last but definitely not least to my

girlfriend and best friend, Monia Glaeske. I only made the decision to study abroad because I knew that our relationship would be able to endure one year of separation. She gave me strength and confidence throughout this year and in the end it was her encouragement that made this thesis possible.

TABLE OF CONTENTS

LIST OF TABLES

LIST OF FIGURES

Images in this thesis are presented in color

Chapter 1

Introduction

1.1 Motivation of This Study

What holds the world together in its inmost folds? The Standard Model (SM) of particle physics is the best answer physics can give to that question at present. Being considered as the most successful theory in the history of physics, the SM is able to describe and predict the behavior of elementary particles under the influence of the electromagnetic, the weak and the strong force with unique precision, all the way to the scale of the nucleon (10^{-15} m).

However, it is clear that the SM is not an ultimate theory. It neglects gravity in the description of the subatomic world and therefore does not encompass all forces of nature. In that respect it does not meet the expectations towards a theory of everything from the outset. Furthermore it requires the masses and the mixing of the fermions and the mass of the Higgs boson as external input parameters instead of providing an unified explanation of how these quantities originate from more fundamental parameters. It lacks the answers to many fundamental questions, such as the nature of dark matter and dark energy or the origin of the baryon asymmetry in the universe. On a more technical level it faces difficulties such as fine-tuning [1] or the

violation of unitarity [2] at high energy scales in the absence of a light Higgs scalar.

In view of all these deficiencies it is one of the main tasks of modern high-energy physics to investigate theories beyond the SM. Theoretical work has to be done on two fronts: On the one hand it is necessary to construct new physics (NP) models and to examine in which directions the SM could be extended. On the other hand the phenomenology of new physics models has to be studied to be able to correctly interpret the data of experiments that aim at measuring effects of new physics. Presently, this second task is as important as never before. The particle physics community is about to enter a new era — in the near future the Large Hadron Collider (LHC) at CERN will collect precise data on the TeV scale and it is widely expected that it will provide evidence for physics beyond the SM. Now, at the eve of the LHC, it is therefore of special importance to study the phenomenology of new physics models. It is the goal of this thesis to contribute to that effort.

We will examine the compatibility of a certain class of models, the so-called $G(221)$ models, with the most recent precision data on a number of electroweak observables. In a global fit analysis we will investigate the constraints on the parameters of these models in order to find out in which regions in parameter space the respective $G(221)$ models are consistent with the data.

1.2 The SM and Its Extension by a Second $SU(2)$

Before we concentrate our attention to the physics beyond the SM we briefly summarize the main characteristics of the SM that will be relevant for our analysis.

The SM is a gauge theory. Its ansatz for the gauge group of the electroweak sector is the $SU(2)_L \otimes U(1)_Y$ in which the $SU(2)_L$ entails weak interactions of left-handed fermion currents and the $U(1)_Y$ acts on fermions that carry hypercharge Y. The fermion content of the SM is accommodated in three generations of leptons

and quarks. Mathematically, they are incorporated in the SM as representations of the electroweak gauge group: Left-handed fermion states form doublets under the $SU(2)_L$, right-handed fermions are represented by $SU(2)_L$-singlets. The hypercharge Y is constructed such that it adds with the third component T_L^3 of the weak isospin to give the electric charge, $Q = T_L^3 + Y$.

If the electroweak gauge symmetry were unbroken in nature the SM would feature four massless vector bosons acting as mediators of the electroweak force. However, we know from the experiment and the fact that the only long-range interactions in nature are those of electromagnetism and gravity that three electroweak gauge bosons are massive. An elegant explanation for that observation is provided by the Higgs mechanism that interprets the masses of the gauge bosons as a consequence of symmetry breaking triggered by a scalar particle, the Higgs field. The SM assumes the simplest case and represents the Higgs boson by a $SU(2)_L$-doublet. In the Higgs mechanism the Higgs boson spontaneously acquires a non-vanishing vacuum expectation value (VEV) which breaks the gauge symmetry of the Lagrangian and results in the occurrence of boson mass terms. In the course of spontaneous symmetry breaking the fundamental gauge bosons mix with each other to form the mass eigenstates that we see in the experiment: The neutral, massive Z boson, the charged and massive W^+ boson as well its anti-particle, the W^- boson, and the neutral and massless photon A.

Many models beyond the SM presume the existence of further gauge bosons that account for new forms of particle interactions at high energy scales. The introduction of new gauge bosons in the theory corresponds to the extentions of the electroweak gauge group by another symmetry group. An additional $U(1)$ results, for instance, in the appearance of a second massive uncharged boson, the Z'. Extensions of the SM with a $SU(2) \otimes U(1)_1 \otimes U(1)_2$ gauge group in the electroweak sector — or with a $G(211)$ gauge structure as we may say equivalently — have been studied in large

detail [3]. One of the next natural steps after adding a $U(1)$ is the extension of the SM gauge group by a second $SU(2)$. In these $G(221)$ models the electroweak gauge group is given as the:

$$G(221): \qquad SU(2)_1 \otimes SU(2)_2 \otimes U(1)_X$$

in which, depending on the specific $G(221)$ model, the two $SU(2)$s can either accommodate left- or right-handed fermion doublets and the $U(1)_X$ introduces a new form of hypercharge X. The inclusion of a second $SU(2)$ results in the presence of three new gauge bosons, the Z', the W'^+ and the W'^-. As these hypothetical gauge bosons have escaped detection so far, they are assumed to be very massive. In this thesis we will study the constraints on a class of $G(221)$ models. One of our key questions will be which masses for the new heavy gauge bosons are still allowed and consistent with the data.

The explicit $G(221)$ models that we will consider in this work are: The left-right model (LR) [4, 5, 6], the leptophobic model (LP), the hadrophobic model (HP) and the fermiophobic model (FP) [7, 8, 9], as well as the ununified model (UU) [10, 11] and the non-universal model (NU) [12]. The LP, HP and UU models are incomplete which manifests itself in the anomalous non-conservation of chiral fermion currents. For purposes of completeness, we will, however, include them into our analysis nonetheless. Especially the LP and the HP models are worth being discussed as they represent, in a sense, intermediate steps in the transition from the LR to the FP model.

In fitting models with a $G(221)$ gauge structure to the electroweak data we follow up the work of many earlier theoretical and phenomenological analyses. In the literature a number of studies can be found that perform global fits to various $G(221)$ models in the same spirit as our work. To be aware of the footing this thesis stands

on we may give a brief overview of these studies now: Polak and Zralek investigated the symmetric version of the LR model in which the new charged vector bosons, the W'^+ and the W'^-, couple with the same strength to the fermions as the charged SM bosons, the W^+ and the W^-. In Refs. [13] and [14] they obtained constraints on the LR parameters from the Z pole observables and from the low-energy data respectively. The non-symmetric case was considered by Chay et al. [15]. They put bounds on the Z' mass and the two mixing angles by combining the precision electroweak data from LEP-I and the experimental data on low-energy neutral-current processes. The tree-level and one-loop calculations in the FP model were carried out by Donini et al. [16]. They showed that precision electroweak data and flavour physics provide stringent constraints on the FP parameter space. Chivukula et al. [17] used the data from precision electroweak measurements to put strong bounds on the UU model.

However, no study encompassing all $G(221)$ models at once has been presented so far. The goal of this thesis will be to close that gap. While the studies in the literature differ in terms of their focus and techniqes, we will present one comprehensive consistent analysis for all $G(221)$ models. In particular, we will pursue an effective Lagrangian approach that will equip us with very universal and flexible expressions for the different fundamental quantities in the $G(221)$ models. Proceeding in this way allows us to address the various $G(221)$ models on an equal footing and ensures that the respective results are contrastable.

We ask ourselves: Which bounds do the experimental data place on $G(221)$ models? We will give an answer to that question in three steps: In the second chapter we will investigate the intrinsic properties of the $G(221)$ models under study. This part of our work mainly aims at providing us with the analytic expressions for the gauge boson masses and the fermion currents. In the third chapter we will use the results of our calculations to derive the new physics corrections to the electroweak observables to which we fit our models. Subsequently, we will give a short introduction to the

Fortran plotting package GAPP [18] that we utilize in a modified form to perform our numerical analysis. The fourth chapter is devoted to the presentation and discussion of our results.

Chapter 2

New Physics Models

To be able to fit the $G(221)$ models to electroweak precision data we need to know how these models are constructed and what their respective properties are. In this chapter we will try to develop an understanding of the models under study by addressing two key points: The masses and the mixing of the gauge bosons and the gauge interactions of the fermions.

The gauge bosons acquire their masses while the fundamental $G(221)$ gauge group is broken down to the $U(1)_{\mathrm{em}}$. This breaking is successively accomplished by two Higgs fields Φ and H that spontaneously acquire non-zero VEVs at different energy scales. Our strategy to extract the gauge boson mass matrices from the Higgs contributions $\mathscr{L}_\Phi$ and $\mathscr{L}_H$ to the fundamental Lagrangian $\mathscr{L}$ is the following: First, we discuss which representations for the Higgs fields comply with the mechanisms by which the fundamental $G(221)$ gauge group can be broken. Once we know the charges of Φ and H under the $G(221)$ symmetry groups we can write down $\mathscr{L}_\Phi$ and $\mathscr{L}_H$ explicitly. We then have to clarify what is meant by the model parameters appearing in these two Lagrangians. When we have fully understood the structure of $\mathscr{L}_\Phi$ and $\mathscr{L}_H$ we can finally concentrate our attention to the breaking of the fundamental symmetries and the generation of the boson masses.

The second contribution to $\mathscr{L}$ that we are interested in is the interaction of the fermion with the gauge boson sector. As, from the perspective of new physics, the electroweak observables appear as low-energy data this is best done in an effective field theory approach. Successively, we will integrate out the massive gauge bosons until we end up with the effective Lagrangian below the electroweak scale and hence the effective four-fermion interactions.

However, before we begin with any calculation we may categorize the $G(221)$ models under study. This will give structure to the analysis that we are going to perform and thereby simplify later considerations significantly.

2.1 Classification

The $G(221)$ models under study are the LR, LP, HP, FP, UU, and NU model. Three criteria will help us to classify these models: The choice of the breaking pattern, the representation of the Higgs field Φ and the charge assignments of the fermions. Fig. 2.1 on the following page gives an overview of the hierarchy among all the classes into which our $G(221)$ models can be grouped. The following discussion basically serves as a comment on that diagram.

2.1.1 Symmetry Breaking Pattern

The gauge group of all $G(221)$ models in the electroweak sector is the $SU(2)_1 \otimes SU(2)_2 \otimes U(1)_X$. If this symmetry were unbroken it would lead to the presence of seven massless gauge bosons in nature. However, experiments tell us that there is only one massless force carrier belonging to the electroweak interaction, the photon. As already discussed in the introduction all other bosons must acquire masses through the effect of spontaneous symmetry breaking.

$G(221)$ models go beyond the SM by extending its gauge group, the $SU(2)_L \otimes$

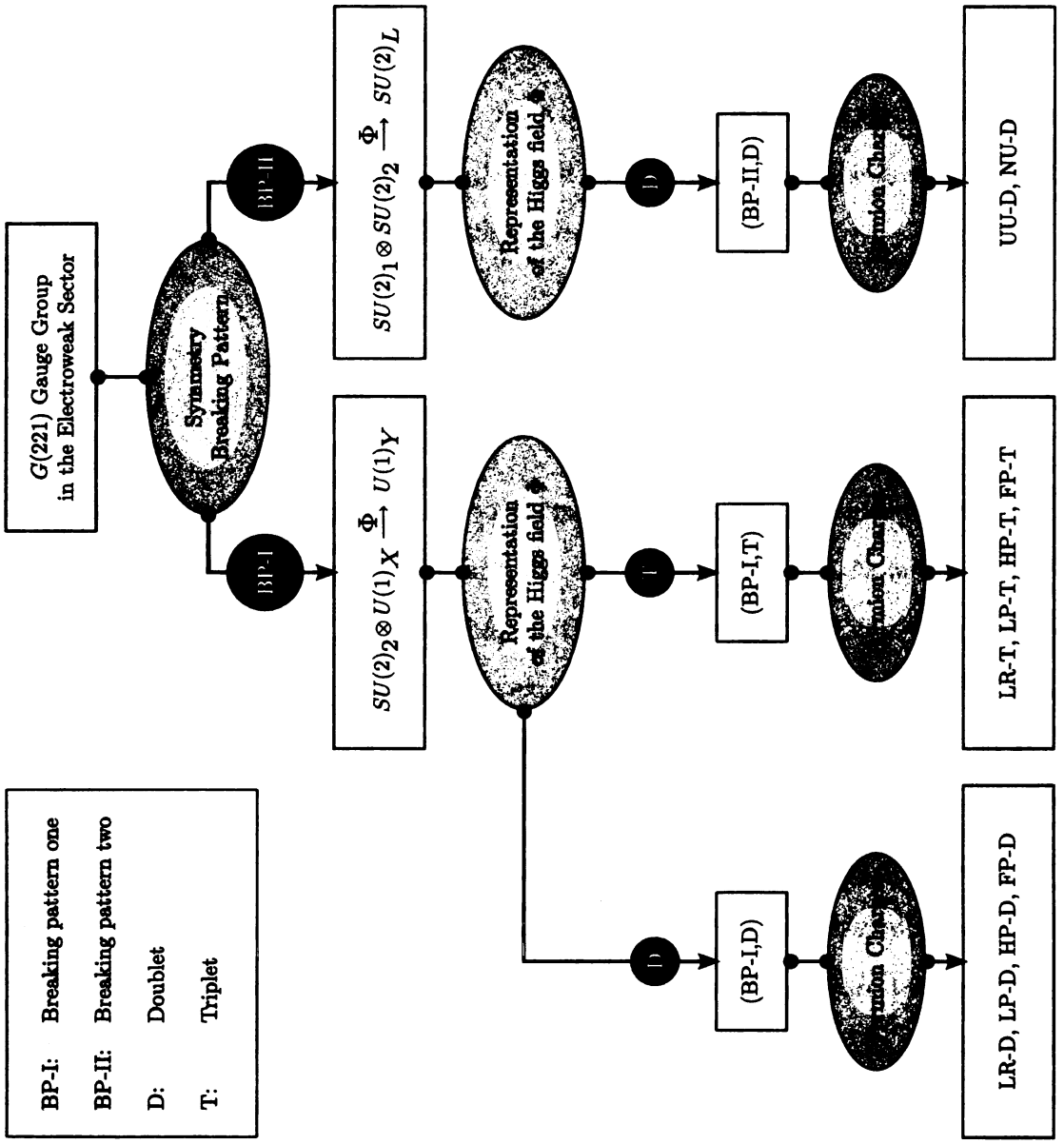

Figure 2.1: Classification of the $G(221)$ models under study — the ten $G(221)$ models considered in this work fall into three distinct classes that differ from each other in terms of the mechanism by which the fundamental $G(221)$ gauge group is broken and the choice for the Higgs representation Φ at the first breaking stage. Two breaking patterns are available; the Higgs field Φ can either be represented by a doublet or triplet. Referring to these three classes of $G(221)$ models we will speak of the (BP-I,D), (BP-I,T) and (BP-II,D) models.

$U(1)_Y$, by an additional $SU(2)$. However, the SM has proven to be a very successful theory at low energies. At a first stage the breaking mechanism of $G(221)$ models therefore has to reproduce the symmetry group of the SM. From there on, the breaking proceeds, of course, as in the SM: At a second breaking stage the SM breaking $SU(2)_L \otimes U(1)_Y \to U(1)_{\rm em}$ is mimicked. It is thus clear that the general $G(221)$ breaking pattern must have the following form:

$$SU(2)_1 \otimes SU(2)_2 \otimes U(1)_X \quad \xrightarrow{\Phi} \quad SU(2)_L \otimes U(1)_Y \quad \xrightarrow{H} \quad U(1)_{\rm em}$$

We have already introduced the two Higgs field Φ and H that are responsible for the two symmetry breakings in the introduction to this chapter. Now we define Φ to be the Higgs field that is responsible for the first breaking and H to be the field responsible for the second breaking. We expect Φ to acquire a VEV at the TeV scale furnishing the new gauge bosons $W'^{\pm}$ and Z' with very heavy masses. H plays the same role as the familiar Higgs doublet in the SM. It gets a VEV of roughly 250 GeV resulting in masses of the $W^{\pm}$ and the Z boson as seen in experiment. Note, that the expected hierarchy of the two VEVs is, in principle, a model assumption.

There are two ways to break the $SU(2)_1 \otimes SU(2)_2 \otimes U(1)_X$ down to the $U(1)_{\rm em}$ splitting the set of all $G(221)$ models naturally into two groups. In the following discussion we will refer to both mechanisms as the first and the second breaking pattern, breaking pattern one and two or just BP-I and BP-II when an abbreviation is needed. The choice of one of either breaking patterns has a substantial phenomenological impact and in fact, it is the most important criterion for the classification of the $G(221)$ models. We now present both patterns in detail:

First breaking pattern: The first breaking mechanism identifies the first $SU(2)$ as the left-handed $SU(2)_L$ that we know from the SM and the second $SU(2)$

as its right-handed counterpart. We would like the first symmetry breaking to provide us with the SM gauge group and as the $SU(2)_L$ is already present right from the beginning — in form of the $SU(2)_1$ — we only have one choice for what to do at the first breaking stage: The $SU(2)_2$ and the $U(1)_X$ have to be broken to the SM hypercharge group $U(1)_Y$:

$$SU(2)_1 \longrightarrow SU(2)_L \quad ; \quad SU(2)_2 \otimes U(1)_X \xrightarrow{\Phi} U(1)_Y$$

Then everything is set up correctly for the second breaking stage at which H can break the $SU(2)_L \otimes U(1)_Y$ to the $U(1)_{\text{em}}$. Fig. 2.2 on page 28 illustrates this first breaking mechanism in a schematic diagram. From the above mentioned models the first four, i.e. the LR, the LP, the HP and the FP model, belong to the first breaking pattern.

Second breaking pattern: The second breaking pattern arrives at the $SU(2)_L$ of the SM by breaking the direct product of the two $SU(2)$s to the diagonal subgroup. As for the remaining group, now the $U(1)_X$, there is again only one choice left. It has to be identified with the $U(1)_Y$ right from the beginning:

$$SU(2)_1 \otimes SU(2)_2 \xrightarrow{\Phi} SU(2)_L \quad ; \quad U(1)_X \longrightarrow U(1)_Y$$

At the second breaking stage we again encounter $SU(2)_L \otimes U(1)_Y \xrightarrow{H} U(1)_{\text{em}}$. Fig. 2.3 on page 29 visualizes this breaking mechanism. The two $G(221)$ models in which the symmetry breaking proceeds according to pattern two are the UU and the NU model.

2.1.2 Higgs Representation at the First Breaking Stage

There are no uniquely defined representations for Φ that have to be employed when either breaking the $SU(2)_2$ and the $U(1)_X$ to the $U(1)_Y$ or the $SU(2)_1 \otimes SU(2)_2$ to the $SU(2)_L$. In fact, we are free to decide between different multiplets for either kind of breaking pattern. In this work we will consider the simplest scenarios and restrict ourselves to: $SU(2)_2$-doublet (D) and $SU(2)_2$-triplet (T) respresentations in the case of breaking pattern one and a bi-doublet (D) representation for breaking pattern two. A bi-triplet would be possible as well for the second breaking mechanism. But as the only expected difference to the bi-doublet case would be a rescaling of some parameters we will neglect that possibility. As opposed to Φ the representations of H are fixed. The condition that the second symmetry breaking has to resemble the SM breaking mechanism respectively leaves only one choice for H in either breaking pattern.

In total we will thus deal with ten different models: four models (LR-D, LP-D, HP-D, FP-D) in which the gauge symmetries are broken according to pattern one and Φ is represented by a $SU(2)_2$-doublet, four models (LR-T, LP-T, HP-T, FP-T) with the same breaking mechanism but utilizing a $SU(2)_2$-triplet representation of Φ instead and two models (UU-D, NU-D) that follow breaking pattern two and use a bi-doublet for Φ.

Since we are only interested in classifying the $G(221)$ models these comments on the Higgs representations should suffice for the moment. In subsection 2.2.1, when we begin to derive the boson masses, we will go into the details.

2.1.3 Assignment of the Fermion Charges

Separating the $G(221)$ models by breaking pattern and Higgs representation at the first breaking stage leads to three subsets of models: (BP-I,D), (BP-I,T) and (BP-

Model	$SU(2)_1$	$SU(2)_2$	$U(1)_X$ Quarks:	$U(1)_X$ Leptons:
LR	$\begin{pmatrix} u_L \\ d_L \end{pmatrix}, \begin{pmatrix} \nu_L \\ e_L \end{pmatrix}$	$\begin{pmatrix} u_R \\ d_R \end{pmatrix}, \begin{pmatrix} \nu_R \\ e_R \end{pmatrix}$	1/6	$-1/2$
LP	$\begin{pmatrix} u_L \\ d_L \end{pmatrix}, \begin{pmatrix} \nu_L \\ e_L \end{pmatrix}$	$\begin{pmatrix} u_R \\ d_R \end{pmatrix}$	1/6	$Y_{\rm SM}$
HP	$\begin{pmatrix} u_L \\ d_L \end{pmatrix}, \begin{pmatrix} \nu_L \\ e_L \end{pmatrix}$	$\begin{pmatrix} \nu_R \\ e_R \end{pmatrix}$	$Y_{\rm SM}$	$-1/2$
FP	$\begin{pmatrix} u_L \\ d_L \end{pmatrix}, \begin{pmatrix} \nu_L \\ e_L \end{pmatrix}$		$Y_{\rm SM}$	$Y_{\rm SM}$
UN	$\begin{pmatrix} u_L \\ d_L \end{pmatrix}$	$\begin{pmatrix} \nu_L \\ e_L \end{pmatrix}$	$Y_{\rm SM}$	$Y_{\rm SM}$
NU	$\begin{pmatrix} u_L \\ d_L \end{pmatrix}_{1^{\rm st},2^{\rm nd}}, \begin{pmatrix} \nu_L \\ e_L \end{pmatrix}_{1^{\rm st},2^{\rm nd}}$	$\begin{pmatrix} u_L \\ d_L \end{pmatrix}_{3^{\rm rd}}, \begin{pmatrix} \nu_L \\ e_L \end{pmatrix}_{3^{\rm rd}}$	$Y_{\rm SM}$	$Y_{\rm SM}$

Table 2.1: Charges of the fermions under the $G(221)$ gauge group — the displayed iso-doublets are eigenstates of the weak interaction. Unless otherwise specified, they represent all three generations. $Y_{\rm SM}$ stands for the usual values of the electroweak hypercharge in the SM: $Y_{\rm SM}(\nu_L) = Y_{\rm SM}(e_L) = -\frac{1}{2}$, $Y_{\rm SM}(e_R) = -1$, $Y_{\rm SM}(u_L) = Y_{\rm SM}(d_L) = \frac{1}{6}$, $Y_{\rm SM}(u_R) = \frac{2}{3}$ and $Y_{\rm SM}(d_R) = -\frac{1}{3}$.

II,D) in shorthand. Within each of these three groups the respective models differ from each other in terms of the fermion charges.

Historically, the LR model represents the original $G(221)$ model. It assumes that the right-handed fermions transform as doublets under the $SU(2)_2$, just as the left-handed fermions transform as doublets under the $SU(2)_1$, viz., the weak $SU(2)$ of the SM. In the LR model all right-handed fermions, thus, interact with the new heavy charged $W'^{\pm}$ bosons. If we let the $W'^{\pm}$ gauge bosons talk to quarks or leptons exclusively we arrive at the LP and HP models. If we only invoke the presence of a second $SU(2)$ in the electroweak gauge group, but assume that the $W'^{\pm}$ gauge bosons do not interact with any SM fermion, we get the FP model. All four models belong to the first breaking pattern.

Regarding the second breaking pattern we can either separate the SM fermion representations by flavor or by generation which provides us with the UU and the (family) NU model respectively. The UU model assigns the quark doublets to the first, the lepton doublets to the second $SU(2)$; the NU model singles out the third fermion generation reserving the $SU(2)_2$ exclusively for it. In that respect the NU model is the only $G(221)$ model under study in which the charge assignements do not apply cross-generationally — the only model that breaks family symmetry.

Tab. 2.1 gives an overview of the fermion charges under the fundamental $G(221)$ gauge groups for all considered models. In order to save space we only include the fermions of the first generation in Tab. 2.1. Unless otherwise specified, these are, however, understood to collectively represent all three fermion generations. Moreover, as indicated in Tab. 2.1 some of our $G(221)$ models not only extend the particle content of the SM by additional gauge bosons but also by new right-handed neutrinos.

Our set of new physics models comprises all phenomenologically different $G(221)$ models. Further $G(221)$ models that we do not include into our analysis could be constructed from the models of the second breaking pattern by exchanging the fermion

representations between the two $SU(2)$s. As such a permutation would, however, only correspond to a redefinition of some model parameters we will not consider these models in our study.

2.2 Masses of the Gauge Bosons

The gauge bosons get their masses and mix with each other in the course of spontaneous symmetry breaking that is triggered by the two Higgs fields Φ and H. To calculate the masses of the physical gauge bosons we first have to discuss the contributions $\mathscr{L}_\Phi$ and $\mathscr{L}_H$ from Φ and H to the total Lagrangian $\mathscr{L}$.

2.2.1 Higgs Representations

In all $G(221)$ models the Lagrangians $\mathscr{L}_\Phi$ and $\mathscr{L}_H$ have the following form:

$$\mathscr{L}_\Phi \sim \mathrm{Tr}\left[(D_\mu\Phi)^\dagger (D^\mu\Phi)\right] \quad ; \quad \mathscr{L}_H \sim \mathrm{Tr}\left[(D_\mu H)^\dagger (D^\mu H)\right]$$

The coefficients of $\mathscr{L}_\Phi$ and $\mathscr{L}_H$ get fixed by the choice of the Higgs representations and the trace symbol only has an effect when the corresponding product of the covariant derivatives is non-scalar — which is the case if a Higgs field is represented by a triplet or a bi-doublet. Constructing the Lagrangians for the two Higgs fields we have to use the covariant derivative D_μ rather than the ordinary partial derivative ∂_μ in order to ensure local gauge invariance.

The goal of our analysis in this subsection is to explicitly write down the covariant derivatives $D_\mu\Phi$ and $D_\mu H$ in terms of the gauge bosons and the gauge couplings. These derivatives depend on the charges of the respective Higgs fields under the $G(221)$ gauge groups. Tab. 2.2 on the next page lists the Higgs representations our models are constructed with. The second column of Tab. 2.2 gives the quantum

1st stage	Repr.	Multiplet and VEV
BP-I (D)	$\Phi \sim \left(1, 2, \frac{1}{2}\right)$	$\Phi = \begin{pmatrix} \phi^+ \\ \phi^0 \end{pmatrix}$; $\langle \Phi \rangle = \frac{1}{\sqrt{2}} \begin{pmatrix} 0 \\ \tilde{u}_{\mathrm{D}} \end{pmatrix}$
BP-I (T)	$\Phi \sim (1, 3, 1)$	$\Phi = \frac{1}{2} \begin{pmatrix} \phi^+ & \sqrt{2}\phi^{++} \\ \sqrt{2}\phi^0 & -\phi^+ \end{pmatrix}$; $\langle \Phi \rangle = \frac{1}{2} \begin{pmatrix} 0 & 0 \\ \tilde{u}_{\mathrm{T}} & 0 \end{pmatrix}$
BP-II	$\Phi \sim (2, \bar{2}, 0)$	$\Phi = \begin{pmatrix} \phi_1^0 & \phi_1^+ \\ \phi_2^- & \phi_2^0 \end{pmatrix}$; $\langle \Phi \rangle = \frac{1}{\sqrt{2}} \begin{pmatrix} \tilde{u} & 0 \\ 0 & \tilde{u} \end{pmatrix}$
2nd stage	Repr.	Multiplet and VEV
BP-I (D)	$H \sim (2, \bar{2}, 0)$	$H = \begin{pmatrix} h_1^0 & h_1^+ \\ h_2^- & h_2^0 \end{pmatrix}$; $\langle H \rangle = \frac{\tilde{v}}{\sqrt{2}} \begin{pmatrix} c_{\tilde{\beta}} & 0 \\ 0 & s_{\tilde{\beta}} \end{pmatrix}$
BP-I (T)	$H \sim (2, \bar{2}, 0)$	$H = \begin{pmatrix} h_1^0 & h_1^+ \\ h_2^- & h_2^0 \end{pmatrix}$; $\langle H \rangle = \frac{\tilde{v}}{\sqrt{2}} \begin{pmatrix} c_{\tilde{\beta}} & 0 \\ 0 & s_{\tilde{\beta}} \end{pmatrix}$
BP-II	$H \sim \left(1, 2, \frac{1}{2}\right)$	$H = \begin{pmatrix} h^+ \\ h^0 \end{pmatrix}$; $\langle H \rangle = \frac{1}{\sqrt{2}} \begin{pmatrix} 0 \\ \tilde{v} \end{pmatrix}$

Table 2.2: Representations of the Higgs fields Φ and H for the three classes of considered models — at the first stage of breaking pattern one Φ can either be chosen to be a doublet or a triplet under the $SU(2)_2$. In the second breaking pattern Φ is represented by a bi-doublet. The second breaking stage mimics the symmetry breaking of the SM; the respective representations of H are therefore fixed.

numbers of Φ and H for all three considered classes of $G(221)$ models in the following format:

$$\text{Higgs field} \sim (T_1, T_2, X)$$

Here T_1 and T_2 denote the main quantum numbers of the $SU(2)_1$ and $SU(2)_2$ isospins and X is the charge under the $U(1)_X$. The actual multiplets that represent Φ and H as well as their VEVs are listed in the third column of Tab. 2.2. We generically denote the non-zero VEVs at the first and second breaking stages by $\tilde{u}$ and $\tilde{v}$ resp. In the case of breaking pattern one we put a small subscript on $\tilde{u}$ to distinguish between the doublet (D) and the triplet (T) representations for Φ. Since the same Higgs H is used in both (BP-I,D) and (BP-I,T) models such a discrimination is, however, not necessary at the second stage. By contrast to pattern two the first breaking pattern introduces a further degree of freedom through the VEVs of the Higgs fields. In the first breaking pattern $\langle H \rangle$ actually features two different VEVs, $\tilde{\kappa}$ and $\tilde{\kappa}'$:

$$\text{BP-I:} \qquad \langle H \rangle = \frac{1}{\sqrt{2}} \begin{pmatrix} \tilde{\kappa} & 0 \\ 0 & \tilde{\kappa}' \end{pmatrix}$$

We obtain the expression given in Tab. 2.2 when we relate the VEV $\tilde{v}$ and the angle $\tilde{\beta}$ to $\tilde{\kappa}$ and $\tilde{\kappa}'$ as follows:

$$\tilde{\kappa} = \tilde{v} \cdot c_{\tilde{\beta}} \quad ; \quad \tilde{\kappa}' = \tilde{v} \cdot s_{\tilde{\beta}}$$

The tilde ($\tilde{}$) over the angle β and the VEVs $\tilde{\kappa}$, $\tilde{\kappa}'$ and $\tilde{v}$ indicates that these parameters are intrinsic model parameters. We will elucidate the details in Subsec. 2.2.2. $c_{\tilde{\beta}}$ and $s_{\tilde{\beta}}$ are, of course, abbreviations for $\cos(\tilde{\beta})$ and $\sin(\tilde{\beta})$. In the following we will abbreviate the trigonometric functions of any arbitrary angle α in this manner:

$$s_\alpha \equiv \sin(\alpha) \quad ; \quad c_\alpha \equiv \cos(\alpha) \quad ; \quad t_\alpha \equiv \tan(\alpha)$$

Two criteria apply to the selection of those multiplet components that acquire non-zero VEVs: On the one hand we require the Lagrangian to remain invariant under $U(1)_{\text{em}}$ transformations while the fundamental gauge symmetries are broken; that is, we have to assign the VEVs to the respective Higgs fields such that the electric charge Q is a good quantum number in the end. On the other hand, as complex or purely imaginary VEVs would lead to, e.g., unphysical mass terms, the Higgs VEVs must be real.

In order to fulfill the first condition we define the electric charge Q to be the sum of T_1^3, T_2^3 and X:

$$Q \equiv T_1^3 + T_2^3 + X \tag{2.1}$$

with T_1^3 and T_2^3 being the third components of the isospin vectors $\vec{T}_1$ and $\vec{T}_2$ and assign the non-zero VEVs to multiplet components for which this sum takes the value zero. The Higgs VEVs then do not carry electric charge and the $U(1)_{\text{em}}$ remains unbroken. In Tab. 2.2 the electric charges of the Higgs fields are indicated by superscripts.

It is not surprising that the relation in Eq. (2.1) represents the proper definition of Q. In models that employ the first breaking pattern T_1^3 is equivalent to T_L^3 and T_2^3 and X add up to Y. If breaking pattern two is used X and Y are the same quantum number and the sum of T_1^3 and T_2^3 equals T_L^3. Eq. (2.1) thus does nothing else than mimicking the familiar SM identity:

$$Q = T_L^3 + Y = T_1^3 + \left(T_2^3 + X\right) = \left(T_1^3 + T_2^3\right) + X$$

Furnishing only the real parts of the respective multiplet components with non-zero VEVs always introduces factors of $\frac{1}{\sqrt{2}}$ when going from a Higgs field to its VEV. To give an example: The h^0 that belongs to the H field of the second breaking pattern is given as:

$$h^0 = \frac{1}{\sqrt{2}}\left(h_r^0 + i \cdot h_i^0\right) \qquad \text{where} \quad h_r^0, h_i^0 \in \mathbb{R}$$

where $\frac{1}{\sqrt{2}}$ plays the role of a normalization factor. $\langle H \rangle$ is supposed to be real and so only h_r^0 gets a VEV and h_i^0 vanishes in the vacuum:

$$\langle h^0 \rangle = \frac{1}{\sqrt{2}}\left(\tilde{u} + i \cdot 0\right) = \frac{u}{\sqrt{2}}$$

With all these general remarks being made, the charges of the Higgs fields Φ and H given in Tab. 2.2 now allow us to explicitly write down the covariant derivatives $D_\mu \Phi$ and $D_\mu H$. Tab. 2.3 on the following page presents the Lagrangians $\mathscr{L}_\Phi$ and $\mathscr{L}_H$ in terms of gauge couplings and vector bosons for all three considered classes of $G(221)$ models. The overall prefactors take care of the proper normalization of $\mathscr{L}_\Phi$ and $\mathscr{L}_H$. They ensure that in both Lagrangians, if expandend in the components of their Higgs multiplets, all terms have a prefactor of 1:

$$\mathscr{L}_\Phi = \sum_i \left(D_\mu \phi_i\right)^\dagger \left(D^\mu \phi_i\right) \quad ; \quad \mathscr{L}_H = \sum_i \left(D_\mu h_i\right)^\dagger \left(D^\mu h_i\right)$$

The gauge couplings of the $SU(2)_1$, the $SU(2)_2$ and the $U(1)_X$ that enter into $\mathscr{L}_\Phi$ and $\mathscr{L}_H$ are denoted by $\tilde{g}_1$, $\tilde{g}_2$ and $\tilde{g}_X$ resp. We will concentrate our attention to them in the next subsection. The gauge bosons belonging to the three fundamental symmetry groups are given as:

$$SU(2)_1 : W_1^1, W_1^2, W_1^3 \quad ; \quad SU(2)_2 : W_2^1, W_2^2, W_2^3 \quad ; \quad U(1)_X : B_X$$

1st stage		Lagrangian
BP-I (D)	$\mathscr{L}_\Phi$	$= \left(D_\mu\Phi\right)^\dagger \left(D^\mu\Phi\right)$
		$= \left(\partial_\mu\Phi^\dagger + i\tilde{g}_2\Phi^\dagger T_2^a \cdot W_{2,\mu}^a + i\tilde{g}_X \frac{1}{2}\Phi^\dagger \cdot B_{X,\mu}\right)\times$
		$\times\left(\partial^\mu\Phi - i\tilde{g}_2 T_2^b\Phi \cdot W_2^{b,\mu} - i\tilde{g}_X \frac{1}{2}\Phi \cdot B_X^\mu\right)$
BP-I (T)	$\mathscr{L}_\Phi$	$= 2\cdot \mathrm{Tr}\Big[\left(D_\mu\Phi\right)^\dagger \left(D^\mu\Phi\right)\Big]$
		$= 2\cdot \mathrm{Tr}\Big[\left(\partial_\mu\Phi^\dagger + i\tilde{g}_2\left[\Phi^\dagger, T_2^a\right] \cdot W_{2,\mu}^a + i\tilde{g}_X\Phi^\dagger \cdot B_{X,\mu}\right)\times$
		$\times\left(\partial^\mu\Phi - i\tilde{g}_2\left[T_2^b, \Phi\right] \cdot W_2^{b,\mu} - i\tilde{g}_X\Phi \cdot B_X^\mu\right)\Big]$
BP-II	$\mathscr{L}_\Phi$	$= \mathrm{Tr}\Big[\left(D_\mu\Phi\right)^\dagger \left(D^\mu\Phi\right)\Big]$
		$= \mathrm{Tr}\Big[\left(\partial_\mu\Phi^\dagger + i\tilde{g}_1\Phi^\dagger T_1^a \cdot W_{1,\mu}^a - i\tilde{g}_2 T_2^b\Phi^\dagger \cdot W_{2,\mu}^b\right)\times$
		$\times\left(\partial^\mu\Phi - i\tilde{g}_1 T_1^c\Phi \cdot W_1^{c,\mu} + i\tilde{g}_2\Phi T_2^d \cdot W_2^{d,\mu}\right)\Big]$

2nd stage		Lagrangian
BP-I	$\mathscr{L}_H$	$= \frac{1}{2}\cdot \mathrm{Tr}\Big[\left(D_\mu H\right)^\dagger \left(D^\mu H\right)\Big]$
		$= \frac{1}{2}\cdot \mathrm{Tr}\Big[\left(\partial_\mu H^\dagger + i\tilde{g}_1 H^\dagger T_1^a \cdot W_{1,\mu}^a - i\tilde{g}_2 T_2^b H^\dagger \cdot W_{2,\mu}^b\right)\times$
		$\times\left(\partial^\mu H - i\tilde{g}_1 T_1^c H \cdot W_1^{c,\mu} + i\tilde{g}_2 H T_2^d \cdot W_2^{d,\mu}\right)\Big]$
BP-II	$\mathscr{L}_H$	$= \left(D_\mu H\right)^\dagger \left(D^\mu H\right)$
		$= \left(\partial_\mu H^\dagger + i\tilde{g}_2\, H^\dagger T_2^a \cdot W_{2,\mu}^a + i\tilde{g}_X \frac{1}{2} H^\dagger \cdot B_{X,\mu}\right)\times$
		$\times\left(\partial^\mu H - i\tilde{g}_2 T_2^b H \cdot W_2^{b,\mu} - i\tilde{g}_X \frac{1}{2} H \cdot B_X^\mu\right)$

Table 2.3: Lagrangians of the Higgs fields Φ and H - depending on their charges under the $G(221)$ gauge group the Higgs fields Φ and H are accounted for by different contributions to the total Lagrangian. Once the Higgs fields acquire their VEVs the gauge symmetry of these Lagrangians gets broken and six linear combinations of the seven fundamental gauge bosons become massive.

Since the Lagrangians $\mathscr{L}_\Phi$ and $\mathscr{L}_H$ are invariant under the full $G(221)$ gauge group, these seven gauge bosons are still massless. The terms in which they appear in $\mathscr{L}_\Phi$ and $\mathscr{L}_H$ represent the gauge interactions of the Higgs fields Φ and H — mass and mass mixing terms do not appear until we break the $G(221)$ symmetry. In our language of Higgs Lagrangians the mechanism of spontaneous symmetry breaking (SSB) is accounted for by the substitution of the Higgs fields Φ and H with their VEVs $\langle\Phi\rangle$ and $\langle H\rangle$:

$$\text{SSB:} \quad \mathscr{L}_\Phi \longrightarrow \mathscr{L}_{\langle\Phi\rangle} \quad ; \quad \mathscr{L}_H \longrightarrow \mathscr{L}_{\langle H\rangle} \tag{2.2}$$

We will examine the effects of these substitutions in Subsec. 2.2.3. Now we focus on the gauge couplings.

2.2.2 Gauge Couplings and Mixing Angles

The treatment of the parameters that are involved in our analysis requires special care: In the next chapter it will be our goal to calculate the new physics corrections of our $G(221)$ models to the electroweak observables and to add these corrections to the GAPP code. GAPP, however, is designed to fit the SM to the electroweak data and therefore employs the usual parameters of the SM. The old physics parameters in our $G(221)$ models differ from these SM parameters, as they receive contributions from new physics, and so we will have to develop a dictionary of relations that will help us translate our parameters to those of the SM, that is to those used by GAPP.

In [19] Burgess et al. present a detailed study of constraints on new physics derived in a model-independent effective Lagrangian approach. They give a detailed discussion of the relation between new physics and SM parameters and in this work we will basically follow their procedure. Burgess et al. distinguish between three different ideas: Model parameters, standard parameters and reference observables.

In the following we will make use of all three concepts which is why we now want to shortly comment on each of them:

Model parameters are the parameters by which the fundamental Lagrangian of our $G(221)$ model is parametrized as well as all other quantities that are derived from them. This definition also applies to the reparametrized Lagrangian in which the VEVs of the Higgs fields are used rather than the fields themselves. Burgess equips these parameters with a tilde; in our previous discussion we already adopted this notation when we introduced the Higgs VEVs $\tilde{u}$ and $\tilde{v}$, the angle $\tilde{\beta}$ and the couplings of the three fundamental gauge groups $\tilde{g}_1$, $\tilde{g}_2$ and $\tilde{g}_X$. The rest of this subsection will deal with the important secondary quantities that can be constructed from these couplings.

Standard parameters are parameters whose analytical relations to the experimental input take exactly the same form as in the SM. In other words: They represent the actual parameters of the SM transfered to and incorporated into our $G(221)$ models. In order to distinguish them from our model parameters we will furnish them with the index SM. It is the standard parameters that are used by GAPP and as mentioned above one of our goals that we have to accomplish before we can start fitting will be to translate our model parameters that have equivalents in the SM to these standard parameters. In fact, the relevant standard parameters will be the fine structure constant, α_{SM}, the VEV of the electroweak symmetry breaking, v^2_{SM}, and the electroweak mixing angle $s^2_{\theta_{\mathrm{SM}}}$. We will come back to the standard parameters in Subsec. 3.1.2.

Reference observables are observables that have been measured with high precision and that can therefore be employed to deduce the numerical values of the standard parameters. GAPP uses the fine structure constant α and Fermi's constant G_F as reference input. Optionally, the mass M_Z of the Z boson can

be fixed. We note that α is identical to $\alpha_{\rm SM}$ — the two notations for the fine structure constant just either emphasize its role as an observable or as a model parameter. Once we have expressed our new physics corrections in terms of the standard parameters the reference observables will serve as the ultimate link between our theoretical analysis and the experimental data.

The breaking of a more fundamental initial gauge group to a smaller subgroup has two effects: First, the new gauge group will be associated with its own gauge couplings that are related to the couplings of the fundamental gauge group. The actual form of the breaking pattern has to tell us how these relations exactly look like. And second, the mechanism of symmetry breaking will lead to the mixing of the gauge bosons belonging to the fundamental symmetry group. It will therefore be convenient to change the basis of the gauge bosons after the symmetry breaking by performing a rotation about a certain angle.

Both the coupling constants of the new gauge groups as well as the mixing angles of the gauge bosons can be constructed from the gauge couplings of the initial symmetry group, in our case $\tilde{g}_1$, $\tilde{g}_2$ and $\tilde{g}_X$. In the following we show how this is respectively done at the first and the second breaking stage of our $G(221)$ models.

First breaking stage The first breaking of pattern one, $SU(2)_2 \otimes U(1)_X \to U(1)_Y$, mimics the SM breaking $SU(2)_L \otimes U(1)_Y \to U(1)_{\rm em}$. Hence, we define the mixing angle $\tilde{\phi}$ between the bosons of the the $SU(2)_2$ and the $U(1)_X$ similarly to the electroweak mixing angle $\theta_{\rm SM}$ — the tangent of $\tilde{\phi}$ is given as the ratio of the $U(1)$ coupling, $\tilde{g}_X$, to the $SU(2)$ coupling, $\tilde{g}_2$. As for breaking pattern two we can either set the tangent of $\tilde{\phi}$ to $\tilde{g}_2/\tilde{g}_1$ or the inverse of that. Breaking the two $SU(2)$s to the diagonal subgroup, $SU(2)_L$, we have to treat both groups on an equal footing and it must therefore not matter which choice we make. We decide for the first option which leads us to:

$$\text{BP-I:} \quad t_{\tilde{\phi}} \equiv \frac{\tilde{g}_X}{\tilde{g}_2} \qquad ; \qquad \text{BP-II:} \quad t_{\tilde{\phi}} \equiv \frac{\tilde{g}_2}{\tilde{g}_1} \tag{2.3}$$

After the first breaking stage we arrive at the $SU(2)_L \otimes U(1)_X$ of the SM for either kind of breaking pattern. Analogously to the standard couplings $g_{L,\mathrm{SM}}$ and $g_{Y,\mathrm{SM}}$ we denote the gauge couplings of this first subgroup of the fundamental $G(221)$ gauge group by $\tilde{g}_L$ and $\tilde{g}_Y$. As the first breaking pattern directly identifies the first $SU(2)$ with the $SU(2)_L$ the corresponding coupling, $\tilde{g}_1$, has to be equivalent to $\tilde{g}_L$. In breaking pattern two $\tilde{g}_L$ follows from the mixing of both fundamental $SU(2)$s:

$$\text{BP-I:} \quad \tilde{g}_L \equiv \tilde{g}_1 \qquad ; \qquad \text{BP-II:} \quad \frac{1}{\tilde{g}_L^2} \equiv \frac{1}{\tilde{g}_1^2} + \frac{1}{\tilde{g}_2^2} \tag{2.4}$$

If we combine Eqs. (2.3) and (2.4) we can rewrite $\tilde{g}_1$ and $\tilde{g}_2$ in terms of the weak isospin coupling constant $\tilde{g}_L$ and the first stage mixing angle $\tilde{\phi}$:

$$\text{BP-II:} \qquad \tilde{g}_1 = \frac{\tilde{g}_L}{s_{\tilde{\phi}}} \quad ; \quad \tilde{g}_2 = \frac{\tilde{g}_L}{c_{\tilde{\phi}}} \qquad \Leftrightarrow \qquad \tilde{g}_L = s_{\tilde{\phi}} \tilde{g}_1 = c_{\tilde{\phi}} \tilde{g}_2 \tag{2.5}$$

Similar arguments apply to the definition of $\tilde{g}_Y$. In breaking pattern two the $U(1)_X$ is not touched during the first symmetry breaking. $\tilde{g}_X$ therefore is equivalent to $\tilde{g}_Y$. The first breaking pattern mixes the $SU(2)_2$ and the $U(1)_X$ at the first stage:

$$\text{BP-I:} \quad \frac{1}{\tilde{g}_Y^2} \equiv \frac{1}{\tilde{g}_2^2} + \frac{1}{\tilde{g}_X^2} \qquad ; \qquad \text{BP-II:} \quad \tilde{g}_Y \equiv \tilde{g}_X \tag{2.6}$$

The combination of Eqs. (2.3) and (2.6) provides us with relations similar to those in Eq. (2.5), now for the first instead of for the second breaking pattern:

$$\text{BP-I:} \qquad \tilde{g}_2 = \frac{\tilde{g}_Y}{s_{\tilde{\phi}}} \quad ; \quad \tilde{g}_X = \frac{\tilde{g}_Y}{c_{\tilde{\phi}}} \qquad \Leftrightarrow \qquad \tilde{g}_Y = s_{\tilde{\phi}} \tilde{g}_2 = c_{\tilde{\phi}} \tilde{g}_X \tag{2.7}$$

Second breaking stage The second breaking stage resembles the electroweak symmetry breaking of the SM. For both breaking patterns the analogue of the Weinberg angle θ_{SM} in our $G(221)$ models, $\tilde{\theta}$, the electric charge $\tilde{e}$ and the fine structure constant $\tilde{\alpha}$ are defined as:

$$t_{\tilde{\theta}} \equiv \frac{\tilde{g}_Y}{\tilde{g}_L} \quad ; \quad \frac{1}{\tilde{e}^2} \equiv \frac{1}{\tilde{g}_L^2} + \frac{1}{\tilde{g}_Y^2} \quad ; \quad \tilde{\alpha} \equiv \frac{\tilde{e}^2}{4\pi}$$

Compare also with Eq. (3.6). Just as in the SM, we then have the following relations between the gauge couplings and the electric charge as well as the electroweak mixing angle:

$$\tilde{g}_L = \frac{\tilde{e}}{s_{\tilde{\theta}}} \quad ; \quad \tilde{g}_Y = \frac{\tilde{e}}{c_{\tilde{\theta}}} \qquad \Leftrightarrow \qquad \tilde{e} = s_{\tilde{\theta}} \tilde{g}_L = c_{\tilde{\theta}} \tilde{g}_Y \tag{2.8}$$

According to the definitions of $\tilde{g}_L$ and $\tilde{g}_Y$ in Eqs. (2.4) and (2.6) the electric charge takes the following form in either breaking pattern:

$$\frac{1}{\tilde{e}^2} = \frac{1}{\tilde{g}_1^2} + \left(\frac{1}{\tilde{g}_2^2} + \frac{1}{\tilde{g}_X^2} \right) = \left(\frac{1}{\tilde{g}_1^2} + \frac{1}{\tilde{g}_2^2} \right) + \frac{1}{\tilde{g}_X^2}$$

GAPP only knows indirectly about coupling constants. Instead of the SM gauge couplings $g_{L,\mathrm{SM}}$ and $g_{Y,\mathrm{SM}}$ the fine structure constant α_{SM} and the electroweak mixing angle θ_{SM} are implemented in the code. When we have come to calculate the corrections to the precision observables we will also discard all gauge couplings trading them for $\tilde{\alpha}$, $\tilde{\theta}$ and $\tilde{\phi}$. The corresponding relations between $\tilde{g}_1$, $\tilde{g}_2$ and $\tilde{g}_X$ on the one side and $\tilde{\alpha}$, $\tilde{\theta}$ and $\tilde{\phi}$ on the other side follow from Eqs. (2.5), (2.7) and (2.8). We present the results in Tab. 2.4 that summarizes all of the important relations discussed in this section.

BP	$\tilde{g}_1/(4\pi\tilde{\alpha})$	$\tilde{g}_2/(4\pi\tilde{\alpha})$	$\tilde{g}_X/(4\pi\tilde{\alpha})$	$\tilde{g}_L^{-2}$	$\tilde{g}_Y^{-2}$	$t_{\tilde{\phi}}$	$t_{\tilde{\theta}}$
I	$s_{\tilde{\theta}}^{-1}$	$c_{\tilde{\theta}}^{-1}s_{\tilde{\phi}}^{-1}$	$c_{\tilde{\theta}}^{-1}c_{\tilde{\phi}}^{-1}$	$\tilde{g}_1^{-2}$	$\tilde{g}_2^{-2}+\tilde{g}_X^{-2}$	$\tilde{g}_X/\tilde{g}_2$	$\tilde{g}_Y/\tilde{g}_L$
II	$s_{\tilde{\theta}}^{-1}s_{\tilde{\phi}}^{-1}$	$s_{\tilde{\theta}}^{-1}c_{\tilde{\phi}}^{-1}$	$c_{\tilde{\theta}}^{-1}$	$\tilde{g}_1^{-2}+\tilde{g}_2^{-2}$	$\tilde{g}_X^{-2}$	$\tilde{g}_2/\tilde{g}_1$	$\tilde{g}_Y/\tilde{g}_L$

Table 2.4: Fundamental gauge couplings and mixing angles — overview of the relations between $\tilde{g}_1$, $\tilde{g}_2$ and $\tilde{g}_X$ on the one side and the parameters $\tilde{\alpha}$, $\tilde{\theta}$ and $\tilde{\phi}$ as well as the couplings constants $\tilde{g}_L$ and $\tilde{g}_Y$ and mixing angles $\tilde{\phi}$ and $\tilde{\theta}$ on the other side.

2.2.3 Mass Matrices and Mixing of the Gauge Bosons

As we now have understood all quantities that enter the two Higgs Lagrangians $\mathscr{L}_\Phi$ and $\mathscr{L}_H$ we can return to Eq. (2.2) and finally perform the symmetry breaking. The first stage of symmetry breaking generates masses for the two heavy gauge bosons $\hat{W}'^{\pm}$ and $\hat{Z}'$:

$$\mathscr{L}_{\langle\Phi\rangle} \equiv \frac{1}{2}\widetilde{M}^2_{\hat{Z}'}\hat{Z}'_\mu\hat{Z}'^{,\mu} + \widetilde{M}^2_{\hat{W}'}\hat{W}'^{+}_\mu\hat{W}'^{-,\mu}$$

The hats ($\hat{}$) over the boson symbols indicate that these gauge bosons are not yet mass eigenstates and thus not physical boson states. During the second symmetry breaking two bosons $\hat{W}^{\pm}$ and $\hat{Z}$ will acquire masses and — that is the point — mix with the $\hat{W}'^{\pm}$ and the $\hat{Z}'$. In order to find the physical gauge bosons it will be necessary to diagonalize the mass matrices in the neutral ($\hat{Z}'$, $\hat{Z}$) and charged ($\hat{W}'^{\pm}$, $\hat{W}^{\pm}$) gauge boson sector. Z', Z, $W'^{\pm}$ and $W^{\pm}$ will then be represented by some linear combinations of the hatted gauge bosons. The tilde over $\widetilde{M}^2_{\hat{Z}'}$ and $\widetilde{M}^2_{\hat{W}'}$ reflects the fact that these masses are only internal model parameters which do not represent masses of physical states. The masses of the physical gauge bosons will be constructed from these tilde masses.

At the second stage of symmetry breaking H gets its VEV furnishing two further

gauge bosons, $\hat{W}^{\pm}$ and $\hat{Z}$, with masses:

$$\begin{aligned}\mathscr{L}_{\langle\Phi\rangle} + \mathscr{L}_{\langle H\rangle} \;\equiv\; & \frac{1}{2}\widetilde{M}^2_{\hat{Z}}\hat{Z}_\mu\hat{Z}^\mu + \frac{1}{2}\left(\widetilde{M}^2_{\hat{Z}'} + \Delta\widetilde{M}^2_{\hat{Z}'}\right)\hat{Z}'_\mu\hat{Z}'^{,\mu} + \delta\widetilde{M}^2_{\hat{Z}\hat{Z}'}\hat{Z}_\mu\hat{Z}'^{,\mu} \\ + \;& \widetilde{M}^2_{\hat{W}}\hat{W}^+_\mu\hat{W}^{-,\mu} + \left(\widetilde{M}^2_{\hat{W}'} + \Delta\widetilde{M}^2_{\hat{W}'}\right)\hat{W}'^+_\mu\hat{W}'^{-,\mu} \\ + \;& \delta\widetilde{M}^2_{\hat{W}\hat{W}'}\left(\hat{W}^+_\mu\hat{W}'^{-,\mu} + \hat{W}^-_\mu\hat{W}'^{+,\mu}\right)\end{aligned} \tag{2.9}$$

The next goal on our way to the masses of the physical gauge bosons is to determine the mass parameters in Eq. (2.9) and to discuss how the hatted bosons are constructed in terms of the fundamental gauge bosons $W^1_{1,2}$, $W^2_{1,2}$, $W^3_{1,2}$ and B_X. We will collect our results for the mass parameters in Tab. 2.5 on page 33.

In a first trivial step we transform the fundamental bosons that belong to the two $SU(2)$s such that they become eigenstates of the electric charge operator:

$$W^+_{1,2} = \frac{1}{\sqrt{2}}\left(W^1_{1,2} - iW^2_{1,2}\right) \quad ; \quad W^-_{1,2} = \frac{1}{\sqrt{2}}\left(W^1_{1,2} + iW^2_{1,2}\right)$$

If we take the bosons $W^{\pm}_{1,2}$, $W^3_{1,2}$ and B_X to be the fundamental basis of the $G(221)$ gauge bosons the effect of the twofold symmetry breaking triggered by Φ and H can be summarized as follows:

$SU(2)_1 \otimes SU(2)_2 \otimes U(1)_X$				Photon	EW bosons	NP bosons
$W^{\pm}_1, W^3_1,$	$W^{\pm}_2, W^3_2,$	B_X	$\longrightarrow$	A	$W^{\pm}, Z$	$W'^{\pm}, Z'$
massless	massless	massless		massless	massive	massive

Figs. 2.2 and 2.3 show diagrammatically the steps that lead from the initial fundamental gauge bosons to the physical states for both breaking patterns. We will now successively examine both stages of symmetry breaking and the diagonalization of the mass matrices. The following discussion can essentially be regarded as a comment on Figs. 2.2 and 2.3.

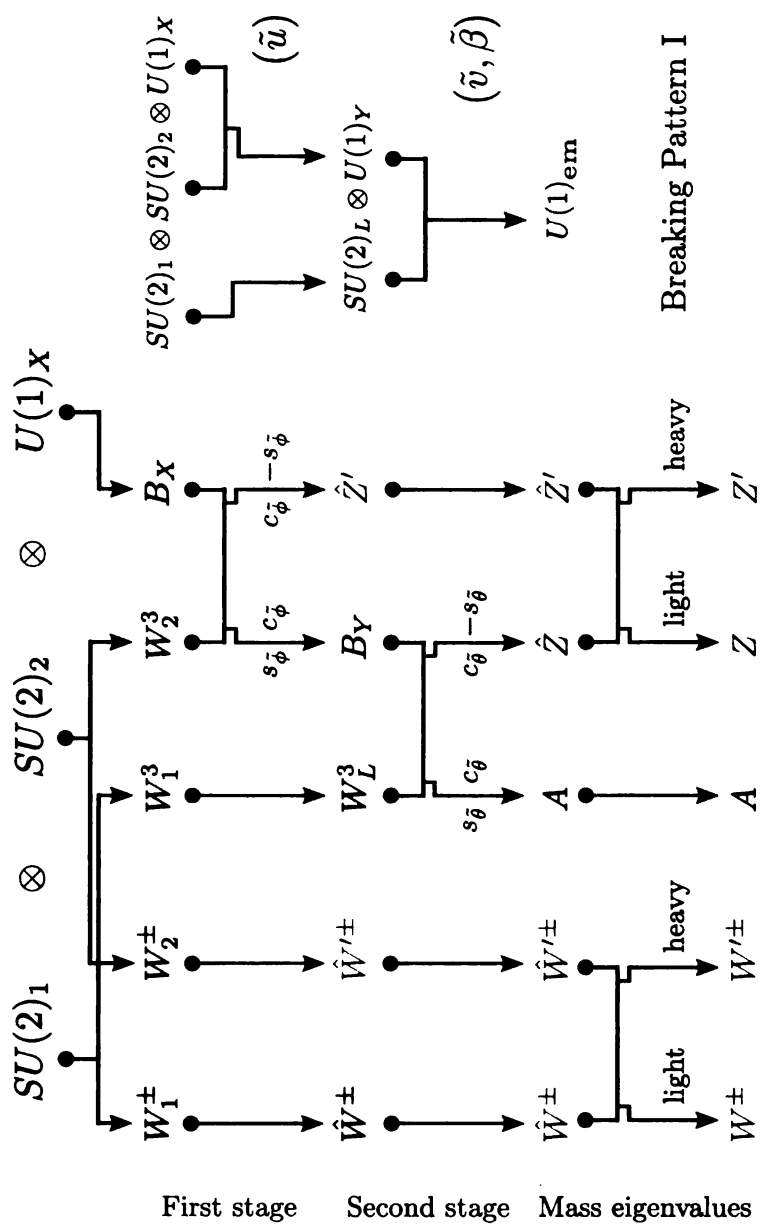

Figure 2.2: Mixing of the gauge bosons due to spontaneous symmetry breaking according the first breaking pattern — the text colors indicate whether the respective bosons have already acquired masses (red symbols) or whether they are still massless (green symbols). For all pairs of bosons that mix at a certain stage of symmetry breaking the respective mixing coefficients are given on either side of the corresponding arrows. Trigonometric functions written on the left-hand / right-hand side of an arrow belong to the left / right boson at the preceding stage of symmetry breaking. See Tab. 2.2 for the definition of the VEVs $\tilde{u}$ and $\tilde{v}$ and the angle $\tilde{\beta}$.

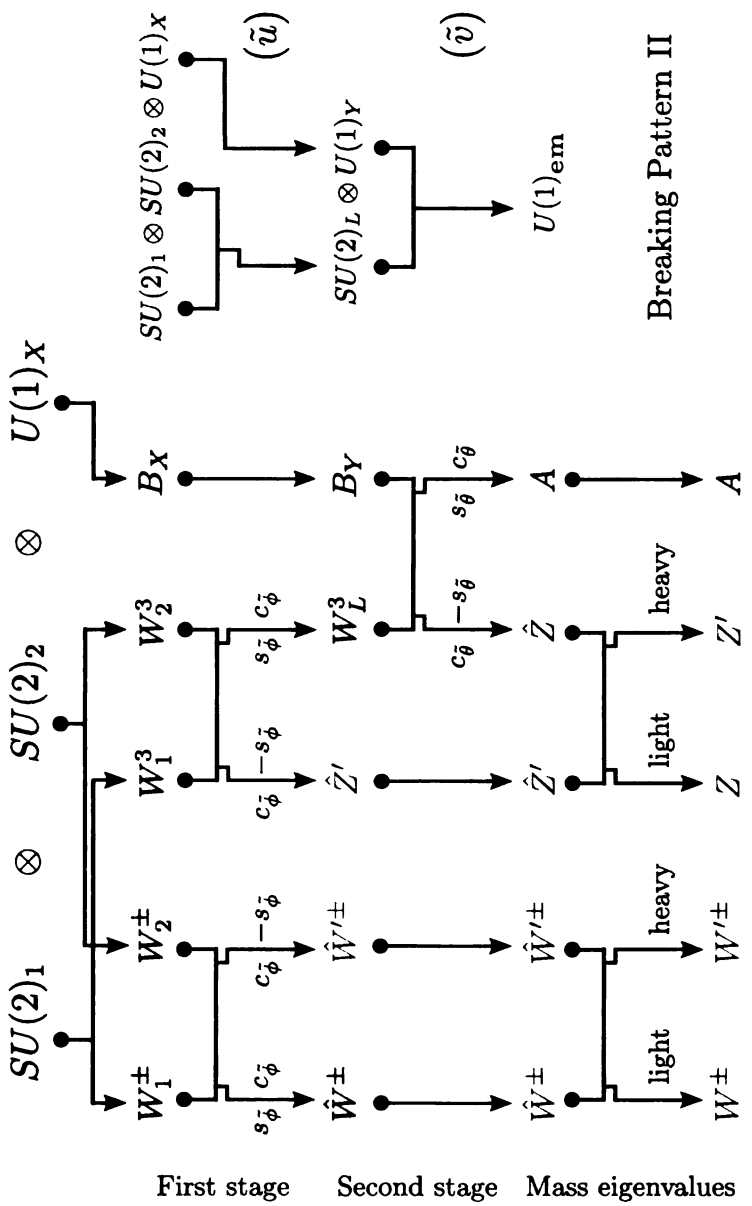

Figure 2.3: Mixing of the gauge bosons due to spontaneous symmetry breaking according to the second breaking pattern — the text colors indicate whether the respective bosons have already acquired masses (red symbols) or whether they are still massless (green symbols). For all pairs of bosons that mix at a certain stage of symmetry breaking the respective mixing coefficients are given on either side of the corresponding arrows. Trigonometric functions written on the left-hand / right-hand side of an arrow belong to the left / right boson at the preceding stage of symmetry breaking. See Tab. 2.2 for the definition of the VEVs $\tilde{u}$ and $\tilde{v}$ and the angle $\tilde{\beta}$.

First Breaking Pattern At the first breaking stage the charged $SU(2)_2$ bosons $W_2^{\pm}$ acquire masses whereas their $SU(2)_1$ equivalents $W_1^{\pm}$ remain massless. These two sets of charged gauge bosons do not mix and so the transition from $W_1^{\pm}$ and $W_2^{\pm}$ to $\hat{W}^{\pm}$ and $\hat{W}'^{\pm}$ is nothing else than a renaming. In the neutral gauge boson sector $\hat{Z}'$ emerges as a certain linear combination of W_2^3 and B_X. The orthogonal linear combination to $\hat{Z}'$ represents the neutral vector boson B_Y of the hypercharge group $U(1)_Y$. We diagonalize the neutral mass matrix by rotating the (W_2^3, B_X) boson basis about the angle $\tilde{\phi}$.

$$\begin{pmatrix} \hat{W}^{\pm} \\ \hat{W}'^{\pm} \end{pmatrix} \equiv \begin{pmatrix} 1 & 0 \\ 0 & 1 \end{pmatrix} \begin{pmatrix} W_1^{\pm} \\ W_2^{\pm} \end{pmatrix} \quad ; \quad \begin{pmatrix} \hat{Z}' \\ B_Y \end{pmatrix} \equiv \begin{pmatrix} c_{\tilde{\phi}} & -s_{\tilde{\phi}} \\ s_{\tilde{\phi}} & c_{\tilde{\phi}} \end{pmatrix} \begin{pmatrix} W_2^3 \\ B_X \end{pmatrix}$$

The coefficients of the boson products $\hat{Z}'_{\mu}\hat{Z}'^{,\mu}$ and $\hat{W}'^{+}_{\mu}\hat{W}'^{-,\mu}$ in the Lagrangian $\mathscr{L}_{\langle\Phi\rangle}$ provide us with the masses $\widetilde{M}^2_{\hat{Z}'}$ and $\widetilde{M}^2_{\hat{W}'}$. As can be seen from Tab. 2.5 these masses depend on the choice for the representation of Φ. In fact, it is this difference in the numerical prefactors of the masses $\widetilde{M}^2_{\hat{Z}'}$ and $\widetilde{M}^2_{\hat{W}'}$ that accounts for the different phenomenology of the (BP-I,D) and the (BP-I,T) models.

Since the Lagrangian $\mathscr{L}_{\Phi}$ does not involve the bosons of the $SU(2)_1$ the neutral W_1^3 stays unaffected during the first symmetry breaking. Once the $SU(2)_2 \otimes U(1)_X$ symmetry is broken to the $U(1)_Y$ we identify the W_1^3 as the neutral boson of the weak isospin group, W_L^3. The bosons that remain massless after the first breaking stage therefore directly correspond to the fundamental gauge bosons of the SM.

At the second stage of symmetry breaking we encounter the usual SM breaking mechanism: The W_L^3 and the B_Y combine resulting in the massive $\hat{Z}$ boson and the massless photon, A. We construct $\hat{Z}$ and A by rotating the (W_L^3, B_Y) basis about the angle $\tilde{\theta}$:

$$\begin{pmatrix} \hat{Z} \\ A \end{pmatrix} \equiv \begin{pmatrix} c_{\tilde{\theta}} & -s_{\tilde{\theta}} \\ s_{\tilde{\theta}} & c_{\tilde{\theta}} \end{pmatrix} \begin{pmatrix} W_L^3 \\ B_Y \end{pmatrix}$$

The charged bosons $\hat{W}^{\pm}$ belonging to the $SU(2)_L$ acquire masses as well. We obtain $\widetilde{M}^2_{\hat{Z}}$ and $\widetilde{M}^2_{\hat{W}}$ as prefactors of $\hat{Z}_\mu \hat{Z}^\mu$ and $\hat{W}^+_\mu \hat{W}^{-,\mu}$ in the Lagrangian $\mathscr{L}_{\langle H \rangle}$. Moreover, the presence of the new physics bosons $\hat{Z}'$ and $\hat{W}'^{\pm}$ results in mass mixing terms $\delta\widetilde{M}^2_{\hat{Z}\hat{Z}'}$ and $\delta\widetilde{M}^2_{\hat{W}\hat{W}'}$. Finally, the second symmetry breaking leads to shifts $\Delta\widetilde{M}^2_{\hat{Z}'}$ and $\Delta\widetilde{M}^2_{\hat{W}'}$ in the masses $\widetilde{M}^2_{\hat{Z}'}$ and $\widetilde{M}^2_{\hat{W}'}$ that are proportional to the VEV $\tilde{v}$ of the low-energy Higgs field H. The results for all these mass parameters are presented in Tab. 2.5. We notice that the angle $\tilde{\beta}$ that we introduced in Subsec. 2.2.1 as the mixing between the two VEVs $\tilde{\kappa}$ and $\tilde{\kappa}'$ appears in Tab. 2.5 exclusively in the $\hat{W}$–$\hat{W}'$ mass mixing parameter $\delta\widetilde{M}^2_{\hat{W}\hat{W}'}$. From now on we will, hence, regard $\tilde{\beta}$ not only as the $\tilde{\kappa}$–$\tilde{\kappa}'$ but also, if not mainly, as the $\hat{W}$–$\hat{W}'$ mixing angle.

Second Breaking Pattern Breaking pattern two involves, of course, the same gauge bosons as the first breaking pattern but constructs the bosons after the first breaking stage in a different way. As opposed to breaking pattern one $W_1^{\pm}$ and $W_2^{\pm}$ do not represent mass eigenstates once Φ has acquired its VEV. $\hat{W}^{\pm}$ and $\hat{W}'^{\pm}$ are now introduced as linear combinations of $W_1^{\pm}$ and $W_2^{\pm}$ after the charged mass matrices has been diagonalized by a rotation about the angle $\tilde{\phi}$. The massive $\hat{Z}'$ does not receive contributions from B_X in the second breaking pattern but is constructed from W_1^3 and W_2^3. The neutral boson of the weak isospin, W_L^3, follows as the linear combination of W_1^3 and W_2^3 that is orthogonal to $\hat{Z}'$:

$$\begin{pmatrix} \hat{W}'^{\pm} \\ \hat{W}^{\pm} \end{pmatrix} \equiv \begin{pmatrix} c_{\tilde{\phi}} & -s_{\tilde{\phi}} \\ s_{\tilde{\phi}} & c_{\tilde{\phi}} \end{pmatrix} \begin{pmatrix} W_1^{\pm} \\ W_2^{\pm} \end{pmatrix} \quad ; \quad \begin{pmatrix} \hat{Z}' \\ W_L^3 \end{pmatrix} \equiv \begin{pmatrix} c_{\tilde{\phi}} & -s_{\tilde{\phi}} \\ s_{\tilde{\phi}} & c_{\tilde{\phi}} \end{pmatrix} \begin{pmatrix} W_1^3 \\ W_2^3 \end{pmatrix}$$

B_Y is identical to B_X; the second stage breaking proceeds as in breaking pattern one. We determine the mass parameters in Eq. (2.9) in the same way as for the first pattern and collect them in Tab. 2.5. As an interesting consequence of the particular structure of the second breaking pattern we notice that the $\hat{Z}'$ and the $\hat{W}'^{\pm}$ are degenerate in terms of their masses and that they receive the same mass corrections in the course of the second symmetry breaking; see also Eq. (2.9):

$$\widetilde{M}^2_{\hat{Z}'} = \frac{1}{4}\left(\tilde{g}_1^2 + \tilde{g}_2^2\right)\tilde{u}^2 = \widetilde{M}^2_{\hat{W}'} \qquad ; \qquad \Delta\widetilde{M}^2_{\hat{Z}'} = \frac{s_{\tilde{\phi}}}{4}\tilde{g}_2^2 v^2 = \Delta\widetilde{M}^2_{\hat{W}'}$$

This behavior is expected since the second breaking pattern breaks the $SU(2)_1 \otimes SU(2)_2$ to the diagonal subgroup not distinguishing between charged and uncharged gauge bosons. The mass generation for the $\hat{Z}'$ and the $\hat{W}'^{\pm}$ proceeds in exactly the same way.

2.2.4 Physical Boson States and Masses

We now know all parameters in the mass Lagrangian of the gauge bosons after the second breaking stage, $\mathscr{L}^{(2)}_{\text{mass}} \equiv \mathscr{L}_{\langle\Phi\rangle} + \mathscr{L}_{\langle H\rangle}$, for all three classes of $G(221)$ models. The considerations that will lead us from $\mathscr{L}^{(2)}_{\text{mass}}$ to the masses of the physical bosons apply generally and so we now return to our BP-independent analysis: $\mathscr{L}^{(2)}_{\text{mass}}$ can be written in its most compact form when we introduce $\widetilde{\mathscr{M}}_{\hat{Z}\hat{Z}'}$ and $\widetilde{\mathscr{M}}_{\hat{W}\hat{W}'}$ as notations for the mass matrices of the neutral and charged gauge bosons:

$$\mathscr{L}^{(2)}_{\text{mass}} = \frac{1}{2}\begin{pmatrix}\hat{Z} & \hat{Z}'\end{pmatrix}\widetilde{\mathscr{M}}_{\hat{Z}\hat{Z}'}\begin{pmatrix}\hat{Z}\\ \hat{Z}'\end{pmatrix} + \begin{pmatrix}\hat{W}^{\pm} & \hat{W}'^{\pm}\end{pmatrix}\widetilde{\mathscr{M}}_{\hat{W}\hat{W}'}\begin{pmatrix}\hat{W}^{\pm}\\ \hat{W}'^{\pm}\end{pmatrix}$$

with $\widetilde{\mathscr{M}}_{\hat{Z}\hat{Z}'}$ and $\widetilde{\mathscr{M}}_{\hat{W}\hat{W}'}$ being of the form:

(BP-I,D)

$\widetilde{M}^2_{\hat{Z}}$	$\widetilde{M}^2_{\hat{Z}'}$	$\widetilde{M}^2_{\hat{W}}$	$\widetilde{M}^2_{\hat{W}'}$
$\frac{1}{4}\left(\tilde{g}_L^2+\tilde{g}_Y^2\right)v^2$	$\frac{1}{4}\left(\tilde{g}_2^2+\tilde{g}_X^2\right)\tilde{u}_{\mathrm{D}}^2$	$\frac{1}{4}\tilde{g}_L^2 v^2$	$\frac{1}{4}\tilde{g}_2^2\tilde{u}_{\mathrm{D}}^2$
$\delta\widetilde{M}^2_{\hat{Z}\hat{Z}'}$	$\Delta\widetilde{M}^2_{\hat{Z}'}$	$\delta\widetilde{M}^2_{\hat{W}\hat{W}'}$	$\Delta\widetilde{M}^2_{\hat{W}'}$
$-\frac{c^2(\tilde{\phi})}{4\tilde{e}}\tilde{g}_L\tilde{g}_2\tilde{g}_X v^2$	$\frac{c^2(\tilde{\phi})}{4}\tilde{g}_2^2 v^2$	$-\frac{s(2\tilde{\beta})}{4}\tilde{g}_L\tilde{g}_2 v^2$	$\frac{1}{4}\tilde{g}_2^2 v^2$

(BP-I,T)

$\widetilde{M}^2_{\hat{Z}}$	$\widetilde{M}^2_{\hat{Z}'}$	$\widetilde{M}^2_{\hat{W}}$	$\widetilde{M}^2_{\hat{W}'}$
$\frac{1}{4}\left(\tilde{g}_L^2+\tilde{g}_Y^2\right)v^2$	$\left(\tilde{g}_2^2+\tilde{g}_X^2\right)\tilde{u}_{\mathrm{T}}^2$	$\frac{1}{4}\tilde{g}_L^2 v^2$	$\frac{1}{2}\tilde{g}_2^2\tilde{u}_{\mathrm{T}}^2$
$\delta\widetilde{M}^2_{\hat{Z}\hat{Z}'}$	$\Delta\widetilde{M}^2_{\hat{Z}'}$	$\delta\widetilde{M}^2_{\hat{W}\hat{W}'}$	$\Delta\widetilde{M}^2_{\hat{W}'}$
$-\frac{c^2(\tilde{\phi})}{4\tilde{e}}\tilde{g}_L\tilde{g}_2\tilde{g}_X v^2$	$\frac{c^2(\tilde{\phi})}{4}\tilde{g}_2^2 v^2$	$-\frac{s(2\tilde{\beta})}{4}\tilde{g}_L\tilde{g}_2 v^2$	$\frac{1}{4}\tilde{g}_2^2 v^2$

(BP-II,D)

$\widetilde{M}^2_{\hat{Z}}$	$\widetilde{M}^2_{\hat{Z}'}$	$\widetilde{M}^2_{\hat{W}}$	$\widetilde{M}^2_{\hat{W}'}$
$\frac{1}{4}\left(\tilde{g}_L^2+\tilde{g}_Y^2\right)v^2$	$\frac{1}{4}\left(\tilde{g}_1^2+\tilde{g}_2^2\right)u^2$	$\frac{1}{4}\tilde{g}_L^2 v^2$	$\frac{1}{4}\left(\tilde{g}_1^2+\tilde{g}_2^2\right)u^2$
$\delta\widetilde{M}^2_{\hat{Z}\hat{Z}'}$	$\Delta\widetilde{M}^2_{\hat{Z}'}$	$\delta\widetilde{M}^2_{\hat{W}\hat{W}'}$	$\Delta\widetilde{M}^2_{\hat{W}'}$
$-\frac{s^2(\tilde{\phi})}{4\tilde{e}}\tilde{g}_1\tilde{g}_2\tilde{g}_Y v^2$	$\frac{s^2(\tilde{\phi})}{4}\tilde{g}_2^2 v^2$	$-\frac{1}{4}\sqrt{\tilde{g}_2^2-\tilde{g}_L^2}\,\tilde{g}_L v^2$	$\frac{1}{4}\left(\tilde{g}_2^2-\tilde{g}_L^2\right)v^2$

Table 2.5: Entries of the fundamental boson mass matrices — the first symmetry breaking generates masses $\widetilde{M}^2_{\hat{Z}'}$ and $\widetilde{M}^2_{\hat{W}'}$ for the $\hat{Z}'$ and the $\hat{W}'^{\pm}$. In the course of the second symmetry breaking the $\hat{Z}$ and the $\hat{W}^{\pm}$ bosons acquire masses $\widetilde{M}^2_{\hat{Z}}$ and $\widetilde{M}^2_{\hat{W}}$. Additionally, the $\hat{Z}'$ and $\hat{W}'^{\pm}$ masses get respectively shifted by $\Delta\widetilde{M}^2_{\hat{Z}'}$ and $\Delta\widetilde{M}^2_{\hat{W}'}$ and mass mixing terms $\delta\widetilde{M}^2_{\hat{Z}\hat{Z}'}$ and $\delta\widetilde{M}^2_{\hat{W}\hat{W}'}$ occur; cf Eq. (2.9).

$$\widetilde{\mathscr{M}}_{\hat{Z}\hat{Z}'} = \begin{pmatrix} \widetilde{M}^2_{\hat{Z}} & \delta\widetilde{M}^2_{\hat{Z}\hat{Z}'} \\ \delta\widetilde{M}^2_{\hat{Z}\hat{Z}'} & \widetilde{M}^2_{\hat{Z}'} + \Delta\widetilde{M}^2_{\hat{Z}'} \end{pmatrix} \quad ; \quad \widetilde{\mathscr{M}}_{\hat{W}\hat{W}'} = \begin{pmatrix} \widetilde{M}^2_{\hat{W}} & \delta\widetilde{M}^2_{\hat{W}\hat{W}'} \\ \delta\widetilde{M}^2_{\hat{W}\hat{W}'} & \widetilde{M}^2_{\hat{W}'} + \Delta\widetilde{M}^2_{\hat{W}'} \end{pmatrix}$$

The masses of the physical gauge bosons are given as the eigenvalues of $\widetilde{\mathscr{M}}_{\hat{Z}\hat{Z}'}$ and $\widetilde{\mathscr{M}}_{\hat{W}\hat{W}'}$, the physical bosons themselves as the corresponding eigenvectors. Since we expect $\widetilde{M}^2_{\hat{Z}'}$ and $\widetilde{M}^2_{\hat{W}'}$ to be very large,

$$\widetilde{M}^2_{\hat{Z}'} \gg \widetilde{M}^2_{\hat{Z}}, \Delta\widetilde{M}^2_{\hat{Z}'}, \delta\widetilde{M}^2_{\hat{Z}\hat{Z}'} \quad ; \quad \widetilde{M}^2_{\hat{W}'} \gg \widetilde{M}^2_{\hat{W}}, \Delta\widetilde{M}^2_{\hat{W}'}, \delta\widetilde{M}^2_{\hat{W}\hat{W}'} ,$$

it is appropriate not to calculate the exact eigenvectors and eigenvalues of $\widetilde{\mathscr{M}}_{\hat{Z}\hat{Z}'}$ and $\widetilde{\mathscr{M}}_{\hat{W}\hat{W}'}$, but to restrict ourselves to a series expansion in powers of $\widetilde{M}^{-2}_{\hat{Z}'}$ and $\widetilde{M}^{-2}_{\hat{W}'}$ resp. We diagonalize the mass matrices by performing rotations about the angles $\tilde{\omega}_{\hat{Z}\hat{Z}'}$ and $\tilde{\omega}_{\hat{W}\hat{W}'}$:

$$\tilde{\omega}_{\hat{Z}\hat{Z}'} = \frac{\delta\widetilde{M}^2_{\hat{Z}\hat{Z}'}}{\widetilde{M}^2_{\hat{Z}'} - \widetilde{M}^2_{\hat{Z}}} \quad ; \quad \tilde{\omega}_{\hat{W}\hat{W}'} = \frac{\delta\widetilde{M}^2_{\hat{W}\hat{W}'}}{\widetilde{M}^2_{\hat{W}'} - \widetilde{M}^2_{\hat{W}}}$$

Up to linear order in $\widetilde{M}^{-2}_{\hat{Z}'}$ or $\widetilde{M}^{-2}_{\hat{W}'}$ the physical bosons Z, Z', $W^{\pm}$ and $W'^{\pm}$ are then given as:

$$Z_\mu \equiv \hat{Z}_\mu - \tilde{\omega}_{\hat{Z}\hat{Z}'}\hat{Z}'_\mu \quad ; \quad Z'_\mu \equiv \hat{Z}'_\mu + \tilde{\omega}_{\hat{Z}\hat{Z}'}\hat{Z}_\mu \tag{2.10}$$

$$W^{\pm}_\mu \equiv \hat{W}^{\pm}_\mu - \tilde{\omega}_{\hat{W}\hat{W}'}\hat{W}'^{\pm}_\mu \quad ; \quad W'^{\pm}_\mu \equiv \hat{W}'^{\pm}_\mu + \tilde{\omega}_{\hat{W}\hat{W}'}\hat{W}^{\pm}_\mu \tag{2.11}$$

The eigenvalues corresponding to these eigenvectors, that is, the physical masses M^2_Z, $M^2_{Z'}$, M^2_W and $M^2_{W'}$, take the following values:

$$M_Z^2 = \widetilde{M}_Z^2 - \frac{\delta\widetilde{M}^4_{Z\dot{Z}'}}{\widetilde{M}^2_{\dot{Z}'}} \quad ; \quad M_{Z'}^2 = \widetilde{M}^2_{\dot{Z}'} + \frac{\delta\widetilde{M}^4_{Z\dot{Z}'}}{\widetilde{M}^2_{\dot{Z}'}} \tag{2.12}$$

$$M_W^2 = \widetilde{M}_W^2 - \frac{\delta\widetilde{M}^4_{W\dot{W}'}}{\widetilde{M}^2_{\dot{W}'}} \quad ; \quad M_{W'}^2 = \widetilde{M}^2_{\dot{W}'} + \frac{\delta\widetilde{M}^4_{W\dot{W}'}}{\widetilde{M}^2_{\dot{W}'}} \tag{2.13}$$

These general relations represent important results in their own right. However, we are also interested in more explicit expressions that tell us how the masses of the six massive gauge bosons depend on the Higgs VEVs, the mixing angles etc. for each of the considered classes of $G(221)$ models. We obtain such expressions in three steps: First, we insert our results for the mass parameters as given in Tab. 2.5 into the above relations. The expressions for M_Z^2, $M_{Z'}^2$, M_W^2 and $M_{W'}^2$ we get this way still involve the gauge couplings of the various symmetry groups. In order to prepare the global fit analysis with GAPP we subsequently rewrite the coupling constants according to Tab. 2.4 in terms of the fine structure constant $\tilde{\alpha}$ and the gauge boson mixing angles. In a third step we introduce the parameter $\tilde{x}$ as the ratio of the squared VEVs $\tilde{u}^2$ and $\tilde{v}^2$,

$$\text{(BP-I,D): } \tilde{x} \equiv \frac{\tilde{u}_{\text{D}}^2}{\tilde{v}^2} \quad ; \quad \text{(BP-I,T): } \tilde{x} \equiv \frac{\tilde{u}_{\text{T}}^2}{\tilde{v}^2} \quad ; \quad \text{(BP-II,D): } \tilde{x} \equiv \frac{\tilde{u}^2}{\tilde{v}^2} \,, \tag{2.14}$$

and expand the physical boson masses in $\frac{1}{\tilde{x}}$. As for M_Z^2 and M_W^2 we consider terms up to first order in $\frac{1}{\tilde{x}}$. In case of the heavy gauge bosons we will only keep terms proportional to $\tilde{x}$. The parameter $\tilde{x}$ allows us to quantify the relation between the scale of the new physics and the electroweak scale. It will play a crucial role in our later analysis: As we will see the corrections to the SM observables in our $G(221)$ models will scale with $\frac{1}{\tilde{x}}$ and depending on which $\tilde{x}$ range in parameter space

	$M_Z^2/(c_{\tilde{\theta}}^{-2}M_0^2)$	$M_{Z'}^2/(c_{\tilde{\phi}}^{-2}M_0^2)$	M_W^2/M_0^2	$M_{W'}^2/M_0^2$
(BP-I,D)	$1-\frac{1}{\tilde{x}}c_{\tilde{\phi}}^4$	$t_{\tilde{\theta}}^2 s_{\tilde{\phi}}^{-2}\tilde{x}$	$1-\frac{1}{\tilde{x}}s_{2\tilde{\beta}}^2$	$t_{\tilde{\theta}}^2 s_{\tilde{\phi}}^{-2}\tilde{x}$
(BP-I,T)	$1-\frac{1}{4\tilde{x}}c_{\tilde{\phi}}^4$	$4t_{\tilde{\theta}}^2 s_{\tilde{\phi}}^{-2}\tilde{x}$	$1-\frac{1}{2\tilde{x}}s_{2\tilde{\beta}}^2$	$2t_{\tilde{\theta}}^2 s_{\tilde{\phi}}^{-2}\tilde{x}$
(BP-II,D)	$1-\frac{1}{\tilde{x}}s_{\tilde{\phi}}^4$	$s_{\tilde{\phi}}^{-2}\tilde{x}$	$1-\frac{1}{\tilde{x}}s_{\tilde{\phi}}^4$	$s_{\tilde{\phi}}^{-2}c_{\tilde{\phi}}^{-2}\tilde{x}$

Table 2.6: Masses of the physical gauge bosons in terms of the model parameters $\tilde{x}$, $\tilde{\phi}$, $\tilde{\theta}$ etc. $M_0 = (\tilde{e}^2\tilde{v}^2)/(4s_{\tilde{\theta}}^2)$ has the same form as the SM mass of the $W^\pm$ boson, but is defined in terms of $G(221)$ model parameters.

is allowed by the experimental data it becomes more likely or less likely that a certain $G(221)$ model can be probed in collider experiments. For that reason the expansion in $\frac{1}{\tilde{x}}$ extracts the leading new physics contributions to the boson masses and sorts out higher order terms that we are not interested in. In that respect expanding in $\frac{1}{\tilde{x}}$ has the same effect as the expansions in $\widetilde{M}_{Z'}^{-2}$ or $\widetilde{M}_{W'}^{-2}$ that we performed above.

The results for M_Z^2, $M_{Z'}^2$, M_W^2 and $M_{W'}^2$ that we obtain after having gone through all three steps are presented in Tab. 2.6. In this table we introduce the mass M_0 that allows us to write down the boson masses in a nice and compact form. M_0 is defined,

$$M_0^2 \equiv \frac{\tilde{e}^2\tilde{v}^2}{4s_{\tilde{\theta}}^2} = \frac{\pi\tilde{\alpha}\tilde{v}^2}{s_{\tilde{\theta}}^2}\,, \tag{2.15}$$

such that it resembles the SM expression for the mass of the $W^\pm$ boson. However, the definition of M_0 employs model and not standard parameters and so M_0 only corresponds to the SM $W^\pm$ mass in the limit $\tilde{x} \to \infty$.

2.3 Gauge Interactions of the Fermions

The fermions that are incorporated into our $G(221)$ models couple to the vector bosons through gauge interactions. In the third chapter, when we will have come to calculate the corrections to the electroweak precision data, these interactions will represent the heart of our analysis — the theoretical description of the various precision observables to which we will fit the $G(221)$ models either requires the fundamental fermion currents or the effective currents that arise in the low-energy theory. In this section we will thus first discuss the direct interactions between fermions and gauge bosons and then present how one arrives at the effective theory by successively integrating out the heavy gauge bosons. The latter part will first lead us to an effective SM-like Lagrangian at the electroweak scale. After removing the electroweak gauge bosons from the theory we will end up with the effective four-fermion interaction below the electroweak scale. The three Lagrangians that we will obtain in this way will represent very powerful and flexible tools that will allow us to perform many calculations for all $G(221)$ models at once.

2.3.1 Fundamental Fermion-Boson Interactions

Our $G(221)$ models accommodate the fermions f in iso-multiplets ψ each of which is represented by a corresponding term $\mathscr{L}_\psi$ in the total Lagrangian $\mathscr{L}$:

$$\mathscr{L}_\psi = i\bar{\psi}\gamma^\mu D_\mu \psi$$

Two things are necessary to ensure that $\mathscr{L}_\psi$ is invariant under local gauge transformations: First, we have to employ the covariant derivative $D_\mu\psi$ instead of the partial derivative $\partial_\mu\psi$. Second, the term $-\bar{\psi}\mathcal{M}_\psi\psi$ reflecting the fermions' masses is not included into $\mathscr{L}_\psi$ but generated through spontaneous symmetry breaking in the Yukawa sector.

BP	$SU(2)_1$ Doublet	$SU(2)_2$ Doublet	Charged under the $U(1)_X$
I	$\tilde{g}_L\bar{\psi}_{\rm L}\gamma^\mu T_1^a W_{1,\mu}^a\psi_{\rm L}$	$\tilde{g}_2\bar{\psi}_{\rm R}\gamma^\mu T_2^b W_{2,\mu}^b\psi_{\rm R}$	$\tilde{g}_X\bar{\psi}\gamma^\mu\left(X_{\rm L}P_{\rm L}+X_{\rm R}P_{\rm R}\right)B_{X,\mu}\psi$
II	$\tilde{g}_1\bar{\psi}_{\rm L}\gamma^\mu T_1^a W_{1,\mu}^a\psi_{\rm L}$	$\tilde{g}_2\bar{\psi}_{\rm L}\gamma^\mu T_2^b W_{2,\mu}^b\psi_{\rm L}$	$\tilde{g}_Y\bar{\psi}\gamma^\mu\left(Y_{\rm L}P_{\rm L}+Y_{\rm R}P_{\rm R}\right)B_{Y,\mu}\psi$

Table 2.7: Building blocks of the fermion Lagrangian $\mathscr{L}_\psi$ that account for the gauge interactions of the fermion multiplet ψ with the vector bosons — $\mathscr{L}_\psi$ is composed as a sum of these blocks according to the chosen breaking pattern and the charges of ψ under the $G(221)$ gauge group.

Just as we expanded the covariant derivatives of the Higgs fields, $D_\mu\Phi$ and $D_\mu H$, in terms of the gauge couplings and bosons in the previous section we will now expand $D_\mu\psi$. Generally, $D_\mu\psi$ can be split into a kinetic part represented by $\partial_\mu\psi$ and terms leading to the gauge interactions. To give an example: In the LR-D and LR-T model the covariant derivative of a lepton multiplet ψ_ℓ and the corresponding Lagrangian $\mathscr{L}_{\psi_\ell}$ read as follows:

$$\begin{aligned}
D_\mu\psi_\ell &= \partial_\mu\psi_\ell - i\tilde{g}_L T_1^a W_{1,\mu}^a P_{\rm L}\psi_{\ell,{\rm L}} - i\tilde{g}_2 T_2^b W_{2,\mu}^b P_{\rm R}\psi_{\ell,{\rm R}} \\
&\quad - i\tilde{g}_X\left(X_{\rm L}P_{\rm L}+X_{\rm R}P_{\rm R}\right)B_{X,\mu}\psi_\ell \\
\mathscr{L}_{\psi_\ell} &= i\bar{\psi}_\ell\gamma^\mu\partial_\mu\psi_\ell + \tilde{g}_L\bar{\psi}_{\ell,{\rm L}}\gamma^\mu T_1^a W_{1,\mu}^a P_{\rm L}\psi_{\ell,{\rm L}} + \tilde{g}_2\bar{\psi}_{\ell,{\rm R}}\gamma^\mu T_2^b W_{2,\mu}^b P_{\rm R}\psi_{\ell,{\rm R}} \\
&\quad + \tilde{g}_X\bar{\psi}_\ell\gamma^\mu\left(X_{\rm L}P_{\rm L}+X_{\rm R}P_{\rm R}\right)B_{X,\mu}\psi_\ell
\end{aligned}$$

The gauge interactions differ from fermion to fermion, though, in dependence of the respective charges under the $G(221)$ symmetry groups. In particular the fermion interactions with the $SU(2)_2$ gauge bosons $W_{2,\mu}^a$ have different chiral structure for both breaking patterns. In Tab. 2.7 we list the pieces that can enter the gauge interaction part of the Lagrangian $\mathscr{L}_\psi$.

The expressions given in Tab. 2.7 stand for the fermion interactions with the weak

eigenstates $W^1_{1,2}$, $W^2_{1,2}$, $W^3_{1,2}$ and B_X. We are, however, interested in the fermion currents that couple to the physical gauge bosons. It will be these couplings that will go into the calculation of the corrections to the electroweak observables. In a first step towards this goal we calculate the fermion couplings to the gauge bosons that we obtain after the second stage of symmetry breaking, $\hat{Z}$, $\hat{Z}'$, $\hat{W}^{\pm}$, $\hat{W}'^{\pm}$ and A. We take the contribution $\mathscr{L}_{\text{int.}}$ to the total Lagrangian $\mathscr{L}$ that accounts for all fermion gauge interactions,

$$\mathscr{L}_{\text{int.}} \equiv \sum_{\psi} \left(\mathscr{L}_{\psi} - i\bar{\psi}\gamma^{\mu}\partial_{\mu}\psi \right) ,$$

transform from the fundamental gauge basis to the basis of the boson charge eigenstates and perform subsequently the rotations that we discussed in Subsec. 2.2.3. The result of this calculation is $\mathscr{L}^{(2)}_{\text{int.}}$, the fermion-boson interaction Lagrangian after the second breaking stage. We may write $\mathscr{L}^{(2)}_{\text{int.}}$ as:

$$\begin{aligned} \mathscr{L}^{(2)}_{\text{int.}} &= \hat{Z}_{\mu} J^{0,\mu} + \hat{W}^{+}_{\mu} J^{+,\mu} + \hat{W}^{-}_{\mu} J^{-,\mu} \\ &+ \hat{Z}'_{\mu} K^{0,\mu} + \hat{W}'^{+}_{\mu} K^{+,\mu} + \hat{W}'^{-}_{\mu} K^{-,\mu} \\ &+ A_{\mu} L^{0,\mu} \end{aligned} \tag{2.16}$$

with J^0, $J^{\pm}$, K^0, $K^{\pm}$ and L^0 denoting the fermion currents coupling to the respective gauge bosons. J^0, $J^{\pm}$ and L^0 correspond to the usual SM currents, K^0 and $K^{\pm}$ represent new fermion currents that emerge due to the new physics in our $G(221)$ models. For the contribution of a particular fermion f to J^0 and L^0 we find:

	$\tilde{g}(\bar{u}, u, \hat{Z}')$	$\tilde{g}(\bar{\nu}, \nu, \hat{Z}')$
LR	$-\frac{1}{6}s_{\tilde{\phi}}\tilde{g}_X P_{\rm L} + (\frac{1}{2}c_{\tilde{\phi}}\tilde{g}_2 - \frac{1}{6}s_{\tilde{\phi}}\tilde{g}_X)P_{\rm R}$	$\frac{1}{2}s_{\tilde{\phi}}\tilde{g}_X P_{\rm L} + (\frac{1}{2}c_{\tilde{\phi}}\tilde{g}_2 + \frac{1}{6}s_{\tilde{\phi}}\tilde{g}_X)P_{\rm R}$
LP	$-\frac{1}{6}s_{\tilde{\phi}}\tilde{g}_X P_{\rm L} + (\frac{1}{2}c_{\tilde{\phi}}\tilde{g}_2 - \frac{1}{6}s_{\tilde{\phi}}\tilde{g}_X)P_{\rm R}$	$\frac{1}{2}s_{\tilde{\phi}}\tilde{g}_X P_{\rm L}$
HP	$-s_{\tilde{\phi}}\tilde{g}_X(\frac{1}{6}P_{\rm L} + \frac{2}{3}P_{\rm R})$	$\frac{1}{2}s_{\tilde{\phi}}\tilde{g}_X P_{\rm L} + (\frac{1}{2}c_{\tilde{\phi}}\tilde{g}_2 + \frac{1}{6}s_{\tilde{\phi}}\tilde{g}_X)P_{\rm R}$
FP	$-s_{\tilde{\phi}}\tilde{g}_X(\frac{1}{6}P_{\rm L} + \frac{2}{3}P_{\rm R})$	$\frac{1}{2}s_{\tilde{\phi}}\tilde{g}_X P_{\rm L}$
UU	$\frac{1}{2}c_{\tilde{\phi}}\tilde{g}_1 P_{\rm L}$	$-\frac{1}{2}s_{\tilde{\phi}}\tilde{g}_2 P_{\rm L}$
NU ($1^{\rm st}$, $2^{\rm nd}$)	$\frac{1}{2}c_{\tilde{\phi}}\tilde{g}_1 P_{\rm L}$	$\frac{1}{2}c_{\tilde{\phi}}\tilde{g}_1 P_{\rm L}$
NU ($3^{\rm rd}$)	$-\frac{1}{2}s_{\tilde{\phi}}\tilde{g}_2 P_{\rm L}$	$-\frac{1}{2}s_{\tilde{\phi}}\tilde{g}_2 P_{\rm L}$

	$\tilde{g}(\bar{d}, d, \hat{Z}')$	$\tilde{g}(\bar{e}, e, \hat{Z}')$
LR	$-\frac{1}{6}s_{\tilde{\phi}}\tilde{g}_X P_{\rm L} - (\frac{1}{2}c_{\tilde{\phi}}\tilde{g}_2 + \frac{1}{6}s_{\tilde{\phi}}\tilde{g}_X)P_{\rm R}$	$\frac{1}{2}s_{\tilde{\phi}}\tilde{g}_X P_{\rm L} - (\frac{1}{2}c_{\tilde{\phi}}\tilde{g}_2 - \frac{1}{6}s_{\tilde{\phi}}\tilde{g}_X)P_{\rm R}$
LP	$-\frac{1}{6}s_{\tilde{\phi}}\tilde{g}_X P_{\rm L} - (\frac{1}{2}c_{\tilde{\phi}}\tilde{g}_2 + \frac{1}{6}s_{\tilde{\phi}}\tilde{g}_X)P_{\rm R}$	$s_{\tilde{\phi}}\tilde{g}_X(\frac{1}{2}P_{\rm L} + P_{\rm R})$
HP	$-s_{\tilde{\phi}}\tilde{g}_X(\frac{1}{6}P_{\rm L} - \frac{1}{3}P_{\rm R})$	$\frac{1}{2}s_{\tilde{\phi}}\tilde{g}_X P_{\rm L} - (\frac{1}{2}c_{\tilde{\phi}}\tilde{g}_2 - \frac{1}{6}s_{\tilde{\phi}}\tilde{g}_X)P_{\rm R}$
FP	$-s_{\tilde{\phi}}\tilde{g}_X(\frac{1}{6}P_{\rm L} - \frac{1}{3}P_{\rm R})$	$s_{\tilde{\phi}}\tilde{g}_X(\frac{1}{2}P_{\rm L} + P_{\rm R})$
UU	$-\frac{1}{2}c_{\tilde{\phi}}\tilde{g}_1 P_{\rm L}$	$\frac{1}{2}s_{\tilde{\phi}}\tilde{g}_2 P_{\rm L}$
NU ($1^{\rm st}$, $2^{\rm nd}$)	$-\frac{1}{2}c_{\tilde{\phi}}\tilde{g}_1 P_{\rm L}$	$-\frac{1}{2}c_{\tilde{\phi}}\tilde{g}_1 P_{\rm L}$
NU ($3^{\rm rd}$)	$\frac{1}{2}s_{\tilde{\phi}}\tilde{g}_2 P_{\rm L}$	$\frac{1}{2}s_{\tilde{\phi}}\tilde{g}_2 P_{\rm L}$

Table 2.8: Fermion couplings to the heavy Z' boson in the current $K^{0,\mu}$ — in the first breaking pattern $K^{0,\mu}$ contains both left- and right-handed parts; in the second breaking pattern it is purely left-handed. Cf. Eqs. (2.16) and (2.21).

	$\tilde{g}(\bar{d}, u, \hat{W}'^{+}), \tilde{g}(\bar{u}, d, \hat{W}'^{-})$	$\tilde{g}(\bar{e}, \nu, \hat{W}'^{+}), \tilde{g}(\bar{\nu}, e, \hat{W}'^{-})$
LR	$\frac{1}{\sqrt{2}}\tilde{g}_2 P_{\mathrm{R}}$	$\frac{1}{\sqrt{2}}\tilde{g}_2 P_{\mathrm{R}}$
LP	$\frac{1}{\sqrt{2}}\tilde{g}_2 P_{\mathrm{R}}$	0
HP	0	$\frac{1}{\sqrt{2}}\tilde{g}_2 P_{\mathrm{R}}$
FP	0	0
UU	$\frac{1}{\sqrt{2}} c_{\tilde{\phi}} \tilde{g}_1 P_{\mathrm{L}}$	$-\frac{1}{\sqrt{2}} s_{\tilde{\phi}} \tilde{g}_2 P_{\mathrm{L}}$
NU (1^{st}, 2^{nd})	$\frac{1}{\sqrt{2}} c_{\tilde{\phi}} \tilde{g}_1 P_{\mathrm{L}}$	$\frac{1}{\sqrt{2}} c_{\tilde{\phi}} \tilde{g}_1 P_{\mathrm{L}}$
NU (3^{rd})	$-\frac{1}{\sqrt{2}} s_{\tilde{\phi}} \tilde{g}_2 P_{\mathrm{L}}$	$-\frac{1}{\sqrt{2}} s_{\tilde{\phi}} \tilde{g}_2 P_{\mathrm{L}}$

Table 2.9: Fermion couplings to the heavy $W'^{\pm}$ boson in the current $K^{\pm,\mu}$ — in the first breaking pattern $K^{\pm,\mu}$ is purely right-handed. It therefore introduces charged fermion interactions with a V+A structure standing in contrast to the charged V-A interactions of the SM. As the contributions from $K^{\pm,\mu}$ are always suppressed by $\frac{1}{\tilde{x}}$ they can, however, be neglected in many cases. In the second breaking pattern $K^{\pm,\mu}$ is purely left-handed. Cf. Eqs. (2.16), (2.22) and (2.23).

$$J_f^{0,\mu} = \frac{\tilde{e}}{s_{\tilde{\theta}} c_{\tilde{\theta}}} \cdot \bar{f}\gamma^\mu \left[\left(T_L^3(f) - s_{\tilde{\theta}}^2 Q_e(f) \right) P_{\mathrm{L}} + \left(-s_{\tilde{\theta}}^2 Q_e(f) \right) P_{\mathrm{R}} \right] f \tag{2.17}$$

$$L_f^{0,\mu} = \tilde{e} Q_e(f) \cdot \bar{f}\gamma^\mu f \tag{2.18}$$

The currents $J^\pm$ belonging to a specific generation of quarks (u, d) or leptons (ν, e) take the following form:

$$J_q^{+,\mu} = \frac{\tilde{g}_L}{\sqrt{2}} \cdot \bar{d}_{\mathrm{L}} \gamma^\mu P_{\mathrm{L}} u_{\mathrm{L}} \quad ; \quad J_l^{+,\mu} = \frac{\tilde{g}_L}{\sqrt{2}} \cdot \bar{e}_{\mathrm{L}} \gamma^\mu P_{\mathrm{L}} \nu_{\mathrm{L}} \tag{2.19}$$

$$J_q^{-,\mu} = \frac{\tilde{g}_L}{\sqrt{2}} \cdot \bar{u}_{\mathrm{L}} \gamma^\mu P_{\mathrm{L}} d_{\mathrm{L}} \quad ; \quad J_l^{-,\mu} = \frac{\tilde{g}_L}{\sqrt{2}} \cdot \bar{\nu}_{\mathrm{L}} \gamma^\mu P_{\mathrm{L}} e_{\mathrm{L}} \tag{2.20}$$

The currents coupling to the light gauge bosons and the photon thus have exactly the same structure as the SM fermion currents. Both sets of currents only differ in the definition of the parameters they employ. In order to be able to present the new physics currents in a compact form we introduce the functions $\tilde{g}(\bar{f}, f, \hat{Z}')$ and $\tilde{g}(\bar{f}, f, \hat{W}'^{\pm})$ that allow us to write K^0 and $K^\pm$ as:

$$K_f^{0,\mu} \equiv \bar{f}\gamma^\mu \tilde{g}(\bar{f}, f, \hat{Z}') f \; ; \tag{2.21}$$

$$K_q^{+,\mu} \equiv \bar{d}\gamma^\mu \tilde{g}(\bar{d}, u, \hat{W}'^{+}) u \; ; \; K_l^{+,\mu} \equiv \bar{e}\gamma^\mu \tilde{g}(\bar{e}, \nu, \hat{W}'^{+}) \nu \tag{2.22}$$

$$K_q^{-,\mu} \equiv \bar{u}\gamma^\mu \tilde{g}(\bar{u}, d, \hat{W}'^{-}) d \; ; \; K_l^{-,\mu} \equiv \bar{\nu}\gamma^\mu \tilde{g}(\bar{\nu}, e, \hat{W}'^{-}) e \tag{2.23}$$

In Tab. 2.8 on page 40 we summarize the results that we get for the fermion couplings to the new heavy $\hat{Z}'$ boson. Tab. 2.9 on the previous page lists the couplings to the new heavy $\hat{W}'^{\pm}$ boson.

The derivation of the fermion currents that couple to the gauge bosons $\hat{Z}$, $\hat{Z}'$,

$\hat{W}^{\pm}$, $\hat{W}'^{\pm}$ and A completes our discussion of those contributions to the fundamental Lagrangian $\mathscr{L}$ that we are interested in. After the second stage of symmetry breaking all information relevant to the further analysis is contained in the sum of $\mathscr{L}^{(2)}_{\text{mass}}$ and $\mathscr{L}^{(2)}_{\text{int.}}$ which we may denote by $\mathscr{L}^{(2)}_{\text{fund.}}$:

$$\begin{aligned}
\mathscr{L}^{(2)}_{\text{fund.}} &\equiv \mathscr{L}^{(2)}_{\text{mass}} + \mathscr{L}^{(2)}_{\text{int.}} \\
&= \frac{1}{2}\widetilde{M}^2_{\hat{Z}}\hat{Z}_\mu\hat{Z}^\mu + \frac{1}{2}\left(\widetilde{M}^2_{\hat{Z}'} + \Delta\widetilde{M}^2_{\hat{Z}'}\right)\hat{Z}'_\mu\hat{Z}'^{,\mu} + \delta\widetilde{M}^2_{\hat{Z}\hat{Z}'}\hat{Z}_\mu\hat{Z}'^{,\mu} \\
&+ \widetilde{M}^2_{\hat{W}}\hat{W}^+_\mu\hat{W}^{-,\mu} + \left(\widetilde{M}^2_{\hat{W}'} + \Delta\widetilde{M}^2_{\hat{W}'}\right)\hat{W}'^+_\mu\hat{W}'^{-,\mu} \\
&+ \delta\widetilde{M}^2_{\hat{W}\hat{W}'}\left(\hat{W}^+_\mu\hat{W}'^{-,\mu} + \hat{W}^-_\mu\hat{W}'^{+,\mu}\right) \\
&+ \hat{Z}_\mu J^{0,\mu} + \hat{W}^+_\mu J^{+,\mu} + \hat{W}^-_\mu J^{-,\mu} \\
&+ \hat{Z}'_\mu K^{0,\mu} + \hat{W}'^+_\mu K^{+,\mu} + \hat{W}'^-_\mu K^{-,\mu} \\
&+ A_\mu L^{0,\mu}
\end{aligned}$$

Since the fermion coupling to the photon will play no role in the further discussion we omit it from now on.

2.3.2 Effective Lagrangian at the Electroweak Scale

At energies below the masses $M_{Z'}$ and $M_{W'}$ the new heavy gauge bosons Z' and $W'^{\pm}$ are too heavy to be produced. In experiments probing observables at the electroweak scale the Z' and the $W'^{\pm}$ are solely noticeable through their virtual interactions. As a consequence, the theoretical description of low-energy processes only accounts for them in form of their propagators, $S^{\mu\nu}_{Z'}(q^2)$ and $S^{\mu\nu}_{W'}(q^2)$:

$$S^{\mu\nu}_{Z'}(q^2) \sim \frac{1}{q^2 - M^2_{Z'}} \quad ; \quad S^{\mu\nu}_{W'}(q^2) \sim \frac{1}{q^2 - M^2_{W'}}$$

As the momentum transfer in these processes, q, is much smaller than $M_{Z'}$ and

(1^{st} step)	Fundamental theory		Effective EW theory
Integrate out Z', $W'^{\pm}$:	$\mathscr{L}^{(2)}_{\text{fund.}}$	$\rightarrow$	$\mathscr{L}_{\text{ew.}}$
(2^{nd} step)	Effective EW theory		Four-fermion interactions
Integrate out Z, $W^{\pm}$:	$\mathscr{L}_{\text{ew.}}$	$\rightarrow$	$\mathscr{L}_{4f}$

Table 2.10: Relations between the Lagrangians $\mathscr{L}^{(2)}_{\text{fund.}}$, $\mathscr{L}_{\text{ew.}}$ and $\mathscr{L}_{4f}$ — the electroweak theory described by $\mathscr{L}_{\text{ew.}}$ can be derived from the fundamental Lagrangian $\mathscr{L}^{(2)}_{\text{fund.}}$ by integrating out the heavy gauge bosons Z' and $W'^{\pm}$. The subsequent removal of Z and $W^{\pm}$ from $\mathscr{L}_{\text{ew.}}$ provides us with the effective four-fermion Lagrangian $\mathscr{L}_{4f}$.

$M_{W'}$, it is justified and fittingly to expand the propagators $S^{\mu\nu}_{Z'}(q^2)$ and $S^{\mu\nu}_{W'}(q^2)$ in inverse powers of the large masses $M^2_{Z'}$ and $M^2_{W'}$. Doing so will lead us to an effective theory at the energy scale of electroweak interactions.

However, we can already take care of the expansions in $M^{-2}_{Z'}$ and $M^{-2}_{W'}$ in the classical Euler-Lagrange equations of motions for Z' and $W'^{\pm}$. In this equivalent approach we do not have to worry about the treatment of Z' and $W'^{\pm}$ as full-fledged boson fields comparable to Z, $W^{\pm}$ and A just to render most of our work dispensable in the end when expanding the propagators $S^{\mu\nu}_{Z'}(q^2)$ and $S^{\mu\nu}_{W'}(q^2)$. We better account for the large masses of the Z' and the $W'^{\pm}$ right from the beginning by expanding the solutions of the equations of motion. If we insert the expressions we get this way for Z' and $W'^{\pm}$ into the Lagrangian $\mathscr{L}^{(2)}_{\text{fund.}}$ we will obtain the effective theory at the electroweak scale as well. The Lagrangian of the effective electroweak theory, $\mathscr{L}_{\text{ew.}}$, will then only contain fermion currents, the Z and the $W^{\pm}$.

Similar arguments apply to processes that take place at even lower energies. If the momentum transfer in a low-energy experiment is smaller than the masses of

the Z and the $W^{\pm}$ we can also integrate out these bosons. This will lead us to the effective four-fermion interaction Lagrangian $\mathscr{L}_{4f}$. Our program for this and the next subsection can thus be summarized as shown in Tab. 2.10.

We begin with integrating out the Z' and the $\hat{W}^{\pm}$. In a first step we have to transform $\mathscr{L}_{\text{fund.}}$ from the basis of the hatted gauge bosons, $\hat{Z}$, $\hat{Z}'$, $\hat{W}^{\pm}$ and $\hat{W}'^{\pm}$, to the basis of the physical bosons, Z, Z', $W^{\pm}$ and $W'^{\pm}$. Eqs. (2.10) and (2.11) tell us how to do that. Subsequently, we formulate the equations of motions for the Z' and the $W'^{\pm}$:

$$\partial_\alpha \frac{\partial \mathscr{L}^{(2)}_{\text{fund.}}}{\partial\left(\partial_\alpha Z'_\mu\right)} - \frac{\partial \mathscr{L}^{(2)}_{\text{fund.}}}{\partial Z'_\mu} = 0 \quad ; \quad \partial_\alpha \frac{\partial \mathscr{L}^{(2)}_{\text{fund.}}}{\partial\left(\partial_\alpha W'^{\pm}_\mu\right)} - \frac{\partial \mathscr{L}^{(2)}_{\text{fund.}}}{\partial W'^{\pm}_\mu} = 0$$

Since $\mathscr{L}_{\text{fund.}}$ does not contain any derivatives of gauge bosons these two equations reduce to the condition that the derivatives of $\mathscr{L}_{\text{fund.}}$ with respect to Z' and $W'^{\pm}$ vanish. Up to first order in $\widetilde{M}^{-2}_{\hat{Z}'}$ and $\widetilde{M}^{-2}_{\hat{W}'}$ we find:

$$\begin{aligned}
\frac{\partial \mathscr{L}^{(2)}_{\text{fund.}}}{\partial Z'_\mu} = 0 \quad &\Rightarrow \quad Z'_\mu = -\frac{K^0_\mu}{\widetilde{M}^2_{\hat{Z}'}} + \mathscr{O}\left(\frac{1}{\widetilde{M}^4_{\hat{Z}'}}\right) \\
\frac{\partial \mathscr{L}^{(2)}_{\text{fund.}}}{\partial W'^{\pm}_\mu} = 0 \quad &\Rightarrow \quad W'^{\mp}_\mu = -\frac{K^{\pm}_\mu}{\widetilde{M}^2_{\hat{W}'}} + \mathscr{O}\left(\frac{1}{\widetilde{M}^4_{\hat{W}'}}\right)
\end{aligned}$$

Plugging these expressions into $\mathscr{L}_{\text{fund.}}$ yields the effective Lagrangian at the electroweak scale:

$$\begin{aligned}
\mathscr{L}_{\text{ew.}} \equiv\ & \frac{1}{2} M_Z^2 Z_\mu Z^\mu + M_W^2 W^+_\mu W^{-,\mu} \\
&+ Z_\mu J^{0,\mu}_{\text{ew.}} + W^+_\mu J^{+,\mu}_{\text{ew.}} + W^-_\mu J^{-,\mu}_{\text{ew.}} + \mathscr{L}^{KK}_{\text{ew.}}.
\end{aligned} \tag{2.24}$$

$\mathscr{L}_{\text{ew.}}$ exhibits three structurally different parts: Ordinary mass terms for the light physical bosons Z and $W^{\pm}$, effective fermion currents $J^{0,\mu}_{\text{ew.}}$ and $J^{\pm,\mu}_{\text{ew.}}$ that couple to

the Z and the $W^{\pm}$ and an effective four-fermion interaction $\mathscr{L}_{\text{ew.}}^{KK}$ that emerges due to the self-interaction of the new physics currents K^0 and $K^{\pm}$. The masses M_Z^2 and M_W^2 and the currents $J_{\text{ew.}}^{0,\mu}$ and $J_{\text{ew.}}^{\pm,\mu}$ are related to the parameters of the fundamental Lagrangian $\mathscr{L}_{\text{fund.}}^{(2)}$ as follows:

$$\begin{aligned} M_Z^2 &= \widetilde{M}_{\hat{Z}}^2 - \frac{\delta\widetilde{M}_{\hat{Z}\hat{Z}'}^2}{\widetilde{M}_{\hat{Z}'}^2} \quad ; \quad M_W^2 = \widetilde{M}_{\hat{W}}^2 - \frac{\delta\widetilde{M}_{\hat{W}\hat{W}'}^2}{\widetilde{M}_{\hat{W}'}^2} \\ J_{\text{ew.}}^{0,\mu} &= J^{0,\mu} - \frac{\delta\widetilde{M}_{\hat{Z}\hat{Z}'}^2}{\widetilde{M}_{\hat{Z}'}^2} K^{0,\mu} \quad ; \quad J_{\text{ew.}}^{\pm,\mu} = J^{\pm,\mu} - \frac{\delta\widetilde{M}_{\hat{W}\hat{W}'}^2}{\widetilde{M}_{\hat{W}'}^2} K^{\pm,\mu} \end{aligned} \tag{2.25}$$

As expected, the results for M_Z^2 and M_W^2 in $\mathscr{L}_{\text{ew.}}$ agree with the expressions in Eqs. (2.12) and (2.13). We find that the low-energy effects of the new heavy gauge bosons Z' and $W'^{\pm}$ are reflected in shifts in the masses and currents that are proportional to the inverse of the heavy masses $\widetilde{M}_{\hat{Z}'}^2$ and $\widetilde{M}_{\hat{W}'}^2$. The Lagrangian $\mathscr{L}_{\text{ew.}}^{KK}$ takes care of the exchange of virtual Z' and $W'^{\pm}$ bosons in four-fermion interactions:

$$\mathscr{L}_{\text{ew.}}^{KK} = -\frac{1}{2\widetilde{M}_{\hat{Z}'}^2} K_\mu^0 K^{0,\mu} - \frac{1}{\widetilde{M}_{\hat{W}'}^2} K_\mu^+ K^{-,\mu} \tag{2.26}$$

2.3.3 Effective Four-Fermion Interactions

Processes at energies below the electroweak scale only involve the Z and the $W^{\pm}$ as virtual off-shell particles. Observables are best described in an effective four-fermion interaction framework in which the Z and the $W^{\pm}$ are integrated out. To arrive at the corresponding Lagrangian, $\mathscr{L}_{4f}$, we repeat the steps of the previous subsection. First, we formulate the equations of motions for the Z and the $W^{\pm}$:

$$\partial_\alpha \frac{\partial\mathscr{L}_{\text{ew.}}}{\partial\left(\partial_\alpha Z_\mu\right)} - \frac{\partial\mathscr{L}_{\text{ew.}}}{\partial Z_\mu} = 0 \quad ; \quad \partial_\alpha \frac{\partial\mathscr{L}_{\text{ew.}}}{\partial\left(\partial_\alpha W_\mu^{\pm}\right)} - \frac{\partial\mathscr{L}_{\text{ew.}}}{\partial W_\mu^{\pm}} = 0$$

which are again equivalent to the condition that the derivatives of the Lagrangian $\mathscr{L}_{\text{ew.}}$ with respect to the Z and the $W^{\pm}$ vanish. Up to linear order in the inverse of the heavy masses we then get:

$$Z_\mu = -\frac{J^0_{\text{ew.},\mu}}{M^2_Z} = -\frac{1}{\widetilde{M}^2_{\hat{Z}}} \cdot \left(J^0_\mu - \frac{\delta \widetilde{M}^2_{Z\hat{Z}'}}{\widetilde{M}^2_{\hat{Z}'}} K^0_\mu \right) - \frac{\delta \widetilde{M}^4_{\hat{Z}\hat{Z}'}}{\widetilde{M}^2_{\hat{Z}'} \widetilde{M}^4_{\hat{Z}}} J^0_\mu + \mathscr{O}\left(\frac{1}{\widetilde{M}^4_{\hat{Z}'}} \right)$$

$$W^{\mp}_\mu = -\frac{J^{\pm}_{\text{ew.},\mu}}{M^2_W} = -\frac{1}{\widetilde{M}^2_{\hat{W}}} \cdot \left(J^{\pm}_\mu - \frac{\delta \widetilde{M}^2_{\hat{W}\hat{W}'}}{\widetilde{M}^2_{\hat{W}'}} K^{\pm}_\mu \right) - \frac{\delta \widetilde{M}^4_{\hat{W}\hat{W}'}}{\widetilde{M}^2_{\hat{W}'} \widetilde{M}^4_{\hat{W}}} J^{\pm}_\mu + \mathscr{O}\left(\frac{1}{\widetilde{M}^4_{\hat{W}'}} \right)$$

Inserting these results into $\mathscr{L}_{\text{ew.}}$ provides us with the effective four-fermion interaction Lagrangian:

$$\begin{aligned}
\mathscr{L}_{4f} \equiv & -\frac{1}{2\widetilde{M}^2_{\hat{Z}}} \left[J^0_\mu J^{0,\mu} - \frac{2\delta \widetilde{M}^2_{\hat{Z}\hat{Z}'}}{\widetilde{M}^2_{\hat{Z}'}} J^0_\mu K^{0,\mu} + \frac{\delta \widetilde{M}^4_{\hat{Z}\hat{Z}'}}{\widetilde{M}^2_{\hat{Z}'} \widetilde{M}^2_{\hat{Z}}} J^0_\mu J^{0,\mu} \right] \\
& - \frac{1}{\widetilde{M}^2_{\hat{W}}} \left[J^+_\mu J^{-,\mu} - \frac{\delta \widetilde{M}^2_{\hat{W}\hat{W}'}}{\widetilde{M}^2_{\hat{W}'}} \left(J^+_\mu K^{-,\mu} + J^-_\mu K^{+,\mu} \right) + \frac{\delta \widetilde{M}^4_{\hat{W}\hat{W}'}}{\widetilde{M}^2_{\hat{W}'} \widetilde{M}^2_{\hat{W}}} J^+_\mu J^{-,\mu} \right] \\
& - \frac{1}{2\widetilde{M}^2_{\hat{Z}'}} K^0_\mu K^{0,\mu} - \frac{1}{\widetilde{M}^2_{\hat{W}'}} K^+_\mu K^{-,\mu}
\end{aligned} \tag{2.27}$$

Neglecting terms that are of second or higher order in $\widetilde{M}^{-2}_{\hat{Z}'}$ or $\widetilde{M}^{-2}_{\hat{W}'}$ this result for the four-fermion Lagrangian $\mathscr{L}_{4f}$ may equivalently be written in terms of the effective currents $J^{0,\mu}_{\text{ew.}}$ and $J^{\pm,\mu}_{\text{ew.}}$ and the KK interactions:

$$\mathscr{L}_{4f} + \mathscr{O}\left(\frac{1}{\widetilde{M}^4_{\hat{Z}'}} \right) + \mathscr{O}\left(\frac{1}{\widetilde{M}^4_{\hat{W}'}} \right) = -\frac{1}{2\widetilde{M}^2_{\hat{Z}}} J^0_{\text{ew.},\mu} J^{0,\mu}_{\text{ew.}} - \frac{1}{\widetilde{M}^2_{\hat{W}}} J^+_{\text{ew.},\mu} J^{-,\mu}_{\text{ew.}} + \mathscr{L}^{KK}_{\text{ew.}}$$

The discussion of $\mathscr{L}_{4f}$ completes our analysis of the fundamental properties and

features of the $G(221)$ models under consideration. In the last two sections we derived and examined the three Lagrangians $\mathscr{L}^{(2)}_{\text{fund.}}$, $\mathscr{L}_{\text{ew.}}$ and $\mathscr{L}_{4f}$ each of which describes the old and new physics that emerge in the $G(221)$ models at a different energy scale. We now have the masses of the physical gauge bosons and the gauge interactions of the fermions at our disposal and are ready to proceed with the preparation our global fit analysis.

Chapter 3

Global Fit Analysis with GAPP

Given the precision that has been reached in measuring the electroweak observables it is a matter of fact that the SM accounts for most of the physics that governs the electroweak interaction and that new physics effects can play the role of corrections to the predictions of the SM. In this chapter we will calculate these corrections to the SM in our $G(221)$ models and examine which regions in the new physics parameter space are still allowed for by the experimental precision data.

Our strategy to obtain constraints on the new physics contributions in the $G(221)$ models is the following: First, we will carefully define the parameters in terms of which the corrections to the SM expressions are going to be parametrized. In this discussion we will link the model to the standard parameters and show how the connection to the reference observables is eventually realized. Once we have established a working base of input and fit parameters we will be able to turn towards the calculation of the new physics corrections. After an overview of the observables that will be included into the fits we will revisit the effective Lagrangians $\mathscr{L}_{\text{ew.}}$ and $\mathscr{L}_{4f}$ and derive the set of those operators in terms of which the electroweak observables are defined. This crucial step will enable us to write down the corrections to any observable that we are interested in.

After all analytical work is done we will turn towards the numerical part of our global fit analysis and alter the code of the plotting package GAPP. In some examples we will present the structure of the GAPP files and illustrate the general procedure by which we implement our results. This modification of the GAPP code will finally allow us to test our $G(221)$ models by comparing their predictions to the electroweak data. For each model we will scan over a grid in parameter space and identify the regions permitted by the data. In this context we will have to explain how the grid must be set up and to develop the algorithm that will provide us with the contours in parameter space.

3.1 Parametrization

The goal of our fit analysis is to examine the bounds on new physics effects. For that reason we now have to review the fundamental model parameters of our $G(221)$ models and clearly separate new from old physics parameters. We will fix those combinations of the fundamental model parameters that have equivalents in the SM by means of experimental data. Parameter combinations that do not correspond to parameters of the SM will serve as free parameters during the numerical fits.

3.1.1 Fundamental Model Parameters

The gauge sector of the SM has $n_{\rm SM} = 3$ model parameters: the coupling constants $g_{L,\rm SM}$ and $g_{Y,\rm SM}$ of the two gauge groups $SU(2)_L$ and $U(1)_Y$ and the VEV $v_{\rm SM}$ of electroweak symmetry breaking. Our $G(221)$ models either feature $\tilde{n}(\text{BP-I}) = 6$ or $\tilde{n}(\text{BP-II}) = 5$ model parameters depending on the mechanism by which the fundamental gauge group is broken. For both breaking patterns the extension of the SM gauge group by a second $SU(2)$ results in an additional coupling constant. In breaking pattern one the VEV of the Higgs field Φ exhibits two degrees of freedom,

in breaking pattern two it exhibits one. According to our discussion in the second chapter the fundamental parameters of all three considered classes of $G(221)$ models are given as:

$$\begin{aligned}
\text{(BP-I,D):} \quad & \{\tilde{g}_1, \tilde{g}_2, \tilde{g}_X, \tilde{u}_{\mathrm{D}}, \tilde{\beta}, \tilde{v}\} \\
\text{(BP-I,T):} \quad & \{\tilde{g}_1, \tilde{g}_2, \tilde{g}_X, \tilde{u}_{\mathrm{T}}, \tilde{\beta}, \tilde{v}\} \\
\text{(BP-II,D):} \quad & \{\tilde{g}_1, \tilde{g}_2, \tilde{g}_X, \tilde{u}, \tilde{v}\}
\end{aligned}$$

Compare especially with Tab. 2.2 on page 16, Fig. 2.2 on page 28 and Fig. 2.3 on page 29. Three combinations of the $G(221)$ model parameters have analogs in the SM and must thus be fixed by the reference observables. Fitting the models belonging to the first breaking pattern we are hence left with three free parameters. In the case of the second breaking pattern we will deal with two fit parameters.

One possibility to distinguish new from old physics parameters would be to consult the relations between the three gauge couplings $\tilde{g}_1$, $\tilde{g}_2$ and $\tilde{g}_X$ and the two SM couplings $g_{L,\mathrm{SM}}$ and $g_{Y,\mathrm{SM}}$ and to fix combinations of these three couplings accordingly. However, gauge couplings represent rather less intuitive parameters since they are only indirectly related to physical quantities and GAPP does not use them. Instead of $g_{L,\mathrm{SM}}$ and $g_{Y,\mathrm{SM}}$ it employs the Weinberg angle θ_{SM} and the fine structure constant α_{SM}. We follow the example of GAPP and trade the couplings $\tilde{g}_1$, $\tilde{g}_2$ and $\tilde{g}_X$ for our model fine structure constant $\tilde{\alpha}$ and the mixing angles $\tilde{\phi}$ and $\tilde{\theta}$. The relations that tell us how this has to be done in principal are listed in Tab. 2.4. Subsequently, we exchange the angle $\tilde{\theta}$ for the sine squared, $s^2_{\tilde{\theta}}$. It is this parameter rather than $\tilde{\theta}$ itself that will frequently appear in our calculations.

Moreover, we expect the ratio squared of the two scales of symmetry breaking, $\tilde{u}$ and $\tilde{v}$, to be the best measure for the effect of new physics on the electroweak

observables. This dimensionless parameter that we introduced as $\tilde{x}$ in Eq. (2.14) sets the mass scale of the new heavy gauge bosons (see Tab. 2.6) which is the key criterion for the impact of new physics. In a second step we thus trade $\tilde{u}$ for $\tilde{x}$ such that we end up with:

$$\text{BP-I: } \{\tilde{\alpha}, \tilde{\phi}, s^2_{\tilde{\theta}}, \tilde{x}, \tilde{\beta}, \tilde{v}\} \quad ; \quad \text{BP-II: } \{\tilde{\alpha}, \tilde{\phi}, s^2_{\tilde{\theta}}, \tilde{x}, \tilde{v}\}$$

Among these model parameters we recognize three parameters that we already know from the SM: $\tilde{\alpha}$, $\tilde{v}$ and $s^2_{\tilde{\theta}}$. We will fix these parameters by the experimental input. The remaining two or three parameters will take the role of the fit parameters. We remove $\tilde{\alpha}$, $\tilde{v}$ and $s^2_{\tilde{\theta}}$ from our calculations by relating them to the standard parameters α_{SM}, v_{SM} and $s^2_{\theta_{\text{SM}}}$ which we carry over from the SM:

$$\alpha \equiv \alpha_{\text{SM}} \equiv \frac{e^2_{\text{SM}}}{4\pi} \quad ; \quad G_F \equiv \frac{1}{\sqrt{2} v^2_{\text{SM}}} \quad ; \quad M_Z^2 \equiv \frac{\pi \alpha_{\text{SM}} v^2_{\text{SM}}}{s^2_{\theta_{\text{SM}}} c^2_{\theta_{\text{SM}}}} \tag{3.1}$$

We obtain numerical values for α_{SM}, v_{SM} and $s^2_{\theta_{\text{SM}}}$ making use of the precise measurements of the fine structure constant α, Fermi's constant G_F and the pole mass M_Z of the Z boson. In conclusion, the way we organize the model parameters can be summarized as depicted in Fig. 3.1:

The new physics effects in our $G(221)$ models all scale with the masses of the new heavy gauge bosons and if we were to take them to infinity our model parameters should be identical to the parameters of the SM. Deviations in $\tilde{\alpha}$, $\tilde{v}$ and $s^2_{\tilde{\theta}}$ from α_{SM}, v_{SM} and $s^2_{\theta_{\text{SM}}}$ thus are expected to appear at first order in $\frac{1}{\tilde{x}}$. In other words: We already know that the relations we are looking for must be of the following form:

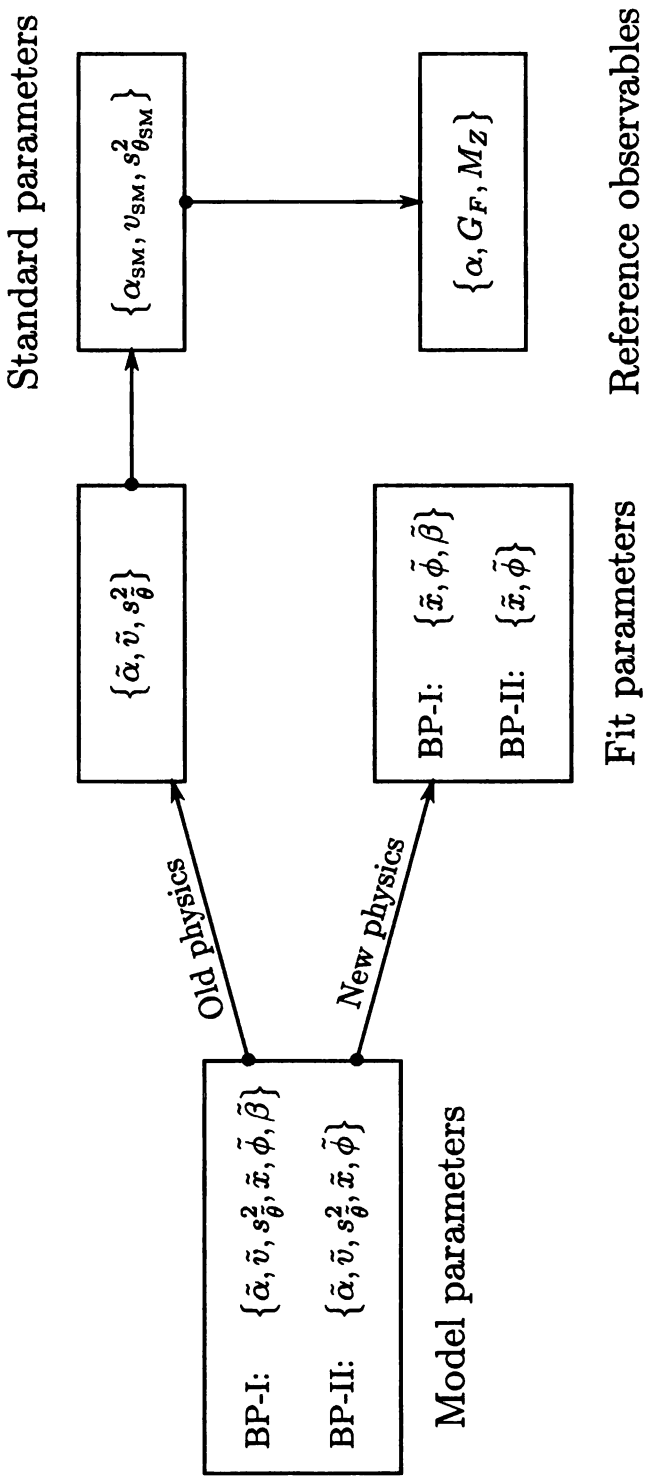

Figure 3.1: Overview of the model, standard and fit parameters — model parameters that do not have an equivalent in the SM (new physics parameters) will be used as fit parameters in our global fit analysis. Parameters with analogs in the SM (old physics parameters) have to be related to the standard parameters and subsequently fixed by the reference observables.

$$\tilde{\alpha} = \alpha_{\mathrm{SM}} \left[1 + \frac{1}{\tilde{x}} C_{\tilde{\alpha}} + \mathcal{O}\left(\frac{1}{\tilde{x}^2} \right) \right] \tag{3.2}$$

$$\tilde{v} = v_{\mathrm{SM}} \left[1 + \frac{1}{\tilde{x}} C_{\tilde{v}} + \mathcal{O}\left(\frac{1}{\tilde{x}^2} \right) \right] \tag{3.3}$$

$$s^2_{\tilde{\theta}} = s^2_{\theta_{\mathrm{SM}}} \left[1 + \frac{1}{\tilde{x}} C_{\tilde{\theta}} + \mathcal{O}\left(\frac{1}{\tilde{x}^2} \right) \right] \tag{3.4}$$

Once we have expressed the coefficients $C_{\tilde{\alpha}}$, $C_{\tilde{v}}$ and $C_{\tilde{\theta}}$ in terms of SM and fit parameters these relations in combination with Eq. (3.1) will enable us to fix the values of $\tilde{\alpha}$, $\tilde{v}$ and $s^2_{\tilde{\theta}}$. In the following subsection we derive $C_{\tilde{\alpha}}$, $C_{\tilde{v}}$ and $C_{\tilde{\theta}}$ one after another.

3.1.2 Relations to the Standard Parameters

Fine structure constant $\tilde{\alpha}$: The first case turns out to be trivial. The electric charge e is defined as the coupling constant of the fermionic gauge interactions with the photon A.

$$L_f^{0,\mu} A_\mu \equiv e \cdot Q_e(f) \bar{f} \gamma^\mu f A_\mu \tag{3.5}$$

A comparison of this definition with our result for $L_f^{0,\mu}$ in Eq. (2.18) lets us conclude that there is no difference at all between all the introduced versions of the fine structure constant:

$$\tilde{e} = e = e_{\mathrm{SM}} \quad \Rightarrow \quad \tilde{\alpha} = \alpha = \alpha_{\mathrm{SM}} \quad \Rightarrow \quad C_{\tilde{\alpha}} = 0 \tag{3.6}$$

VEV of the Electroweak Symmetry Breaking $\tilde{v}$: We derive the coefficient $C_{\tilde{v}}$ by relating the two VEVs $\tilde{v}$ and v_{SM} to Fermi's constant G_F. As G_F is determined from experiment its numerical value is fixed. It is the same in any model and can

thus serve as a link between $\tilde{v}$ and $v_{\rm SM}$. The definition of $v_{\rm SM}$ in terms of G_F is given in Eq. (3.1). To obtain the corresponding relation between $\tilde{v}$ and G_F we first have to understand the origin of Eq. (3.1): G_F is model independently defined as prefactor in the analytical expression for the lifetime τ_μ of the muon μ, compare with [20]:

$$\begin{aligned}\tau_\mu^{-1} \equiv\ & G_F^2 \cdot \frac{m_\mu^5}{192\pi^3} \cdot F\left(\frac{m_e^2}{m_\mu^2}\right)\left(1+\frac{3}{5}\frac{m_\mu^2}{M_W^2}\right) \times \\ & \times \left[1+\left(\frac{25}{8}-\frac{\pi^2}{2}\right)\frac{\alpha\left(m_\mu\right)}{\pi}+C_2\frac{\alpha^2\left(m_\mu\right)}{\pi^2}\right]\end{aligned}$$

where:

$$\begin{aligned}F(x) &= 1-8x+8x^3-x^4-12x^2\ln x \\ C_2 &= \frac{156815}{5184}-\frac{518}{81}\pi^2-\frac{895}{36}\zeta(3)+\frac{67}{720}\pi^4+\frac{53}{6}\pi^2\ln 2 \\ \alpha^{-1}\left(m_\mu\right) &= \alpha^{-1}-\frac{2}{3\pi}\ln\left(\frac{m_\mu}{m_e}\right)+\frac{1}{6\pi}\end{aligned}$$

As we are only interested in the leading order shift in $v_{\rm SM}$ the higher order corrections to τ_μ^{-1} are of no interest for us. For the moment it is sufficient to only consider the tree-level expression for the muon lifetime; $\tau_\mu^{-1} = (G_F^2 m_\mu^5)/(192\pi^3)$. The explicit computation of τ_μ in the SM is based on the effective theory below the electroweak scale which is governed by the Lagrangian $\mathscr{L}_{\rm SM,4f}$. As for the decay of the muon, we are only interested in the contribution $\mathscr{L}^{\rm ch}_{\rm SM,4f}$ to $\mathscr{L}_{\rm SM,4f}$ that takes care of the interaction of charged currents:

$$\mathscr{L}^{\rm ch}_{\rm SM,4f} = -\frac{1}{M^2_{W,\rm SM}} J^+_{\rm SM,\mu} J^{-,\mu}_{\rm SM}$$

The muon μ^- decays into an electron e^-, a muon neutrino ν_μ and an electron anti-neutrino $\bar{\nu}_e$: $\mu^- \rightarrow e^- + \nu_\mu + \bar{\nu}_e$. The corresponding fermion currents are

consequently given as:

$$J^{+,\mu}_{\mathrm{SM}} = \frac{g_{L,\mathrm{SM}}}{\sqrt{2}} \cdot \bar{e}\gamma^{\mu} P_{\mathrm{L}} \nu_e \quad ; \quad J^{-,\mu}_{\mathrm{SM}} = \frac{g_{L,\mathrm{SM}}}{\sqrt{2}} \cdot \bar{\nu}_{\mu}\gamma^{\mu} P_{\mathrm{L}} \mu$$

Inserting these currents into $\mathscr{L}^{\mathrm{ch}}_{\mathrm{SM},4f}$ and going through the algebra yields the SM expression for the muon lifetime:

$$\tau^{-1}_{\mu,\mathrm{SM}} = \frac{g^4_{L,\mathrm{SM}}}{32 M^4_{W,\mathrm{SM}}} \cdot \frac{m^5_{\mu}}{192\pi^3}$$

This result allows us to identify G_F. Employing the relation $M^2_{W,\mathrm{SM}} = \frac{1}{4} g^2_{L,\mathrm{SM}} v^2_{\mathrm{SM}}$ we recover Eq. (3.1):

$$G_F = \frac{\sqrt{2}}{8} \cdot \frac{g^2_{L,\mathrm{SM}}}{M^2_{W,\mathrm{SM}}} = \frac{1}{\sqrt{2} v^2_{\mathrm{SM}}}$$

We observe that G_F is determined by the prefactors of the fermion couplings to the charged bosons W^+ and W^- in the effective four-fermion Lagrangian. This insight sets up our strategy to relate $\tilde{v}$ to G_F: We will take that part of $\mathscr{L}_{4f}$ that accounts for charged interactions, $\mathscr{L}^{\mathrm{ch.}}_{4f}$, compute the effective couplings to the charged gauge bosons and relate the results to τ^{-1}_{μ} and G_F as in the SM. $\mathscr{L}^{\mathrm{ch.}}_{4f}$ has been calculated in Subsec. 2.3.3:

$$\begin{aligned}\mathscr{L}^{\mathrm{ch.}}_{4f} = & -\frac{1}{\widetilde{M}^2_{\hat{W}}} \left[J^+_{\mu} J^{-,\mu} - \frac{\delta \widetilde{M}^2_{\hat{W}\hat{W}'}}{\widetilde{M}^2_{\hat{W}'}} \left(J^+_{\mu} K^{-,\mu} + J^-_{\mu} K^{+,\mu} \right) + \frac{\delta \widetilde{M}^4_{\hat{W}\hat{W}'}}{\widetilde{M}^2_{\hat{W}'} \widetilde{M}^2_{\hat{W}}} J^+_{\mu} J^{-,\mu} \right] \\ & - \frac{1}{\widetilde{M}^2_{\hat{W}'}} K^+_{\mu} K^{-,\mu}\end{aligned}$$

Depending on their chiral structure the new physics currents $K^{+,\mu}$ and $K^{-,\mu}$ might or might not enter the calculation of τ^{-1}_{μ} in our $G(221)$ models. The reason lies in the fact that it is the square of G_F that enters the expression for the muon lifetime.

Repeating the SM calculation we have to square the fermion couplings to the charged gauge bosons. The contributions from the currents $K^{+,\mu}$ and $K^{-,\mu}$ are, however, suppressed by the mass $\widetilde{M}^2_{\hat{W}'}$ of the new heavy $\hat{W}'^{\pm}$ gauge boson. If $K^{+,\mu}$ and $K^{-,\mu}$ are right-handed – being the case for the models of the first breaking pattern — the JK and KK operators do not interfere with the left-handed JJ operators in the limit of massless fermions. The non-zero terms involving the currents $K^{+,\mu}$ and $K^{-,\mu}$ that we are left with are all of order $\widetilde{M}^{-4}_{\hat{W}'}$ and hence negligible. By contrast, in the models belonging to the second breaking pattern the new physics currents are left-handed resulting in non-vanishing interference terms. In the following we discuss both cases separately.

We derived the currents $J^{+,\mu}$ and $J^{-,\mu}$ in Subsec. 2.3.1 and found that they have the same structure as their SM analogs; see Eqs. (2.19) and (2.20). To calculate G_F for the first breaking pattern we therefore only have to replace $g_{L,\text{SM}}$ by $\tilde{g}_L$ and take into account that the shift in the $W^{\pm}$ mass introduces a second JJ operator in the effective Lagrangian:

$$\text{BP-I:} \qquad G_F = \frac{\sqrt{2}}{8} \cdot \frac{\tilde{g}_L^2}{\widetilde{M}^2_{\hat{W}}} \left(1 + \frac{\delta \widetilde{M}^4_{\hat{W}\hat{W}'}}{\widetilde{M}^2_{\hat{W}'} \widetilde{M}^2_{\hat{W}}} \right)$$

Making use of the expressions for $\tilde{g}_L$ and the $W^{\pm}$ mass parameters in terms of the fundamental model parameters that we collected in the last chapter we can rewrite this result as follows:

$$\text{(BP-I,D):} \quad G_F = \frac{1}{\sqrt{2}\tilde{v}^2} \left(1 + \frac{s^2_{2\tilde{\beta}}}{\tilde{x}} \right) \quad ; \quad \text{(BP-I,T):} \quad G_F = \frac{1}{\sqrt{2}\tilde{v}^2} \left(1 + \frac{s^2_{2\tilde{\beta}}}{2\tilde{x}} \right)$$

The dependence on the representation of the Higgs field Φ is induced by the mass $\widetilde{M}^2_{W'}$ that takes different values for different Φ representations. Keeping terms up to

first order in $\frac{1}{\tilde{x}}$ the comparison with the SM result finally yields:

$$\text{(BP-I,D):}\quad \tilde{v} = v_{\text{SM}}\left(1+\frac{s^2_{2\tilde{\beta}}}{2\tilde{x}}\right) \quad ; \quad \text{(BP-I,T):}\quad \tilde{v} = v_{\text{SM}}\left(1+\frac{s^2_{2\tilde{\beta}}}{4\tilde{x}}\right)$$

In other words: The coefficient $C_{\tilde{v}}$ takes the value $C_{\tilde{v}} = \frac{1}{2}s^2_{2\tilde{\beta}}$ if Φ is represented by a doublet the value $C_{\tilde{v}} = \frac{1}{4}s^2_{2\tilde{\beta}}$ if the triplet representation is chosen for Φ. In the models of the second breaking pattern the currents $K^{+,\mu}$ and $K^{-,\mu}$ may be written as:

$$K^{+,\mu} = \frac{\tilde{g}_K}{\sqrt{2}}\cdot\bar{e}\gamma^\mu P_{\text{L}}\nu \quad ; \quad K^{-,\mu} = \frac{\tilde{g}_K}{\sqrt{2}}\cdot\bar{\nu}\gamma^\mu P_{\text{L}}e$$

where $\tilde{g}_K$ corresponds to the entries in Tab. 2.9 with the factor $\frac{1}{\sqrt{2}}$ and the projection operators taken out. Now all operators in $\mathscr{L}^{\text{ch.}}_{4f}$ contribute to G_F and we obtain:

$$\begin{aligned}\text{BP-II:}\quad G_F &= \frac{\sqrt{2}}{8}\cdot\frac{\tilde{g}_L^2}{\widetilde{M}^2_{\hat{W}}}\left(1+\frac{\delta\widetilde{M}^4_{\hat{W}\hat{W}'}}{\widetilde{M}^2_{\hat{W}'}\widetilde{M}^2_{\hat{W}}}\right) - \frac{\sqrt{2}}{8}\cdot 2\frac{\delta\widetilde{M}^2_{\hat{W}\hat{W}'}}{\widetilde{M}^2_{\hat{W}'}\widetilde{M}^2_{\hat{W}}}\tilde{g}_L\tilde{g}_K + \frac{\sqrt{2}}{8}\cdot\frac{\tilde{g}_K^2}{\widetilde{M}^2_{\hat{W}'}} \\ &= \frac{\sqrt{2}}{8}\cdot\frac{\tilde{g}_L^2}{\widetilde{M}^2_{\hat{W}}}\left[1+\frac{\widetilde{M}^2_{\hat{W}}}{\widetilde{M}^2_{\hat{W}'}}\left(\frac{\delta\widetilde{M}^4_{\hat{W}\hat{W}'}}{\widetilde{M}^4_{\hat{W}}} - 2\frac{\delta\widetilde{M}^2_{\hat{W}\hat{W}'}}{\widetilde{M}^2_{\hat{W}}}\cdot\frac{\tilde{g}_K}{\tilde{g}_L}+\frac{\tilde{g}_K^2}{\tilde{g}_L^2}\right)\right]\end{aligned}$$

In the UU-D and the NU-D model all corrections due to new physics cancel each other and Fermi's constant G_F reduces to the same expression as in the SM:

$$\text{BP-II:}\qquad G_F = \frac{1}{\sqrt{2}\tilde{v}^2} \quad \Rightarrow \quad \tilde{v} = v_{\text{SM}} \quad \Rightarrow \quad C_{\tilde{v}} = 0$$

Electroweak Mixing Angle $s^2_{\tilde{\theta}}$ We obtain the shift in the electroweak mixing angle $s^2_{\tilde{\theta}}$ by equating the SM expression for the mass of the Z boson M_Z in Eq. (3.1)

with our $G(221)$ results that are listed in Tab. 2.6. With M_0 being defined as in Eq. (2.15) we can write for M_Z^2:

$$\begin{aligned}
\text{(BP-I,D):} \quad M_Z^2 &= \frac{M_0^2}{c_{\tilde{\theta}}^2}\left(1-\frac{c_{\tilde{\phi}}^4}{\tilde{x}}\right) = \frac{\pi\tilde{\alpha}\tilde{v}^2}{s_{\tilde{\theta}}^2 c_{\tilde{\theta}}^2}\left(1-\frac{c_{\tilde{\phi}}^4}{\tilde{x}}\right) \\
\text{(BP-I,T):} \quad M_Z^2 &= \frac{M_0^2}{c_{\tilde{\theta}}^2}\left(1-\frac{c_{\tilde{\phi}}^4}{4\tilde{x}}\right) = \frac{\pi\tilde{\alpha}\tilde{v}^2}{s_{\tilde{\theta}}^2 c_{\tilde{\theta}}^2}\left(1-\frac{c_{\tilde{\phi}}^4}{4\tilde{x}}\right) \\
\text{(BP-II,D):} \quad M_Z^2 &= \frac{M_0^2}{c_{\tilde{\theta}}^2}\left(1-\frac{s_{\tilde{\phi}}^4}{\tilde{x}}\right) = \frac{\pi\tilde{\alpha}\tilde{v}^2}{s_{\tilde{\theta}}^2 c_{\tilde{\theta}}^2}\left(1-\frac{s_{\tilde{\phi}}^4}{\tilde{x}}\right)
\end{aligned}$$

The results of our previous discussion of $\tilde{\alpha}$ and $\tilde{v}$ allow us to remove all model parameters from M_Z^2 expect for the mixing angle $\tilde{\theta}$. Up to linear order in $\frac{1}{\tilde{x}}$ we obtain:

$$\begin{aligned}
\text{(BP-I,D):} \quad M_Z^2 &= \frac{\pi\alpha_{\rm SM} v_{\rm SM}^2}{s_{\tilde{\theta}}^2 c_{\tilde{\theta}}^2}\left[1-\frac{1}{\tilde{x}}\left(c_{\tilde{\phi}}^4 - s_{2\tilde{\beta}}^2\right)\right] \\
\text{(BP-I,T):} \quad M_Z^2 &= \frac{\pi\alpha_{\rm SM} v_{\rm SM}^2}{s_{\tilde{\theta}}^2 c_{\tilde{\theta}}^2}\left[1-\frac{1}{\tilde{x}}\left(\frac{1}{4}c_{\tilde{\phi}}^4 - \frac{1}{2}s_{2\tilde{\beta}}^2\right)\right] \\
\text{(BP-II,D):} \quad M_Z^2 &= \frac{\pi\alpha_{\rm SM} v_{\rm SM}^2}{s_{\tilde{\theta}}^2 c_{\tilde{\theta}}^2}\left[1-\frac{1}{\tilde{x}}s_{\tilde{\phi}}^4\right]
\end{aligned}$$

The comparison with Eq. (3.1) then yields:

$$\text{(BP-I,D):} \quad s_{\tilde{\theta}}^2 c_{\tilde{\theta}}^2 = s_{\theta_{\rm SM}}^2 c_{\theta_{\rm SM}}^2\left[1-\frac{1}{\tilde{x}}\left(c_{\tilde{\phi}}^4 - s_{2\tilde{\beta}}^2\right)\right] \tag{3.7}$$

$$\text{(BP-I,T):} \quad s_{\tilde{\theta}}^2 c_{\tilde{\theta}}^2 = s_{\theta_{\rm SM}}^2 c_{\theta_{\rm SM}}^2\left[1-\frac{1}{\tilde{x}}\left(\frac{1}{4}c_{\tilde{\phi}}^4 - \frac{1}{2}s_{2\tilde{\beta}}^2\right)\right] \tag{3.8}$$

$$\text{(BP-II,D):} \quad s_{\tilde{\theta}}^2 c_{\tilde{\theta}}^2 = s_{\theta_{\rm SM}}^2 c_{\theta_{\rm SM}}^2\left[1-\frac{1}{\tilde{x}}s_{\tilde{\phi}}^4\right] \tag{3.9}$$

	$C_{\tilde{\alpha}}$	$C_{\tilde{v}}$	$C_{\tilde{\theta}}$
(BP-I,D)	0	$\frac{1}{2}s^2_{2\tilde{\beta}}$	$-f(\theta_{\rm SM})\cdot\left(c^4_{\tilde{\phi}}-s^2_{2\tilde{\beta}}\right)$
(BP-I,T)	0	$\frac{1}{4}s^2_{2\tilde{\beta}}$	$-f(\theta_{\rm SM})\cdot\left(\frac{1}{4}c^4_{\tilde{\phi}}-\frac{1}{2}s^2_{2\tilde{\beta}}\right)$
(BP-II,D)	0	0	$-f(\theta_{\rm SM})\cdot s^4_{\tilde{\phi}}$

Table 3.1: Results for the coefficients $C_{\tilde{\alpha}}$, $C_{\tilde{v}}$ and $C_{\tilde{\theta}}$ that parametrize the shifts in the model parameters $\tilde{\alpha}$, $\tilde{v}$ and $\tilde{\theta}$ resp. at first order in $\frac{1}{\tilde{x}}$ — compare also with Eqs. (3.2), (3.3) and (3.4). $f(\theta_{\rm SM})$ is given as $f(\theta_{\rm SM}) \equiv c^2_{\theta_{\rm SM}}/\left(c^2_{\theta_{\rm SM}}-s^2_{\theta_{\rm SM}}\right)$.

Replacing $c^2_{\tilde{\theta}}$ by $1-s^2_{\tilde{\theta}}$ we can solve these three equations for $s^2_{\tilde{\theta}}$:

$$\text{(BP-I,D):}\quad s^2_{\tilde{\theta}} = s^2_{\theta_{\rm SM}}\left[1-\frac{1}{\tilde{x}}\cdot\frac{c^2_{\theta_{\rm SM}}}{c^2_{\theta_{\rm SM}}-s^2_{\theta_{\rm SM}}}\left(c^4_{\tilde{\phi}}-s^2_{2\tilde{\beta}}\right)\right]$$

$$\text{(BP-I,T):}\quad s^2_{\tilde{\theta}} = s^2_{\theta_{\rm SM}}\left[1-\frac{1}{\tilde{x}}\cdot\frac{c^2_{\theta_{\rm SM}}}{c^2_{\theta_{\rm SM}}-s^2_{\theta_{\rm SM}}}\left(\frac{1}{4}c^4_{\tilde{\phi}}-\frac{1}{2}s^2_{2\tilde{\beta}}\right)\right]$$

$$\text{(BP-II,D):}\quad s^2_{\tilde{\theta}} = s^2_{\theta_{\rm SM}}\left[1-\frac{1}{\tilde{x}}\cdot\frac{c^2_{\theta_{\rm SM}}}{c^2_{\theta_{\rm SM}}-s^2_{\theta_{\rm SM}}}s^4_{\tilde{\phi}}\right]$$

These findings for the electroweak mixing angle complete our analysis of the model parameters. Tab. 3.1 summarizes our results for the coefficients $C_{\tilde{\alpha}}$, $C_{\tilde{v}}$ and $C_{\tilde{\theta}}$ that we found in this subsection. Together with Eqs. (3.2), (3.3) and (3.4) and the definition of the SM parameters in Eq. (3.1) this table enables us to fix the values of $\tilde{\alpha}$, $\tilde{v}$ and $s^2_{\tilde{\theta}}$. We are now prepared to return to the effective Lagrangians $\mathscr{L}_{\rm eff.}$ and $\mathscr{L}_{4f}$ and to parameterize the operators that we need for the calculation of the new physics corrections in terms of the fit parameters $\tilde{x}$, $\tilde{\phi}$ and $\tilde{\beta}$. First of all we will, however, discuss the considered electroweak observables in more detail.

3.2 Electroweak Observables

The corrections to the SM expressions for the electroweak observables constitute the foundation of our global fit analysis. Before we turn to the explicit algebra we, however, first have to introduce and define all the observables that we are going to consider. After we have developed an understanding of all the quantities that will enter our fits we will proceed with the actual calculations.

3.2.1 Overview of the Included Observables

The electroweak precision observables to which we will fit the $G(221)$ models fall into two classes: Observables defined in terms of operators that appear in the effective Lagrangian $\mathscr{L}_{\text{ew.}}$ at the electroweak scale and observables that are related to operators in the four-fermion Lagrangian $\mathscr{L}_{4f}$ below the electroweak scale. Both classes can be further subdivided into certain sets of observables. We now briefly characterize these groups mentioning in each case which and how many observables they contain and how much experimental data is available respectively. In total we will fit 37 observables; 46 experimental values are at our disposal.

Observables derived from $\mathscr{L}_{\text{ew.}}$:

- *Z pole data:* Partial decay widths $\Gamma_Z\left(f\bar{f}\right)$ of the Z boson, fermion left-right asymmetries $A_{LR}(f)$ and various other observables that can be constructed from these quantities. 21 observables, 25 experimental values (LEP and SLAC data).

- $W^{\pm}$ *pole data:* Mass M_W and total width Γ_W of the $W^{\pm}$ boson. Two observables, four experimental values (LEP and TeVatron data).

- *Mass m_t of the top quark t:* One observable, one experimental value (total TeVatron average).

Observables derived from $\mathscr{L}_{4f}$:

- *Neutrino-nucleon scattering:* Left- and right-handed neutral current quark couplings $g_L^{\nu N}$ and $g_R^{\nu N}$ and ratios of neutral-to-charged current cross sections R_ν and $R_{\bar{\nu}}$. Five observables, eight experimental values.

- *Neutrino-electron scattering:* Vector and axial neutral current electron couplings $g_V^{\nu e}$ and $g_A^{\nu e}$. Two observables, two experimental values.

- *Parity-violating processes:* Weak charges of cesium, thallium and the electron, $Q_W\left(^{133}\mathrm{Cs}\right)$, $Q_W\left(^{205}\mathrm{Tl}\right)$ and $Q_W(e)$. Two linear combinations C_1 and C_2 of the quark vector couplings C_{1u} and C_{1d}. Five observables, five experimental values.

- *Lifetime τ_τ of the τ lepton:* One observable, one experimental value (world average).

This selection of observables differs slightly from the set of observables that is used by the default 2009 version of the GAPP code [21]. Originally, GAPP does not consider the width Γ_W of the $W^\pm$ boson but additionally includes the value of the anomalous magnetic magnetic of the muon $\frac{1}{2}(g_\mu - 2)$, the measurement of the unitary of the first row in the CKM-matrix and data related to the $b \to s\gamma$ decay. $\frac{1}{2}(g_\mu - 2)$ and the $b \to s\gamma$ amplitude only receive new physics corrections at the loop-level. Since we are only interested in tree-level effects induced by new physics we do not include the corresponding observables into our analysis. In this study we consider the new physics tree-level corrections, if $\tilde{x}$ is large, to be of the same order of magnitude as SM loop effects — new physics loop terms are therefore negligible. Furthermore, we take out the experimental constraints on the CKM unitarity as we do not consider new physics in the flavor sector in this analysis.

In the following we will allude to all these groups of observables separately. We will introduce the respective quantities in terms of which the individual observables are defined and set up everything such that we are prepared to calculate the new physics corrections in Subsec. 3.2.2.

High-energy observables derived from $\mathscr{L}_{\mathbf{ew}}$.

Z pole data: At tree-level the partial width $\Gamma_Z\left(f\bar{f}\right)$ of the decay of a Z boson into a fermion pair $f\bar{f}$ is given as:

$$\Gamma_Z\left(f\bar{f}\right) \equiv \frac{n_c(f)}{3} \cdot \frac{M_Z \alpha}{s_\theta^2 c_\theta^2} \left(\left[g_V^Z(f)\right]^2 + \left[g_A^Z(f)\right]^2 \right) \tag{3.10}$$

By writing the parameters appearing in this expression without tilde or SM index we indicate that this relation holds independently of the model employed. When we have come to calculate the new physics corrections in Subsec. 3.2.2 we will evaluate this general expression for $\Gamma_Z\left(f\bar{f}\right)$ and all the other definitions presented here in the SM as well as in our $G(221)$ models. $g_V^Z(f)$ and $g_A^Z(f)$ denote the vector and the axial couplings of the fermion f to the Z boson. They are related to the left- and right-handed couplings $g_L^Z(f)$ and $g_R^Z(f)$ as follows

$$g_V^Z(f) \equiv \frac{1}{2}\left(g_R^Z(f) + g_L^Z(f)\right) \quad ; \quad g_A^Z(f) \equiv \frac{1}{2}\left(g_R^Z(f) - g_L^Z(f)\right)$$

and parametrize the coupling of the Z boson to the neutral fermion current $J_f^{0,\mu}$:

$$\begin{aligned} J_{f,\mu}^0 Z^\mu &\equiv \frac{e}{s_\theta c_\theta} \bar{f}\left(g_V^Z(f)\gamma_\mu + g_A^Z(f)\gamma_\mu\gamma_5\right) f Z^\mu \\ &\equiv \frac{e}{s_\theta c_\theta} \bar{f}\gamma_\mu\left(g_L^Z(f) P_{\mathrm{L}} + g_R^Z(f) P_{\mathrm{R}}\right) f Z^\mu \end{aligned} \tag{3.11}$$

$n_c(f)$ in Eq. (3.10) stands for the color multiplicity of the fermion f. The charged

leptons ℓ as well as the corresponding neutrinos ν_ℓ are represented by color singlets, the quarks q come in tree colors --- red, green, blue:

$$n_c(\ell) = 1 \quad ; \quad n_c(\nu_\ell) = 1 \quad ; \quad n_c(q) = 3$$

M_Z is the experimental value for the mass of the Z boson. If we sum over the partial widths $\Gamma_Z(f\bar{f})$ of all fermion pairs to which the Z can decay, that is, all pairs expect for the top pair $t\bar{t}$, we obtain the total width Γ_Z of the Z peak. Summing only over quarks q in the final state provides us with the hadronic decay width Γ_Z (had.):

$$\Gamma_Z \equiv \sum_{f \neq t} \Gamma_Z(f\bar{f}) \quad ; \quad \Gamma_Z(\text{had.}) \equiv \sum_{q \neq t} \Gamma_Z(q\bar{q})$$

The individual partial widths $\Gamma_Z(f\bar{f})$ for decays into fermion pairs $f\bar{f}$, the total width Γ_Z and the hadronic width Γ_Z (had.) are the ingredients for a wealth of secondary observables. For instance, the total hadronic cross section $\sigma_{\text{had.}}$ representing a fundamental QCD quantity that is accessible experimentally can be expressed in terms of $\Gamma_Z(e\bar{e})$, Γ_Z and Γ_Z (had.):

$$\sigma_{\text{had.}} \equiv \frac{12\pi}{M_Z^2 \Gamma_Z^2} \cdot \Gamma_Z(e^- e^+) \, \Gamma_Z(\text{had.})$$

The partial widths for decays into charged leptons $\Gamma_Z(\ell\bar{\ell})$ and decays into quarks $\Gamma_Z(q\bar{q})$ are used to define the hadron-to-lepton ratios $R(\ell)$ and the hadronic branching ratios $R(q)$ respectively:

$$R(\ell) \equiv \frac{\Gamma_Z(\text{had.})}{\Gamma_Z(\ell\bar{\ell})} \quad ; \quad \ell \in \{e, \mu, \tau\}$$

$$R(q) \equiv \frac{\Gamma_Z(q\bar{q})}{\Gamma_Z(\text{had.})} \quad ; \quad q \in \{u, d, c, s, b\}$$

As for the light quarks, u, d and s, experimental data is available for the ratio of $R(s)$ to the total branching into light quarks:

$$\mathcal{R}(s) \equiv \frac{R(s)}{R(u) + R(d) + R(s)}$$

Coming back to the left- and right-handed fermion couplings $g_L^Z(f)$ and $g_R^Z(f)$ to the Z boson we can write the polarization or left-right asymmetry $A_{LR}(f)$ of a fermion f as follows:

$$A_{LR}(f) \equiv \frac{\left[g_L^Z(f)\right]^2 - \left[g_R^Z(f)\right]^2}{\left[g_L^Z(f)\right]^2 + \left[g_R^Z(f)\right]^2} \tag{3.12}$$

The combination of the quark branching ratios $R(q)$ and the left-right asymmetries $A_{LR}(q)$ yields the hadronic left-right asymmetry Q_{LR}:

$$Q_{LR} \equiv \sum_{q=d,s,b} R(q) A_{LR}(q) - \sum_{q=u,c} R(q) A_{LR}(q)$$

A second class of asymmetries, the forward-backward asymmetries $A_{FB}(f)$, emerges from the convolution of the $A_{LR}(f)$ asymmetries with the polarization asymmetry $A_{LR}(e)$ of the electron. The hadronic charge asymmetry Q_{FB} is defined accordingly:

$$A_{FB}(f) \equiv \frac{3}{4} A_{LR}(e) A_{LR}(f) \quad ; \quad Q_{FB} \equiv \frac{3}{4} A_{LR}(e) Q_{LR}$$

Having introduced these last two quantities we have covered all relevant definitions pertaining the Z pole data. We will include the following 21 observables into our global fit analysis:

Γ_Z	,	$\sigma_{\text{had.}}$	,	$R(e)$	,	$R(\mu)$	,	$R(\tau)$	,	$\mathcal{R}(s)$	,						
$R(c)$	,	$R(b)$	,	$A_{LR}(e)$	,	$A_{LR}(\mu)$	,	$A_{LR}(\tau)$	,	$A_{LR}(s)$	,						
$A_{LR}(c)$	,	$A_{LR}(b)$	,	$A_{FB}(e)$	,	$A_{FB}(\mu)$	,	$A_{FB}(\tau)$	,	$A_{FB}(s)$	,						
$A_{FB}(c)$	,	$A_{FB}(b)$	,	Q_{FB}													

$W^{\pm}$ pole data Due to their opposite charges the two charged electroweak bosons, W^+ and W^-, couple to different fermion pairs. Respectively, the following decays are allowed:

$$W^+ \rightarrow \ell^+ \nu_\ell \quad ; \quad W^+ \rightarrow u_i \bar{d}_j \tag{3.13}$$

$$W^- \rightarrow \ell^- \bar{\nu}_\ell \quad ; \quad W^- \rightarrow \bar{u}_i d_j \tag{3.14}$$

with $i = 1, 2$ and $j = 1, 2, 3$ representing generation indices. Since the top quark t is too heavy to be produced in $W^{\pm}$ decay $i = 3$ is excluded. The respective decay widths of the W^+ and the W^- are, of course, identical. In order to avoid writing down every expression twice we will consider the properties of the W^+ only in the following discussion. All results derived for the W^+ will apply to the W^- as well.

In analogy to Eq. (3.10) the tree-level expression for the partial width of a W^+ decaying into a lepton-neutrino pair $\ell^+ \nu_\ell$ reads as:

$$\Gamma_W \left(\ell^+ \nu_\ell\right) \equiv \frac{n_c(\ell)}{48\pi} \cdot M_W \left(\left[g_L^W(\ell)\right]^2 + \left[g_R^W(\ell)\right]^2 \right)$$

The left- and right-handed couplings $g_L^W(f)$ and $g_R^W(f)$ of the fermions to the $W^{\pm}$ are defined similarly as the corresponding couplings to the Z boson:

$$J^{+}_{\ell,\mu}W^{+,\mu} \equiv \frac{1}{\sqrt{2}}\bar{\ell}\gamma_\mu\left(g^W_L(\ell)P_{\rm L}+g^W_R(\ell)P_{\rm R}\right)\nu_\ell W^{+,\mu}$$
$$J^{+}_{q,\mu}W^{+,\mu} \equiv \frac{1}{\sqrt{2}}\bar{d}\gamma_\mu\left(g^W_L(\ell)P_{\rm L}+g^W_R(\ell)P_{\rm R}\right)uW^{+,\mu}$$

In the SM the $W^{\pm}$ does not couple to right-handed fermion currents. The only reason why we include $g^W_R(f)$ into our discussion is that it might play a role in our $G(221)$ models later on. However, we learnt from our calculation of the muon lifetime in Subsec. 3.1.2 that right-handed contributions are always suppressed by the mass $\widetilde{M}^2_{W'}$ in the $G(221)$ models. As it is $\left[g^W_R(f)\right]^2$ that enters the partial decay width $\Gamma_W\left(\ell^+\nu_\ell\right)$ these contributions will be negligible. Calculating the $W^{\pm}$ decay width explicitly up to order $\mathcal{O}\left(\widetilde{M}^{-2}_{W'}\right)$ we will therefore always use the following relation:

$$\Gamma_W\left(\ell^+\nu_\ell\right) \equiv \frac{n_c(\ell)}{48\pi}\cdot M_W\left[g^W_L(\ell)\right]^2 \tag{3.15}$$

The partial width for the decay into a quark pair $\Gamma_W\left(u_i\bar{d}_j\right)$ is slightly more complicated than $\Gamma_W\left(\ell^+\nu_\ell\right)$. To take into account the mixing of the strong eigenstates of the down-type quarks in the case of weak interactions we have to include the entries of the CKM-matrix V into $\Gamma_W\left(u_i\bar{d}_j\right)$:

$$\Gamma_W\left(u_i\bar{d}_j\right) \equiv \left|V_{ij}\right|^2\cdot\frac{n_c(u_i)}{48\pi}\cdot M_W\left[g^W_L(u_i)\right]^2$$

Owing to the unitarity of V these coefficients become irrelevant once we only consider the combined widths $\Gamma_W(u_i)$:

$$\sum_j\left|V_{ij}\right|^2=1 \quad\Rightarrow\quad \Gamma_W(u_i)\equiv\sum_j\Gamma_W\left(u_i\bar{d}_j\right)=\frac{n_c(u_i)}{48\pi}\cdot M_W\left[g^W_L(u_i)\right]^2 \tag{3.16}$$

The arguments ℓ and u_i of $g_L^W(f)$ in Eqs. (3.15) and (3.16) are not intended to indicate a dependence of $g_L^W(f)$ on the quantum numbers of the lepton ℓ or the up-type quark u_i but are supposed to reflect the fact that $g_L^W(f)$ may vary between fermions belonging to different $SU(2)$s in our $G(221)$ models.

If we finally sum up all leptonic and hadronic decay widths we obtain the total width Γ_W of the $W^\pm$ boson:

$$\Gamma_W \equiv \sum_\ell \Gamma_W\left(\ell^+\nu_\ell\right) + \sum_i \Gamma_W\left(u_i\right)$$

This is one of the two $W^\pm$ pole observables to which we will fit our $G(221)$ models; the other being the mass M_W of the $W^\pm$ boson:

$$\boxed{\Gamma_W \quad , \quad M_W}$$

Mass of the top quark: Besides the mass of the $W^\pm$ boson we will also include the pole mass m_t of the top quark into our fits.

$$\boxed{m_t}$$

In the $G(221)$ models that we consider m_t, however, does not receive corrections due to new physics. To see why that is we must have a closer look at the origin of m_t within the theory: In the SM as well as in our $G(221)$ models the masses of the fermions are generated in the Yukawa sector through spontaneous symmetry breaking. The fermions couple to the Higgs bosons — once the Higgs fields acquire their VEVs the Yukawa interactions turn into fermionic mass terms. The generated masses are then given in terms of the Higgs VEVs and the initial Yukawa couplings G_f. In the case of our $G(221)$ models we may write for m_t:

$$m_t = \tilde{G}_t \cdot f\left(\tilde{x}, \tilde{v}\right) \tag{3.17}$$

where the functional form of $f(\tilde{x}, \tilde{v})$ depends on the details of the respective model. Eq. (3.17) shows us that the value of m_t can always be set to any desired value just by choosing the Yukawa coupling $\tilde{G}_t$ accordingly. In fact, $\tilde{G}_t$ is an additional fundamental parameter of our $G(221)$ models. Due to its trivial relation to m_t the problem of constraining $\tilde{G}_t$ can, however, be completely separated from the remaining analysis. In this work we will choose $\tilde{G}_t$ such that the $G(221)$ prediction of m_t corresponds to the SM value:

$$m_t \equiv m_{t,\mathrm{SM}}$$

Note that it is the on-shell mass m_t of the top quark that we will use as an observable. Fitting the $G(221)$ models to the data in Subsec. 3.3 we will, by contrast, employ the $\overline{\mathrm{MS}}$ mass $\bar{m}_t$ as a free fit parameter. In appendix B we briefly outline the relation between these two definitions of the top quark mass.

Low-energy observables derived from $\mathscr{L}_{4f}$

Neutrino-Nucleon Scattering Deep inelastic scattering (DIS) experiments allow to probe the coupling of neutrinos ν to nucleons inside an atomic nucleus N. For measuring the electroweak mixing angle, it is advantageous to choose an isoscalar target. As neutrinos are capable of exchanging both Z and $W^{\pm}$ bosons with the up and the down quarks that constitute the nucleons neutral (NC) as well as charged (CC) current interactions occur in ν-DIS experiments. In the case of, for instance, incident muon neutrinos ν_μ and muon anti-neutrinos $\bar{\nu}_\mu$ the following reactions take place:

$$\begin{aligned} \text{NC:} \quad & \nu_\mu N \to \nu_\mu X \;\; ; \;\; \bar{\nu}_\mu N \to \bar{\nu}_\mu X \\ \text{CC:} \quad & \nu_\mu N \to \mu^- X \;\; ; \;\; \bar{\nu}_\mu N \to \mu^+ X \end{aligned}$$

where X denotes an arbitrary hadronic final state. These weak interaction processes are governed by the effective four-fermion Lagrangian $\mathscr{L}_{4f}$ below the electroweak scale. If we assume that only the usual left-handed SM neutrinos play a role in ν-DIS experiments the contribution $\mathscr{L}_{4f}^{\mathrm{NC},\nu N}$ to $\mathscr{L}_{4f}$ that accounts for the neutral current neutrino interactions with the up and the down quarks is given by:

$$\mathscr{L}_{4f}^{\mathrm{NC},\nu N} \equiv -\frac{G_F}{\sqrt{2}} \bar{\nu} \gamma_\mu \left(1-\gamma_5\right) \nu \sum_{q=u,d} \bar{q} \gamma^\mu \left[\varepsilon_L\left(q\right)\left(1-\gamma_5\right) + \varepsilon_R\left(q\right)\left(1+\gamma_5\right)\right] q$$

As the chiral fermion structures that we encounter in this Lagrangian will appear over and over again in the analysis that is still to come we now introduce the following notation for left- and right-handed as well as vector and axial fermionic spinor products:

$$\begin{aligned} \bar{f}_1 \gamma^\mu \left(1-\gamma_5\right) f_2 &\equiv \left(\bar{f}_1 f_2\right)_L^\mu \;\; ; \;\; \bar{f}_1 \gamma^\mu \left(1+\gamma_5\right) f_2 \equiv \left(\bar{f}_1 f_2\right)_R^\mu \\ \bar{f}_1 \gamma^\mu f_2 &\equiv \left(\bar{f}_1 f_2\right)_V^\mu \;\; ; \;\; \bar{f}_1 \gamma^\mu \gamma_5 f_2 \equiv \left(\bar{f}_1 f_2\right)_A^\mu \end{aligned}$$

With these abbreviations we can write $\mathscr{L}_{4f}^{\mathrm{NC},\nu N}$ in a more compact form:

$$\mathscr{L}_{4f}^{\mathrm{NC},\nu N} = -\frac{G_F}{\sqrt{2}} \left(\bar{\nu}\nu\right)_{L,\mu} \sum_{q=u,d} \left[\varepsilon_L\left(q\right)\left(\bar{q}q\right)_L^\mu + \varepsilon_R\left(q\right)\left(\bar{q}q\right)_R^\mu\right] \tag{3.18}$$

The Lagrangian $\mathscr{L}_{4f}^{\mathrm{CC},\nu N}$ which is the counterpart of $\mathscr{L}_{4f}^{\mathrm{NC},\nu N}$ being responsible for charged current interactions has the following structure in the case of muon neutrino experiments:

$$\mathscr{L}_{4f}^{\mathrm{CC},\nu N} \equiv -\frac{G_F}{\sqrt{2}}\left[\left(\bar{\mu}\nu_\mu\right)_{L,\mu}\left(\bar{u}d\right)_L^\mu + \left(\bar{\nu}_\mu\mu\right)_{L,\mu}\left(\bar{d}u\right)_L^\mu\right] + \mathscr{L}_{\mathrm{NP},4f}^{\mathrm{CC},\nu N}$$

with $\mathscr{L}_{\mathrm{NP},4f}^{\mathrm{CC},\nu N}$ accounting for effects beyond the SM. The actual physics of neutrino-hadron scattering is contained in the coefficients $\varepsilon_L(q)$ and $\varepsilon_R(q)$ of the effective four-fermion operators in the neutral current Lagrangian. In Subsec. 3.2.2 we will calculate the shifts of all ν-DIS observables just be determining the new physics corrections to $\varepsilon_L(q)$ and $\varepsilon_R(q)$. At tree level the left- and right-handed neutral current quark couplings $g_L^{\nu N}$ and $g_R^{\nu N}$ can be expressed in terms of the coefficients $\varepsilon_L(q)$ and $\varepsilon_R(q)$ as follows:

$$g_L^{\nu N} \equiv \varepsilon_L^2(u) + \varepsilon_L^2(d) \quad ; \quad g_R^{\nu N} \equiv \varepsilon_R^2(u) + \varepsilon_R^2(d)$$

Accordingly, the differences between the respective coefficients can be used to define the quantities $\delta_L^{\nu N}$ and $\delta_R^{\nu N}$:

$$\delta_L^{\nu N} \equiv \varepsilon_L^2(u) - \varepsilon_L^2(d) \quad ; \quad \delta_R^{\nu N} \equiv \varepsilon_R^2(u) - \varepsilon_R^2(d)$$

Combining $\delta_L^{\nu N}$ and $\delta_R^{\nu N}$ with the left- and right-handed couplings $g_L^{\nu N}$ and $g_R^{\nu N}$ allows us to construct the observable $\kappa^{\nu N}$:

$$\kappa^{\nu N} \equiv C_L^g \cdot \left(g_L^{\nu N}\right)^2 + C_R^g \cdot \left(g_R^{\nu N}\right)^2 + C_L^\delta \cdot \left(\delta_L^{\nu N}\right)^2 + C_R^\delta \cdot \left(\delta_R^{\nu N}\right)^2 \tag{3.19}$$

$\kappa^{\nu N}$ can be understood as a measure for the effective $\nu\nu qq$ coupling in ν-DIS processes [22]. It has been measured experimentally by the CCFR collaboration at

Fermilab; cf. Ref. [23]. In Eq. (3.19) C_L^q, C_R^q, C_L^δ and C_R^δ represent weight factors that depend on the specific experimental setup; according to GAPP C_L^q and C_R^q are of order $\mathcal{O}(1)$, C_L^δ and C_R^δ of order $\mathcal{O}\left(10^{-2}\right)$.

However, the actual observables of interest in the context of ν-DIS experiments are the ratios R_ν and $R_{\bar{\nu}}$ of the neutral-to-charged current cross sections which we denote by $\sigma_{\nu N}^{\mathrm{NC}}$ and $\sigma_{\nu N}^{\mathrm{CC}}$ in the case of neutrinos and by $\sigma_{\bar{\nu}N}^{\mathrm{NC}}$ and $\sigma_{\bar{\nu}N}^{\mathrm{CC}}$ in the case of anti-neutrinos. By construction many theoretical uncertainties cancel in R_ν and $R_{\bar{\nu}}$. For that reason it is these quantities that many ν-DIS experiments are interested in. In the lowest-order approximation we may write:

$$R_\nu \equiv \frac{\sigma_{\nu N}^{\mathrm{NC}}}{\sigma_{\nu N}^{\mathrm{CC}}} \equiv \left(g_L^{\nu N}\right)^2 + \left(g_R^{\nu N}\right)^2 r \quad ; \quad R_{\bar{\nu}} \equiv \frac{\sigma_{\bar{\nu}N}^{\mathrm{NC}}}{\sigma_{\bar{\nu}N}^{\mathrm{CC}}} \equiv \left(g_L^{\nu N}\right)^2 + \frac{1}{r}\left(g_R^{\nu N}\right)^2 \tag{3.20}$$

$r \equiv \sigma_{\bar{\nu}N}^{\mathrm{CC}}/\sigma_{\nu N}^{\mathrm{CC}}$ denotes the ratio of the charged current cross sections $\sigma_{\bar{\nu}N}^{\mathrm{CC}}$ and $\sigma_{\nu N}^{\mathrm{CC}}$ and can be measured directly. R_ν and $R_{\bar{\nu}}$ complete the set of neutrino-nucleon scattering observables that we will use in our fit analysis.

$$\boxed{\left(g_L^{\nu N}\right)^2 \;,\; \left(g_R^{\nu N}\right)^2 \;,\; \kappa^{\nu N} \;,\; R_\nu \;,\; R_{\bar{\nu}}}$$

The expressions for R_ν and $R_{\bar{\nu}}$ in Eq. (3.20) involve the ratio r that we do not have a handle on. However, this does not represent a problem. In practice, R_ν and $R_{\bar{\nu}}$ are usually written as linear combinations of $\varepsilon_L(q)$ and $\varepsilon_R(q)$:

$$\begin{aligned} R_\nu &= (1-\delta)\left[a_L(u)\varepsilon_L^2(u) + a_L(d)\varepsilon_L^2(d) + a_R(u)\varepsilon_R^2(u) + a_R(u)\varepsilon_R^2(d)\right] \\ R_{\bar{\nu}} &= \left(1-\bar{\delta}\right)\left[\bar{a}_L(u)\varepsilon_L^2(u) + \bar{a}_L(d)\varepsilon_L^2(d) + \bar{a}_R(u)\varepsilon_R^2(u) + \bar{a}_R(u)\varepsilon_R^2(d)\right] \end{aligned}$$

The advantage of this notation is that it clearly separates experimental from theoretical influences on R_ν and $R_{\bar{\nu}}$. While the coefficients δ, $\bar{\delta}$, $a_{L,R}(q)$ and $\bar{a}_{L,R}(q)$

are fixed by the conditions under which the experiment is carried out the theoretical details are entirely incorporated into $\varepsilon_L(q)$ and $\varepsilon_R(q)$. Higher-order corrections to R_ν and $R_{\bar{\nu}}$ only apply to $\varepsilon_L(q)$ and $\varepsilon_R(q)$; the coefficients are always the same. The values of δ, $\bar{\delta}$, $a_{L,R}(q)$ and $\bar{a}_{L,R}(q)$ for the various ν-DIS experiments are implemented in the GAPP code. Our task will be to derive $\varepsilon_L(q)$ and $\varepsilon_R(q)$ in our $G(221)$ models.

Neutrino-Electron Scattering Not only the scattering of neutrinos off nucleons but also off electrons can be probed in low-energy measurements. The most precise data on neutrino-electron scattering comes from the CHARM II [24] experiment at CERN that utilized muon neutrinos and anti-neutrinos. In the theoretical description of the CHARM II measurements we only need to consider the Lagrangian $\mathscr{L}_{4f}^{\mathrm{NC},\nu e}$ that takes care of neutral current interactions. $\mathscr{L}_{4f}^{\mathrm{NC},\nu e}$ is identical to the Lagrangian $\mathscr{L}_{4f}^{\mathrm{NC},\nu N}$ that accounts for neutral current neutrino-hadron interactions, see Eq. (3.18), except for the fact that it involves electrons instead of quarks:

$$\mathscr{L}_{4f}^{\mathrm{NC},\nu e} = -\frac{G_F}{\sqrt{2}}(\bar{\nu}\nu)_{L,\mu}\left[\varepsilon_L(e)(\bar{e}e)_L^\mu + \varepsilon_R(e)(\bar{e}e)_R^\mu\right] \tag{3.21}$$

In the case of scattering of electron neutrinos ν_e off electrons also the charged interaction Lagrangian $\mathscr{L}_{4f}^{\mathrm{CC},\nu e}$ has to be included.

$$\mathscr{L}_{4f}^{\mathrm{CC},\nu e} \equiv -\frac{G_F}{\sqrt{2}}\left[(\bar{e}\nu_e)_{L,\mu}(\bar{e}e)_L^\mu + (\bar{\nu}_e e)_{L,\mu}(\bar{e}e)_L^\mu\right] + \mathscr{L}_{\mathrm{NP},4f}^{\mathrm{CC},\nu e}$$

However, the physically relevant information is again entirely contained in the coefficients $\varepsilon_L(e)$ and $\varepsilon_R(e)$ of the four-fermion operators of the neutral current Lagrangian. Just as in the hadronic case these two coefficients are used to define the effective four-fermion couplings. Instead of employing left- and right-handed couplings one usually formulates the neutrino-electron interaction in terms of vector and axial couplings $g_V^{\nu e}$ and $g_A^{\nu e}$:

$$g_V^{\nu e} \equiv \varepsilon_R(e) + \varepsilon_L(e) \quad ; \quad g_A^{\nu e} \equiv \varepsilon_R(e) - \varepsilon_L(e)$$

$\mathscr{L}_{4f}^{\mathrm{NC},\nu e}$ can then equivalently be written as:

$$\mathscr{L}_{4f}^{\mathrm{NC},\nu e} = -\frac{G_F}{\sqrt{2}}(\bar{\nu}\nu)_{L,\mu}\left[g_V^{\nu e}(\bar{e}e)_V^{\mu} + g_A^{\nu e}(\bar{e}e)_A^{\mu}\right]$$

The observables that are typically measured in the experiment are the total cross sections $\sigma_{\nu e}^{\mathrm{NC}}$ and $\sigma_{\bar{\nu}e}^{\mathrm{NC}}$ or their ratio $\sigma_{\nu e}^{\mathrm{NC}}/\sigma_{\bar{\nu}e}^{\mathrm{NC}}$. In the limit of large incident neutrino energies, $E_\nu \gg m_e$, the cross sections are given as:

$$\sigma_{\nu e}^{\mathrm{NC}} = \frac{G_F^2 m_e E_\nu}{2\pi}\left[\left(g_V^{\nu e} + g_A^{\nu e}\right)^2 + \frac{1}{3}\left(g_V^{\nu e} - g_A^{\nu e}\right)^2\right]$$
$$\sigma_{\bar{\nu}e}^{\mathrm{NC}} = \frac{G_F^2 m_e E_\nu}{2\pi}\left[\left(g_V^{\nu e} - g_A^{\nu e}\right)^2 + \frac{1}{3}\left(g_V^{\nu e} + g_A^{\nu e}\right)^2\right]$$

If the scattering of electron neutrinos ν_e is studied the contribution from the charged current interactions must be considered as well. Effectively, the corresponding cross sections $\sigma_{\nu e}$ and $\sigma_{\bar{\nu}e}$ are obtained by substituting $g_{V,A}^{\nu e} + 1$ for $g_{V,A}^{\nu e}$ in $\sigma_{\nu e}^{\mathrm{NC}}$ and $\sigma_{\bar{\nu}e}^{\mathrm{NC}}$. We do not have to care about these details as the experimental results are usually boiled down to the fundamental couplings $g_V^{\nu e}$ and $g_A^{\nu e}$. In our fit analysis with GAPP these two couplings will be the only observables related to neutrino-electron scattering:

$$\boxed{\boxed{g_V^{\nu e} \quad , \quad g_A^{\nu e}}}$$

Parity Violating Processes: The interaction of charged leptons with other charged fermions is dominated by the Coulomb force. For the most part it is described by the QED Lagrangian $\mathscr{L}_{\mathrm{QED}} = L_f^{0,\mu} A_\mu$, see Eq. (3.5), in which the fermion current $L_f^{0,\mu}$ has a vector structure. Taking the product of $L_f^{0,\mu}$ with the vector field A^μ results

in a scalar Lagrangian $\mathscr{L}_{\mathrm{QED}}$. QED processes are therefore invariant under parity inversion. However, the electroweak force as we know it from the SM has a V-A structure resulting in maximal parity violation. New physics effects may introduce V+A interactions softening the extent of parity violation. But as they will always be suppressed at low energies parity violation is an intrinsic property of the electroweak force below the scale of new physics.

Since the detection of parity violation in the mid 1950's [25] many experiments were devoted to the investigation of parity-violating interactions in electroweak processes. The related observables that we will consider in our analysis originate from three different measurements: The observation of atomic parity violation (APV), the study of left-right asymmetries in Møller scattering [26] and the analysis of deep inelastic electron scattering on nuclear targets. APV and electron-hadron scattering experiments probe parity-violating interactions between electrons and the quarks in atomic nuclei. In the case of APV it is the atomic electrons that interact with the nucleons in the core. e-DIS experiments feature free electrons beams. The Møller scattering experiments examine electron-electron instead of electron-hadron interactions.

To account for the parity violation in these experiments one introduces the weak vector charge Q_W. In the description of APV experiments the electroweak physics is accommodated in the weak charge $Q_W\left({}^{A}\mathrm{Z}\right)$ of the isotope under study where Z and A denote atomic charge and mass number respectively. In this work we will consider the weak charges of cesium-133 and thallium-205. Møller scattering experiments allow to extract the weak charge of the electron $Q_W(e)$.

To understand what is meant by $Q_W\left({}^{A}\mathrm{Z}\right)$ we first have to define the weak vector charge $Q_W(q)$ at the quark level. In a first step we introduce the Lagrangian $\mathscr{L}_{4f}^{\mathrm{NC},eq}$ that incorporates the parity-violating contributions to the effective quark-electron interactions below the electroweak scale:

$$\mathscr{L}_{4f}^{\mathrm{NC},eq} \equiv -\frac{G_F}{\sqrt{2}} \sum_q \left[C_{1q} \left(\bar{e}e\right)_{A,\mu} \left(\bar{q}q\right)_V^\mu + C_{2q} \left(\bar{e}e\right)_{V,\mu} \left(\bar{q}q\right)_A^\mu \right] \tag{3.22}$$

The coefficients C_{1f} and C_{2f} in this Lagrangian play a similar role as $\varepsilon_L(q)$ and $\varepsilon_R(q)$ in $\mathscr{L}_{4f}^{\mathrm{NC},\nu N}$ or $g_V^{\nu e}$ and $g_A^{\nu e}$ in $\mathscr{L}_{4f}^{\mathrm{NC},\nu e}$. We will focus on them when it comes to calculating the new physics corrections in Subsec. 3.2.2. Since $\mathscr{L}_{4f}^{\mathrm{NC},eq}$ mixes vectorial with axial fermion products, that is, parity-odd with parity-even terms, it transforms as a pseudoscalar under parity transformations — hence the parity violation in the quark-electron interactions. The general idea behind $Q_W(q)$ is to mimic the parametrization of the QED vector current $L_q^{0,\mu}$ in terms of the electric charge $Q_e(q)$. If we define $Q_W(q)$ as:

$$Q_W(q) \equiv 2 \cdot C_{1q}$$

we can rewrite the SM tree-level expression for the electroweak neutral current $J_q^{0,\mu}$ as follows:

$$J_{\mathrm{SM},q,\mu}^0 Z^\mu \equiv \frac{e}{s_{\theta_{\mathrm{SM}}} c_{\theta_{\mathrm{SM}}}} \left| g_{A,\mathrm{SM}}^Z(q) \right| \cdot \left[Q_{W,\mathrm{SM}}(q) \left(\bar{q}q\right)_{V,\mu} \pm \left(\bar{q}q\right)_{A,\mu} \right] Z^\mu$$

The comparison of this form of the neutral current with the one given in Eq. (3.11) allows us to relate $Q_{W,\mathrm{SM}}(q)$ to the vector and axial couplings $g_{V,\mathrm{SM}}^Z(q)$ and $g_{A,\mathrm{SM}}^Z(q)$:

$$Q_{W,\mathrm{SM}}(q) = \frac{g_{V,\mathrm{SM}}^Z(q)}{\left| g_{A,\mathrm{SM}}^Z(q) \right|}$$

By convention $Q_{W,\mathrm{SM}}(q)$ is normalized such that the prefactor of the axial part in $J_{q,\mathrm{SM}}^{0,\mu}$ has an absolute value of 1. The sign of the axial component is given by the sign of $g_{A,\mathrm{SM}}^Z(q)$. As we now know how the weak charges of the up and the down

quark are defined we can write down the weak charges of composite particles. The weak charges of the nucleons, the proton p and the neutron n, are given as:

$$Q_W(p) \equiv 2Q_W(u) + Q_W(d) \quad ; \quad Q_W(n) \equiv Q_W(u) + 2Q_W(d)$$

Equipped with these basic charges we are able to calculate the weak charge $Q_W\left({}^A\mathrm{Z}\right)$ of an atomic nucleus consisting of Z protons and $N = A - Z$ neutrons:

$$Q_W\left({}^A\mathrm{Z}\right) \equiv Z \cdot Q_W(p) + N \cdot Q_W(n) = 2 \cdot [(Z + A) \cdot C_{1u} + (2A - Z) \cdot C_{1d}]$$

To take care of parity-violating interactions in electron-electron scattering processes we introduce the pseudoscalar Lagrangian $\mathscr{L}_{4f}^{\mathrm{NC},ee}$:

$$\mathscr{L}_{4f}^{\mathrm{NC},ee} = -\frac{G_F}{\sqrt{2}} \cdot C_{1e}(\bar{e}e)_{A,\mu}(\bar{e}e)_V^{\mu} \tag{3.23}$$

In analogy to $Q_W(q)$ the weak charge of the electron is essentially given by the coupling constant C_{1e}:

$$Q_W(e) \equiv 2 \cdot C_{1e}$$

Finally, it is possible to extract certain linear combinations of the coupling coefficients C_{1u} and C_{1d} from polarized electron-hadron scattering data. In our global fit analysis we will use the values for the linear combinations $\mathcal{C}_1$ and $\mathcal{C}_2$ that were determined experimentally by Young et al. [27]:

$$\mathcal{C}_1 \equiv 9 \cdot C_{1u} + 4 \cdot C_{1d} \quad ; \quad \mathcal{C}_2 \equiv -4 \cdot C_{1u} + 9 \cdot C_{1d}$$

In summary, the included observables related to parity-violating processes present

themselves as follows:

$$\boxed{Q_W\left(^{133}\mathrm{Cs}\right) \quad , \quad Q_W\left(^{205}\mathrm{Tl}\right) \quad , \quad Q_W(e) \quad , \quad C_1 \quad , \quad C_2}$$

Lifetime of the tau lepton: Lastly, we can extract the lifetime τ_τ of the tau τ from the effective four-fermion Lagrangian $\mathscr{L}_{4f}$.

$$\boxed{\tau_\tau}$$

The derivation of τ_τ in the effective theory below the electroweak scale follows exactly the same steps as the computation of the lifetime τ_μ of the muon; cf. our discussion of τ_μ, Fermi's constant G_F and the electroweak VEV $\tilde{v}$ in Subsec. 3.1.2. There is, however, one detail that we have to pay attention to in repeating the calculation of τ_μ: The τ lepton might couple differently to the currents $K^{\pm,\mu}$ than the fermions to which it decays. In the UU-D model this caveat applies to the hadronic decay modes of the τ; in the NU-D model — as the τ belonging to the third fermion generation only decays to first and second generation fermions — the final state couplings always differ from the initial state couplings. Deriving τ_μ we did not have to worry about this subtleness since we were only dealing with purely leptonic decays within the first two fermion generations, $\mu^- \to e^- + \nu_\mu + \bar{\nu}_e$.

Although these differences are of theoretical interest as they illustrate the different features of the respective models they are of no practical importance to our analysis. Just as in Subsec. 3.1.2 it turns out that the fermion couplings to the new physics currents $K^{\pm,\mu}$ do not contribute to the tau lifetime τ_τ once we discard all terms that are of order $\mathscr{O}\left(\tilde{x}^{-2}\right)$. In the lowest-order approximation we thus find for τ_τ:

$$\tau_\tau^{-1} = G_F^2 \cdot \frac{m_\tau^5}{192\pi^3}$$

Given the heavy mass of the τ we also include the leading-order correction to the tree-level result into our expression for τ_τ:

$$\tau_\tau^{-1} = G_F^2 \cdot \frac{m_\tau^5}{192\pi^3} \left[1 + 3 \left(\frac{m_\tau^2}{M_W^2} \right)^{1/5} \right] \tag{3.24}$$

3.2.2 New Physics Corrections

The aim of this work is to examine the leading-order effects of new physics in the $G(221)$ models. Calculating the new physics corrections to the SM predictions we will therefore only work at tree-level. For a given electroweak observable $\mathcal{O}$ that we want to include into our fit analysis the GAPP code already knows the SM tree-level expression $\mathcal{O}_{\rm SM}^{\rm tree}$. The task that is left to us is to calculate the corresponding expression $\mathcal{O}_{\rm NP}^{\rm tree}$ in our $G(221)$ models. Consequently, the dominating effects of new physics, $\Delta\mathcal{O}^{\rm tree}$, are reflected in the deviation of $\mathcal{O}_{\rm NP}^{\rm tree}$ from $\mathcal{O}_{\rm SM}^{\rm tree}$:

$$\Delta\mathcal{O}^{\rm tree} \equiv \mathcal{O}_{\rm NP}^{\rm tree} - \mathcal{O}_{\rm SM}^{\rm tree} \tag{3.25}$$

In this and the next subsection we will calculate $\Delta\mathcal{O}^{\rm tree}$ for all fundamental observables, that is, all observables that cannot be constructed from other basic observables. The computation of the secondary observables will then be taken care of by GAPP. We will organize our discussion in the same way as our overview of the included observables in Subsec. 3.2.1. First, we will revisit the Lagrangian $\mathscr{L}_{\rm ew.}$. Subsequently, we will concentrate our attention to the low-energy data.

Corrections to the high-energy observables

Z pole data: All Z pole observables can be formulated either in terms of the partial decay widths $\Gamma_Z\left(f\bar{f}\right)$ or the polarization asymmetries $A_{LR}(f)$. It therefore suffices to only calculate the corrections to these two quantities. All other Z pole observables will then be covered automatically. We obtain $\Delta\Gamma_Z(f)$ and $\Delta A_{LR}(f)$ by comparing the SM expressions $\Gamma_{Z,\rm SM}(f\bar{f})$ and $A_{LR,\rm SM}(f)$ with their equivalents in the $G(221)$

models. According to Eqs. (3.10) and (3.12) we may write:

$$\begin{aligned}
\Gamma_{Z,\mathrm{SM}}(f\bar{f}) &= \frac{n_c(f)}{3}\cdot\frac{M_Z\alpha}{s^2_{\theta_{\mathrm{SM}}}c^2_{\theta_{\mathrm{SM}}}}\left(\left[g^Z_{V,\mathrm{SM}}(f)\right]^2+\left[g^Z_{A,\mathrm{SM}}(f)\right]^2\right)\\
A_{LR,\mathrm{SM}}(f) &= \frac{\left[g^Z_{L,\mathrm{SM}}(f)\right]^2-\left[g^Z_{R,\mathrm{SM}}(f)\right]^2}{\left[g^Z_{L,\mathrm{SM}}(f)\right]^2+\left[g^Z_{R,\mathrm{SM}}(f)\right]^2} \qquad (3.26)\\
\Gamma_Z\left(f\bar{f}\right) &= \frac{n_c(f)}{3}\cdot\frac{M_Z\alpha}{s^2_{\tilde{\theta}}c^2_{\tilde{\theta}}}\left(\left[\tilde{g}^Z_V(f)\right]^2+\left[\tilde{g}^Z_A(f)\right]^2\right)\\
A_{LR}(f) &= \frac{\left[\tilde{g}^Z_L(f)\right]^2-\left[\tilde{g}^Z_R(f)\right]^2}{\left[\tilde{g}^Z_L(f)\right]^2+\left[\tilde{g}^Z_R(f)\right]^2} \qquad (3.27)
\end{aligned}$$

The fermionic couplings to the Z boson play a key role for both observables. In a first step towards $\Delta\Gamma_Z(f)$ and $\Delta A_{LR}(f)$ we therefore focus on these couplings. The SM gives the following expressions for $g^Z_{L,\mathrm{SM}}(f)$, $g^Z_{R,\mathrm{SM}}(f)$, $g^Z_{V,\mathrm{SM}}(f)$ and $g^Z_{A,\mathrm{SM}}(f)$:

$$g^Z_{L,\mathrm{SM}}(f)=T^3_L(f)-s^2_{\theta_{\mathrm{SM}}}Q_e(f) \quad ; \quad g^Z_{R,\mathrm{SM}}(f)=-s^2_{\theta_{\mathrm{SM}}}Q_e(f) \qquad (3.28)$$

$$g^Z_{V,\mathrm{SM}}(f)=\frac{1}{2}T^3_L(f)-s^2_{\theta_{\mathrm{SM}}}Q_e(f) \quad ; \quad g^Z_{V,\mathrm{SM}}(f)=-\frac{1}{2}T^3_L(f) \qquad (3.29)$$

In our $G(221)$ models two effects lead to deviations from the SM couplings. First of all, $\tilde{g}^Z_L(f)$, $\tilde{g}^Z_R(f)$, $\tilde{g}^Z_V(f)$ and $\tilde{g}^Z_A(f)$ depend on the model parameters rather than on the SM parameters. We gave a detailed discussion of the shifts in the respective parameters in Sec. 3.1. Anyway, if this were the only difference the $G(221)$ couplings would still have the same form as the SM expressions; compare with the result for the electroweak neutral current $J^{0,\mu}_f$ in Eq. (2.17). The second effect that we have to consider is the mixing of the $\hat{Z}$ boson with the new heavy $\hat{Z}'$ in the electroweak theory. At the electroweak scale the Z couples effectively to the fermion current $J^{0,\mu}_{\mathrm{ew.}}$,

see Eq. (2.25), that also involves the new physics current $K^{0,\mu}$. The shifts in the model parameters as well as the explicit form of $K^{0,\mu}$ are model-dependent which is why we cannot state universal results for the fermion couplings to the Z boson that apply likewise to all $G(221)$ models. What the couplings in the different models, however, do have in common is that they all reduce to the SM expressions in the limit $\tilde{x} \to \infty$:

$$\tilde{g}_L^Z(f) \equiv g_{L,\mathrm{SM}}^Z(f) + \delta g_L^Z(f) \quad ; \quad \tilde{g}_R^Z(f) \equiv g_{R,\mathrm{SM}}^Z(f) + \delta g_R^Z(f) \tag{3.30}$$

$$\tilde{g}_V^Z(f) \equiv g_{V,\mathrm{SM}}^Z(f) + \delta g_V^Z(f) \quad ; \quad \tilde{g}_A^Z(f) \equiv g_{A,\mathrm{SM}}^Z(f) + \delta g_A^Z(f) \tag{3.31}$$

The deviations $\delta g_L^Z(f)$, $\delta g_R^Z(f)$, $\delta g_V^Z(f)$ and $\delta g_A^Z(f)$ can be expanded in inverse powers of $\tilde{x}$ with the lowest-order terms being proportional to $\frac{1}{\tilde{x}}$. As hitherto we will only keep these contributions and neglect higher orders. Tab. 3.2 summarizes our results for $\delta g_L^Z(f)$, $\delta g_R^Z(f)$; in Tab. 3.3 we present our results for $\delta g_V^Z(f)$ and $\delta g_A^Z(f)$. To get an impression of the values behind the left- and right handed couplings $g_L^Z(f)$ and $g_R^Z(f)$ for the different fermions f in the different $G(221)$ models we numerically evaluate the expressions that we derived in this subsection; see Tabs. D.1 to D.11 in the appendix. The experimental input values that were employed to generate these tables are given in Subsec A.1.

The deviations $\delta g_L^Z(f)$ and $\delta g_R^Z(f)$ in the left- and right-handed couplings enable us to calculate the corrections $\Delta A_{LR}(f)$ to the polarization asymmetries. $\delta g_V^Z(f)$ and $\delta g_A^Z(f)$ allow us to write down the shifts $\Delta\Gamma_Z(f)$ in the partial decay widths. With the aid of Eqs. (3.7), (3.8) and (3.9) we obtain the following results for $\Delta\Gamma_Z(f)$:

	$\tilde{x}\delta g_L^Z(f)$
(BP-I,D)	$f(\theta_{\rm SM})\left(c_{\tilde{\phi}}^4 - s_{2\tilde{\beta}}^2\right) Q_e(f) + s_{\tilde{\phi}}^2 c_{\tilde{\phi}}^2 \left[T_L^3(f) - Q_e(f)\right]$
(BP-I,T)	$f(\theta_{\rm SM})\left(\frac{1}{4}c_{\tilde{\phi}}^4 - \frac{1}{2}s_{2\tilde{\beta}}^2\right) Q_e(f) + \frac{1}{4}s_{\tilde{\phi}}^2 c_{\tilde{\phi}}^2 \left[T_L^3(f) - Q_e(f)\right]$
(BP-II,D)	$f(\theta_{\rm SM}) \cdot s_{\tilde{\phi}}^4 Q_e(f) + s_{\tilde{\phi}}^2 \left[c_{\tilde{\phi}}^2 T_1^3(f) - s_{\tilde{\phi}}^2 T_2^3(f)\right]$

	$\tilde{x}\delta g_R^Z(f)$
(BP-I,D)	$f(\theta_{\rm SM})\left(c_{\tilde{\phi}}^4 - s_{2\tilde{\beta}}^2\right) Q_e(f) + s_{\tilde{\phi}}^2 c_{\tilde{\phi}}^2 \left[T_2^3(f) - Q_e(f)\right] + c_{\tilde{\phi}}^4 T_2^3(f)$
(BP-I,T)	$f(\theta_{\rm SM})\left(\frac{1}{4}c_{\tilde{\phi}}^4 - \frac{1}{2}s_{2\tilde{\beta}}^2\right) Q_e(f) + \frac{1}{4}s_{\tilde{\phi}}^2 c_{\tilde{\phi}}^2 \left[T_2^3(f) - Q_e(f)\right] + \frac{1}{4}c_{\tilde{\phi}}^4 T_2^3(f)$
(BP-II,D)	$f(\theta_{\rm SM}) \cdot s_{\tilde{\phi}}^4 Q_e(f)$

Table 3.2: Shifts $\delta g_L^Z(f)$ and $\delta g_R^Z(f)$ in the left- and right-handed couplings $g_L^Z(f)$ and $g_R^Z(f)$ of the fermions to the Z boson — compare also with Tabs. D.1 to D.11 in Subsec. D.1.1. The function $f(\theta_{\rm SM})$ is given as $f(\theta_{\rm SM}) \equiv s_{\theta_{\rm SM}}^2 c_{\theta_{\rm SM}}^2 / \left(c_{\theta_{\rm SM}}^2 - s_{\theta_{\rm SM}}^2\right)$.

	$\tilde{x}\delta g_V^Z(f)$
(BP-I,D)	$f(\theta_{\rm SM})\left(c_{\tilde{\phi}}^4 - s_{2\tilde{\beta}}^2\right) Q_e(f)$ $+\frac{1}{2}s_{\tilde{\phi}}^2 c_{\tilde{\phi}}^2 \left[T_L^3(f) + T_2^3(f) - 2Q_e(f)\right] + \frac{1}{2}c_{\tilde{\phi}}^4 T_2^3(f)$
(BP-I,T)	$f(\theta_{\rm SM})\left(\frac{1}{4}c_{\tilde{\phi}}^4 - \frac{1}{2}s_{2\tilde{\beta}}^2\right) Q_e(f)$ $+\frac{1}{8}s_{\tilde{\phi}}^2 c_{\tilde{\phi}}^2 \left[T_L^3(f) + T_2^3(f) - 2Q_e(f)\right] + \frac{1}{8}c_{\tilde{\phi}}^4 T_2^3(f)$
(BP-II,D)	$f(\theta_{\rm SM}) \cdot s_{\tilde{\phi}}^4 Q_e(f) + \frac{1}{2}s_{\tilde{\phi}}^2 \left[c_{\tilde{\phi}}^2 T_1^3(f) - s_{\tilde{\phi}}^2 T_2^3(f)\right]$

	$\tilde{x}\delta g_A^Z(f)$
(BP-I,D)	$\frac{1}{2}s_{\tilde{\phi}}^2 c_{\tilde{\phi}}^2 \left[T_2^3(f) - T_L^3(f)\right] + \frac{1}{2}c_{\tilde{\phi}}^4 T_2^3(f)$
(BP-I,T)	$\frac{1}{8}s_{\tilde{\phi}}^2 c_{\tilde{\phi}}^2 \left[T_2^3(f) - T_L^3(f)\right] + \frac{1}{8}c_{\tilde{\phi}}^4 T_2^3(f)$
(BP-II,D)	$-\frac{1}{2}s_{\tilde{\phi}}^2 \left[c_{\tilde{\phi}}^2 T_1^3(f) - s_{\tilde{\phi}}^2 T_2^3(f)\right]$

Table 3.3: Shifts $\delta g_V^Z(f)$ and $\delta g_A^Z(f)$ in the vector and axial couplings $g_V^Z(f)$ and $g_A^Z(f)$ of the fermions to the Z boson. The function $f(\theta_{\rm SM})$ is given as $f(\theta_{\rm SM}) \equiv s_{\theta_{\rm SM}}^2 c_{\theta_{\rm SM}}^2 / \left(c_{\theta_{\rm SM}}^2 - s_{\theta_{\rm SM}}^2\right)$.

$$\text{(BP-I,D):}\quad \Delta\Gamma_Z(f) = \frac{n_c(f)}{3}\cdot\frac{M_Z\alpha}{s^2_{\theta_{\rm SM}}c^2_{\theta_{\rm SM}}}\Big\{2g^Z_{V,\rm SM}(f)\delta g^Z_V(f)+2g^Z_{A,\rm SM}(f)\delta g^Z_A(f)$$
$$+\frac{1}{\tilde{x}}\left(\left[g^Z_{V,\rm SM}(f)\right]^2+\left[g^Z_{A,\rm SM}(f)\right]^2\right)\left(c^4_{\tilde{\theta}}-s^2_{2\tilde{\beta}}\right)\Big\} \qquad (3.32)$$

$$\text{(BP-I,T):}\quad \Delta\Gamma_Z(f) = \frac{n_c(f)}{3}\cdot\frac{M_Z\alpha}{s^2_{\theta_{\rm SM}}c^2_{\theta_{\rm SM}}}\Big\{2g^Z_{V,\rm SM}(f)\delta g^Z_V(f)+2g^Z_{A,\rm SM}(f)\delta g^Z_A(f)$$
$$+\frac{1}{\tilde{x}}\left(\left[g^Z_{V,\rm SM}(f)\right]^2+\left[g^Z_{A,\rm SM}(f)\right]^2\right)\left(\frac{1}{4}c^4_{\tilde{\theta}}-\frac{1}{2}s^2_{2\tilde{\beta}}\right)\Big\} \qquad (3.33)$$

$$\text{(BP-II,D):}\quad \Delta\Gamma_Z(f) = \frac{n_c(f)}{3}\cdot\frac{M_Z\alpha}{s^2_{\theta_{\rm SM}}c^2_{\theta_{\rm SM}}}\Big\{2g^Z_{V,\rm SM}(f)\delta g^Z_V(f)+2g^Z_{A,\rm SM}(f)\delta g^Z_A(f)$$
$$+\frac{1}{\tilde{x}}\left(\left[g^Z_{V,\rm SM}(f)\right]^2+\left[g^Z_{A,\rm SM}(f)\right]^2\right)s^4_{\tilde{\phi}}\Big\} \qquad (3.34)$$

In Eqs. (3.32), (3.33) and (3.34) we present the corrections $\Delta\Gamma_Z(f)$ to the partial decay widths in a compact form. To obtain the actual expressions that we will implement in the GAPP code we still need to replace the couplings $g^Z_{V,\rm SM}(f)$ and $g^Z_{A,\rm SM}(f)$ and the deviations $\delta g^Z_V(f)$ and $\delta g^Z_A(f)$ by the terms that are given in Eq. (3.29) and Tab. 3.3 respectively. As these expressions will turn out to be rather cumbersome and as they will not yield further insight into the physics behind the corrections $\Delta\Gamma_Z(f)$ we do not present them here. This argument applies to all new physics corrections that we are going to discuss in this and the next subsection. In each case we will only show as many steps of the respective calculations as necessary to illustrate our procedure. However, notice that we will still employ the corrections $\Delta\Gamma_Z(f)$ as an example for the modification of the GAPP code in Subsec 3.3.2.

Making use of Eqs. (3.26), (3.27), (3.30), (3.31) we obtain the following expression for the corrections $\Delta A_{LR}(f)$ to the left-right asymmetries:

$$\Delta A_{LR}(f) = 4g^Z_{L,\rm SM}(f)g^Z_{R,\rm SM}(f)\frac{g^Z_{R,\rm SM}(f)\delta g^Z_R(f)-g^Z_{L,\rm SM}(f)\delta g^Z_L(f)}{\left(\left[g^Z_{L,\rm SM}(f)\right]^2+\left[g^Z_{R,\rm SM}(f)\right]^2\right)^2}$$

Our results for $\Delta\Gamma_Z(f)$ and $\Delta A_{LR}(f)$ is everything we need to implement the shifts in the Z pole observables in the GAPP code. We can now proceed with the width Γ_W and the mass M_W of the $W^\pm$ boson.

$W^\pm$ pole data: According to Eqs. (3.15) and (3.16) we need the mass M_W of the $W^\pm$ first before we can calculate its width. In the SM the tree-level expression for M_W is given as:

$$M_{W,\mathrm{SM}} = c_{\theta_{\mathrm{SM}}} \cdot M_Z = \frac{\sqrt{\pi\alpha}v_{\mathrm{SM}}}{s_{\theta_{\mathrm{SM}}}}$$

To obtain ΔM_W we simply have to consult our results for M_W^2 listed in Tab. 2.6, express M_0^2 in terms of the standard and fit parameters, take the square root and substract $M_{W,\mathrm{SM}}$. These steps result in:

$$\begin{aligned}
\text{(BP-I,D):}\quad \Delta M_W/M_{W,\mathrm{SM}} &= \frac{1}{2\tilde{x}} \cdot \frac{c^2_{\theta_{\mathrm{SM}}}}{c^2_{\theta_{\mathrm{SM}}} - s^2_{\theta_{\mathrm{SM}}}} \left(c^4_{\tilde{\phi}} - s^2_{2\tilde{\beta}}\right) \\
\text{(BP-I,T):}\quad \Delta M_W/M_{W,\mathrm{SM}} &= \frac{1}{2\tilde{x}} \cdot \frac{c^2_{\theta_{\mathrm{SM}}}}{c^2_{\theta_{\mathrm{SM}}} - s^2_{\theta_{\mathrm{SM}}}} \left(\frac{1}{4}c^4_{\tilde{\phi}} - \frac{1}{2}s^2_{2\tilde{\beta}}\right) \\
\text{(BP-II,D):}\quad \Delta M_W/M_{W,\mathrm{SM}} &= \frac{1}{2\tilde{x}} \cdot \frac{s^2_{\theta_{\mathrm{SM}}}}{c^2_{\theta_{\mathrm{SM}}} - s^2_{\theta_{\mathrm{SM}}}} s^4_{\tilde{\phi}}
\end{aligned}$$

In the SM the left-handed coupling $g^W_{L,\mathrm{SM}}(f)$ of a fermion f to the $W^\pm$ boson is just given by the gauge coupling $g_{L,\mathrm{SM}}$ of the left-handed $SU(2)_L$. The SM partial decay widths $\Gamma_{W,\mathrm{SM}}(f)$ can therefore be written as:

$$\Gamma_{W,\mathrm{SM}}(f) = n_c(f) \cdot \frac{g^2_{L,\mathrm{SM}}}{48\pi} M_{W,\mathrm{SM}}$$

In the $G(221)$ models that belong to the first breaking pattern the right-handed

	$\tilde{x}\delta g_L^W(f)/g_{L,\mathrm{SM}}$
(BP-I,D)	$\frac{1}{2}f(\theta_{\mathrm{SM}})\left(c_{\tilde{\phi}}^4 - s_{2\tilde{\beta}}^2\right)$
(BP-I,T)	$\frac{1}{2}f(\theta_{\mathrm{SM}})\left(\frac{1}{4}c_{\tilde{\phi}}^4 - \frac{1}{2}s_{2\tilde{\beta}}^2\right)$
(BP-II,D)	$\frac{1}{2}f(\theta_{\mathrm{SM}})\, s_{\tilde{\phi}}^4 + 2s_{\tilde{\phi}}^2\left[c_{\tilde{\phi}}^2 T_1(f) - s_{\tilde{\phi}}^2 T_2(f)\right]$

Table 3.4: Shifts $\delta g_L^W(f)$ in the left-handed coupling $g_L^W(f)$ of the fermions to the $W^\pm$ boson. The function $f(\theta_{\mathrm{SM}})$ is given as $f(\theta_{\mathrm{SM}}) \equiv c_{\theta_{\mathrm{SM}}}^2 / \left(c_{\theta_{\mathrm{SM}}}^2 - s_{\theta_{\mathrm{SM}}}^2\right)$.

couplings $g_R^W(f)$ are suppressed by $\frac{1}{\tilde{x}}$ which is why we do not have to consider them in the $W^\pm$ width. The left-handed couplings unchangeably correspond to the $SU(2)_L$ gauge coupling $\tilde{g}_L$. As for the second breaking pattern the fermion coupling is purely left-handed and the mixing between the $\hat{W}^\pm$ and the $\hat{W}'^\pm$ introduces a shift in $g_R^W(f)$. Our result for the charged fermion current $J_{\mathrm{ew.}}^{\pm,\mu}$ in Eq. (2.25) leads us to:

$$\begin{aligned} \text{BP-I:} \quad & g_L^W(f) = \tilde{g}_L \\ \text{BP-II:} \quad & g_L^W(f) = \tilde{g}_L\left(1 + \frac{2}{\tilde{x}}s_{\tilde{\phi}}^2\left[c_{\tilde{\phi}}^2 T_1(f) - s_{\tilde{\phi}}^2 T_2(f)\right]\right) \end{aligned}$$

In a last step we take into account the deviation of $\tilde{g}_L$ from its SM analog $g_{L,\mathrm{SM}}$ due to the shift in the electroweak mixing angle. Doing so we obtain the corrections $\delta g_L^W(f)$ to the left-handed fermion couplings $g_L^W(f)$, see Tab. 3.4.

$$g_L^W(f) \equiv g_{L,\mathrm{SM}}^W(f) + \delta g_L^W(f) \equiv g_{L,\mathrm{SM}} + \delta g_L^W(f)$$

With the results for $\delta g_L^W(f)$ at hand we can write down the shifts $\Delta\Gamma_W(f)$ in the

partial $W^{\pm}$ widths $\Gamma_W(f)$:

$$\Delta\Gamma_W(f) = \frac{n_c(f)}{48\pi}\left(2g_{L,\mathrm{SM}}\delta g_L^W(f)M_{W,\mathrm{SM}} + g_{L,\mathrm{SM}}^2\Delta M_W\right)$$

Corrections to the Low-Energy Observables

Neutrino Scattering and Parity Violation All of our observables that are extracted from either ν-DIS, Møller scattering, e-DIS, or APV experiments can be traced back to the couplings in the effective four-fermion Lagrangian $\mathscr{L}_{4\mathrm{f}}$. In the case of neutrino-hadron scattering the left- and right handed quark couplings $\varepsilon_L(q)$ and $\varepsilon_R(q)$ are the quantities of interest, see Eq. (3.18), to calculate the vector and axial electron couplings $g_V^{\nu e}$ and $g_A^{\nu e}$ in neutrino-electron scattering we need the coefficients $\varepsilon_L(e)$ and $\varepsilon_R(e)$, see Eq. (3.21), and to obtain the weak charges of atomic nuclei, $Q_W\left({}^A\mathrm{Z}\right)$, and the electron, $Q_W(e)$, we have to know the couplings C_{1q} and C_{1e}, see Eqs. (3.22) and (3.23). Because of these similarities we can address the corrections to most of the low-energy observables in one go. Only the calculation of the shift in the τ lifetime has to be taken care of separately; we will discuss $\Delta\tau_\tau$ in the next subsection.

Before we turn to the new physics corrections we still have to hand in the SM expressions for the effective four-fermion couplings that are involved in our analysis. One finds for the couplings $\varepsilon_{L,\mathrm{SM}}(f)$ and $\varepsilon_{R,\mathrm{SM}}(f)$ of a charged fermion f — an up or down quark or an electron in our case - to the neutrino:

$$\varepsilon_{L,\mathrm{SM}}(f) = 2g_{L,\mathrm{SM}}^Z(\nu)g_{L,\mathrm{SM}}^Z(f) \quad ; \quad \varepsilon_{R,\mathrm{SM}}(f) = 2g_{L,\mathrm{SM}}^Z(\nu)g_{R,\mathrm{SM}}^Z(f) \quad ; \quad f \in \{u,d,e\}$$

The couplings $g_{L,\mathrm{SM}}^Z(f)$ and $g_{R,\mathrm{SM}}^Z(f)$ are given explicitly in Eq. (3.28). With $T_L^3(\nu) =$

$\frac{1}{2}$ and $Q_e(\nu) = 0$ we obtain:

$$\varepsilon_{L,\mathrm{SM}}(f) = g^Z_{L,\mathrm{SM}}(f) = T^3_L(f) - s^2_{\theta_{\mathrm{SM}}} Q(f) \quad ; \quad \varepsilon_{R,\mathrm{SM}}(f) = g^Z_{R,\mathrm{SM}}(f) = -s^2_{\theta_{\mathrm{SM}}} Q(f)$$

The corresponding couplings $C_{1q,\mathrm{SM}}$ and $C_{1e,\mathrm{SM}}$ in electron-quark and electron-electron interactions are very similar to these results. We find:

$$C_{1f,\mathrm{SM}} = 8 g^Z_{A,\mathrm{SM}}(e) g^Z_{V,\mathrm{SM}}(f) \quad ; \quad f \in \{u, d, e\}$$

In accordance with Eq. (3.29) and using $T^3_L = -\frac{1}{2}$ we rewrite $C_{1f,\mathrm{SM}}$ as:

$$C_{1f,\mathrm{SM}} = T^3_L(f) - 2 s^2_{\theta_{\mathrm{SM}}} Q_e(f)$$

In the next step we calculate the corrections to these expressions. Most of the work has already been done. We derived the effective four-fermion Lagrangian $\mathscr{L}_{4f}$ in Subsec. 2.3.3. The fermion currents and the boson masses that constitute $\mathscr{L}_{4f}$ were the subject of the discussion throughout the entire second chapter. Now we reap the fruits of our labor. Instead of only calculating those couplings in terms of which our observables are defined we perform a general analysis and compute all effective four-fermion couplings. First, we write the neutral and charged current components of $\mathscr{L}_{4f}$ as follows:

$$\mathscr{L}^{\mathrm{NC}}_{4f} \equiv -\frac{G_F}{\sqrt{2}} \sum_{f_1, f_2} \sum_{i,j} C^{\mathrm{NC}}_{4f} \left(f_{1,i}, f_{2,j}\right) \left(\bar{f}_1 f_1\right)_{i,\mu} \left(\bar{f}_2 f_2\right)^{\mu}_{j}$$

$$\mathscr{L}^{\mathrm{CC}}_{4f} \equiv -\frac{G_F}{\sqrt{2}} \sum_{f_1, f_3} \sum_{i,j} C^{\mathrm{CC}}_{4f} \left(f_{1,i}, f_{3,j}\right) \left(\bar{f}_1 f_2\right)_{i,\mu} \left(\bar{f}_3 f_4\right)^{\mu}_{j}$$

The fermion sums run over up and down quarks, neutrinos and electrons, $f \in \{u, d, \nu, e\}$ and i and j denote the chirality of the respective fermions, $i, j \in \{L, R\}$.

The fermion pairs (f_1, f_2) and (f_3, f_4) in $\mathscr{L}_{4f}^{\rm CC}$ represent iso-doublets under either of the two $SU(2)$s in our models.

Similarly, we can rewrite the effective four-fermion interactions $\mathscr{L}_{\rm ew.}^{KK}$ in the Lagrangian at the electroweak scale $\mathscr{L}_{\rm ew.}$: We separate $\mathscr{L}_{\rm ew.}^{KK}$ into neutral and charged current contributions, compare with Eq. (2.26),

$$\mathscr{L}_{\rm ew.}^{KK} \equiv \mathscr{L}_{\rm ew.}^{NC} + \mathscr{L}_{\rm ew.}^{CC}$$

and define the coupling coefficients $C_{ew.}^{\rm NC}\left(f_{1,i}, f_{2,j}\right)$ and $C_{ew.}^{\rm CC}\left(f_{1,i}, f_{3,j}\right)$ such that $\mathscr{L}_{ew.}^{\rm NC}$ and $\mathscr{L}_{ew.}^{\rm CC}$ turn into:

$$\mathscr{L}_{ew.}^{\rm NC} \equiv -\frac{G_F}{\sqrt{2}} \sum_{f_1,f_2} \sum_{i,j} C_{ew.}^{\rm NC}\left(f_{1,i}, f_{2,j}\right) \left(\bar{f}_1 f_1\right)_{i,\mu} \left(\bar{f}_2 f_2\right)_j^{\mu} \qquad ; i,j = L,R$$

$$\mathscr{L}_{ew.}^{\rm CC} \equiv -\frac{G_F}{\sqrt{2}} \sum_{f_1,f_3} \sum_{i,j} C_{ew.}^{\rm CC}\left(f_{1,i}, f_{3,j}\right) \left(\bar{f}_1 f_2\right)_{i,\mu} \left(\bar{f}_3 f_4\right)_j^{\mu} \qquad ; i,j = L,R$$

The couplings in $\mathscr{L}_{ew.}^{\rm NC}$ and $\mathscr{L}_{ew.}^{\rm CC}$ do not directly appear in the definitions of our low-energy observables, but contribute indirectly to them as they are integrated in the low-energy couplings $C_{4f}^{\rm NC}\left(f_{1,i}, f_{2,j}\right)$ and $C_{4f}^{\rm CC}\left(f_{1,i}, f_{3,j}\right)$. Besides that they are also important in their own right as they represent major consequences of the new physics in the $G(221)$ models at the electroweak scale. We therefore do not restrict our analysis to the four-fermion interactions in $\mathscr{L}_{4f}$, but also examine the couplings in $\mathscr{L}_{ew.}^{\rm KK}$.

We obtain $C_{ew.}^{\rm NC}\left(f_{1,i}, f_{2,j}\right)$, $C_{ew.}^{\rm CC}\left(f_{1,i}, f_{3,j}\right)$, $C_{4f}^{\rm NC}\left(f_{1,i}, f_{2,j}\right)$ and $C_{4f}^{\rm CC}\left(f_{1,i}, f_{3,j}\right)$ from the Lagrangians $\mathscr{L}_{ew.}$ and $\mathscr{L}_{4f}$ in Eqs. (2.24) and (2.27) by inserting our results for the effective fermion currents and boson masses and trading the model parameters that we are not going to fit for the standard parameters. Inserting the experimental values for the reference observables provides us with numerical results which we

present in the appendix – see Tabs. D.13 to D.22 for $C_{ew.}^{\mathrm{NC}}\left(f_{1,i}, f_{2,j}\right)$, Tabs. D.23 to D.26 for $C_{ew.}^{\mathrm{CC}}\left(f_{1,i}, f_{3,j}\right)$, Tabs. D.27 to D.36 for $C_{4f}^{\mathrm{NC}}\left(f_{1,i}, f_{2,j}\right)$ and Tabs. D.37 to D.45 for $C_{4f}^{\mathrm{CC}}\left(f_{1,i}, f_{3,j}\right)$.

Finally, we remark that the modification of the GAPP code requires the analytical expressions for the four-fermion couplings. As the explicit results are rather lengthy we, however, do not present them here.

Lifetime of the Tau Calculating the corrections to the τ lifetime turns out to be trivial: The only quantity in our expression for τ_τ that receives a shift is the mass M_W of the $W^\pm$ boson; compare with Eq. (3.24). We can immediately write down the leading-order shift $\Delta\tau_\tau^{-1}$ as:

$$\Delta\tau_\tau^{-1} = G_F^2 \cdot \frac{m_\tau^5}{192\pi^3} \cdot 3 \left(\frac{m_\tau^2}{M_{W,\mathrm{SM}}^2}\right)^{1/5} \cdot \left(-\frac{2}{5} \cdot \frac{\Delta M_W}{M_{W,\mathrm{SM}}}\right)$$

Notice that the corrections to τ_τ only emerge from the subleading term in Eq. (3.24). $\Delta\tau_\tau^{-1}$ is consequently suppressed by the ratio of the mass of the τ to the SM mass of the $W^\pm$ boson which is why we expect the shift in the τ lifetime to play only a minor role in our global fit analysis.

3.3 Numerical Analysis

With the calculation of the corrections to our 37 observables we have completed the analytical part of our study. Now we are ready to determine the bounds on our new physics parameters numerically with GAPP. In this section we will give a short introduction to GAPP, say how the code has to modified in order to accommodate the $G(221)$ model and discuss how we actually run it. For the moment we focus on the technical details of our fit analysis – the results that we obtain are presented in the next chapter.

3.3.1 Introduction to GAPP

GAPP, short for *Global Analysis of Particle Properties*, is a Fortran package developed by J. Erler that allows to perform precision tests of the SM and to determine its fundamental parameters. For this work J. Erler kindly provided us with the most recent GAPP version which is up-to-date as of 2009. GAPP is written in such a way that extensions of the SM can be easily accommodated in the code: The default version of GAPP already comes with the option to examine various models beyond the SM that feature a Z' as a new heavy gauge boson; in this work we utilize GAPP to test our $G(221)$ models.

At its core GAPP calculates the deviation of the theoretical predictions for the various precision observables from the experimental data in terms of chi-square, χ^2:

$$\chi^2 \equiv \sum_i \mathcal{P}_i^2 \equiv \sum_i \frac{1}{\sigma_i^2} \left(\bar{\mathcal{O}}_i^{\text{exp.}} - \mathcal{O}_i^{\text{theo.}} \right)^2$$

Here $\bar{\mathcal{O}}_i^{\text{exp.}}$ stands for the central value, σ_i for the total uncertainty of the experimental result; $\mathcal{O}_i^{\text{exp.}} = \bar{\mathcal{O}}_i^{\text{exp.}} \pm \sigma_i$. σ_i subsumes the experimental errors as well as the theoretical uncertainties that affect the interpretation of the experimental data. The individual contributions to χ^2 from the different observables, also called the pulls, are denoted with $\mathcal{P}_i$.

Confronting a given theoretical model with experimental data χ^2 is a measure for the agreement between theory and experiment -- the larger the value of χ^2 the less likely is it that the physics underlying the experiment is described by the considered model. In other words: If χ^2 takes a too large value one can conclude that the testes model is ruled out by the experiment. On the other hand, if one assumes that a given theory represents the correct description of the experiment, χ^2 can be employed to determine or constrain the values of the parameters in the examined model. In this case χ^2 is regarded as a function of the model parameters; those parameter values for

which χ^2 takes a minimum value are considered to be the best estimate for the true values.

The calculation and minimization of χ^2 is the actual purpose of GAPP. In order to find the smallest possible χ^2 value it employs the minimization program MINUIT [28] that is included in the CERN program library. MINIUT can either be initialized by external data or it can directly be driven by Fortran subroutine calls. The current version of GAPP runs MINUIT in the data-driven mode. This means for us that the fit parameters have to be defined in an external data file. In this file, called `smfit.dat` in the default GAPP version, each parameter is assigned a number, a name, a starting value and a starting step size. Additionally, one is able to set bounds on the ranges in which the respective fit parameters are allowed to vary during the minimization. In the same file MINIUT is given all the commands that specify which actions it is supposed to perform. In our analysis we will either use GAPP to calculate χ^2 for a given set of parameter values or to find the minimum value of χ^2. Accordingly, we will either just give a simple `return` command to MINUIT or feed it with the commands `minimize`, `improve` and `seek`.

MINUIT always requires a Fortran subroutine that calculates the value of the function of interest. In the case of GAPP this subroutine is called `fcn` and located in the file `chi2.f`. Before χ^2 is calculated `fcn` defines certain constants, initializes the quantum numbers of the fermions and sets flags that trigger the inclusion of various higher-order corrections. Subsequently, it calls the Fortran function `chi2` that is contained in the same file and that takes care of the calculation of χ^2. `chi2` stores the experimental values and errors, calls the different subroutines that compute the theoretical predictions, calculates the pulls and finally determines χ^2. Once `chi2` has returned the χ^2 value to `fcn` any final computations are processed. Depending on how the flags were set by the user the likelihood $\mathcal{L} \sim \exp\left(-\chi^2/2\right)$ corresponding to the calculated χ^2 value might be determined or the results of the computation might

	File	Subroutines	Observables
Z pole data	`lep100.f`	`z0pole`	$\Gamma_Z(f\bar{f})$, $A_{LR}(f)$
$W^{\pm}$ pole data	`sin2th.f`	`sin2thetaw`	M_W
	`wwidth.f`	`wwprod`	$\Gamma_W(f)$
νN scattering	`dis.f`	`nuh`	$\varepsilon_L(q)$, $\varepsilon_R(q)$
νe scattering	`nue.f`	`nue`	$g_V^{\nu e}$, $g_A^{\nu e}$
PV processes	`pnc.f`	`apv`	C_{1q}
	"	`moller`	$Q_W(e)$
τ lifetime	`taulife.f`	`taulifetime`	τ_τ^{-1}

Table 3.5: Overview of the modified GAPP files — the subroutines in these files compute the SM quantities for which we have calculated the $G(221)$ corrections in Subsec 3.2.2. Once we have implemented the new physics shifts into these files the values for the electroweak observables calculated by GAPP will automatically represent the predictions of our $G(221)$ models.

be written to an output file.

In Subsec. 3.2.2 we calculated the new physics corrections to a variety of fundamental quantities with which all of our observables can be constructed. These quantities are calculated by GAPP in seven different Fortran files; see Tab. 3.5. Setting up the GAPP code such that we can fit our $G(221)$ models we will have to modify these files. The calculation of the observables will then be taken care of by GAPP.

3.3.2 Modification of the Code

In order to implement our $G(221)$ models into the GAPP code three modifications are basically necessary: The new physics fit parameters have to be defined in the input file that drives the fit, the additional quantum numbers of the fermions have

to be provided to the function `fcn` and the corrections to the observables have to be added to the SM expressions in the respective Fortran files. In the following we will comment on each of these modifications. As the inclusion of the new quantum numbers represents the simplest step we allude to it first.

Additional Quantum Numbers

In the models belonging to the first breaking pattern we have to introduce two new quantum numbers: The third component $T_2^3(f)$ of the $SU(2)_2$ isospin $\vec{T}_2(f)$ and the charge $X(f)$ under the $U(1)_X$ gauge group. As $X(f)$ may be depend on the chirality of the fermion f it effectively represents two quantum numbers: $X_L(f)$ and $X_R(f)$, the charges of the left- and right-handed versions of f. The models of the second breaking pattern do without the introduction of new quantum numbers: $T_1^3(f)$ and $T_2^3(f)$ correspond to the weak isospin quantum number $T_L^3(f)$; $X(f)$ is identical to the weak hypercharge $Y(f)$.

We take care of the different charge assignments by creating for each model a Fortran file (`sm.f`, `lr-d.f`, `hp-d.f`, ..., `nu-d.f`) in which we specify the numerical values of the new quantum numbers $T_2^3(f)$, $X_L(f)$ and $X_R(f)$. In the SM, the UU-D and the NU-D model these quantum numbers are set to zero for all fermions. Within the function `fcn` we import these files using the Fortran command `include`.

Fit Parameters

In Subsec. 2.3.1 we came to the conclusion that the new physics corrections to the electroweak observables are best parametrized in terms of $\tilde{x}$, $\tilde{\phi}$ and, in the case of breaking pattern one, $\tilde{\beta}$. As this is certainly true, we will, however, not give these three parameters as direct input to MINUIT. In analyzes like ours one usually chooses fit parameters that are defined on the whole real axis. Additionally, we consider it natural to define the fit parameter such that they reflect the structure of the fitted

analytical expressions as well as possible. Instead of $\tilde{x}$, $\tilde{\phi}$ and $\tilde{\beta}$ we therefore let GAPP scan over $\ln\tilde{x}$, $t^2_{\tilde{\phi}}$ and $s^2_{2\tilde{\beta}}$:

$$\left\{\tilde{x}, \tilde{\phi}, \tilde{\beta}\right\} \quad \rightarrow \quad \left\{\ln\tilde{x}, t^2_{\tilde{\phi}}, s^2_{2\tilde{\beta}}\right\}$$

The advantage of $\ln\tilde{x}$ and $t^2_{\tilde{\phi}}$ over $\tilde{x}$ and $\tilde{\phi}$ is that both functions range over the whole real axis. $s^2_{2\tilde{\beta}}$ takes, of course, only values between 0 and 1. Essentially in every expression that depends on $\tilde{\beta}$ it, however, appears in the form $s^2_{2\tilde{\beta}}$. Every other choice would therefore be unnatural.

Moreover, $t^2_{\tilde{\phi}}$ represents a convenient compromise between two functions, $c^2_{\tilde{\phi}}$ and $s^2_{\tilde{\phi}}$, that are particularly important in the two breaking patterns that we are considering. Due to the different definition of the mixing angle $\tilde{\phi}$ in both breaking patterns it is either $c^2_{\tilde{\phi}}$ or $s^2_{\tilde{\phi}}$ that appears all over in the analytical expressions describing the respective $G(221)$ models; see for example the $\frac{1}{\tilde{x}}$ contributions to the Z mass in Tab. 2.5 that are either proportional to $c^4_{\tilde{\phi}}$ or $s^4_{\tilde{\phi}}$. It is this difference in the expressions for M_Z that leads to the different shifts in $s^2_{\tilde{\theta}}$ in the first and second breaking pattern; compare with the calculation in Subsec. 3.1.2. In the end, all these distinctions can be traced back to the fundamental relation of the $SU(2)_2$ coupling $\tilde{g}_2$ to the mixing angle $\tilde{\phi}$:

$$\text{BP-I:} \quad \frac{\tilde{g}_2}{\sqrt{\tilde{g}_2^2 + \tilde{g}_X^2}} = c_{\tilde{\phi}} \quad ; \quad \text{BP-II:} \quad \frac{\tilde{g}_2}{\sqrt{\tilde{g}_1^2 + \tilde{g}_2^2}} = s_{\tilde{\phi}}$$

Having decided for $\ln\tilde{x}$, $t^2_{\tilde{\phi}}$ and $s^2_{2\tilde{\beta}}$ as fit parameters we include them in the GAPP input file. To prevent GAPP from scanning unphysical parameter values or values that we are not interested in we set bound on the ranges over which our parameters are allowed to vary:

$$\text{BP-I:}\quad \ln\tilde{x}\in[0.00,10.00]\quad;\quad t^2_{\tilde{\phi}}\in[0.01,100.00]\quad;\quad s^2_{2\tilde{\beta}}\in[0.00,1.00] \tag{3.35}$$

$$\text{BP-II:}\quad \ln\tilde{x}\in[0.00,10.00]\quad;\quad t^2_{\tilde{\phi}}\in[0.03,30.00] \tag{3.36}$$

If $\ln\tilde{x}$ becomes very large the new physics in our $G(221)$ models decouples from the energy scale of the SM and thereby from the physics that is essential to the electroweak observables. At large values of $\ln\tilde{x}$ we will therefore not be able to discriminate between our $G(221)$ models which is why we set an upper bound of $\ln\tilde{x}_{\text{max}}=10$ on $\ln\tilde{x}$. The bounds on $t^2_{\tilde{\phi}}$ originate from the intrinsic structure of our $G(221)$ models and the condition that perturbativity must not be violated: Depending on the breaking pattern $t_{\tilde{\phi}}$ is either defined in terms of $\tilde{g}_X$ and $\tilde{g}_2$ or $\tilde{g}_1$ and $\tilde{g}_2$, see Eq. (2.3). In both cases the gauge couplings cannot take arbitrary values as they are related to the electroweak couplings $\tilde{g}_L$ and $\tilde{g}_Y$, compare with Eqs. (2.4) and (2.6), which are constrained by the experiment. Using the experimental data listed in Appendix A.1 we find that $g_{L,\text{SM}}$ and $g_{Y,\text{SM}}$ take approximately the following values in the SM:

$$g_{L,\text{SM}}=\frac{e}{s_{\theta_{\text{SM}}}}\approx 0.626\quad;\quad g_{Y,\text{SM}}=\frac{e}{c_{\theta_{\text{SM}}}}\approx 0.346$$

These numbers represent lower bounds on $\tilde{g}_1$, $\tilde{g}_2$ and $\tilde{g}_X$, $\tilde{g}_2$ respectively:

$$\text{BP-I:}\quad \tilde{g}_X,\tilde{g}_2>g_{Y,\text{SM}}\quad;\quad \text{BP-II:}\quad \tilde{g}_1,\tilde{g}_2>g_{L,\text{SM}}$$

Our $G(221)$ models are perturbative quantum field theories in which the typical expansion parameters are given as $\alpha_1\equiv\tilde{g}_1^2/4\pi$, $\alpha_2\equiv\tilde{g}_2^2/4\pi$ and $\alpha_X\equiv\tilde{g}_X^2/4\pi$. To ensure the validity of perturbation theory all three parameters must be smaller than 1. This places an upper constraints on $\tilde{g}_1$, $\tilde{g}_2$ and $\tilde{g}_X$.

$$\tilde{g}_1, \tilde{g}_2, \tilde{g}_X < \sqrt{4\pi}$$

Combining both arguments and putting the numerical values into Eqs. (2.3), (2.4) and (2.6) we are able to roughly estimate the bounds on $t^2_{\tilde{\phi}}$; see Eqs. (3.35) and (3.36). We expect that for high $\tilde{x}$ values changes in $t^2_{\tilde{\phi}}$ will be irrelevant to the calculation of the observables. Setting limits on the allowed range of $t^2_{\tilde{\phi}}$ therefore does not only take care of the mentioned theoretical constraints but also avoids the risk of GAPP getting lost during the minimization of χ^2 while it scans over always higher $t^2_{\tilde{\phi}}$ values.

Fitting the $G(221)$ models to the electroweak observables we will also allow the $\overline{\text{MS}}$ mass of the top quark $\bar{m}_t$, see appendix B, and the mass of the SM Higgs boson M_H to float. In doing so we will see how much of an effect the new physics in our $G(221)$ model has on these crucial SM parameters. Especially we are interested in the question whether the considered extensions to the SM are consistent with larger masses of the Higgs or whether they constrain M_H to similar values as the SM. In order to find the minimum value of χ^2 in the respective models we will thus let GAPP vary five parameters.

$$\boxed{\ln \tilde{x} \quad , \quad t^2_{\tilde{\phi}} \quad , \quad s^2_{2\tilde{\beta}} \quad , \quad \bar{m}_t \quad , \quad M_H}$$

When it comes to scanning the parameter space of the new physics parameters we will fix $\bar{m}_t$ and M_H at their respective best fit values.

New Physics Corrections

In Subsec. 3.2.2 we calculated the new physics corrections $\Delta\mathcal{O}^{\text{tree}}$ to the electroweak observables $\mathcal{O}$ at tree-level. After providing GAPP with the new quantum numbers of the fermions and the definition of the fit parameters we now are ready to implement the results of our calculations into the GAPP code. The crucial question in this context is where to put our expressions for $\Delta\mathcal{O}^{\text{tree}}$. In the case of some observables

the GAPP code is structured in the best possible way from our perspective: First GAPP computes the tree-level expression $\mathcal{O}_{\text{SM}}^{\text{tree}}$, higher-order corrections $\mathcal{O}_{\text{SM}}^{\text{HO}} = \mathcal{O}_{\text{SM}}^{\text{1-loop}} + \mathcal{O}_{\text{SM}}^{\text{2-loop}} + ...$ are calculated subsequently and successively added to the tree-level result.

$$\mathcal{O}_{\text{SM}} = \mathcal{O}_{\text{SM}}^{\text{tree}} + \mathcal{O}_{\text{SM}}^{\text{1-loop}} + \mathcal{O}_{\text{SM}}^{\text{2-loop}} + ...$$

When then just have to add $\Delta\mathcal{O}^{\text{tree}}$ to $\mathcal{O}_{\text{SM}}^{\text{tree}}$ in order to get the theoretical prediction $\mathcal{O}_{\text{NP}}$ of our new physics models.

$$\mathcal{O}_{\text{NP}} \approx \left(\mathcal{O}_{\text{SM}}^{\text{tree}} + \Delta\mathcal{O}^{\text{tree}}\right) + \mathcal{O}_{\text{SM}}^{\text{1-loop}} + \mathcal{O}_{\text{SM}}^{\text{2-loop}} + ... \tag{3.37}$$

However, in other cases the pure tree-level SM expressions are not accessible in the code. GAPP might start the calculation of $\mathcal{O}_{\text{SM}}$ using quantities that already contain higher-order terms right from the beginning. $\mathcal{O}_{\text{SM}}$ would then be initialized by some approximation that is constructed from tree-level as well as loop terms $\mathcal{O}_{\text{SM}}^{(\text{tree,HO})}$. Moreover, GAPP might also include higher-order contributions multiplicatively instead of just adding them to $\mathcal{O}_{\text{SM}}$:

$$\mathcal{O}_{\text{SM}} = \mathcal{O}_{\text{SM}}^{\text{tree}} \cdot \left(1 + \mathcal{O}_{\text{SM}}^{\text{1-loop}}/\mathcal{O}_{\text{SM}}^{\text{tree}}\right) \cdot (1 + ...)$$

In any case, no matter how GAPP calculates $\mathcal{O}_{\text{SM}}$, we stick to the procedure illustrated in Eq. (3.37). As early as possible after their initialization we modify the individual SM quantities in the GAPP code. Doing so will introduce mixing terms in the calculation of some observables that we actually do not want to include into our analysis. For instance we will get products of our new physics corrections $\Delta\mathcal{O}^{\text{tree}}$ with SM loop terms. However, all terms that we introduce unintentionally are small and can be neglected:

$$\Delta\mathcal{O}^{\text{tree}} \cdot \mathcal{O}_{\text{SM}}^{\text{1-loop}} \approx \Delta\mathcal{O}^{\text{tree}} \cdot \mathcal{O}_{\text{SM}}^{\text{2-loop}} \approx \ldots \approx 0$$

According to the general comments made in this subsection we now implement our results for $\Delta\mathcal{O}^{\text{tree}}$ in the respective Fortran files, see Tab. 3.5. The shifts in the electroweak observables differ from model to model. We take care of that by introducing a switch variable `modtype` in the Fortran code that allows to respectively include only those new physics corrections that correspond to the model that is being fitted. Implementing the corrections in that way gives a modular structure to our modification. Once the code is set up for one specific class of $G(221)$ models it is easy to add the corrections for all other models. The extension of GAPP by further models that are similar to our $G(221)$ models should be accomplishable without much effort.

3.3.3 Fitting and Scanning the Models

Finally, GAPP is configured in such a way that we can run it and examine the compatibility of our $G(221)$ models with the electroweak precision data. Two tasks are on our agenda: First, we will let GAPP minimize χ^2 for each model. These *model fits* will tell us which values for the new physics parameters and which masses for the top quark and the Higgs boson are most preferred by the data. Subsequently, we will scan the parameter space of the new physics parameters in the respective models. Based on these *model scans* will be able to identify the parameter values that are still consistent with the data.

Minimization of χ^2: For each model we determine the smallest possible value $\chi^2_{\text{min.}}$ of χ^2. In order to find $\chi^2_{\text{min.}}$ we let GAPP vary five parameters: $\ln\tilde{x}$, $t^2_{\tilde{\phi}}$, $s^2_{2\tilde{\beta}}$, $\bar{m}_t$ and M_H. This first step is trivial as it just requires a simple call to MINUIT. The

	$n=1$	$n=2$	$n=3$
$\Delta\chi^2\,(95\%, n)$	3.84146	5.99146	7.81473

Table 3.6: Maximum allowed deviations $\Delta\chi^2$ from $\chi^2_{\text{min.}}$ at 95% CL for one, two or three free model parameters — at these values of χ^2 the cumulative distribution function $F\left(\chi^2, n\right)$ of the χ^2 distribution with n degrees of freedom takes the value $F\left(\chi^2, n\right) = 0.95$.

results of this first numerical analysis are presented in Subsec. 4.1.1. See especially Tabs. 4.1 and 4.2 and Figs. 4.1 and 4.2.

Constraints on the new physics parameters: In our second analysis we fix $\bar{m}_t$ and M_H at their respective best fit values and focus exclusively on the bounds on the new physics parameters. The criterion by which we decide whether a certain set of values for $\ln\tilde{x}$, $t^2_{\tilde{\phi}}$, $s^2_{2\tilde{\beta}}$ is viable and consistent with the data is the deviation $\Delta\chi^2$ in χ^2 from the respective minimum value $\chi^2_{\text{min.}}$. If χ^2 is larger than $\chi^2_{\text{ref.}} = \chi^2_{\text{min.}} + \Delta\chi^2$ for some parameter values we conclude that these values are ruled out by the data; all parameter values that yield a χ^2 smaller than $\chi^2_{\text{min.}} + \Delta\chi^2$ are still feasible.

$$\chi^2 < \chi^2_{\text{min.}} + \Delta\chi^2 \quad \Rightarrow \quad \text{Parameter values are allowed.}$$
$$\chi^2 > \chi^2_{\text{min.}} + \Delta\chi^2 \quad \Rightarrow \quad \text{Parameter values are ruled out.}$$

The choice of $\Delta\chi^2 = \Delta\chi^2\,(\text{CL}, n)$ depends on the desired confidence level CL and the number n of free model parameters. In this work we would like to describe the properties of the parameter space at a 95% CL. The models belonging to the first breaking pattern feature three, the models of the second breaking pattern two new physics parameters. In Subsec. 4.1.2 we will examine the M_H dependence of χ^2. In

that context we will need $\Delta\chi^2$ corresponding to one free parameter. We calculate $\Delta\chi^2\,(95\%, 1)$, $\Delta\chi^2\,(95\%, 2)$ and $\Delta\chi^2\,(95\%, 3)$ employing the cumulative distribution function $F\left(\chi^2, n\right)$ of the χ^2 distribution with n degrees of freedom and present the results in Tab. 3.6.

The points of interest in the parameter space are those where χ^2 falls below the threshold of $\chi^2_{\text{min.}} + \Delta\chi^2$ or where it becomes larger than $\chi^2_{\text{min.}} + \Delta\chi^2$. Together these points form the boundaries for the allowed regions in parameter space which represent the goal of our analysis. To find these points we let GAPP scan over a grid in parameter space and calculate χ^2 at each point. If χ^2 is larger (smaller) than $\chi^2_{\text{ref.}}$ at a given grid point and smaller (larger) than $\chi^2_{\text{ref.}}$ at the following grid point we lineally interpolate between the involved parameter values to find the values on the boundary between the allowed and forbidden regions.

Chapter 4

Results

Our global fit analysis provides us with a wealth of information about the $G(221)$ models under study. After we have given a detailed discussion of our numerical approach in the last chapter we now discuss our results and draw conclusions about the underlying physics.

First we will present the values of the fit parameters that minimize χ^2 in the individual models. These best fit values will give us an idea of the scale of the new physics in the $G(221)$ models and they will tell us which masses M_H of the Higgs boson are respectively most preferred by the data. As we will see M_H tends to take smaller values than in the SM for the models of the first breaking pattern and roughly the same value as in the SM for models of the second breaking pattern. To get bounds on M_H for all ten $G(221)$ models as well as for the SM we will plot χ^2 as a function of M_H. Doing so will allows us to read off those M_H values for which $\Delta\chi^2$ is smaller than $\Delta\chi^2(95\%, 1)$. To get a better understanding of the χ^2 plots we will also examine the pulls $\mathcal{P}_i$ of the electroweak observables for M_H either fixed at a very small or a very large value. The corresponding pull distributions will help us identify the observables that constrain M_H.

In the second step we will turn to our parameter scans and present the bounds

on the new physics parameters. Subsequently, we will translate the boundaries in parameter space to bounds on the masses of the new heavy gauge bosons. These results will show us which gauge boson masses are still consistent with the data and whether one could hope to detect the Z' and / or the $W'^{\pm}$ at the LHC. Again we will examine the pull distributions to identify those observables which drive the parameter plots. In a last section we will calculate the explicit numerical expressions for these important observables in the respective models and try to reconstruct the plots of the bounds in parameter space.

4.1 Fits to the Electroweak Data

4.1.1 Best Fit Values

In Subsec. 3.3.3 we described how we minimized χ^2 for the ten $G(221)$ models under consideration as well as for the SM by varying the values of $\ln \tilde{x}$, $t^2_{\tilde{\phi}}$, $s^2_{2\tilde{\beta}}$, M_H and $\bar{m}_t$. The results of that analysis are now presented in Tab. 4.1.

Inspecting Tab. 4.1 we make several interesting observations: First of all, we notice that the values of $\chi^2_{\text{min.}}$ for the $G(221)$ models are of the same order as for the SM. This finding tells us on the one hand that none of the $G(221)$ modles is ruled out by the data — all models yield reasonable $\chi^2_{\text{min.}}$ values that are comparable to the one of the SM. On the other hand we also see that our results in Tab. 4.1 prove once more how excellently the experimental data is described by the SM. Our $G(221)$ models can barely improve the SM value of $\chi^2_{\text{min.}}$; only in four models, the LP-D, LP-T, FP-D and the FP-T model, we obtain a slightly smaller value. The other four models that belong to the first breaking pattern yield approximately the same value as the SM; the UU-D and NU-D values of $\chi^2_{\text{min.}}$ are slightly higher. As we will see later it is not just by chance that the models of breaking pattern one split into two groups. The analysis of the pulls of the electroweak observables in Subsec. 4.2.2 will

reveal that the fits of the LP and the FP model and the fits of the LR and the HP are respectively driven by the same sets of observables.

Given the best fit values for $\tilde{x}$ it is, however, obvious why the minimum χ^2 values are so close to each other. The scale of the new physics in the $G(221)$ models is throughout very high. In all models $\tilde{x}$ is pushed to very large values resulting in a substantial suppression of the new physics corrections. It is a testament to the power of the SM that the experimental data apparently favors small up to negligible contributions from new physics. In none of the considered models the best fit value for $\tilde{x}$ is smaller than 160. In the case of the NU-D model we even reach the bound that we set on $\ln \tilde{x}$ — we demanded that $\ln \tilde{x}$ must not take values larger than $\ln \tilde{x} = 10$. With $\tilde{x} = 22026$ in the NU-D model we exactly reach that limit. This explains why we put a long dash (–) into the corresponding entry in Tab. 4.1. As the NU-D model apparantly favors neglible new physics corrections the best fit value for $t^2_{\tilde{\phi}}$ is meaningless as well.

In summary, we conclude: The smaller the deviation from the SM the better in agreement with the experiment are the predictions of the $G(221)$ models. This insight will help us in the further interpretation of our results. Especially, when we have come to discuss the bounds on the new physics parameters in Sec. 4.2 we will take the SM as the best description of the experimental data – the fact that some regions in parameter space are ruled out by the data can then be explained with the new physics corrections being too large in these regions.

Moreover, we find that the best fit value for $\tilde{x}$ in any (BP-I,T) model is always smaller than in the corresponding (BP-I,D) model. This relation is expected since choosing a triplet instead of a doublet representation for H in any model of the first breaking pattern leads to suppressing prefactors of the $c^4_{\tilde{\phi}}$ and $s^2_{2\tilde{\beta}}$ terms in the new physics corrections; see, e.g., Tab. 3.1. In (BP-I,T) models the $c^4_{\tilde{\phi}}$ contributions are always four times smaller than in the (BP-I,D) models. The $s^2_{2\tilde{\beta}}$ terms receive a

Model	$\chi^2_{\text{min.}}$	$\tilde{x}$	$t^2_{\tilde{\phi}}$	$s^2_{2\tilde{\beta}}$	$\bar{m}_t$ [GeV]	M_H [GeV]
SM	41.95	--	--	--	162.8	93.24
LR-D	42.46	2028	99.99	0.9998	162.8	72.33
LP-D	41.60	1055	100.0	0.5499	162.7	68.94
HP-D	42.24	641.9	100.0	0.3348	162.7	70.88
FP-D	41.09	812.9	64.05	0.4312	162.7	67.50
LR-T	42.44	997.1	99.95	0.9992	162.8	72.17
LP-T	41.60	263.8	100.0	0.2750	162.7	68.94
HP-T	42.24	160.5	100.0	0.1674	162.7	70.88
FP-T	41.09	203.1	64.72	0.2153	162.7	67.48
UU-D	43.16	318.6	0.03016	--	162.8	94.60
NU-D	43.34	--	--	--	162.8	93.48

Table 4.1: Best fit values of $\tilde{x}$, $t^2_{\tilde{\phi}}$, $s^2_{2\tilde{\beta}}$, M_H and $\bar{m}_t$ for all ten $G(221)$ models as well as for the SM — the bounds that were set on $\ln\tilde{x}$, $t^2_{\tilde{\phi}}$, $s^2_{2\tilde{\beta}}$ are given in Eqs. (3.35) and (3.36). In the case of the NU-D model $\tilde{x}$ reaches the maximum allowed value; the corresponding best fit $t^2_{\tilde{\phi}}$ value is thus meaningless.

prefactor of $\frac{1}{2}$. This effect will also be evident in the plots of the bounds on the new physics parameters: In Subsec. will see that the boundaries that separate allowed from forbidden regions in parameter space are always shifted to lower $\tilde{x}$ values if H is chosen to be a triplet.

In most models $t^2_{\tilde{\phi}}$ reaches either the lower or the upper bound that we set on that parameter. In the models of the first breaking pattern a high $t^2_{\tilde{\phi}}$ value seems to be preferred; in the models belonging to the second breaking pattern $t^2_{\tilde{\phi}}$ tends to take smaller values. Both observations lead us to the same conclusion: The experimental data can be best explained if the coupling $\tilde{g}_2$ of the second $SU(2)_2$ in the $G(221)$ gauge group is taken to be small – which is just another way of saying how successful the ansatz of the $SU(2)_L \otimes U(1)_Y$ gauge group in the SM is.

4.1.2 Higgs Mass Dependence

Another insight that we gain from Tab. 4.1 is that the $G(221)$ models prefer a Higgs mass M_H in the same range as the SM. The best fit values for M_H in the models of the first breaking pattern are smaller than the SM value by roughly 20 GeV. Our results for the second breaking pattern are almost identical to the SM value. Again we notice that the models belonging to breaking pattern one fall into two groups: The Higgs mass values of the LR and the HP models on the one hand and the results for the LP and the FP models on the other hand are respectively comparable to each other.

To get a better impression of how χ^2 depends on the mass of the Higgs boson we calculate χ^2 for values of M_H between 30 and 300 GeV in all $G(221)$ models and in the SM. Doing so we fix all other fit parameters at their best fit values such that the Higgs mass remains as the only free parameter. The results of that step are shown in Fig. 4.1. Since the Higgs mass always appears logarithmically in loop contributions to the electroweak observables, a quadratic dependence on $\ln(M_H)$ is expected if we

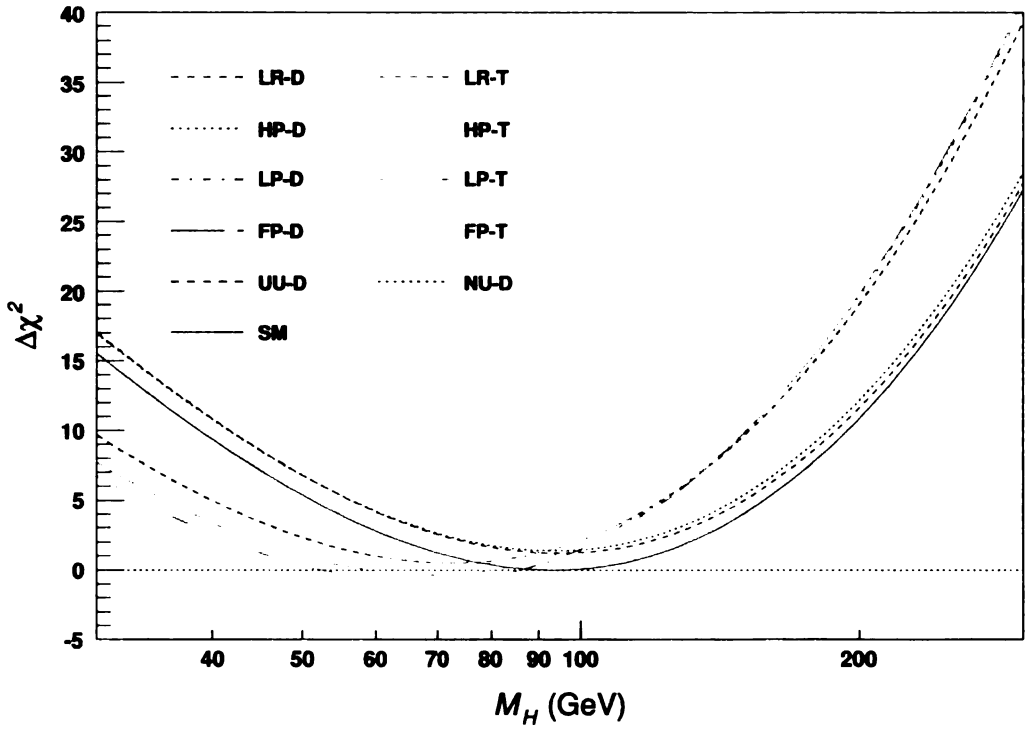

Figure 4.1: χ^2 in dependence of the Higgs mass M_H for all ten $G(221)$ models and the SM — the χ^2 curves of the (BP-I,D) models differ so little form the curves of the corresponding (BP-I,T) models that they are mostly covered by them. See Tab. 4.2 for the allowed ranges of the Higgs mass that we deduce from this plot.

expand χ^2 around its minimum value. For small deviations from $\chi^2_{\text{min.}}$ the plots in Fig. 4.1 certainly confirm this expectation.

Fig. 4.1 cannot only tell us the χ^2 value for a given Higgs mass but also help us to answer the reverse question: Which masses M_H correspond to a certain value of χ^2? According to our considerations in Subsec. 3.3.3 all values of M_H that correspond to a χ^2 smaller than $\chi^2_{\text{ref.}} = \chi^2_{\text{min.}} + \Delta\chi^2\,(95\%, 1)$ are consistent with the experimental data at 95% CL. We determine these allowed ranges of the Higgs mass for all $G(221)$ models as well as for the SM and present the results in Tab. 4.2.

We find that in none of the considered models M_H can be smaller than 38 GeV or much larger than 150 GeV. To find out which observables constrain the Higgs mass we perform two further fits with M_H being fixed at $M_H = 25\,\text{GeV}$ and $M_H = 250\,\text{GeV}$ respectively. During both finds we let GAPP vary $\ln\tilde{x}$, $t^2_{\tilde{\phi}}$, $s^2_{2\tilde{\beta}}$ and $\bar{m}_t$ to minimize χ^2. Proceeding in this way removes the dependence of the pulls on the new physics parameters and the top mass — we isolate the contributions from the Higgs mass. The pull distributions after our fits point onto three observables that significantly deviate from the measured values: For $M_H = 25\,\text{GeV}$ the forward-backward asymmetry of the bottom quark $A_{FB}(b)$ (observable № 17) contributes with a large pull to χ^2. If M_H is set to $M_H = 250\,\text{GeV}$, the theoretical predictions for the left-right asymmetry of the electron $A_{LR}(e)$ (observable № 21) and the $W^\pm$ mass M_W (observable № 29) are far off the experimental results.

The physically relevant observation is that the measurement of the $W^\pm$ mass constrains the allowed range for the Higgs mass. Such a correlation is expected as M_H enters the expression for M_W at the loop-level, in the SM as well as in our $G(221)$ models. In Fig. 4.1 we observe that the allowed M_H ranges of the BP-I models are shifted towards lower M_H values compared to the curves belonging to the SM and the BP-II models. In other words: The BP-I models prefer smaller Higgs masses than the SM or the BP-II models; compare with Tab. 4.2. A closer look at the new physics

Model	$M_H^{\text{low}}\,(\chi^2_{\text{ref.}})$ [GeV]	$M_H\,(\chi^2_{\text{min.}})$ [GeV]	$M_H^{\text{up}}\,(\chi^2_{\text{ref.}})$ [GeV]
SM	55.37	93.24	148.12
LR-D	41.91	72.33	117.76
LP-D	39.62	68.94	112.91
HP-D	40.94	70.88	115.64
FP-D	38.62	67.50	110.85
LR-T	41.80	72.17	117.47
LP-T	39.62	68.94	112.91
HP-T	40.94	70.88	115.64
FP-T	38.63	67.48	110.89
UU-D	56.17	94.60	150.30
NU-D	55.50	93.48	148.51

Table 4.2: Bounds on the Higgs mass M_H — M_H^{low} and M_H^{up} are those masses of the Higgs boson for which χ^2 takes the value $\chi^2_{\text{ref.}} = \chi^2_{\text{min.}} + \Delta\chi^2\,(95\%, 1)$. Therefore M_H^{low} represents a lower and M_H^{up} an upper bound on the Higgs masses that are consistent with the data. Note that the values of M_H for which the χ^2 curves in Fig. 4.1 reach their respective minima are identical to the best fit values given in Tab. 4.1.

corrections ΔM_W to the $W^\pm$ mass reveals why that is: In Tab. 4.5 in Subsec. 4.2.2 we present numerical expressions for the shift ΔM_W — plugging the best fit values for $c^2_{\tilde{\phi}}$ and $s^2_{2\tilde{\beta}}$ or $s^2_{\tilde{\phi}}$ respectively into our results for ΔM_W we notice that the $\tilde{\phi}$-dependent contributions are almost negligible: Consequently, ΔM_W is practically zero in the UU-D and NU-D models. In the models of the first breaking pattern the shift does not vanish; it is clearly dominated by the $s^2_{2\tilde{\beta}}$ term. The best fit M_H values in the BP-I models therefore differ from the SM value in order to compensate the non-zero new physics contributions ΔM_W to M_W. On the other hand, due to the negligible new physics shift in the BP-II models, the best fit values for the Higgs mass in these models are basically the same as in the SM.

The large pulls for $A_{FB}(b)$ and $A_{LR}(e)$ are less meaningfull in the context of the M_H dependence of χ^2: In the best fits of all of our models $A_{FB}(b)$ is the observable with the largest contribution to χ^2 anyway, see Tab. A.1. The pull of observable № 21, $A_{LR}(e)$, is prone to been blown up by the exceptionally small experimental error.

In a last step we address the question of how χ^2 behaves if we do not vary M_H but the top mass $\bar{m}_t$. For all models under study we calculate χ^2 for a set of fixed $\bar{m}_t$ values and show the result in Fig. 4.2. As the best fit values for $\bar{m}_t$ in Tab. 4.1 are already almost the same for all models we expect $\bar{m}_t$ to be constrained to a very narrow range. Fig. 4.2 exactly confirms this expectation: If we demand that $\Delta\chi^2$ is smaller than $\Delta\chi^2\,(95\%, 1)$ the top mass $\bar{m}_t$ cannot be smaller than $\sim 160\,\text{GeV}$ and larger than $\sim 165\,\text{GeV}$ in any model.

4.2 Allowed Regions in Parameter Space

Figs. C.1 to C.9 in the appendix show the main results of our study: The bounds on the new physics parameters for all $G(221)$ models and – for all models of the first

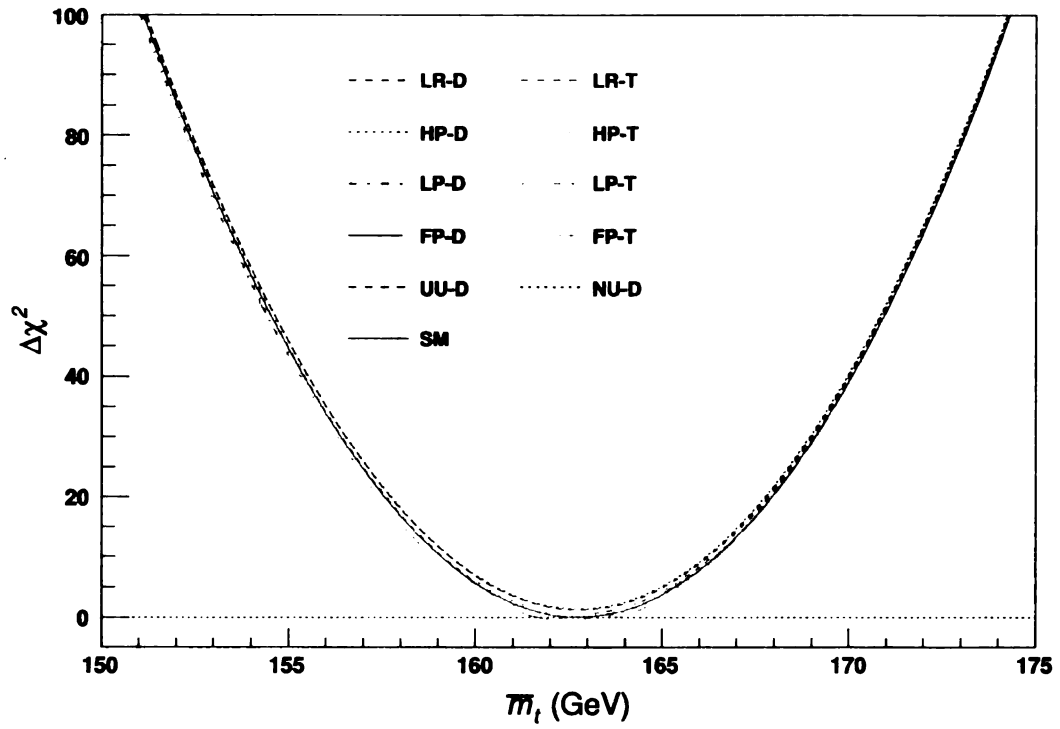

Figure 4.2: χ^2 in dependence of the top mass $\bar{m}_t$ for all ten $G(221)$ models and the SM — the χ^2 curves of the (BP-I,D) models differ so little form the curves of the corresponding (BP-I,T) models that they are mostly covered by them.

breaking pattern — the bounds on the masses $M_{Z'}$ and $M_{W'}$ of the new heavy gauge bosons. We obtain the plots of the gauge boson masses by taking the parameter values on the contours in parameter space and plugging them into the expressions for $M_{Z'}$ and $M_{W'}$ that we derived in Subsec. 2.2.4, see Tab. 2.6. In that respect the mass plots are nothing else than direct translations of the parameter bounds into constraints on the masses of the Z' and the $W'^{\pm}$. In the UU-D and the NU-D model the masses of the Z' and the $W'^{\pm}$ boson are degenerate which is why we do not include mass plots for these models. They would just show straight lines in the $M_{Z'}$–$M_{W'}$ plane. We find that the minimum masses of the Z' and the $W'^{\pm}$ that would still be consistent with the data are respectively given as 2.49 GeV and 3.66 GeV in these two models.

In the following subsection we will discuss the general properties of the parameter and mass plots. Subsequently, we will identify the observables that drive the plots and try to quantitatively understand how the plots come to their specific shapes.

4.2.1 General Features

As discussed in Subsec. 3.3.2 $\tilde{\phi}$ either enters the new physics corrections to the electroweak observables in form of the $c_{\tilde{\phi}}$ or the $s_{\tilde{\phi}}$. For that reason we decide to plot the bounds on the parameters in the $\tilde{x}$–$c_{\tilde{\phi}}$ or $\tilde{x}$-$s_{\tilde{\phi}}$ plane respectively. The parameter space of the models belonging to breaking pattern one in which $s^2_{2\tilde{\beta}}$ introduces a further degree of freedom is actually three-dimensional. In fact, the boundaries between the allowed and the forbidden parameter values are given by two-dimensional surfaces in these models. However, we stick to a two-dimensional representation and color-code the values of $s^2_{2\tilde{\beta}}$ on the parameter contours.

If we fix $s^2_{2\tilde{\beta}}$ at different values we obtain different parameter bounds in the $\tilde{x}$–$c_{\tilde{\phi}}$ plane. In other words: Looking at different *slices* of the two-dimensional boundary surface along the $s^2_{2\tilde{\beta}}$ axis changes the bounds on $\tilde{x}$ and $c_{\tilde{\phi}}$. The allowed regions shown in Figs. C.1 to C.8 represent the maximum allowed regions that we obtain combining

the projections of all slices in respectively one plot. Proceeding in this way represents a conservative approach: We exclude as few parameter values as possible. Only when no value for $s^2_{2\tilde{\beta}}$ leads to a $\chi^2 < \chi^2_{\text{ref.}}$ we say that a given set of $\tilde{x}$ and $c_{\tilde{\phi}}$ values is ruled out by the data.

For each model we include two different parameter contours into our plots: One contour that has been calculated with M_H and $\bar{m}_t$ being fixed at the best fit values M_H^{NP} and $\bar{m}_t^{\text{NP}}$ of the respective model and one contour calculated with M_H and $\bar{m}_t$ being set to the values $M_H^{\text{SM}} = 93.24\,\text{GeV}$ and $\bar{m}_t^{\text{SM}} = 162.8\,\text{GeV}$ that we obtained fitting the SM. With the Higgs and the top mass given by M_H^{NP} and $\bar{m}_t^{\text{NP}}$ the contours are more relaxed — M_H and $\bar{m}_t$ are harmonized with the specific properties of the $G(221)$ models and larger regions in parameter space can be opened up.

In all plots we indicate the bounds that we set on the parameter $t^2_{\tilde{\phi}}$ for our numerical analysis, see Eqs. (3.35) and (3.36), by dotted lines. In the parameter plots showing the $\tilde{x}$-$c_{\tilde{\phi}}$ or the $\tilde{x}$-$s_{\tilde{\phi}}$ plane these bounds simply result in straight horizontal lines that cut off regions where $c_{\tilde{\phi}}$ or $s_{\tilde{\phi}}$ takes too high or low values. As for the models of the first breaking pattern, these boundaries in the $\tilde{x}$-$c_{\tilde{\phi}}$ plane are independent of the value of $s^2_{2\tilde{\beta}}$. If we translate these parameter bounds into the $M_{Z'}$-$M_{W'}$ plane we can, in principle, choose between different $s^2_{2\tilde{\beta}}$ values. Depending on our choice we would get slightly different constraints on the gauge boson masses. As it turns out the effects of the $s^2_{2\tilde{\beta}}$ contributions to $M_{Z'}$ and $M_{W'}$ are, however, very small. They are suppressed by $\tilde{x}^{-1/2}$ and calculating the bounds on $M_{Z'}$ and $M_{W'}$ that follow from the constraints on $c_{\tilde{\phi}}$ we can just neglect them. The dotted lines that are shown in the mass plots correspond to a $s^2_{2\tilde{\beta}}$ value of $s^2_{2\tilde{\beta}} = 0$.

The fact that $s^2_{2\tilde{\beta}}$ becomes larger when we follow the parameter contours to higher values of $c_{\tilde{\phi}}$ can be explained with the different signs of the $c^4_{\tilde{\phi}}$ and $s^2_{2\tilde{\beta}}$ terms in the shifts of the electroweak observables, compare with Tab. 3.1. As discussed in our analysis of the best fit values, see Subsec. 4.1.1, the experimental data apparently requires

the contributions from new physics to be small. In order to keep the corrections low $s^2_{2\tilde{\beta}}$ has to increase when we reach higher values of $c_{\tilde{\phi}}$.

Furthermore, we observe that the parameter plots of the (BP-I,T) models are all shifted to lower $\tilde{x}$ values with respect to the corresponding (BP-I,D) models. This can again be attributed to the changes in the prefactors of the $c^4_{\tilde{\phi}}$ and $s^2_{2\tilde{\beta}}$ terms that occur when the doublet representation of Φ is replaced by a triplet representation. The prefactors of $c^4_{\tilde{\phi}}$ and $s^2_{2\tilde{\beta}}$ also explain why $s^2_{2\tilde{\beta}}$ tends to take smaller values in the upper $c_{\tilde{\phi}}$ regions if Φ is a triplet: Multiplying $c^4_{\tilde{\phi}}$ by $\frac{1}{4}$ and $s^2_{2\tilde{\beta}}$ by $\frac{1}{2}$ effectively enhances the effect of the $s^2_{2\tilde{\beta}}$ terms by a factor of 2. To keep the new physics contributions small we now have to choose smaller values for $s^2_{2\tilde{\beta}}$.

An obvious feature of the parameter plots for the first breaking pattern is that they again fall into the same two groups: The plots for the LR-D, LR-T, HP-D and HP-T models and the plots for the LP-D, LP-T, FP-D and FP-T models respectively resemble each other. Furthermore, the models of breaking pattern two seem to join either of these groups: The UU-D parameter contours have the same shape as those of the LR and HP models. Our results for the NU-D model look similar to what we get for the LP and FP models. These similarities can be explained with the respective observables that yield the largest to contributions to χ^2 in the individual models. In the next subsection we will identify those observables and try to quantitatively reconstruct our parameter plots.

4.2.2 Observables Driving the Plots

For each $G(221)$ model under study we set the new physics parameters to some exemplary values in the forbidden regions in parameter space and plot the resulting pull distributions, see Figs. C.10 to C.14. These plots directly point onto those observables due to which the respective regions are ruled out. We, however, note that the pull distributions shown in the appendix represent rather auxiliary material than

actual results of our analysis. They just allow us to identify the important observables — once we know which observables we have to look at our further discussion will be based on the explicit expressions for those observables.

In the first place, the pull distributions confirm that models with similar contours in parameter space are driven by the same observables: In the LR and HP models as well as in the UU-D model the hadronic cross section $\sigma_{\text{had.}}$ in e^-e^+ annihilation (observable № 3) clearly has the largest pull. Further large contributions come from the forward-backward asymmetry of the bottom quark $A_{FB}(b)$ (observable № 17) and the $W^\pm$ mass M_W (observable № 29).

As expected also the LP and FP models are driven by the same observables. At low values of $c_{\tilde{\phi}}$ the weak vector charge $Q_W\left(^{133}\text{Cs}\right)$ of cesium-133 (observable № 61) apparently plays an important role. We present the corresponding pull distribution for the FP models in Fig. C.13. For the same value of $c_{\tilde{\phi}}$ the pulls of the LP models would basically look the same. If $c_{\tilde{\phi}}$ is set to higher values $Q_W\left(^{133}\text{Cs}\right)$ looses its influence and the left-handed neutrino-nucleon coupling $\left(g_L^{\nu N}\right)^2$ (observable № 48) becomes the driving force behind the plots. We show an example pull distribution for the LP model in Fig. C.11. Again, at the same $c_{\tilde{\phi}}$ value the result for the FP model would be similar. For even larger values of $c_{\tilde{\phi}}$ we would see that also in the LP and FP models the pulls of $A_{FB}(b)$ and mass M_W can go up. In the NU-D model $\left(g_L^{\nu N}\right)^2$ is the most important observable.

To understand the origin of the pulls we compute the relative new physics corrections to $\sigma_{\text{had.}}$, $A_{FB}(b)$, M_W, $\left(g_L^{\nu N}\right)^2$ and $Q_W\left(^{133}\text{Cs}\right)$ in all $G(221)$ models and insert the values of the experimental reference observables α, G_F and M_Z, see Subsec. A.1. The results of our calculation are shown in Tabs. 4.3 to 4.7. We now list the most important conclusions that we draw from these results. First, we focus on the models of breaking pattern one. The upshot of our argumentation is pictorially summarized in the sketches shown in Fig. 4.3.

	$\tilde{x}\Delta\sigma_{\rm had.}/\sigma_{\rm had.,SM}$
LR-D	$-1.13\cdot c^2_{\tilde{\phi}} - 0.142\cdot c^4_{\tilde{\phi}} + 0.0432\cdot s^2_{2\tilde{\beta}}$
LP-D	$0.346\cdot c^2_{\tilde{\phi}} - 0.142\cdot c^4_{\tilde{\phi}} + 0.0432\cdot s^2_{2\tilde{\beta}}$
HP-D	$-1.38\cdot c^2_{\tilde{\phi}} - 0.142\cdot c^4_{\tilde{\phi}} + 0.0432\cdot s^2_{2\tilde{\beta}}$
FP-D	$0.0985\cdot c^2_{\tilde{\phi}} - 0.142\cdot c^4_{\tilde{\phi}} + 0.0432\cdot s^2_{2\tilde{\beta}}$
UU-D	$-0.889\cdot s^2_{\tilde{\phi}} - 0.0132\cdot s^4_{\tilde{\phi}}$
NU-D	$0.583\cdot s^2_{\tilde{\phi}} - 0.0132\cdot s^4_{\tilde{\phi}}$

Table 4.3: Numerical evaluation of $\Delta\sigma_{\rm had.}/\sigma_{\rm had.,SM}$ — the expressions for the (BP-I,T) models follow from the (BP-I,D) results by multiplying $c^2_{\tilde{\phi}}$ and $c^4_{\tilde{\phi}}$ by $\frac{1}{4}$ and $s^2_{2\tilde{\beta}}$ by $\frac{1}{2}$.

	$\tilde{x}\Delta A_{FB}(b)/A_{FB,\rm SM}(b)$
LR-D	$-30.0\cdot c^2_{\tilde{\phi}} + 67.6\cdot c^4_{\tilde{\phi}} - 20.6\cdot s^2_{2\tilde{\beta}}$
LP-D	$-46.1\cdot c^2_{\tilde{\phi}} + 67.6\cdot c^4_{\tilde{\phi}} - 20.6\cdot s^2_{2\tilde{\beta}}$
HP-D	$-30.9\cdot c^2_{\tilde{\phi}} + 67.6\cdot c^4_{\tilde{\phi}} - 20.6\cdot s^2_{2\tilde{\beta}}$
FP-D	$-47.0\cdot c^2_{\tilde{\phi}} + 67.6\cdot c^4_{\tilde{\phi}} - 20.6\cdot s^2_{2\tilde{\beta}}$
UU-D	$0.161\cdot s^2_{\tilde{\phi}} + 6.29\cdot s^4_{\tilde{\phi}}$
NU-D	$14.2\cdot s^2_{\tilde{\phi}} + 6.29\cdot s^4_{\tilde{\phi}}$

Table 4.4: Numerical evaluation of $\Delta A_{FB}(b)/A_{FB,\rm SM}(b)$ — the expressions for the (BP-I,T) models follow from the (BP-I,D) results by multiplying $c^2_{\tilde{\phi}}$ and $c^4_{\tilde{\phi}}$ by $\frac{1}{4}$ and $s^2_{2\tilde{\beta}}$ by $\frac{1}{2}$.

	$\tilde{x}\Delta M_W/M_{W,\mathrm{SM}}$
(BP-I,D)	$0.719 \cdot c_{\tilde{\phi}}^4 - 0.719 \cdot s_{2\tilde{\beta}}^2$
(BP-I,T)	$0.180 \cdot c_{\tilde{\phi}}^4 - 0.360 \cdot s_{2\tilde{\beta}}^2$
UU-D	$0.219 \cdot s_{\tilde{\phi}}^4$
NU-D	$0.219 \cdot s_{\tilde{\phi}}^4$

Table 4.5: Numerical evaluation of $\Delta M_W/M_{W,\mathrm{SM}}$

	$\tilde{x}\Delta \left(g_L^{\nu N}\right)^2 / \left(g_{L,\mathrm{SM}}^{\nu N}\right)^2$
(BP-I,D)	$0.0875 + 1.91 \cdot c_{\tilde{\phi}}^2 + 0.839 \cdot c_{\tilde{\phi}}^4 - 2.84 \cdot s_{2\tilde{\beta}}^2$
(BP-I,T)	$0.0219 + 0.478 \cdot c_{\tilde{\phi}}^2 + 0.210 \cdot c_{\tilde{\phi}}^4 - 1.42 \cdot s_{2\tilde{\beta}}^2$
UU-D	$0.839 \cdot s_{\tilde{\phi}}^4$
NU-D	$2.58 - 0.583 \cdot s_{\tilde{\phi}}^2 + 0.839 \cdot s_{\tilde{\phi}}^4$

Table 4.6: Numerical evaluation of $\Delta \left(g_L^{\nu N}\right)^2 / \left(g_{L,\mathrm{SM}}^{\nu N}\right)^2$

	$\tilde{x}\Delta Q_W\left(^{133}\mathrm{Cs}\right)/Q_{W,\mathrm{SM}}\left(^{133}\mathrm{Cs}\right)$
LR-D	$-0.855\cdot c_{\tilde{\phi}}^4 - 0.145\cdot s_{2\tilde{\beta}}^2$
LP-D	$3.35 - 1.95\cdot c_{\tilde{\phi}}^2 - 0.855\cdot c_{\tilde{\phi}}^4 - 0.145\cdot s_{2\tilde{\beta}}^2$
HP-D	$-0.855\cdot c_{\tilde{\phi}}^4 - 0.145\cdot s_{2\tilde{\beta}}^2$
FP-D	$2.95 - 1.95\cdot c_{\tilde{\phi}}^2 - 0.855\cdot c_{\tilde{\phi}}^4 - 0.145\cdot s_{2\tilde{\beta}}^2$
UU-D	$-0.855\cdot s_{\tilde{\phi}}^4$
NU-D	$0.406 + 0.594\cdot s_{\tilde{\phi}}^2 - 0.855\cdot s_{\tilde{\phi}}^4$

Table 4.7: Numerical evaluation of $\Delta Q_W\left(^{133}\mathrm{Cs}\right)/Q_{W,\mathrm{SM}}\left(^{133}\mathrm{Cs}\right)$ -- the expressions for the (BP-I,T) models follow from the (BP-I,D) results by multiplying $c_{\tilde{\phi}}^2$ and $c_{\tilde{\phi}}^4$ by $\frac{1}{4}$ and $s_{2\tilde{\beta}}^2$ by $\frac{1}{2}$.

- The corrections to $A_{FB}(b)$, M_W and $\left(g_L^{\nu N}\right)^2$ all prefer smaller values of $c_{\tilde{\phi}}$. If $c_{\tilde{\phi}}$ chosen too large the new physics shifts increase and the respective pulls are blown up. $\Delta\left(g_L^{\nu N}\right)^2$ and ΔM_W are especially sensitive to high $c_{\tilde{\phi}}$ values: In $\Delta\left(g_L^{\nu N}\right)^2$ the $c_{\tilde{\phi}}^2$ and the $c_{\tilde{\phi}}^4$ terms have the same sign so that they cannot cancel each other; ΔM_W only involves a $c_{\tilde{\phi}}^4$ contribution. $A_{FB}(b)$ has the largest effect on the parameter bounds in the LR and HP models as for these models the coefficient of $c_{\tilde{\phi}}^2$ has a smaller absolute value which leads to bad cancellation.

- The reason for the large impact of $Q_W\left(^{133}\mathrm{Cs}\right)$ on the LP and FP bounds lies in the fact that the corrections $\Delta Q_W\left(^{133}\mathrm{Cs}\right)$ involve an absolute term in these models. Only for large $c_{\tilde{\phi}}$ values the negative $c_{\tilde{\phi}}^2$ and $c_{\tilde{\phi}}^4$ terms can compete with that absolute contribution. The consequences are that the low-$c_{\tilde{\phi}}$ region is ruled out in the LP and FP models and that the parameter contours start at higher $\tilde{x}$ values than in the LR and HP models. At higher $c_{\tilde{\phi}}$ values, once $Q_W\left(^{133}\mathrm{Cs}\right)$

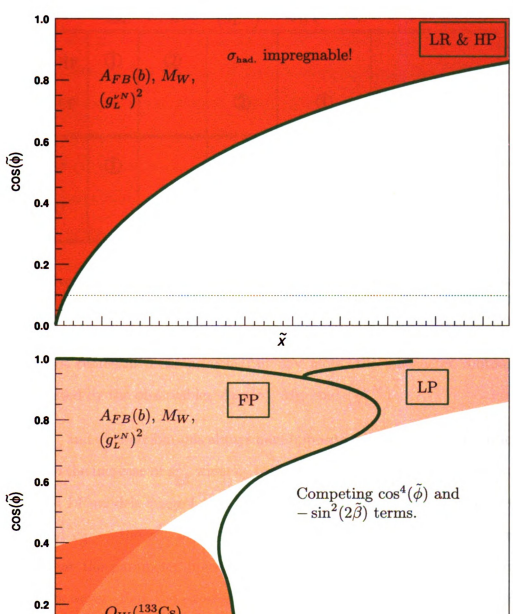

Figure 4.3: Sketches illustrating the influences of some key observables on the parameter bounds for the models of the first breaking pattern — the parameter contours in the (BP-I,T) models are shifted to lower $\tilde{x}$ values compared to the corresponding (BP-I,D) models. Omitting the tick labels on the $\tilde{x}$ axis we ensure that the sketches apply to (BP-I,D) and (BP-I,T) models alike. The UU-D parameter contour is driven by $\sigma_{\text{had.}}$ as well. In the NU-D model $\left(g_L^{\nu N}\right)^2$ is the most important observable.

	$\sigma_{\text{had.}}$	$A_{FB}(b)$	$\left(g_L^{\nu N}\right)^2$	$Q_W(^{133}\text{Cs})$	Set of other obs.
LR, HP	①	②			
LP, FP			②	①	
UU	①				②
NU			①		②

Table 4.8: Overview of the observables driving the parameter plots — the most and second most important observables are respectively marked with the symbols ① and ②. In the UU and NU models only one observable significantly contributes to χ^2.

does not represent a strong constrait any more, the parameter contours are dominated by the observables $A_{FB}(b)$, M_W and $\left(g_L^{\nu N}\right)^2$.

- The $s^2_{2\tilde{\beta}}$ and $c^4_{\tilde{\phi}}$ contributions always have opposite sign. As discussed earlier this leads to the increase of $s^2_{2\tilde{\beta}}$ when $c_{\tilde{\phi}}$ becomes larger. The parameter plots of the FP and LP models suggest that — depending on the exact interplay between $s^2_{2\tilde{\beta}}$ and $c_{\tilde{\phi}}$ — the $s^2_{2\tilde{\beta}}$ terms are be able to overcome the $c^4_{\tilde{\phi}}$ contributions such that the parameter boundaries are pulled back towards lower $\tilde{x}$ values. Note, however, that the expressions given in Tabs. 4.3 to 4.7 cannot explain the branching between the LP and FP contours. To account for that effect we certainly would have to extend our discussion to other observables as well.

- In the case of the LR and HP models the $s^2_{2\tilde{\beta}}$ terms do not have a chance: The $c^2_{\tilde{\phi}}$ and $c^4_{\tilde{\phi}}$ contributions to $\Delta\sigma_{\text{had.}}$ have the same sign and the $s^2_{2\tilde{\beta}}$ term is suppressed by a small prefactor. The pull of $\sigma_{\text{had.}}$ therefore represents a hindrance for the LR and HP models that is impregnable for large $c_{\tilde{\phi}}$.

After these comments on the models of the first breaking pattern it is easy to

understand the shape of the parameter contours in the second breaking pattern: In the UU-D model all corrections that we present in Tab. 4.3 to 4.7 favor small $s_{\tilde{\phi}}$ values. Especially the fact that the $s^2_{\tilde{\phi}}$ and $s^4_{\tilde{\phi}}$ terms in $\Delta\sigma_{\text{had.}}$ have the same sign leads to the exclusion of the high-$s_{\tilde{\phi}}$ region. For that reason the UU-D plot looks similar to the plots of the LR and HP models. The contour of the NU-D model is mainly influenced by the correction to $\left(g_L^{\nu N}\right)^2$. Since $\Delta\left(g_L^{\nu N}\right)^2$ is small if $s_{\tilde{\phi}}$ takes some intermediate value we observe a bump in the NU-D contour towards lower $\tilde{x}$ values for $s_{\tilde{\phi}}$ values around ~ 0.65.

In conclusion, we summarize our observations as follows: The shapes of the contours for LR, HP and UU models are driven by $\sigma_{\text{had.}}$. For the LR and HP models, $A_{FB}(b)$ also plays an important role. In the LP and FP models, at low $c_{\tilde{\phi}}$ values, $Q_W\left(^{133}\text{Cs}\right)$ is the most important observable. At higher $c_{\tilde{\phi}}$ the coupling $\left(g_L^{\nu N}\right)^2$ is responsible for the shape of the parameter contours. (To some degree, $A_{FB}(b)$ has the same effect on the LP and FP contours as on the LR and HP contours, though subdominant compared to the other observables. The same applies to $\left(g_L^{\nu N}\right)^2$ for the LR and HP models.) The NU contour is mainly driven by the pull of $\left(g_L^{\nu N}\right)^2$. Tab. 4.8 on the previous page presents these results in a tabular form.

4.3 Concluding Remarks

4.3.1 Constraints From Triple Gauge Boson Couplings

The aim of our analysis is to confront the $G(221)$ models with all important precision data that is available for electroweak observables. In this last section we may thus include the precise LEP 2 measurement of the ZW^+W^- triple gauge boson coupling into our discussion. The γW^+W^- boson coupling has been measured at LEP 2 as well. We, however, do not consider this coupling here: Due to QED gauge invariance

the γW^+W^- coupling is the same in the $G(221)$ models as in the SM. It does not shift which is why it cannot help us to constrain the new physics parameters. In addition to that, it has been measured with less precision than the ZW^+W^- coupling, anyway.

Employing the Hagiwara parametrization [29] we can write the ZW^+W^- vertex factor g_{ZWW} as a function of the parameter g_1^Z:

$$g_{ZWW} = g_{ZWW}\left(g_1^Z\right)$$

which takes the value unity in the SM. The experimental value for g_1^Z extracted from the LEP 2 data reads as [30]:

$$g_1^Z = 1.001 \pm 0.027 \pm 0.013$$

where the uncertainties are the 1σ statistical and systematic uncertainties, respectively. The total experimental uncertainty Δg_1^Z in g_1^Z follows from adding these two uncertainties in quadrature:

$$g_1^Z = 1.001 \pm \Delta g_1^Z \quad ; \quad \Delta g_1^Z = 0.030 \tag{4.1}$$

This result is obtained from the analysis of $e^-e^+ \to W^+W^-$ events. One deduces the scattering amplitude $\mathcal{A}_{\text{exp.}}$ from the experimental data and determines g_1^Z in a single-parameter fit in which all other couplings are kept fixed to their SM values:

$$\mathcal{A}_{\text{exp.}} \equiv \mathcal{A}_{\text{SM}}^{\gamma} + g_1^Z \mathcal{A}_{\text{SM}}^{Z} + \mathcal{A}_{\text{SM}}^{\nu} \tag{4.2}$$

The three amplitudes $\mathcal{A}_{\text{SM}}^{\gamma}$, $\mathcal{A}_{\text{SM}}^{Z}$ and $\mathcal{A}_{\text{SM}}^{\nu}$ denote the respective contributions from the s-channel γ exchange, s-channel Z exchange and t-channel ν exchange in the $e^-e^+ \longrightarrow W^+W^-$ transition. We can now use the result for g_1^Z in Eq. (4.1) to further

constrain our new physics parameters. In the $G(221)$ models the total amplitude $\mathcal{A}_{\text{exp.}}$ is given as:

$$\mathcal{A}_{\text{exp.}} = \mathcal{A}^{\gamma}_{\text{NP}} + \mathcal{A}^{Z}_{\text{NP}} + \mathcal{A}^{\nu}_{\text{NP}} \tag{4.3}$$

where the $G(221)$ amplitudes can respectively be written as the sum of the corresponding SM amplitude and a new physics correction that is proportional to $\frac{1}{\tilde{x}}$:

$$\mathcal{A}^{a}_{\text{NP}} = \mathcal{A}^{a}_{\text{SM}} + \Delta\mathcal{A}^{a} \quad ; \quad \Delta\mathcal{A}^{a} = \frac{1}{\tilde{x}} \cdot \delta\mathcal{A}^{a}\left(\tilde{\phi}, \tilde{\beta}\right) \quad ; \quad a \in \{\gamma, Z, \nu\}$$

In order to find the regions in parameter space that are excluded due to the $ZW^{+}W^{-}$ constraints we have to calculate the three amplitudes contributing to $\mathcal{A}_{\text{exp.}}$ in both the $G(221)$ models and in the SM. This is best be done employing the helicity amplitude method [31]. In Ref. [29] Hagiwara et al. present general expressions for the relevant amplitudes for all possible combinations of $e^{\pm}$ and $W^{\pm}$ helicities which allow us to quickly compute the $G(221)$ and SM helicity amplitudes — we only have to either plug our $G(221)$ results for the various couplings and masses or the corresponding SM expressions into the expressions given by Hagiwara et al.

For the explicit helicity amplitudes we refer to Ref. [29]. Here, we only note the key features of the dependencies on the scattering angle θ (not to be confused with the Weinberg angle). For a given configuration of incoming and outgoing helicities, all three amplitudes $\mathcal{A}^{\gamma}$, $\mathcal{A}^{Z}$ and $\mathcal{A}^{\nu}$ are proportional to the Wigner d-functions. For the s-channel amplitudes, we have:

$$\mathcal{A}^{\gamma}, \mathcal{A}^{Z} \propto d^{\Delta\sigma,\Delta\lambda}_{\Delta J}(\theta).$$

As for the t-channel ν exchange, we have an additional θ dependence from the ν-propagator:

$$\mathcal{A}^{\nu} \propto \left(B - \frac{C}{1 + \beta^2 - 2\beta\cos\theta}\right) d^{\Delta\sigma,\Delta\lambda}_{\Delta J}(\theta),$$

where B and C depend on the helicity configuration, but are independent of θ. To finally constrain our new physics parameters, we peform a partial-wave analysis. For any of the three involved amplitudes we project out the $d_{\Delta J}^{\Delta\sigma,\Delta\lambda}(\theta)$ component:

$$\tilde{\mathcal{A}}^a \equiv \int_{-1}^{1} d(\cos\theta)\, \mathcal{A}^a \cdot d_{\Delta J}^{\Delta\sigma,\Delta\lambda}(\theta) \quad ; \quad a \in \{\gamma, Z, \nu\}$$

By equating the two expressions for $\mathcal{A}_{\text{exp.}}$ in Eqs. (4.2) and (4.3) and projecting out the $d_{\Delta J}^{\Delta\sigma,\Delta\lambda}(\theta)$ component we finally obtain the constraint on the new physics parameters — $\tilde{x}$, $\tilde{\phi}$ and $\tilde{\beta}$ can only take values for which the following relation holds:

$$\tilde{\mathcal{A}}^{\gamma}_{\text{NP}} + \tilde{\mathcal{A}}^{Z}_{\text{NP}} + \tilde{\mathcal{A}}^{\nu}_{\text{NP}} = \tilde{\mathcal{A}}^{\gamma}_{\text{SM}} + \left(1.001 \pm \Delta g_1^Z\right) \tilde{\mathcal{A}}^{Z}_{\text{SM}} + \tilde{\mathcal{A}}^{\nu}_{\text{SM}}$$

According to this condition we calculate the bounds on $\tilde{x}$, $\tilde{\phi}$ and $\tilde{\beta}$ for all possible helicity configurations. Once we have done that, we combine our results and determine the maximum regions in parameter space that are ruled out due to the experimental value of Δg_1^Z.

Our calculations show that the experimental data on the ZW^+W^- vertex generally does not put stronger bounds on the new physics parameters than the electroweak precision observables. To illustrate which regions in parameter space are typically excluded by the data on the ZW^+W^- coupling we show our results for the (BP-I,D) models in Fig. 4.4. As the only fermion quantum numbers that we have to take into account are those of the electron we are able to respectively combine our results for the LR-D and HP-D and the LP-D and FP-D models in common plots. For both pairs of (BP-I,D) models we present the parameter bounds for the extreme $s^2_{2\tilde{\beta}}$ values of $s^2_{2\tilde{\beta}} = 0$ and $s^2_{2\tilde{\beta}} = 1$.

In the case of the LR-D and HP-D models the ZW^+W^- constraints do not affect the results of our global fit analysis at all: For low $c_{\tilde{\phi}}$ values $s^2_{2\tilde{\beta}}$ is small on the LR-D

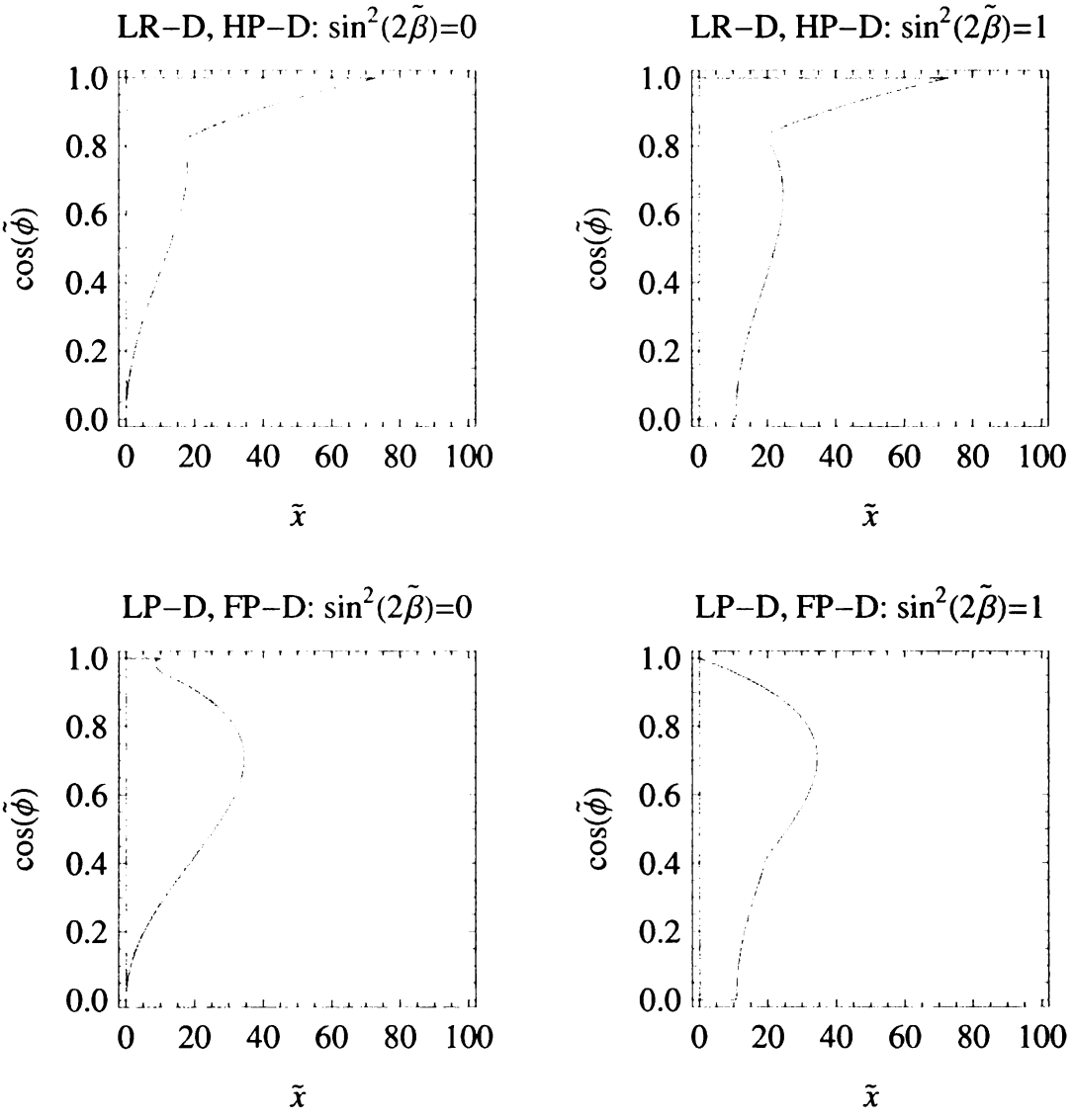

Figure 4.4: Bounds on the (BP-I,D) models from the ZW^+W^- vertex — the shaded regions are excluded, the blank regions consistent with the measurement of the ZW^+W^- coupling.

and HP-D parameter contours — in which case the ZW^+W^- data is only able to rule out points in parameter space with $\tilde{x} \lesssim 20$. In the LP-D model our boundary between allowed and forbidden parameter values is located at $\tilde{x}$ values larger than 250. The ZW^+W^- constraints do not reach up to that high $\tilde{x}$ values. Only in the FP-D the ZW^+W^- contour comes at least close to the one that we found earlier in our global fit analysis. If $\tilde{x}$ is chosen small and $s^2_{2\tilde{\beta}}$ set to 1 the contours meet each other at $c_{\tilde{\phi}} = 1$. However, as the FP-D curve has a much smaller slope than the ZW^+W^- contour the ZW^+W^- data does not exclude parameter values that were not already ruled out by our global fit analysis.

In conclusion, we can say that at present the constraints from the ZW^+W^- vertex cannot compete with the bounds set by the electroweak precision data. Our global fit analysis therefore represent the complete answer to the question that we posed in the introduction: Which bounds do the experimental data place on $G(221)$ models? All information on the bounds is contained in the plots of the parameter space and the masses of the new heavy gauge bosons that we show in the appendix.

4.3.2 Future Prospects

The Q-weak [32] collaboration at Jefferson Lab intends to determine the weak charge of the proton, $Q_W(p)$, by measuring the parity violating asymmetry in elastic e^-p scattering at $Q^2 = 0.03\,\mathrm{GeV}^2$. Meanwhile the e2ePV collaboration [33], also at Jefferson Lab, proposes a Møller scattering experiment at $Q^2 = 0.0056\,\mathrm{GeV}^2$ that would allow to infer the weak charge of the electron, $Q_W(e)$, with ultra-high precision. The experimental results that are anticipated by both collaborations are already implemented into the GAPP code:

$$Q_W(p) = 0.0715 \pm 0.0029 \quad ; \quad Q_W(e) = -0.046900 \pm 0.001079$$

Given the accurancy that both experiments are aiming at we feel tempted to investigate how much of an effect it would be if we added these two precise values to our global fit analysis. In a last step we thus repeat our scans of the $G(221)$ parameter space with $Q_W(p)$ and the e2ePV value for $Q_W(e)$ included as additional constraints. While the bounds on the LR, HP, UU-D and NU-D models are only slightly affected the results for the LP and FP models change drastically. As an example we present the $\tilde{x}$-$c_{\tilde{\phi}}$ parameter contour for the LP-D model in Fig. 4.5. At low values of $c_{\tilde{\phi}}$ the boundary between allowed and forbidden values is pushed to much larger $\tilde{x}$ values. To find out which observable is responsible for that shift we again pick a point in the excluded region and examine the distribution of the pulls. It turns out that the anticipated value for the weak charge of the electron causes the dramatic change of the LP and FP contours. The effect of $Q_W(e)$ on the LP and FP models is thus comparable to the one of $Q_W(^{133}\mathrm{Cs})$ with the only difference being that the region exluded by $Q_W(e)$ extends to much higher $\tilde{x}$ values, compare also with Fig. 4.3. As a consequence of these further constraints from $Q_W(p)$ and the e2ePV value for $Q_W(e)$ the allowed region in the $M_{Z'}$–$M_{W'}$ plane shrinks as well, see Fig. 4.5. The minimum allowed mass for the $W'^{\pm}$ increases, for instance, from $\approx 0.6\,\mathrm{TeV}$ to $\approx 1.2\,\mathrm{TeV}$.

This last analysis therefore shows us that our study can only be understood as a snapshot that tries to capture the current constraints on the $G(221)$ models. Future experiments such as the measurements of weak charges at low energies might be able to yield significant corrections to the picture that we have drawn in this thesis. However, this prospect shall not discourage us. It is exactly the interplay between increasingly more precise experiments and phenomenological studies like ours that harbors the chance of detecting new physics beyond the SM.

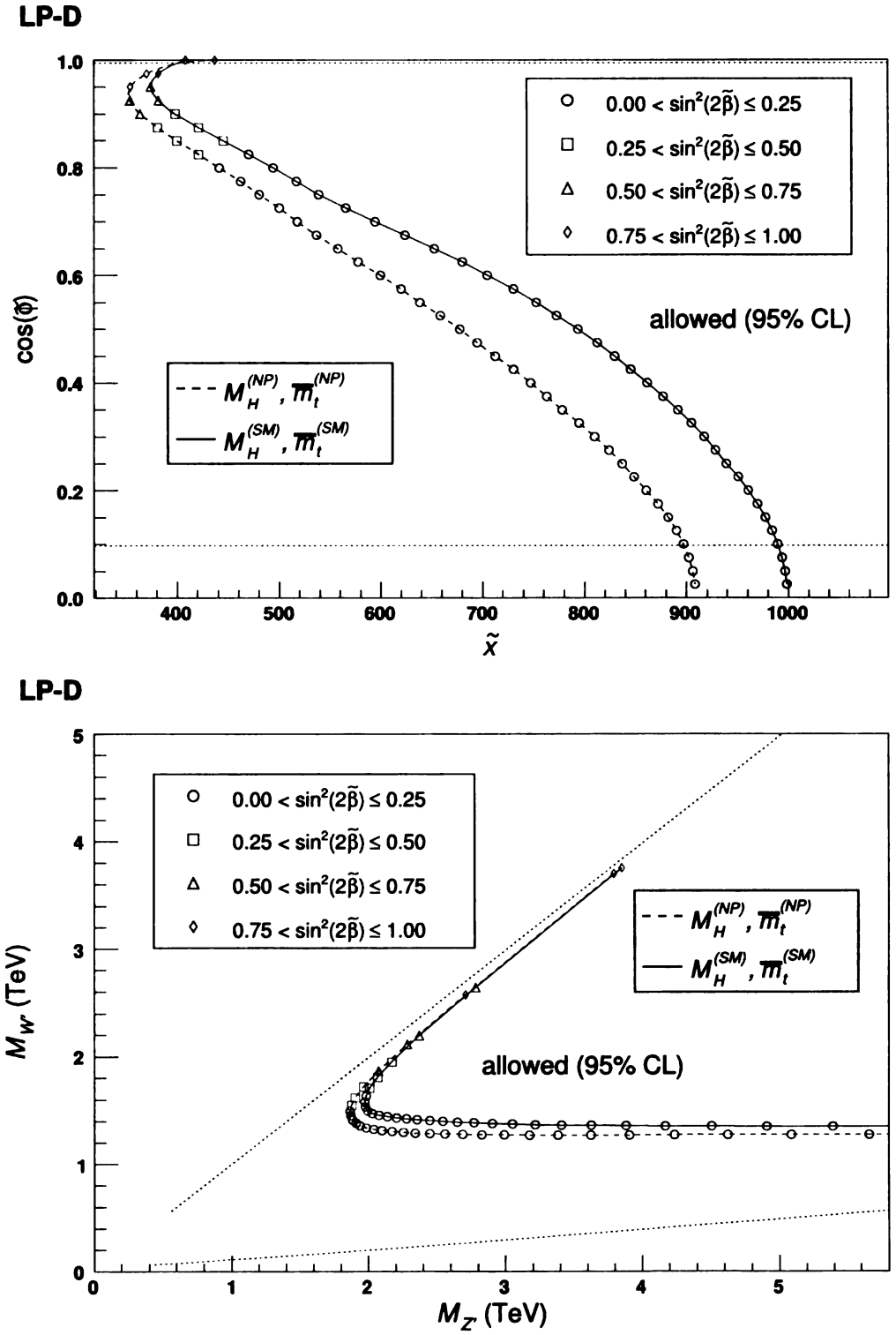

Figure 4.5: Bounds on the the LP-D model with the anticipated values for $Q_W(p)$ and $Q_W(e)$ being included into the analysis -- compare to Fig. C.2.

Appendix A

Experimental Input

We give the experimental results for the reference observables α, G_F and M_Z that are used by the GAPP code and determine the numerical values of the standard parameters $s^2_{\theta_{\rm SM}}$ and $v_{\rm SM}$. Subsequently, we list the experimental values of all electroweak observables to which we fit our $G(221)$ models. The experimental data implemented in the 2009 version of GAPP [21] agrees for the most part with the values given in the 2008 PDG book; compare with [20].

A.1 Reference Observables α, G_F and M_Z

The most recent version of the GAPP code uses the following numbers:

$$\alpha = 1/137.03599911 \quad ; \quad G_F = 1.16637 \cdot 10^{-5}\,\mathrm{GeV}^{-2} \quad ; \quad M_Z = 91.1876\,\mathrm{GeV}$$

The value for α represents the low-energy limit of the fine structure constant. Going to higher and higher energies in the experiment scale-dependent loop corrections will cause α to *run*, that is, to become progressively larger. We have to consider the running of the fine structure constant when we deduce the numerical value of

$s^2_{\theta_{\rm SM}}$ from the Z mass. Expressing M_Z in terms of α, $s^2_{\theta_{\rm SM}}$ and $v_{\rm SM}$, see Eq. (3.1), the involved α does not take the value 1/137.036. Instead it is given as the running coupling $\alpha(\mu)$ evaluated at the Z mass scale. The explicit value of $\alpha\,(M_Z)$ depends on the employed renormalization scheme. GAPP is based on the modified minimal substraction ($\overline{\rm MS}$) scheme. The $\overline{\rm MS}$ value $\hat{\alpha}\,(M_Z)$ for $\alpha\,(M_Z)$ is calculated by GAPP and turns out to be $\hat{\alpha}\,(M_Z) = 1/127.918$. Eq. in Subsec. then actually reads as:

$$M_Z^2 \equiv \hat{\alpha}\,(M_Z) \cdot \frac{\pi v_{\rm SM}^2}{s^2_{\theta_{\rm SM}} c^2_{\theta_{\rm SM}}}$$

We solve this equation for $s^2_{\theta_{\rm SM}}$ and obtain:

$$s^2_{\theta_{\rm SM}} = 0.233652 \quad ; \quad c^2_{\theta_{\rm SM}} = 0.766348$$

The value for Fermi's constant G_F results in a electroweak VEV of:

$$v_{\rm SM} = 246.221\,\text{GeV}$$

A.2 Electroweak Observables

We present the measured values for the electroweak observables in two tables: Tab. A.1 on the following page lists the experimental results for the Z and $W^\pm$ pole data as well as the top mass; Tab. A.2 on page 132 presents the experimental data that is available for the low-energy observables. Both tables also give the numbers by which the GAPP code refers to the individual observables, our best fit results for the SM and the corresponding pulls.

№	Obs.	Exp.	SM	Pull
(2)	Γ_Z [GeV]	2.4952 ± 0.0023	2.4956	-0.163
(3)	$\sigma_{\text{had.}}$ [nb]	41.541 ± 0.037	41.480	1.658
(4)	$R(e)$	20.804 ± 0.050	20.740	1.278
(5)	$R(\mu)$	20.785 ± 0.033	20.740	1.355
(6)	$R(\tau)$	20.764 ± 0.045	20.786	-0.478
(14)	$\mathcal{R}(s)$	0.371 ± 0.022	0.359	0.535
(16)	$R(c)$	0.1721 ± 0.0300	0.1722	-0.048
(15)	$R(b)$	0.21629 ± 0.00066	0.21580	0.741
(11)	$A_{LR}(e)$	0.1498 ± 0.0049	0.14737	0.495
(21)		0.15138 ± 0.00216	— " —	1.855
(22)		0.1544 ± 0.0060	— " —	1.171
(25)		0.162 ± 0.043	— " —	0.340
(23)	$A_{LR}(\mu)$	0.142 ± 0.015	— " —	-0.358
(10)	$A_{LR}(\tau)$	0.1439 ± 0.0043	— " —	-0.808
(24)		0.136 ± 0.015	— " —	-0.758
(26)	$A_{LR}(s)$	0.895 ± 0.091	0.936	-0.447
(20)	$A_{LR}(c)$	0.670 ± 0.027	0.668	0.078
(19)	$A_{LR}(b)$	0.923 ± 0.020	0.935	-0.588
(7)	$A_{FB}(e)$	0.0145 ± 0.0025	0.0163	-0.716
(8)	$A_{FB}(\mu)$	0.0169 ± 0.0013	— " —	0.470
(9)	$A_{FB}(\tau)$	0.0188 ± 0.0017	— " —	1.477
(13)	$A_{FB}(s)$	0.0980 ± 0.0110	0.1034	-0.493
(18)	$A_{FB}(c)$	0.0707 ± 0.0035	0.0738	-0.892
(17)	$A_{FB}(b)$	0.0992 ± 0.0016	0.1033	-2.573
(12)	Q_{FB}	0.0403 ± 0.0026	0.0423	-0.781
(28)	Γ_W [GeV]	2.196 ± 0.083	2.092	1.257
(30)		2.057 ± 0.062	— " —	-0.559
(27)	M_W [GeV]	80.376 ± 0.033	80.378	-0.051
(29)		80.432 ± 0.039	— " —	1.393
(42)	m_t [GeV]	172.40 ± 1.34	172.45	-0.035

Table A.1: Experimental values for the Z and $W^{\pm}$ pole observables and the top mass that we employed for our numerical analysis — see the PDG book [20] for references. The SM values and the corresponding pulls represent our best fit results.

№	Obs.	Exp.	SM	Pull
(47)	τ_τ [fs]	290.93 ± 0.48	289.08	0.771
(48)	$\left(g_L^{\nu N}\right)^2$	0.3010 ± 0.0015	0.3039	-1.944
(49)	$\left(g_R^{\nu N}\right)^2$	0.0308 ± 0.0011	0.0300	0.720
(50)	$\kappa^{\nu N}$	0.5820 ± 0.0041	0.5830	-0.252
(51)	R_ν	0.3021 ± 0.0041	0.3091	-1.705
(52)		0.3096 ± 0.0043	— " —	0.119
(53)	$R_{\bar{\nu}}$	0.403 ± 0.016	0.386	1.058
(54)		0.384 ± 0.018	— " —	-0.115
(55)		0.365 ± 0.016	0.381	-1.031
(56)	$g_V^{\nu e}$	-0.040 ± 0.015	-0.040	-0.016
(57)	$g_A^{\nu e}$	-0.507 ± 0.014	-0.506	-0.044
(58)	$Q_W(e)$	-0.0403 ± 0.0053	-0.0472	1.309
(61)	$Q_W\left({}^{133}\mathrm{Cs}\right)$	-73.16 ± 0.35	-73.15	-0.032
(62)	$Q_W\left({}^{205}\mathrm{Tl}\right)$	-116.40 ± 3.64	-116.75	0.096
(63)	C_1	-0.0285 ± 0.0043	-0.0335	1.170
(64)	C_2	0.342 ± 0.063	0.3885	-0.739

Table A.2: Experimental values for the low-energy observables that we employed for our numerical analysis — see the PDG book [20] for references. The numbers № in the first column refer to the numeration of the observables in the GAPP code, the SM values and the corresponding pulls represent our best fit results.

Appendix B

MS-Bar Mass of the Top Quark

To renormalize a perturbative quantum field theory one introduces counter terms that absorb the infinities arising beyond the tree-level. These counter terms are, however, not unambiguously defined. Different renormalization schemes are available each of which fixes the counter terms in a different way and each of which, hence, entails different definitions of important quantities such as masses and coupling strengths.

Common schemes include the on-shell scheme in which the particle masses are set to their physical values on the mass shell and the modified minimal subtraction ($\overline{\text{MS}}$) scheme which absorbs infinite as well as large logarithmic terms in the renormalization constants. In this study we require the mass of the top quark in both schemes: The on-shell mass m_t is one of our 37 observables; see Subsec. 3.2.1. The $\overline{\text{MS}}$ mass $\bar{m}_t$ is one of our five fit parameters; see Subsec. 3.3.2. In this appendix we will briefly outline the relation between these two definitions of the top quark mass.

All loop insertions into the top quark propagator contribute, in principle, to the mass renormalization of the top quark. In this discussion we will restrict ourselves to a couple of example loop effects: We consider diagrams involving a gluon G, a Higgs boson H, a longitudinal Z boson Z_L and a longitudinal W^+ boson W_L^+ respectively. The contributions from transverse electroweak gauge bosons are sub-leading which

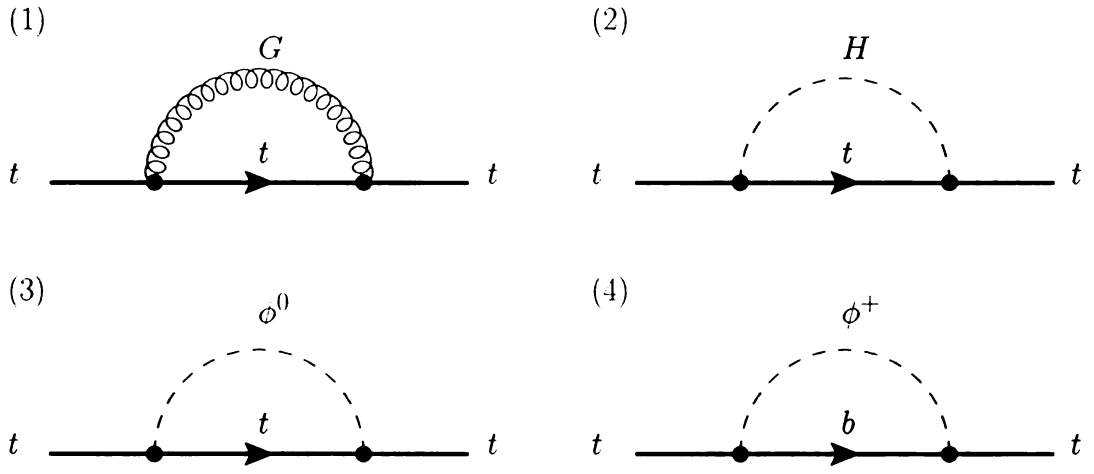

Figure B.1: The four considered example diagrams that contribute to the mass renormalization of the top quark — the Goldstone bosons ϕ^0 and ϕ^+ substitute the longitudinal electroweak gauge bosons Z_L and W_L^+.

is why we neglect them here. By virtue of the Goldstone-boson equivalence theorem (ET) [34, 35, 36] it is possible to replace the longitudinal gauge bosons Z_L and W_L^+ by their corresponding unphysical Higgs bosons ϕ^0 and ϕ^+. The ET only requires that $m_t > M_W, M_Z$ which certainly is the case. Fig. B.1 presents the four diagrams under study.

In the on-shell renormalization scheme the bare top mass m_t^{bare} is related to the pole mass m_t as follows:

$$m_t^{\text{bare}} = m_t \left(1 + \frac{\delta_{m_t}}{m_t}\right) = m_t \left(1 + \frac{\delta_{m_t}^{\text{QCD}}}{m_t} + \frac{\delta_{m_t}^{\text{Yuk.}}}{m_t} + \ldots\right)$$

where $\delta_{m_t}^{\text{Yuk.}}$ subsumes all contributions from the Yukawa couplings of the top quark to the Higgs bosons H, ϕ^0 and ϕ^+, that is, the contributions from diagrams № 2 to № 4 in Fig. B.1. The dots represent the contributions from all diagrams that we do not discuss in this appendix. Evaluating diagram № 1 we obtain an expression for $\delta_{m_t}^{\text{QCD}}/m_t$:

$$\frac{\delta_{m_t}^{\text{QCD}}}{m_t} = \frac{3\alpha_s}{4\pi} C_F \left(-\Delta + \ln\left(\frac{m_t^2}{\mu^2}\right) - \frac{4}{3}\right) \tag{B.1}$$

Here, α_s stands for the strong coupling constant. At the top mass scale it has a value of $\alpha_s(m_t) = 0.11$ [20]. C_F is a color factor that takes the value $C_F = \frac{4}{3}$ in QCD. $\Delta \equiv \frac{2}{4-N} - \gamma_E + \ln(4\pi)$ denotes the regulator that appears in dimensional regularization. $\gamma_E = 0.577...$ is the Euler-Mascheroni constant. The mass parameter μ is a measure for the energy scale.

Ref. [37] provides us with an expression for $\delta_{m_t}^{\text{Yuk.}}/m_t$:

$$\frac{\delta_{m_t}^{\text{Yuk.}}}{m_t} = \frac{g_L^2}{16\pi^2}\frac{m_t^2}{8M_W^2}\left[3\Delta - 3\ln\left(\frac{m_t^2}{\mu^2}\right) + 1 - 4I\left(\frac{M_H^2}{m_t^2}\right) + 2J\left(\frac{M_H^2}{m_t^2}\right) + i\pi\right] \quad \text{(B.2)}$$

where

$$I(\xi) = \int_0^1 dx\, \ln\left[x^2 + (1-x)\xi - i\epsilon\right] \quad ; \quad J(\xi) = \int_0^1 dx\, x \ln\left[x^2 + (1-x)\xi - i\epsilon\right]$$

In the on-shell scheme the entire shift δ_{m_t} in the top quark mass is absorbed in the corresponding counter term. The $\overline{\text{MS}}$ scheme includes, by contrast, the finite real parts of δ_{m_t} in the definition of the mass $\bar{m}_t$. Only the infinite and logarithmic pieces are cancelled by the renormalization constant. According to Eqs. (B.1) and (B.2) the difference between m_t and $\bar{m}_t$ thus amounts to:

$$\begin{aligned}\bar{m}_t &= m_t + \Delta_{m_t}^{\text{QCD}} + \Delta_{m_t}^{\text{Yuk.}} + ... \\ &= m_t + \frac{3\alpha_s}{4\pi}C_F \cdot \left(-\frac{4}{3}\right) + \frac{g_L^2}{16\pi^2}\frac{m_t^2}{8M_W^2}\left[1 - 4I\left(\frac{M_H^2}{m_t^2}\right) + 2J\left(\frac{M_H^2}{m_t^2}\right)\right] + ...\end{aligned}$$

To obtain numerical results for $\Delta_{m_t}^{\text{QCD}}$ and $\Delta_{m_t}^{\text{Yuk.}}$ we employ the following data: The experimental value for the pole mass, $m_t = 172.40\,\text{GeV}$, the strong coupling at the top mass scale, $\alpha_s(m_t) = 0.11$, the SM value $g_{L,\text{SM}} = 0.63$ for g_L, the weighted mean of the two measurements of the $W^\pm$ mass, $M_W = 80.40\,\text{GeV}$, and the SM best-fit

value for the Higgs mass, $M_H = 93.24\,\mathrm{GeV}$. We find:

$$\Delta_{m_t}^{\mathrm{QCD}} = -8.05\,\mathrm{GeV} \quad ; \quad \Delta_{m_t}^{\mathrm{Yuk.}} = 0.93\,\mathrm{GeV}$$

The comparison of the SM prediction for the pole mass, $m_t = 172.5\,\mathrm{GeV}$, with the SM best-fit value for the $\overline{\mathrm{MS}}$ mass, $\bar{m}_t = 162.8\,\mathrm{GeV}$, shows that the contribution from the neglected diagrams must add up to roughly $\approx -2.6\,\mathrm{GeV}$.

Appendix C

Bounds on the $G(221)$ Models

In this appendix we present plots for each $G(221)$ model that indicate which regions in parameter space are consistent with the electroweak data and to which masses $M_{Z'}$ and $M_{W'}$ of the new heavy gauge bosons these viable parameter values correspond. Subsequently, we show pull distributions for each model that were calculated for exemplary points in the forbidden parameter regions. These pull distributions point onto the observables that are responsible for the respective parameter bounds.

C.1 Parameter and Mass Plots

For the models of the first breaking pattern the parameter plots present the $\tilde{x}$–$c_{\tilde{\phi}}$ plane; for the UU-D and the NU-D models the $\tilde{x}$- $s_{\tilde{\phi}}$ plane is shown. The boundary between allowed and forbidden parameter values is determined twice for each model: With M_H and $\bar{m}_t$ being fixed at the SM best fit values in the one case and with M_H and $\bar{m}_t$ being re-fitted in the new physics models in the second case. In the plots for the models of breaking pattern one the information on $s^2_{2\tilde{\beta}}$ is color-coded. For each $c_{\tilde{\phi}}$ the $s^2_{2\tilde{\beta}}$ value corresponding to the lowest $\tilde{x}$ is chosen. The dotted lines indicate the bounds on $t^2_{\tilde{\phi}}$ that we discussed in Subsec. 3.3.2.

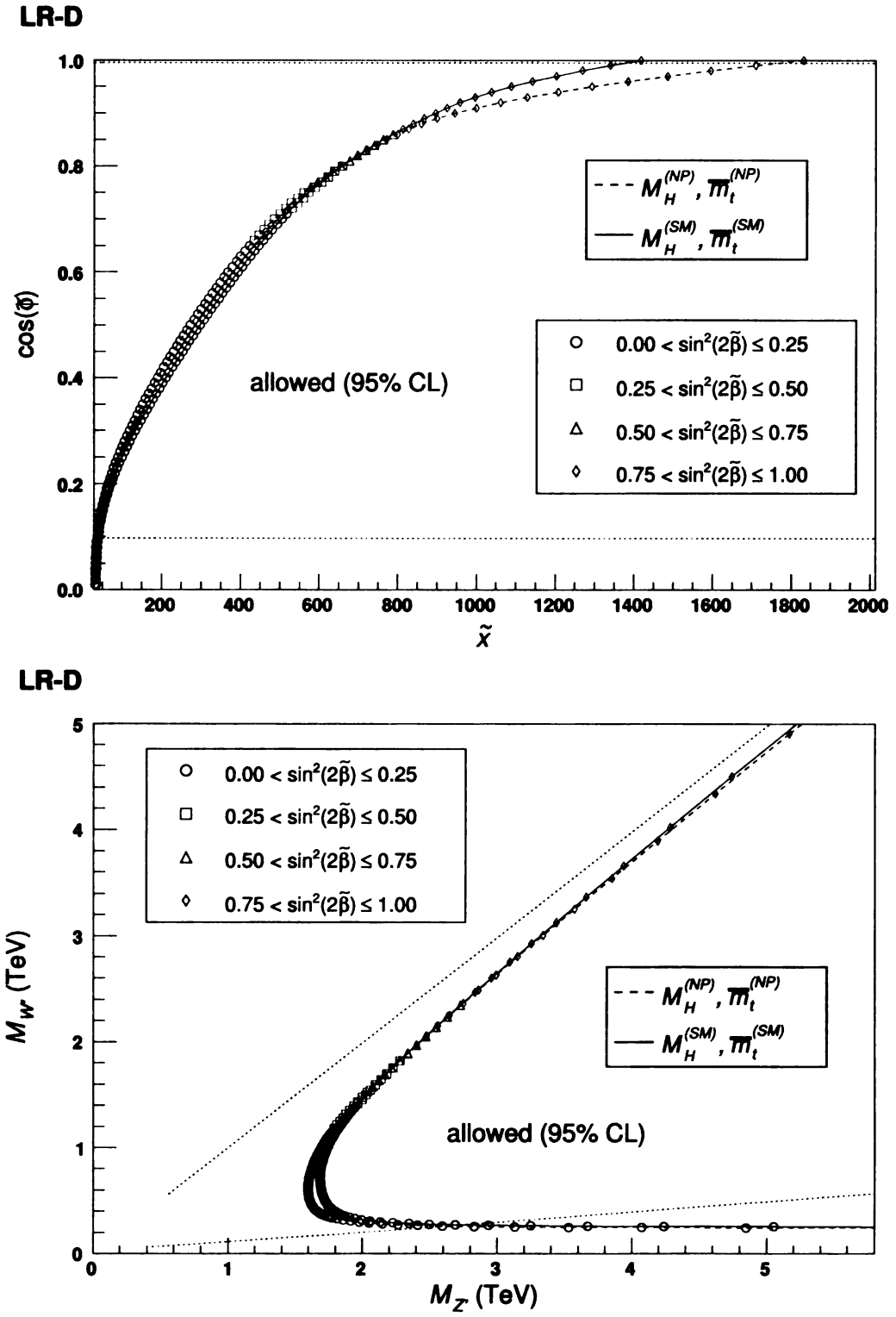

Figure C.1: Bounds on the new physics parameters and the masses of the new heavy gauge bosons in the LR-D model.

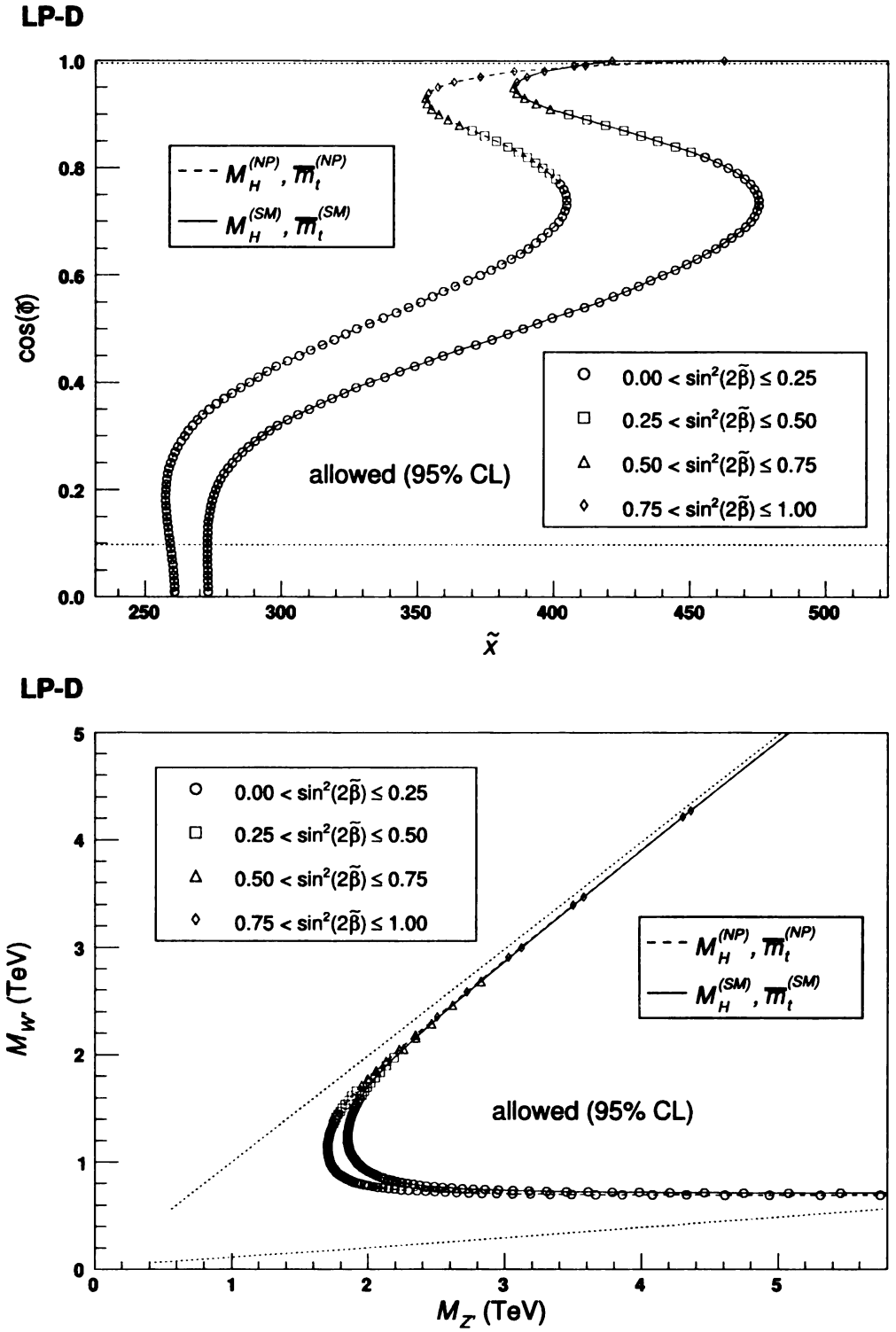

Figure C.2: Bounds on the new physics parameters and the masses of the new heavy gauge bosons in the LP-D model.

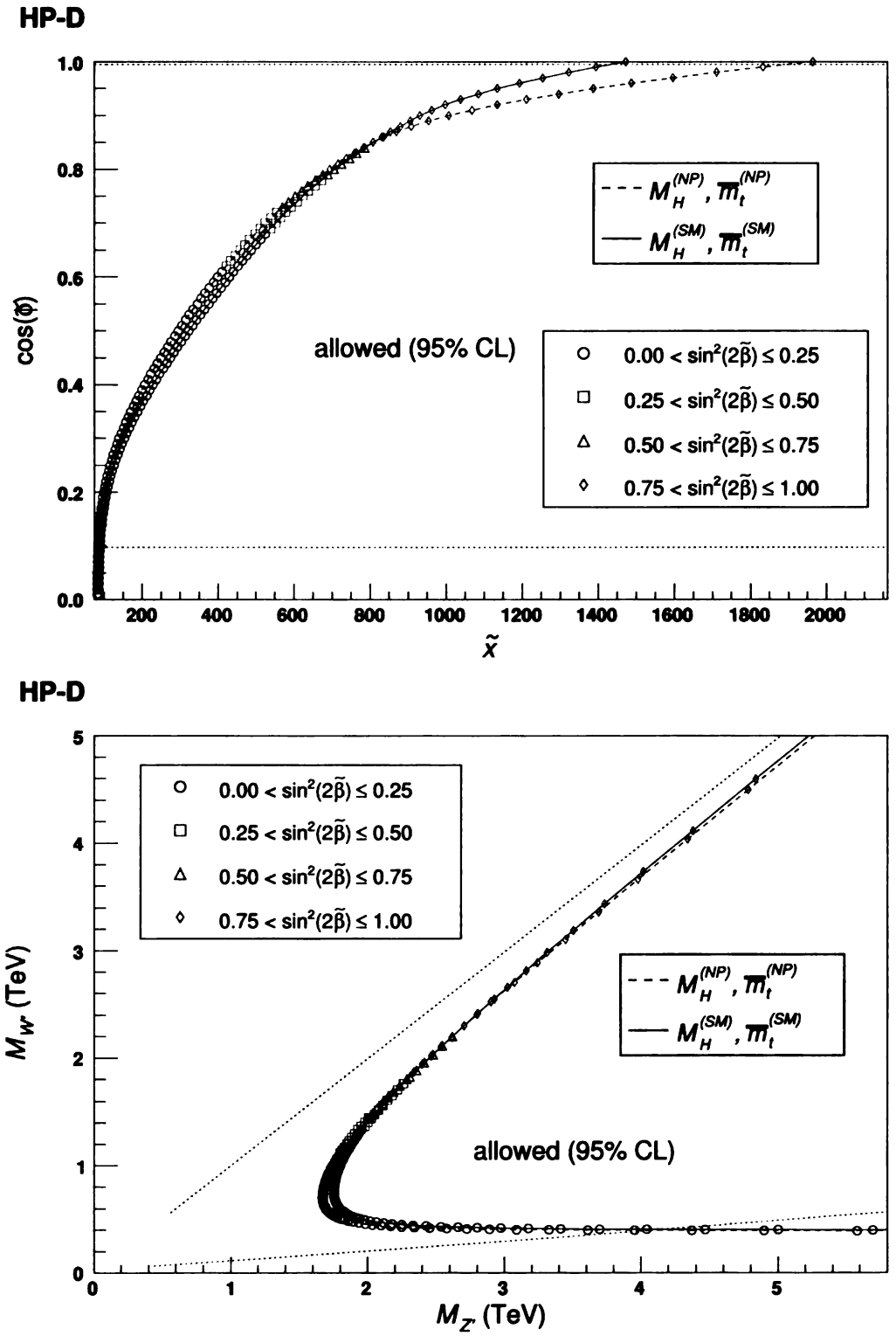

Figure C.3: Bounds on the new physics parameters and the masses of the new heavy gauge bosons in the HP-D model.

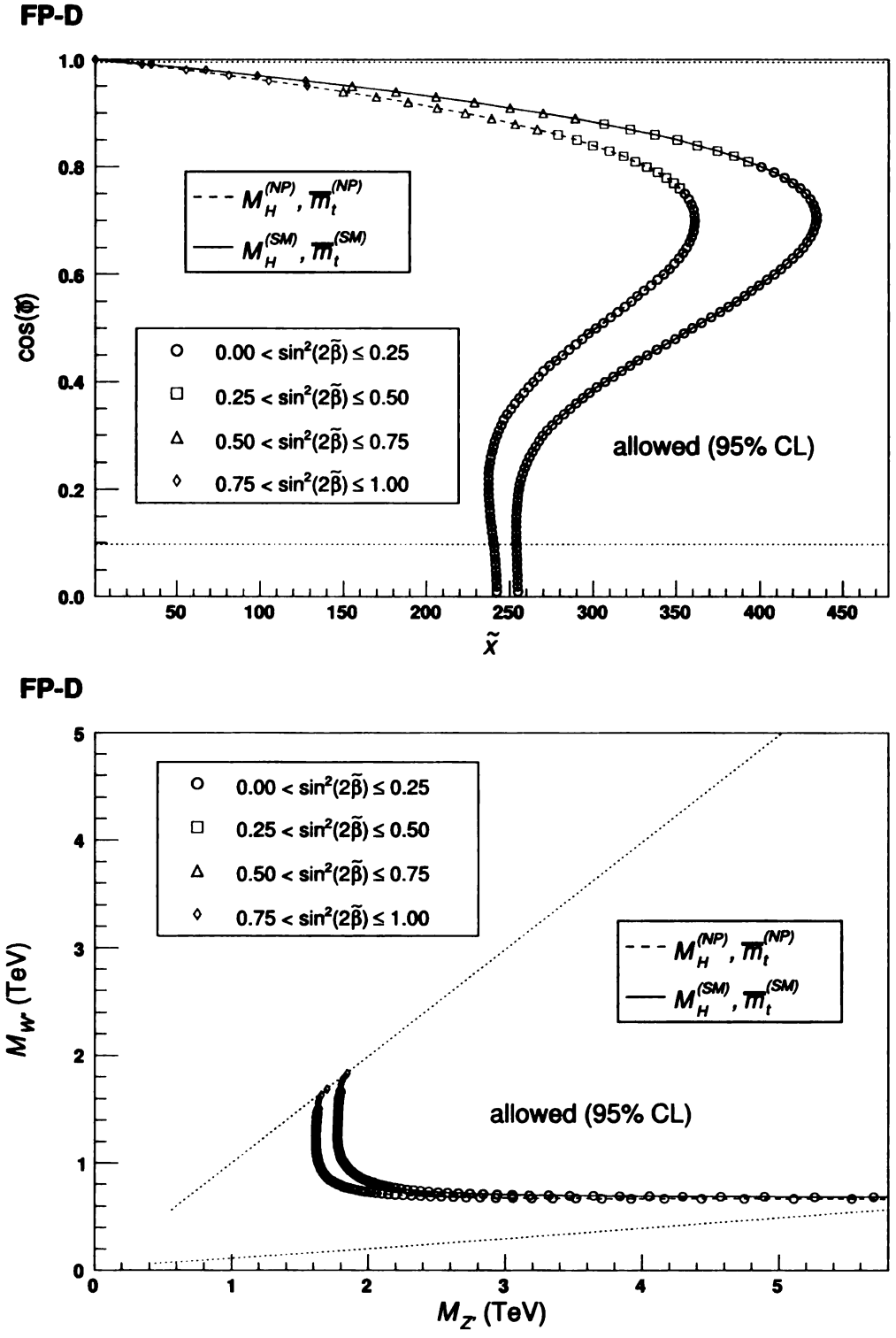

Figure C.4: Bounds on the new physics parameters and the masses of the new heavy gauge bosons in the FP-D model.

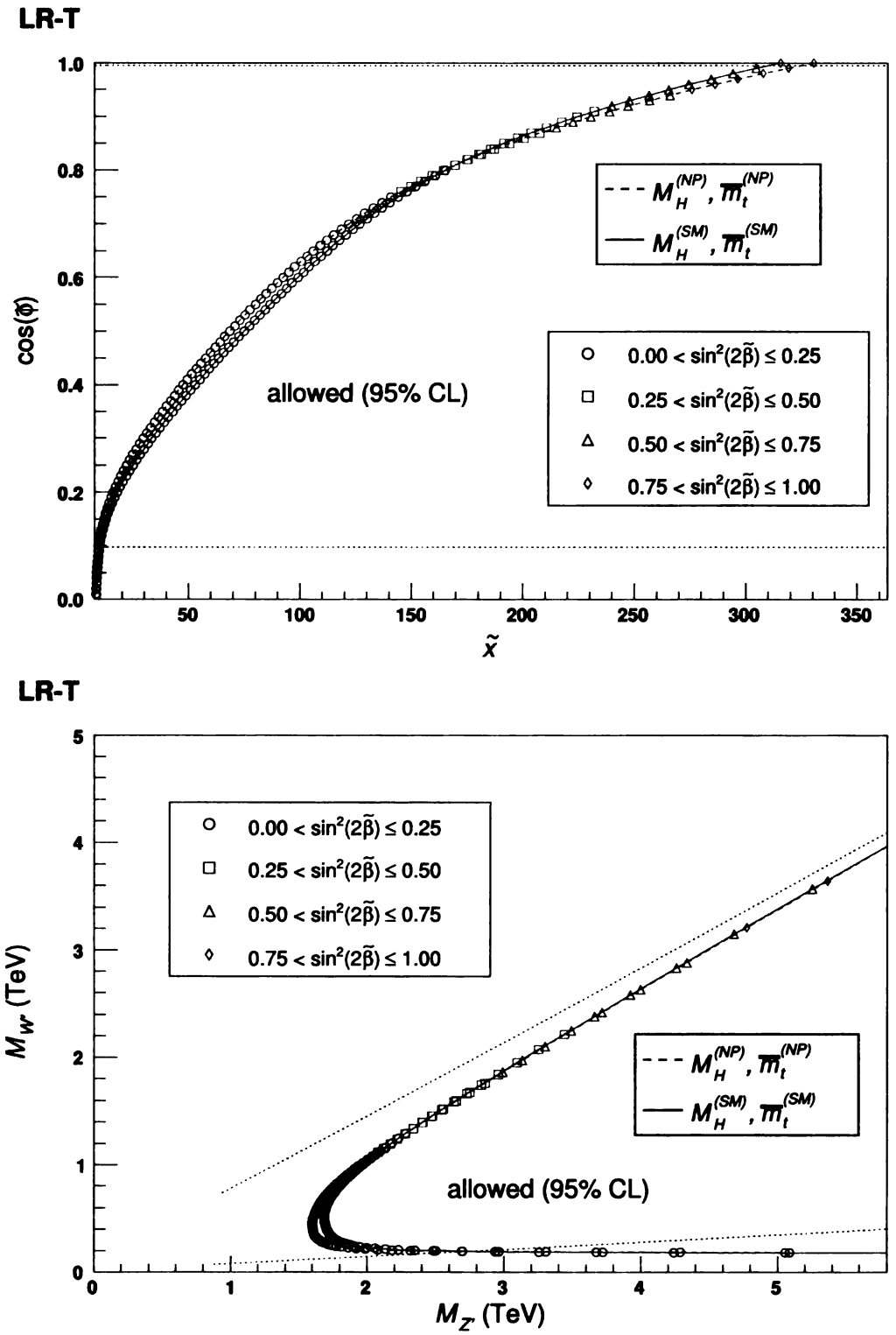

Figure C.5: Bounds on the new physics parameters and the masses of the new heavy gauge bosons in the LR-T model.

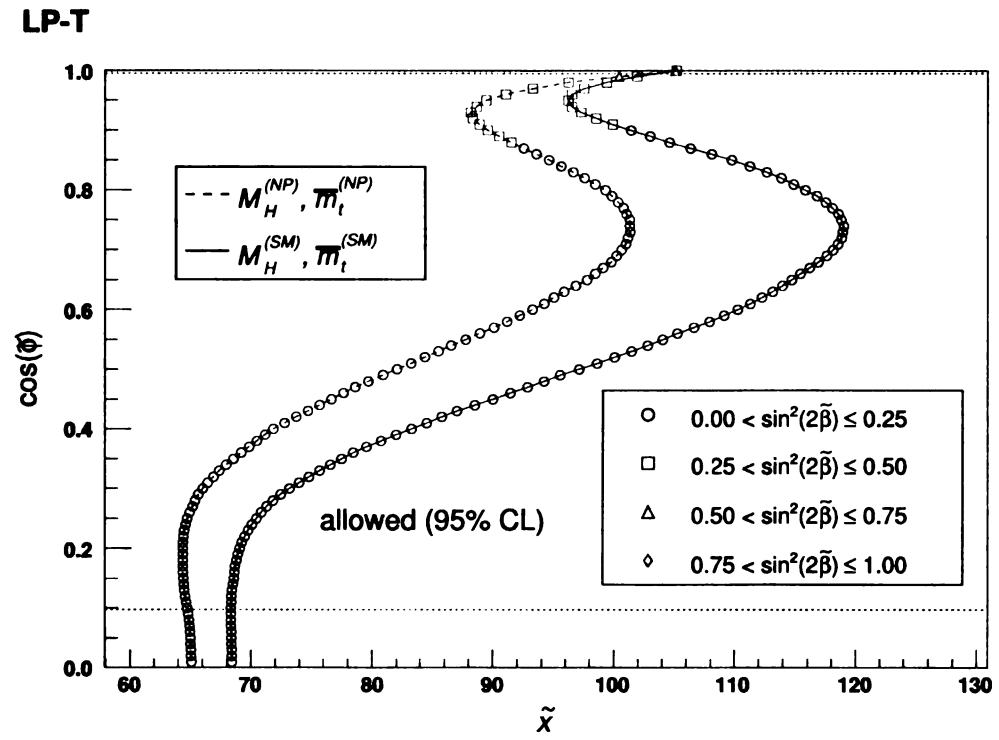

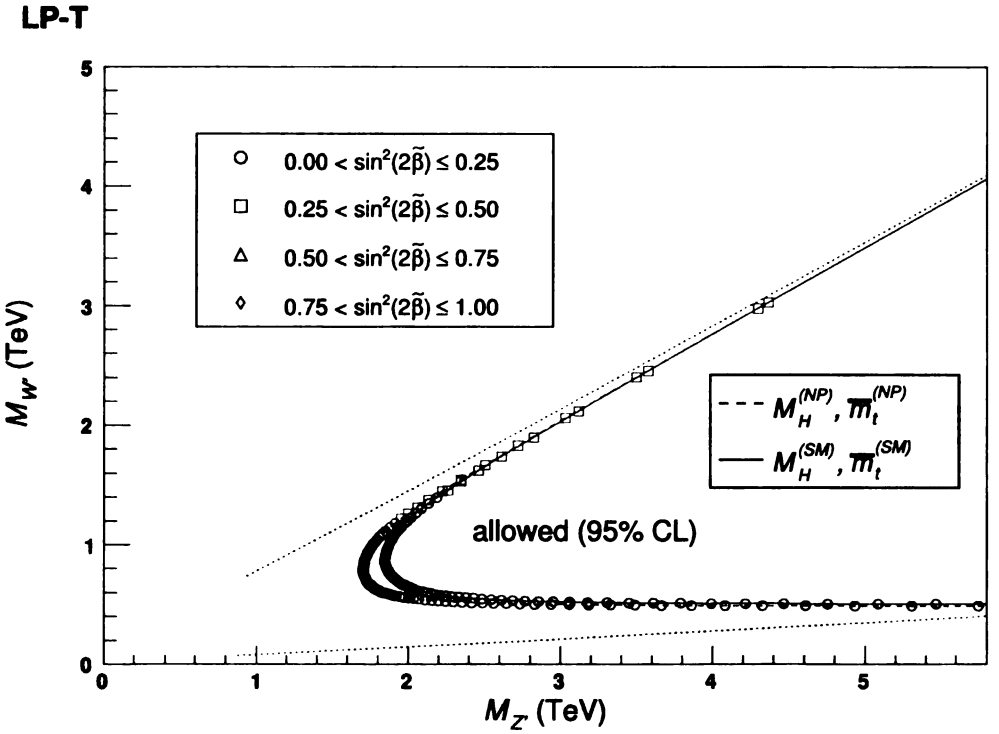

Figure C.6: Bounds on the new physics parameters and the masses of the new heavy gauge bosons in the LP-T model.

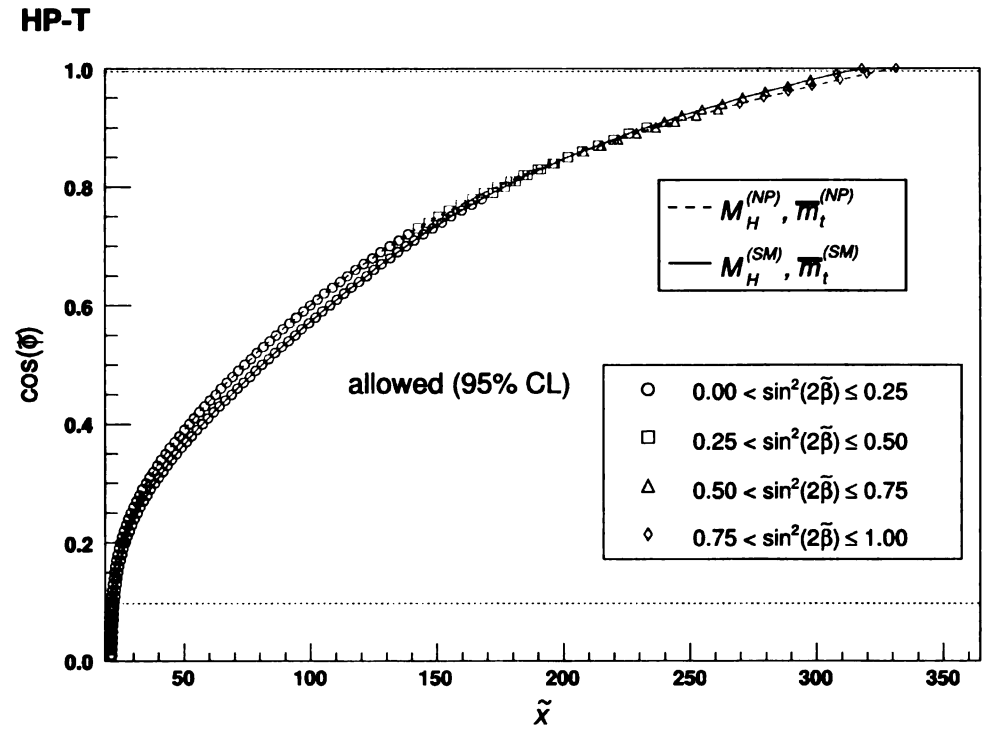

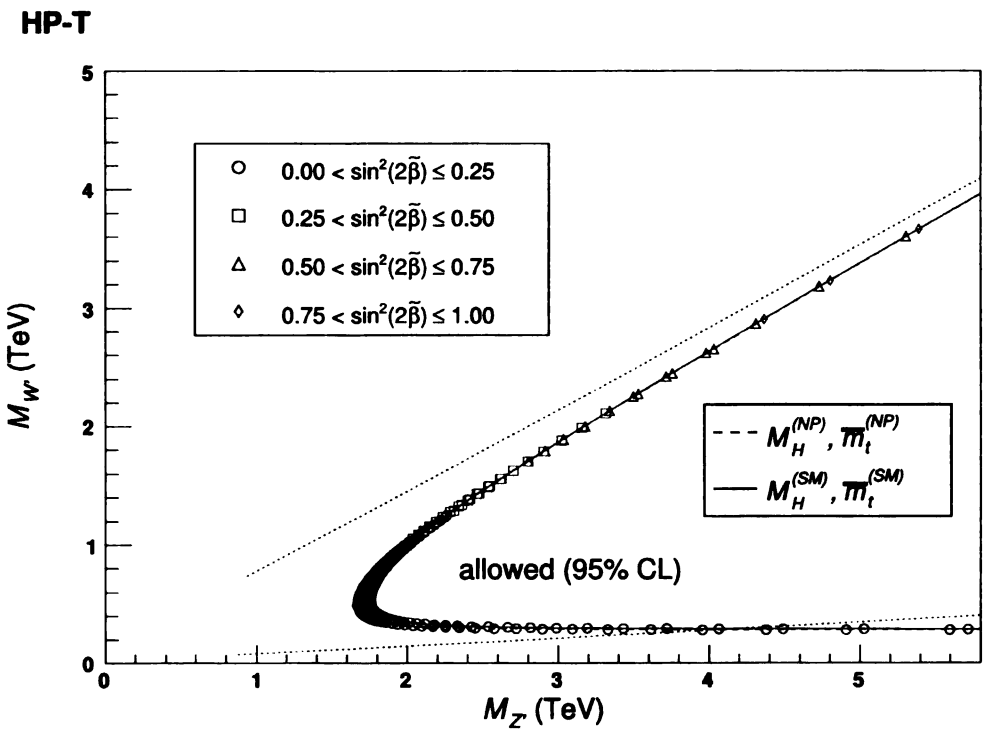

Figure C.7: Bounds on the new physics parameters and the masses of the new heavy gauge bosons in the HP-T model.

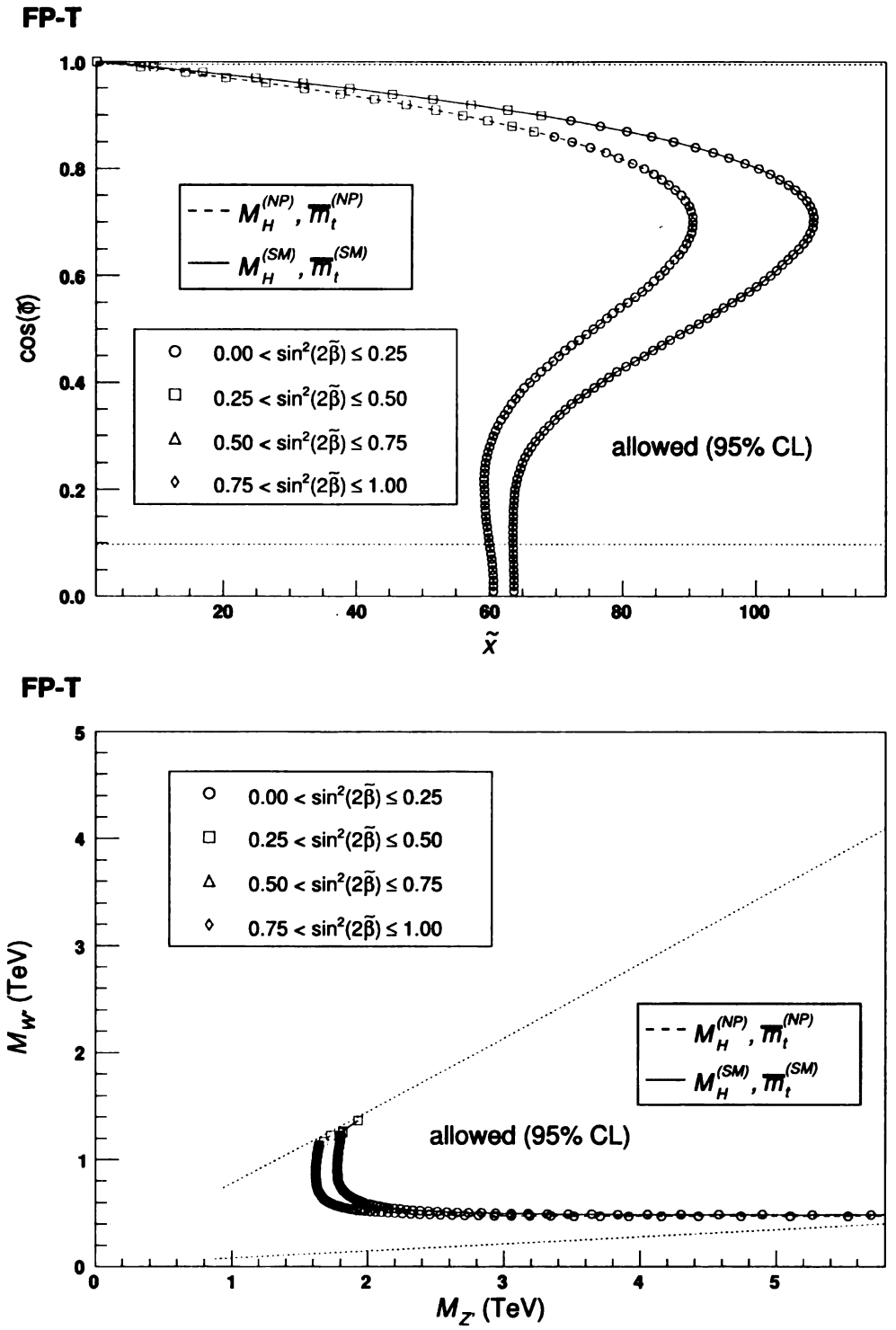

Figure C.8: Bounds on the new physics parameters and the masses of the new heavy gauge bosons in the FP-T model.

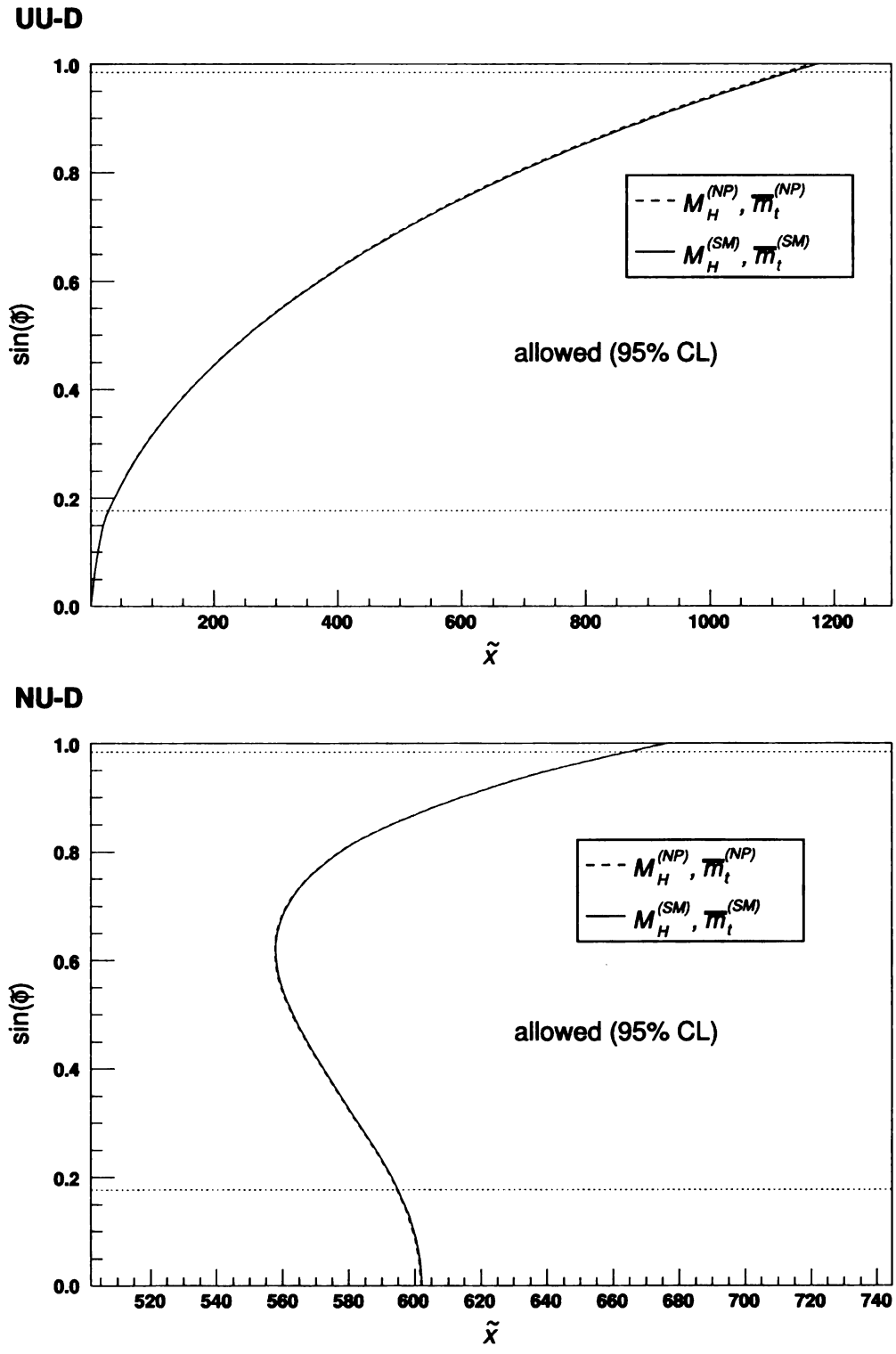

Figure C.9: Bounds on the new physics parameters in the UU-D and the NU-D model.

C.2 Pull Distributions

For each model the pull distribution at a specific point in the excluded part of the parameter space is shown. The goal in choosing the values of the parameters was to find parameter configurations in which the respective features of the pull distributions are clearly visible. The colors of the bars in Fig. C.10 to C.14 indicate the signs of the pulls: Blue bars stands for positive pulls; negative pulls correspond to orange bars.

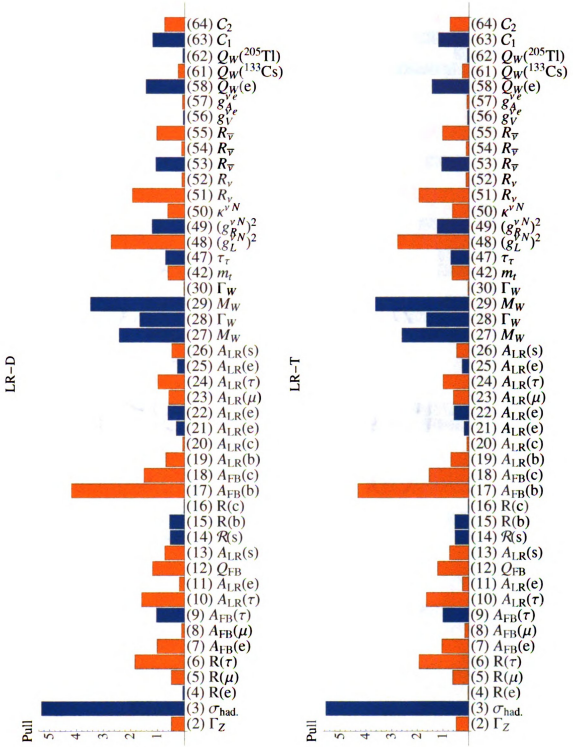

Figure C.10: Pull distributions in the LR models. Parameter values: $\tilde{x} = 300$, $c_{\tilde{\phi}} = 0.90$, $s^2_{2\tilde{\beta}} = 0.00$ (LR-D); $\tilde{x} = 70$, $c_{\tilde{\phi}} = 0.90$, $s^2_{2\tilde{\beta}} = 0.00$ (LR-T).

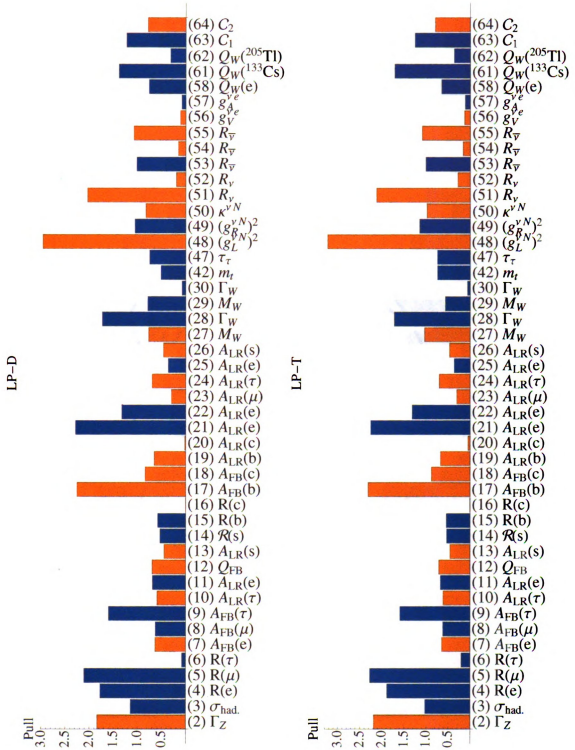

Figure C.11: Pull distributions in the LP models. Parameter values: $\tilde{x} = 300$, $c_{\tilde{\phi}} = 0.71$, $s^2_{2\tilde{\beta}} = 0.00$ (LP-D); $\tilde{x} = 60$, $c_{\tilde{\phi}} = 0.71$, $s^2_{2\tilde{\beta}} = 0.00$ (LP-T).

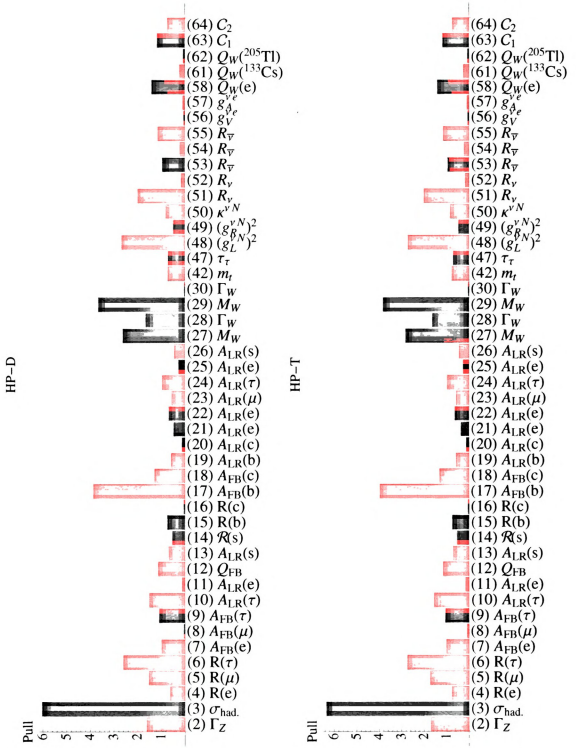

Figure C.12: Pull distributions in the HP models. Parameter values: $\tilde{x} = 300$, $c_{\tilde{\phi}} = 0.90$, $s^2_{2\tilde{\beta}} = 0.00$ (HP-D); $\tilde{x} = 70$, $c_{\tilde{\phi}} = 0.90$, $s^2_{2\tilde{\beta}} = 0.00$ (HP-T).

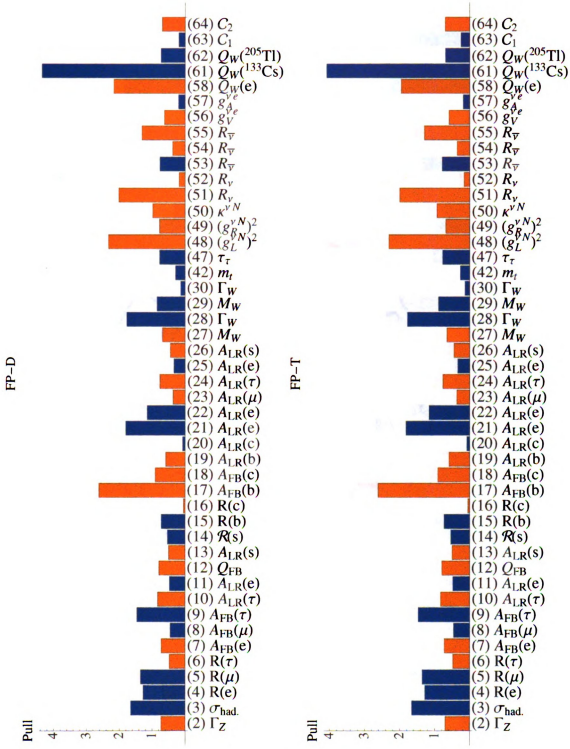

Figure C.13: Pull distributions in the FP models. Parameter values: $\tilde{x} = 150$, $c_{\tilde{\phi}} = 0.20$, $s^2_{2\tilde{\beta}} = 0.00$ (FP-D); $\tilde{x} = 40$, $c_{\tilde{\phi}} = 0.20$, $s^2_{2\tilde{\beta}} = 0.00$ (FP-T).

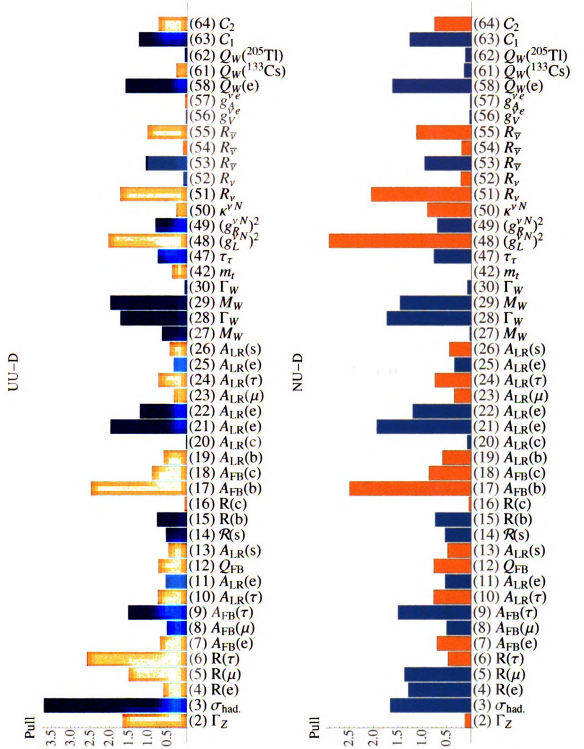

Figure C.14: Pull distributions in the UU-D and NU-D models. Parameter values: $\tilde{x} = 400$, $s_{\tilde{\phi}} = 0.90$ (UU-D); $\tilde{x} = 500$, $c_{\tilde{\phi}} = 0.71$ (NU-D).

Appendix D

Coupling Coefficients

D.1 Couplings in $\mathscr{L}_{\text{ew.}}$

D.1.1 Fermion Couplings to the Z Boson

Left-Handed Couplings $\tilde{g}_L^Z(f)$

The left-handed coupling $\tilde{g}_L^Z(f)$ of a fermion f to the Z boson at the electroweak scale can be written as the sum of the SM coupling $g_{L,\text{SM}}^Z(f)$ and various model-dependent new physics corrections that are proportional to $\frac{1}{\tilde{x}}$.

$$\tilde{g}_L^Z(f) = g_{L,\text{SM}}^Z(f) + \frac{1}{\tilde{x}} \cdot N_1 + \frac{1}{\tilde{x}} s_{2\tilde{\beta}}^2 \cdot N_2 + \frac{1}{\tilde{x}} s_{\tilde{\phi}}^2 \cdot N_3 + \frac{1}{\tilde{x}} s_{\tilde{\phi}}^4 \cdot N_4 \qquad \text{(D.1)}$$

Tabs. D.1 to D.3 list the numerical values of the coefficients N_1, N_2, N_3 and N_4 in Eq. (D.1) for all fermions f and for all considered $G(221)$ models.

Right-Handed Couplings $\tilde{g}_R^Z(f)$

The right-handed coupling $\tilde{g}_R^Z(f)$ of a fermion f to the Z boson at the electroweak scale can be written as the sum of the SM coupling $g_{R,\text{SM}}^Z(f)$ and various model-

f	$g^Z_{L,\mathrm{SM}}$	$\frac{1}{\tilde{x}}$	$\frac{1}{\tilde{x}}s^2_{2\tilde{\beta}}$	$\frac{1}{\tilde{x}}s^2_{\tilde{\phi}}$	$\frac{1}{\tilde{x}}s^4_{\tilde{\phi}}$	Eqn.
u	0.344	0.224	-0.224	-0.615	0.391	(D.2)
d	-0.422	-0.112	0.112	0.0574	0.0546	(D.3)
ν	0.500	0	0	0.500	-0.500	(D.4)
e	-0.266	-0.336	0.336	1.17	-0.836	(D.5)

Table D.1: Left-handed couplings $\tilde{g}^Z_L(f)$ of the fermions to the Z boson in the LR-D, LP-D, HP-D and FP-D model. See text and Eq. (D.1) on the previous page for details.

f	$g^Z_{L,\mathrm{SM}}$	$\frac{1}{\tilde{x}}$	$\frac{1}{\tilde{x}}s^2_{2\tilde{\beta}}$	$\frac{1}{\tilde{x}}s^2_{\tilde{\phi}}$	$\frac{1}{\tilde{x}}s^4_{\tilde{\phi}}$	Eqn.
u	0.344	0.0560	-0.112	-0.154	0.0977	(D.6)
d	-0.422	-0.0280	0.0560	0.0144	0.0137	(D.7)
ν	0.500	0	0	0.125	-0.125	(D.8)
e	-0.266	-0.0840	0.168	0.293	-0.209	(D.9)

Table D.2: Left-handed couplings $\tilde{g}^Z_L(f)$ of the fermions to the Z boson in the LR-T, LP-T, HP-T and FP-T model. See text and Eq. (D.1) on the previous page for details.

f	$g^Z_{L,\mathrm{SM}}$	$\frac{1}{\tilde{x}}s^2_{\tilde{\phi}}$ (UU-D)	$\frac{1}{\tilde{x}}s^2_{\tilde{\phi}}$ (NU-D)	$\frac{1}{\tilde{x}}s^4_{\tilde{\phi}}$	Eqn.
u	0.344	0.500	0.500	-0.276	(D.10)
d	-0.422	-0.500	-0.500	0.388	(D.11)
ν	0.500	0	0.500	-0.500	(D.12)
e	-0.266	0	-0.500	0.164	(D.13)

Table D.3: Left-handed couplings $\tilde{g}^Z_L(f)$ of the fermions to the Z boson in the UU-D and NU-D model. The SM values and the coffecients of the $\frac{1}{\tilde{x}}s^4_{\tilde{\phi}}$ term are the same in both models. The results for the NU-D model apply to the first two fermion generations. See text and Eq. (D.1) on the previous page for details.

f	$g^Z_{R,\mathrm{SM}}$	$\frac{1}{\tilde{x}}$	$\frac{1}{\tilde{x}}s^2_{2\tilde{\beta}}$	$\frac{1}{\tilde{x}}s^2_{\tilde{\varphi}}$	$\frac{1}{\tilde{x}}s^4_{\tilde{\varphi}}$	Eqn.
u	-0.156	0.724	-0.224	-1.61	0.891	(D.15)
d	0.0779	-0.612	0.112	1.06	-0.445	(D.16)
ν	0	0.500	0	-0.500	0	(D.17)
e	0.234	-0.836	0.336	2.17	-1.34	(D.18)

Table D.4: Right-handed couplings $\tilde{g}^Z_R(f)$ of the fermions to the Z boson in the LR-D model. See text and Eq. (D.14) on the current page for details.

f	$g^Z_{R,\mathrm{SM}}$	$\frac{1}{\tilde{x}}$	$\frac{1}{\tilde{x}}s^2_{2\tilde{\beta}}$	$\frac{1}{\tilde{x}}s^2_{\tilde{\varphi}}$	$\frac{1}{\tilde{x}}s^4_{\tilde{\varphi}}$	Eqn.
u	-0.156	0.724	-0.224	-1.61	0.891	(D.19)
d	0.0779	-0.612	0.112	1.06	-0.445	(D.20)
ν	0	0	0	0	0	(D.21)
e	0.234	-0.336	0.336	1.67	-1.34	(D.22)

Table D.5: Right-handed couplings $\tilde{g}^Z_R(f)$ of the fermions to the Z boson in the LP-D model. See text and Eq. (D.14) on the current page for details.

dependent new physics corrections that are proportional to $\frac{1}{\tilde{x}}$.

$$\tilde{g}^Z_R(f) = g^Z_{R,\mathrm{SM}}(f) + \frac{1}{\tilde{x}}\cdot N_1 + \frac{1}{\tilde{x}}s^2_{2\tilde{\beta}}\cdot N_2 + \frac{1}{\tilde{x}}s^2_{\tilde{\varphi}}\cdot N_3 + \frac{1}{\tilde{x}}s^4_{\tilde{\varphi}}\cdot N_4 \qquad \text{(D.14)}$$

Tabs. D.4 to D.12 list the numerical values of the coefficients N_1, N_2, N_3 and N_4 in Eq. (D.14) for all fermions f and for all considered $G(221)$ models.

f	$g^Z_{R,\mathrm{SM}}$	$\frac{1}{\tilde{x}}$	$\frac{1}{\tilde{x}}s^2_{2\tilde{\beta}}$	$\frac{1}{\tilde{x}}s^2_{\tilde{\phi}}$	$\frac{1}{\tilde{x}}s^4_{\tilde{\phi}}$	Eqn.
u	-0.156	0.224	-0.224	-1.11	0.891	(D.23)
d	0.0779	-0.112	0.112	0.557	-0.445	(D.24)
ν	0	0.500	0	-0.500	0	(D.25)
e	0.234	-0.836	0.336	2.17	-1.34	(D.26)

Table D.6: Right-handed couplings $\tilde{g}^Z_R(f)$ of the fermions to the Z boson in the HP-D model. See text and Eq. (D.14) on the previous page for details.

f	$g^Z_{R,\mathrm{SM}}$	$\frac{1}{\tilde{x}}$	$\frac{1}{\tilde{x}}s^2_{2\tilde{\beta}}$	$\frac{1}{\tilde{x}}s^2_{\tilde{\phi}}$	$\frac{1}{\tilde{x}}s^4_{\tilde{\phi}}$	Eqn.
u	-0.156	0.224	-0.224	-1.11	0.891	(D.27)
d	0.0779	-0.112	0.112	0.557	-0.445	(D.28)
ν	0	0	0	0	0	(D.29)
e	0.234	-0.336	0.336	1.67	-1.34	(D.30)

Table D.7: Right-handed couplings $\tilde{g}^Z_R(f)$ of the fermions to the Z boson in the FP-D model. See text and Eq. (D.14) on the previous page for details.

f	$g^Z_{R,\mathrm{SM}}$	$\frac{1}{\tilde{x}}$	$\frac{1}{\tilde{x}}s^2_{2\tilde{\beta}}$	$\frac{1}{\tilde{x}}s^2_{\tilde{\phi}}$	$\frac{1}{\tilde{x}}s^4_{\tilde{\phi}}$	Eqn.
u	-0.156	0.181	-0.112	-0.404	0.223	(D.31)
d	0.0779	-0.153	0.0560	0.264	-0.111	(D.32)
ν	0	0.125	0	-0.125	0	(D.33)
e	0.234	-0.209	0.168	0.543	-0.334	(D.34)

Table D.8: Right-handed couplings $\tilde{g}^Z_R(f)$ of the fermions to the Z boson in the LR-T model. See text and Eq. (D.14) on the previous page for details.

f	$g^Z_{R,\mathrm{SM}}$	$\frac{1}{\tilde{x}}$	$\frac{1}{\tilde{x}}s^2_{2\tilde{\beta}}$	$\frac{1}{\tilde{x}}s^2_{\tilde{\phi}}$	$\frac{1}{\tilde{x}}s^4_{\tilde{\phi}}$	Eqn.
u	-0.156	0.181	-0.112	-0.404	0.223	(D.35)
d	0.0779	-0.153	0.0560	0.264	-0.111	(D.36)
ν	0	0	0	0	0	(D.37)
e	0.234	-0.0840	0.168	0.418	-0.334	(D.38)

Table D.9: Right-handed couplings $\tilde{g}^Z_R(f)$ of the fermions to the Z boson in the LP-T model. See text and Eq. (D.14) on the previous page for details.

f	$g^Z_{R,\mathrm{SM}}$	$\frac{1}{\tilde{x}}$	$\frac{1}{\tilde{x}}s^2_{2\tilde{\beta}}$	$\frac{1}{\tilde{x}}s^2_{\tilde{\phi}}$	$\frac{1}{\tilde{x}}s^4_{\tilde{\phi}}$	Eqn.
u	-0.156	0.0560	-0.112	-0.279	0.223	(D.39)
d	0.0779	-0.0280	0.0560	0.139	-0.111	(D.40)
ν	0	0.125	0	-0.125	0	(D.41)
e	0.234	-0.209	0.168	0.543	-0.334	(D.42)

Table D.10: Right-handed couplings $\tilde{g}^Z_R(f)$ of the fermions to the Z boson in the HP-T model. See text and Eq. (D.14) on page 155 for details.

f	$g^Z_{R,\mathrm{SM}}$	$\frac{1}{\tilde{x}}$	$\frac{1}{\tilde{x}}s^2_{2\tilde{\beta}}$	$\frac{1}{\tilde{x}}s^2_{\tilde{\phi}}$	$\frac{1}{\tilde{x}}s^4_{\tilde{\phi}}$	Eqn.
u	-0.156	0.0560	-0.112	-0.279	0.223	(D.43)
d	0.0779	-0.0280	0.0560	0.139	-0.111	(D.44)
ν	0	0	0	0	0	(D.45)
e	0.234	-0.0840	0.168	0.418	-0.334	(D.46)

Table D.11: Right-handed couplings $\tilde{g}^Z_R(f)$ of the fermions to the Z boson in the FP-T model. See text and Eq. (D.14) on page 155 for details.

f	$g^Z_{R,\mathrm{SM}}$	$\frac{1}{\tilde{x}}s^4_{\tilde{\phi}}$	Eqn.
u	-0.156	0.224	(D.47)
d	0.0779	-0.112	(D.48)
ν	0	0	(D.49)
e	0.234	-0.336	(D.50)

Table D.12: Right-handed couplings $\tilde{g}^Z_R(f)$ of the fermions to the Z boson in the UU-D and NU-D model. The results for the NU-D model apply to the first two fermion generations. See text and Eq. (D.14) on page 155 for details.

D.1.2 Couplings of the New Physics Currents

Couplings of the Neutral Fermion Currents

The coupling coefficients $C_{ew.}^{\mathrm{NC}}\left(f_{1,i}, f_{2,j}\right)$ of the neutral current four-fermion interactions in the effective Lagrangian at the electroweak scale are defined such that the Lagrangian $\mathscr{L}_{ew.}^{\mathrm{NC}} = -\frac{1}{2}\widetilde{M}_{\tilde{Z}'}^{-2} K_{\mu}^{0} K^{0,\mu}$ takes the following form:

$$\mathscr{L}_{ew.}^{\mathrm{NC}} \equiv -\frac{G_F}{\sqrt{2}} \sum_{f_1,f_2} \sum_{i,j} C_{ew.}^{\mathrm{NC}}\left(f_{1,i}, f_{2,j}\right) \left(\bar{f}_1 f_1\right)_{i,\mu} \left(\bar{f}_2 f_2\right)_j^{\mu} \qquad ; i,j = L,R$$

They can be written as the sum of various model-dependent new physics corrections that are proportional to $\frac{1}{\tilde{x}}$.

$$C_{ew.}^{\mathrm{NC}}\left(f_{1,i}, f_{2,j}\right) = \frac{1}{\tilde{x}} \cdot N_1 + \frac{1}{\tilde{x}} s_{\tilde{\phi}}^2 \cdot N_2 + \frac{1}{\tilde{x}} s_{\tilde{\phi}}^4 \cdot N_3 \tag{D.51}$$

Absolute terms that are independent of $\tilde{x}$ do not appear in $C_{ew.}^{\mathrm{NC}}\left(f_{1,i}, f_{2,j}\right)$ since the four-fermion interactions in $\mathscr{L}_{ew.}$ represent a pure effect of the new physics in the $G(221)$ models. Tabs. D.13 to D.22 list the numerical values of the coefficients N_1, N_2 and N_3 in Eq. (D.51) for all possible fermion pairs $\left(f_{1,i}, f_{2,j}\right)$ and for all considered $G(221)$ models.

Couplings of the Charged Fermion Currents

The coupling coefficients $C_{ew.}^{\mathrm{CC}}\left(f_{1,i}, f_{3,j}\right)$ of the charged current four-fermion interactions in the effective Lagrangian at the electroweak scale are defined such that the Lagrangian $\mathscr{L}_{ew.}^{\mathrm{CC}} = -\widetilde{M}_{W'}^{-2} K_{\mu}^{+} K^{--,\mu}$ takes the following form:

$$\mathscr{L}_{ew.}^{\mathrm{CC}} \equiv -\frac{G_F}{\sqrt{2}} \sum_{f_1, f_3} \sum_{i,j} C_{ew.}^{\mathrm{CC}}\left(f_{1,i}, f_{3,j}\right) \left(\bar{f}_1 f_2\right)_{i,\mu} \left(\bar{f}_3 f_4\right)_j^{\mu} \qquad ; i,j = L,R$$

They can be written as the sum of various model-dependent new physics corrections that are proportional to $\frac{1}{\tilde{x}}$.

$$C_{ew.}^{\mathrm{CC}}\left(f_{1,i}, f_{3,j}\right) = \frac{1}{\tilde{x}} \cdot N_1 + \frac{1}{\tilde{x}} s_{\tilde{\phi}}^2 \cdot N_2 + \frac{1}{\tilde{x}} s_{\tilde{\phi}}^4 \cdot N_3 \tag{D.412}$$

Absolute terms that are independent of $\tilde{x}$ do not appear in $C_{ew.}^{\mathrm{CC}}\left(f_{1,i}, f_{3,j}\right)$ since the four-fermion interactions in $\mathscr{L}_{ew.}$ represent a pure effect of the new physics in the $G(221)$ models. Tabs. D.23 to D.26 list the numerical values of the coefficients N_1, N_2 and N_3 in Eq. (D.412) for all possible fermion pairs $\left(f_{1,i}, f_{3,j}\right)$ and for all considered $G(221)$ models. The couplings in the models of the first breaking pattern have a very simple form which allows us to combine our results for the (BP-I,D) and the (BP-I,T) models in one table each.

$(\bar{f}_1 f_1)_{L,R}$	$(\bar{f}_2 f_2)_{L,R}$	$\frac{1}{\tilde{x}}$	$\frac{1}{\tilde{x}} s^2_{\tilde{\phi}}$	$\frac{1}{\tilde{x}} s^4_{\tilde{\phi}}$	Eqn.
$(\bar{u}u)_L$	$(\bar{u}u)_L$	0	0	0.0556	(D.52)
$(\bar{u}u)_L$	$(\bar{u}u)_R$	0	-0.167	0.222	(D.53)
$(\bar{u}u)_L$	$(\bar{d}d)_L$	0	0	0.0556	(D.54)
$(\bar{u}u)_L$	$(\bar{d}d)_R$	0	0.167	-0.111	(D.55)
$(\bar{u}u)_L$	$(\bar{\nu}\nu)_L$	0	0	-0.167	(D.56)
$(\bar{u}u)_L$	$(\bar{\nu}\nu)_R$	0	-0.167	0	(D.57)
$(\bar{u}u)_L$	$(\bar{e}e)_L$	0	0	-0.167	(D.58)
$(\bar{u}u)_L$	$(\bar{e}e)_R$	0	0.167	-0.333	(D.59)
$(\bar{u}u)_R$	$(\bar{u}u)_R$	0.500	-1.33	0.889	(D.60)
$(\bar{u}u)_R$	$(\bar{d}d)_L$	0	-0.167	0.222	(D.61)
$(\bar{u}u)_R$	$(\bar{d}d)_R$	-0.500	1.00	-0.444	(D.62)
$(\bar{u}u)_R$	$(\bar{\nu}\nu)_L$	0	0.500	-0.667	(D.63)
$(\bar{u}u)_R$	$(\bar{\nu}\nu)_R$	0.500	-0.667	0	(D.64)
$(\bar{u}u)_R$	$(\bar{e}e)_L$	0	0.500	-0.667	(D.65)
$(\bar{u}u)_R$	$(\bar{e}e)_R$	-0.500	1.67	-1.33	(D.66)
$(\bar{d}d)_L$	$(\bar{d}d)_L$	0	0	0.0556	(D.67)
$(\bar{d}d)_L$	$(\bar{d}d)_R$	0	0.167	-0.111	(D.68)
$(\bar{d}d)_L$	$(\bar{\nu}\nu)_L$	0	0	-0.167	(D.69)
$(\bar{d}d)_L$	$(\bar{\nu}\nu)_R$	0	-0.167	0	(D.70)
$(\bar{d}d)_L$	$(\bar{e}e)_L$	0	0	-0.167	(D.71)
$(\bar{d}d)_L$	$(\bar{e}e)_R$	0	0.167	-0.333	(D.72)
$(\bar{d}d)_R$	$(\bar{d}d)_R$	0.500	-0.667	0.222	(D.73)
$(\bar{d}d)_R$	$(\bar{\nu}\nu)_L$	0	-0.500	0.333	(D.74)
$(\bar{d}d)_R$	$(\bar{\nu}\nu)_R$	-0.500	0.333	0	(D.75)
$(\bar{d}d)_R$	$(\bar{e}e)_L$	0	-0.500	0.333	(D.76)
$(\bar{d}d)_R$	$(\bar{e}e)_R$	0.500	-1.33	0.667	(D.77)
$(\bar{\nu}\nu)_L$	$(\bar{\nu}\nu)_L$	0	0	0.500	(D.78)
$(\bar{\nu}\nu)_L$	$(\bar{\nu}\nu)_R$	0	0.500	0	(D.79)
$(\bar{\nu}\nu)_L$	$(\bar{e}e)_L$	0	0	0.500	(D.80)
$(\bar{\nu}\nu)_L$	$(\bar{e}e)_R$	0	-0.500	1.00	(D.81)
$(\bar{\nu}\nu)_R$	$(\bar{\nu}\nu)_R$	0.500	0	0	(D.82)
$(\bar{\nu}\nu)_R$	$(\bar{e}e)_L$	0	0.500	0	(D.83)
$(\bar{\nu}\nu)_R$	$(\bar{e}e)_R$	-0.500	1.00	0	(D.84)
$(\bar{e}e)_L$	$(\bar{e}e)_L$	0	0	0.500	(D.85)
$(\bar{e}e)_L$	$(\bar{e}e)_R$	0	-0.500	1.00	(D.86)
$(\bar{e}e)_R$	$(\bar{e}e)_R$	0.500	-2.00	2.00	(D.87)

Table D.13: Couplings $C^{\rm NC}_{ew.}(f_{1,i}, f_{2,j})$ of the neutral fermion currents at the electroweak scale in the LR-D model. See text and Eq. (D.51) on page 158 for details.

$(\bar{f}_1 f_1)_{L,R}$	$(\bar{f}_2 f_2)_{L,R}$	$\frac{1}{\tilde{x}}$	$\frac{1}{\tilde{x}} s^2_{\tilde{\phi}}$	$\frac{1}{\tilde{x}} s^4_{\tilde{\phi}}$	Eqn.
$(\bar{u}u)_L$	$(\bar{u}u)_L$	0	0	0.0556	(D.88)
$(\bar{u}u)_L$	$(\bar{u}u)_R$	0	-0.167	0.222	(D.89)
$(\bar{u}u)_L$	$(\bar{d}d)_L$	0	0	0.0556	(D.90)
$(\bar{u}u)_L$	$(\bar{d}d)_R$	0	0.167	-0.111	(D.91)
$(\bar{u}u)_L$	$(\bar{\nu}\nu)_L$	0	0	-0.167	(D.92)
$(\bar{u}u)_L$	$(\bar{\nu}\nu)_R$	0	0	0	(D.93)
$(\bar{u}u)_L$	$(\bar{e}e)_L$	0	0	-0.167	(D.94)
$(\bar{u}u)_L$	$(\bar{e}e)_R$	0	0	-0.333	(D.95)
$(\bar{u}u)_R$	$(\bar{u}u)_R$	0.500	-1.33	0.889	(D.96)
$(\bar{u}u)_R$	$(\bar{d}d)_L$	0	-0.167	0.222	(D.97)
$(\bar{u}u)_R$	$(\bar{d}d)_R$	-0.500	1.00	-0.444	(D.98)
$(\bar{u}u)_R$	$(\bar{\nu}\nu)_L$	0	0.500	-0.667	(D.99)
$(\bar{u}u)_R$	$(\bar{\nu}\nu)_R$	0	0	0	(D.100)
$(\bar{u}u)_R$	$(\bar{e}e)_L$	0	0.500	-0.667	(D.101)
$(\bar{u}u)_R$	$(\bar{e}e)_R$	0	1.00	-1.33	(D.102)
$(\bar{d}d)_L$	$(\bar{d}d)_L$	0	0	0.0556	(D.103)
$(\bar{d}d)_L$	$(\bar{d}d)_R$	0	0.167	-0.111	(D.104)
$(\bar{d}d)_L$	$(\bar{\nu}\nu)_L$	0	0	-0.167	(D.105)
$(\bar{d}d)_L$	$(\bar{\nu}\nu)_R$	0	0	0	(D.106)
$(\bar{d}d)_L$	$(\bar{e}e)_L$	0	0	-0.167	(D.107)
$(\bar{d}d)_L$	$(\bar{e}e)_R$	0	0	-0.333	(D.108)
$(\bar{d}d)_R$	$(\bar{d}d)_R$	0.500	-0.667	0.222	(D.109)
$(\bar{d}d)_R$	$(\bar{\nu}\nu)_L$	0	-0.500	0.333	(D.110)
$(\bar{d}d)_R$	$(\bar{\nu}\nu)_R$	0	0	0	(D.111)
$(\bar{d}d)_R$	$(\bar{e}e)_L$	0	-0.500	0.333	(D.112)
$(\bar{d}d)_R$	$(\bar{e}e)_R$	0	-1.00	0.667	(D.113)
$(\bar{\nu}\nu)_L$	$(\bar{\nu}\nu)_L$	0	0	0.500	(D.114)
$(\bar{\nu}\nu)_L$	$(\bar{\nu}\nu)_R$	0	0	0	(D.115)
$(\bar{\nu}\nu)_L$	$(\bar{e}e)_L$	0	0	0.500	(D.116)
$(\bar{\nu}\nu)_L$	$(\bar{e}e)_R$	0	0	1.00	(D.117)
$(\bar{\nu}\nu)_R$	$(\bar{\nu}\nu)_R$	0	0	0	(D.118)
$(\bar{\nu}\nu)_R$	$(\bar{e}e)_L$	0	0	0	(D.119)
$(\bar{\nu}\nu)_R$	$(\bar{e}e)_R$	0	0	0	(D.120)
$(\bar{e}e)_L$	$(\bar{e}e)_L$	0	0	0.500	(D.121)
$(\bar{e}e)_L$	$(\bar{e}e)_R$	0	0	1.00	(D.122)
$(\bar{e}e)_R$	$(\bar{e}e)_R$	0	0	2.00	(D.123)

Table D.14: Couplings $C^{\rm NC}_{ew.}\left(f_{1,i}, f_{2,j}\right)$ of the neutral fermion currents at the electroweak scale in the LP-D model. See text and Eq. (D.51) on page 158 for details.

$(\bar{f}_1 f_1)_{L,R}$	$(\bar{f}_2 f_2)_{L,R}$	$\frac{1}{\tilde{x}}$	$\frac{1}{\tilde{x}} s^2_{\tilde{\phi}}$	$\frac{1}{\tilde{x}} s^4_{\tilde{\phi}}$	Eqn.
$(\bar{u}u)_L$	$(\bar{u}u)_L$	0	0	0.0556	(D.124)
$(\bar{u}u)_L$	$(\bar{u}u)_R$	0	0	0.222	(D.125)
$(\bar{u}u)_L$	$(\bar{d}d)_L$	0	0	0.0556	(D.126)
$(\bar{u}u)_L$	$(\bar{d}d)_R$	0	0	-0.111	(D.127)
$(\bar{u}u)_L$	$(\bar{\nu}\nu)_L$	0	0	-0.167	(D.128)
$(\bar{u}u)_L$	$(\bar{\nu}\nu)_R$	0	-0.167	0	(D.129)
$(\bar{u}u)_L$	$(\bar{e}e)_L$	0	0	-0.167	(D.130)
$(\bar{u}u)_L$	$(\bar{e}e)_R$	0	0.167	-0.333	(D.131)
$(\bar{u}u)_R$	$(\bar{u}u)_R$	0	0	0.889	(D.132)
$(\bar{u}u)_R$	$(\bar{d}d)_L$	0	0	0.222	(D.133)
$(\bar{u}u)_R$	$(\bar{d}d)_R$	0	0	-0.444	(D.134)
$(\bar{u}u)_R$	$(\bar{\nu}\nu)_L$	0	0	-0.667	(D.135)
$(\bar{u}u)_R$	$(\bar{\nu}\nu)_R$	0	-0.667	0	(D.136)
$(\bar{u}u)_R$	$(\bar{e}e)_L$	0	0	-0.667	(D.137)
$(\bar{u}u)_R$	$(\bar{e}e)_R$	0	0.667	-1.33	(D.138)
$(\bar{d}d)_L$	$(\bar{d}d)_L$	0	0	0.0556	(D.139)
$(\bar{d}d)_L$	$(\bar{d}d)_R$	0	0	-0.111	(D.140)
$(\bar{d}d)_L$	$(\bar{\nu}\nu)_L$	0	0	-0.167	(D.141)
$(\bar{d}d)_L$	$(\bar{\nu}\nu)_R$	0	-0.167	0	(D.142)
$(\bar{d}d)_L$	$(\bar{e}e)_L$	0	0	-0.167	(D.143)
$(\bar{d}d)_L$	$(\bar{e}e)_R$	0	0.167	-0.333	(D.144)
$(\bar{d}d)_R$	$(\bar{d}d)_R$	0	0	0.222	(D.145)
$(\bar{d}d)_R$	$(\bar{\nu}\nu)_L$	0	0	0.333	(D.146)
$(\bar{d}d)_R$	$(\bar{\nu}\nu)_R$	0	0.333	0	(D.147)
$(\bar{d}d)_R$	$(\bar{e}e)_L$	0	0	0.333	(D.148)
$(\bar{d}d)_R$	$(\bar{e}e)_R$	0	-0.333	0.667	(D.149)
$(\bar{\nu}\nu)_L$	$(\bar{\nu}\nu)_L$	0	0	0.500	(D.150)
$(\bar{\nu}\nu)_L$	$(\bar{\nu}\nu)_R$	0	0.500	0	(D.151)
$(\bar{\nu}\nu)_L$	$(\bar{e}e)_L$	0	0	0.500	(D.152)
$(\bar{\nu}\nu)_L$	$(\bar{e}e)_R$	0	-0.500	1.00	(D.153)
$(\bar{\nu}\nu)_R$	$(\bar{\nu}\nu)_R$	0.500	0	0	(D.154)
$(\bar{\nu}\nu)_R$	$(\bar{e}e)_L$	0	0.500	0	(D.155)
$(\bar{\nu}\nu)_R$	$(\bar{e}e)_R$	-0.500	1.00	0	(D.156)
$(\bar{e}e)_L$	$(\bar{e}e)_L$	0	0	0.500	(D.157)
$(\bar{e}e)_L$	$(\bar{e}e)_R$	0	-0.500	1.00	(D.158)
$(\bar{e}e)_R$	$(\bar{e}e)_R$	0.500	-2.00	2.00	(D.159)

Table D.15: Couplings $C^{\rm NC}_{ew.}\left(f_{1,i}, f_{2,j}\right)$ of the neutral fermion currents at the electroweak scale in the HP-D model. See text and Eq. (D.51) on page 158 for details.

$(\bar{f}_1 f_1)_{L,R}$	$(\bar{f}_2 f_2)_{L,R}$	$\frac{1}{x}$	$\frac{1}{x}s_\phi^2$	$\frac{1}{x}s_\phi^4$	Eqn.
$(\bar{u}u)_L$	$(\bar{u}u)_L$	0	0	0.0556	(D.160)
$(\bar{u}u)_L$	$(\bar{u}u)_R$	0	0	0.222	(D.161)
$(\bar{u}u)_L$	$(\bar{d}d)_L$	0	0	0.0556	(D.162)
$(\bar{u}u)_L$	$(\bar{d}d)_R$	0	0	-0.111	(D.163)
$(\bar{u}u)_L$	$(\bar{\nu}\nu)_L$	0	0	-0.167	(D.164)
$(\bar{u}u)_L$	$(\bar{\nu}\nu)_R$	0	0	0	(D.165)
$(\bar{u}u)_L$	$(\bar{e}e)_L$	0	0	-0.167	(D.166)
$(\bar{u}u)_L$	$(\bar{e}e)_R$	0	0	-0.333	(D.167)
$(\bar{u}u)_R$	$(\bar{u}u)_R$	0	0	0.889	(D.168)
$(\bar{u}u)_R$	$(\bar{d}d)_L$	0	0	0.222	(D.169)
$(\bar{u}u)_R$	$(\bar{d}d)_R$	0	0	-0.444	(D.170)
$(\bar{u}u)_R$	$(\bar{\nu}\nu)_L$	0	0	-0.667	(D.171)
$(\bar{u}u)_R$	$(\bar{\nu}\nu)_R$	0	0	0	(D.172)
$(\bar{u}u)_R$	$(\bar{e}e)_L$	0	0	-0.667	(D.173)
$(\bar{u}u)_R$	$(\bar{e}e)_R$	0	0	-1.33	(D.174)
$(\bar{d}d)_L$	$(\bar{d}d)_L$	0	0	0.0556	(D.175)
$(\bar{d}d)_L$	$(\bar{d}d)_R$	0	0	-0.111	(D.176)
$(\bar{d}d)_L$	$(\bar{\nu}\nu)_L$	0	0	-0.167	(D.177)
$(\bar{d}d)_L$	$(\bar{\nu}\nu)_R$	0	0	0	(D.178)
$(\bar{d}d)_L$	$(\bar{e}e)_L$	0	0	-0.167	(D.179)
$(\bar{d}d)_L$	$(\bar{e}e)_R$	0	0	-0.333	(D.180)
$(\bar{d}d)_R$	$(\bar{d}d)_R$	0	0	0.222	(D.181)
$(\bar{d}d)_R$	$(\bar{\nu}\nu)_L$	0	0	0.333	(D.182)
$(\bar{d}d)_R$	$(\bar{\nu}\nu)_R$	0	0	0	(D.183)
$(\bar{d}d)_R$	$(\bar{e}e)_L$	0	0	0.333	(D.184)
$(\bar{d}d)_R$	$(\bar{e}e)_R$	0	0	0.667	(D.185)
$(\bar{\nu}\nu)_L$	$(\bar{\nu}\nu)_L$	0	0	0.500	(D.186)
$(\bar{\nu}\nu)_L$	$(\bar{\nu}\nu)_R$	0	0	0	(D.187)
$(\bar{\nu}\nu)_L$	$(\bar{e}e)_L$	0	0	0.500	(D.188)
$(\bar{\nu}\nu)_L$	$(\bar{e}e)_R$	0	0	1.00	(D.189)
$(\bar{\nu}\nu)_R$	$(\bar{\nu}\nu)_R$	0	0	0	(D.190)
$(\bar{\nu}\nu)_R$	$(\bar{e}e)_L$	0	0	0	(D.191)
$(\bar{\nu}\nu)_R$	$(\bar{e}e)_R$	0	0	0	(D.192)
$(\bar{e}e)_L$	$(\bar{e}e)_L$	0	0	0.500	(D.193)
$(\bar{e}e)_L$	$(\bar{e}e)_R$	0	0	1.00	(D.194)
$(\bar{e}e)_R$	$(\bar{e}e)_R$	0	0	2.00	(D.195)

Table D.16: Couplings $C_{ew.}^{\mathrm{NC}}\left(f_{1,i}, f_{2,j}\right)$ of the neutral fermion currents at the electroweak scale in the FP-D model. See text and Eq. (D.51) on page 158 for details.

$(\bar{f}_1 f_1)_C$	$(\bar{f}_2 f_2)_C$	$\frac{1}{\tilde{x}}$	$\frac{1}{\tilde{x}} s^2_{\tilde{\phi}}$	$\frac{1}{\tilde{x}} s^4_{\tilde{\phi}}$	Eqn.
$(\bar{u}u)_L$	$(\bar{u}u)_L$	0	0	0.0139	(D.196)
$(\bar{u}u)_L$	$(\bar{u}u)_R$	0	-0.0417	0.0556	(D.197)
$(\bar{u}u)_L$	$(\bar{d}d)_L$	0	0	0.0139	(D.198)
$(\bar{u}u)_L$	$(\bar{d}d)_R$	0	0.0417	-0.0278	(D.199)
$(\bar{u}u)_L$	$(\bar{\nu}\nu)_L$	0	0	-0.0417	(D.200)
$(\bar{u}u)_L$	$(\bar{\nu}\nu)_R$	0	-0.0417	0	(D.201)
$(\bar{u}u)_L$	$(\bar{e}e)_L$	0	0	-0.0417	(D.202)
$(\bar{u}u)_L$	$(\bar{e}e)_R$	0	0.0417	-0.0833	(D.203)
$(\bar{u}u)_R$	$(\bar{u}u)_R$	0.125	-0.333	0.222	(D.204)
$(\bar{u}u)_R$	$(\bar{d}d)_L$	0	-0.0417	0.0556	(D.205)
$(\bar{u}u)_R$	$(\bar{d}d)_R$	-0.125	0.250	-0.111	(D.206)
$(\bar{u}u)_R$	$(\bar{\nu}\nu)_L$	0	0.125	-0.167	(D.207)
$(\bar{u}u)_R$	$(\bar{\nu}\nu)_R$	0.125	-0.167	0	(D.208)
$(\bar{u}u)_R$	$(\bar{e}e)_L$	0	0.125	-0.167	(D.209)
$(\bar{u}u)_R$	$(\bar{e}e)_R$	-0.125	0.417	-0.333	(D.210)
$(\bar{d}d)_L$	$(\bar{d}d)_L$	0	0	0.0139	(D.211)
$(\bar{d}d)_L$	$(\bar{d}d)_R$	0	0.0417	-0.0278	(D.212)
$(\bar{d}d)_L$	$(\bar{\nu}\nu)_L$	0	0	-0.0417	(D.213)
$(\bar{d}d)_L$	$(\bar{\nu}\nu)_R$	0	-0.0417	0	(D.214)
$(\bar{d}d)_L$	$(\bar{e}e)_L$	0	0	-0.0417	(D.215)
$(\bar{d}d)_L$	$(\bar{e}e)_R$	0	0.0417	-0.0833	(D.216)
$(\bar{d}d)_R$	$(\bar{d}d)_R$	0.125	-0.167	0.0556	(D.217)
$(\bar{d}d)_R$	$(\bar{\nu}\nu)_L$	0	-0.125	0.0833	(D.218)
$(\bar{d}d)_R$	$(\bar{\nu}\nu)_R$	-0.125	0.0833	0	(D.219)
$(\bar{d}d)_R$	$(\bar{e}e)_L$	0	-0.125	0.0833	(D.220)
$(\bar{d}d)_R$	$(\bar{e}e)_R$	0.125	-0.333	0.167	(D.221)
$(\bar{\nu}\nu)_L$	$(\bar{\nu}\nu)_L$	0	0	0.125	(D.222)
$(\bar{\nu}\nu)_L$	$(\bar{\nu}\nu)_R$	0	0.125	0	(D.223)
$(\bar{\nu}\nu)_L$	$(\bar{e}e)_L$	0	0	0.125	(D.224)
$(\bar{\nu}\nu)_L$	$(\bar{e}e)_R$	0	-0.125	0.250	(D.225)
$(\bar{\nu}\nu)_R$	$(\bar{\nu}\nu)_R$	0.125	0	0	(D.226)
$(\bar{\nu}\nu)_R$	$(\bar{e}e)_L$	0	0.125	0	(D.227)
$(\bar{\nu}\nu)_R$	$(\bar{e}e)_R$	-0.125	0.250	0	(D.228)
$(\bar{e}e)_L$	$(\bar{e}e)_L$	0	0	0.125	(D.229)
$(\bar{e}e)_L$	$(\bar{e}e)_R$	0	-0.125	0.250	(D.230)
$(\bar{e}e)_R$	$(\bar{e}e)_R$	0.125	-0.500	0.500	(D.231)

Table D.17: Couplings $C^{\rm NC}_{ew.}\left(f_{1,i}, f_{2,j}\right)$ of the neutral fermion currents at the electroweak scale in the LR-T model. See text and Eq. (D.51) on page 158 for details.

$(\bar{f}_1 f_1)_C$	$(\bar{f}_2 f_2)_C$	$\frac{1}{\tilde{x}}$	$\frac{1}{\tilde{x}} s^2_{\tilde{\phi}}$	$\frac{1}{\tilde{x}} s^4_{\tilde{\phi}}$	Eqn.
$(\bar{u}u)_L$	$(\bar{u}u)_L$	0	0	0.0139	(D.232)
$(\bar{u}u)_L$	$(\bar{u}u)_R$	0	-0.0417	0.0556	(D.233)
$(\bar{u}u)_L$	$(\bar{d}d)_L$	0	0	0.0139	(D.234)
$(\bar{u}u)_L$	$(\bar{d}d)_R$	0	0.0417	-0.0278	(D.235)
$(\bar{u}u)_L$	$(\bar{\nu}\nu)_L$	0	0	-0.0417	(D.236)
$(\bar{u}u)_L$	$(\bar{\nu}\nu)_R$	0	0	0	(D.237)
$(\bar{u}u)_L$	$(\bar{e}e)_L$	0	0	-0.0417	(D.238)
$(\bar{u}u)_L$	$(\bar{e}e)_R$	0	0	-0.0833	(D.239)
$(\bar{u}u)_R$	$(\bar{u}u)_R$	0.125	-0.333	0.222	(D.240)
$(\bar{u}u)_R$	$(\bar{d}d)_L$	0	-0.0417	0.0556	(D.241)
$(\bar{u}u)_R$	$(\bar{d}d)_R$	-0.125	0.250	-0.111	(D.242)
$(\bar{u}u)_R$	$(\bar{\nu}\nu)_L$	0	0.125	-0.167	(D.243)
$(\bar{u}u)_R$	$(\bar{\nu}\nu)_R$	0	0	0	(D.244)
$(\bar{u}u)_R$	$(\bar{e}e)_L$	0	0.125	-0.167	(D.245)
$(\bar{u}u)_R$	$(\bar{e}e)_R$	0	0.250	-0.333	(D.246)
$(\bar{d}d)_L$	$(\bar{d}d)_L$	0	0	0.0139	(D.247)
$(\bar{d}d)_L$	$(\bar{d}d)_R$	0	0.0417	-0.0278	(D.248)
$(\bar{d}d)_L$	$(\bar{\nu}\nu)_L$	0	0	-0.0417	(D.249)
$(\bar{d}d)_L$	$(\bar{\nu}\nu)_R$	0	0	0	(D.250)
$(\bar{d}d)_L$	$(\bar{e}e)_L$	0	0	-0.0417	(D.251)
$(\bar{d}d)_L$	$(\bar{e}e)_R$	0	0	-0.0833	(D.252)
$(\bar{d}d)_R$	$(\bar{d}d)_R$	0.125	-0.167	0.0556	(D.253)
$(\bar{d}d)_R$	$(\bar{\nu}\nu)_L$	0	-0.125	0.0833	(D.254)
$(\bar{d}d)_R$	$(\bar{\nu}\nu)_R$	0	0	0	(D.255)
$(\bar{d}d)_R$	$(\bar{e}e)_L$	0	-0.125	0.0833	(D.256)
$(\bar{d}d)_R$	$(\bar{e}e)_R$	0	-0.250	0.167	(D.257)
$(\bar{\nu}\nu)_L$	$(\bar{\nu}\nu)_L$	0	0	0.125	(D.258)
$(\bar{\nu}\nu)_L$	$(\bar{\nu}\nu)_R$	0	0	0	(D.259)
$(\bar{\nu}\nu)_L$	$(\bar{e}e)_L$	0	0	0.125	(D.260)
$(\bar{\nu}\nu)_L$	$(\bar{e}e)_R$	0	0	0.250	(D.261)
$(\bar{\nu}\nu)_R$	$(\bar{\nu}\nu)_R$	0	0	0	(D.262)
$(\bar{\nu}\nu)_R$	$(\bar{e}e)_L$	0	0	0	(D.263)
$(\bar{\nu}\nu)_R$	$(\bar{e}e)_R$	0	0	0	(D.264)
$(\bar{e}e)_L$	$(\bar{e}e)_L$	0	0	0.125	(D.265)
$(\bar{e}e)_L$	$(\bar{e}e)_R$	0	0	0.250	(D.266)
$(\bar{e}e)_R$	$(\bar{e}e)_R$	0	0	0.500	(D.267)

Table D.18: Couplings $C^{\rm NC}_{ew.}\left(f_{1,i}, f_{2,j}\right)$ of the neutral fermion currents at the electroweak scale in the LP-T model. See text and Eq. (D.51) on page 158 for details.

$(\bar{f}_1 f_1)_C$	$(\bar{f}_2 f_2)_C$	$\frac{1}{\tilde{x}}$	$\frac{1}{\tilde{x}} s^2_{\tilde{\phi}}$	$\frac{1}{\tilde{x}} s^4_{\tilde{\phi}}$	Eqn.
$(\bar{u}u)_L$	$(\bar{u}u)_L$	0	0	0.0139	(D.268)
$(\bar{u}u)_L$	$(\bar{u}u)_R$	0	0	0.0556	(D.269)
$(\bar{u}u)_L$	$(\bar{d}d)_L$	0	0	0.0139	(D.270)
$(\bar{u}u)_L$	$(\bar{d}d)_R$	0	0	-0.0278	(D.271)
$(\bar{u}u)_L$	$(\bar{\nu}\nu)_L$	0	0	-0.0417	(D.272)
$(\bar{u}u)_L$	$(\bar{\nu}\nu)_R$	0	-0.0417	0	(D.273)
$(\bar{u}u)_L$	$(\bar{e}e)_L$	0	0	-0.0417	(D.274)
$(\bar{u}u)_L$	$(\bar{e}e)_R$	0	0.0417	-0.0833	(D.275)
$(\bar{u}u)_R$	$(\bar{u}u)_R$	0	0	0.222	(D.276)
$(\bar{u}u)_R$	$(\bar{d}d)_L$	0	0	0.0556	(D.277)
$(\bar{u}u)_R$	$(\bar{d}d)_R$	0	0	-0.111	(D.278)
$(\bar{u}u)_R$	$(\bar{\nu}\nu)_L$	0	0	-0.167	(D.279)
$(\bar{u}u)_R$	$(\bar{\nu}\nu)_R$	0	-0.167	0	(D.280)
$(\bar{u}u)_R$	$(\bar{e}e)_L$	0	0	-0.167	(D.281)
$(\bar{u}u)_R$	$(\bar{e}e)_R$	0	0.167	-0.333	(D.282)
$(\bar{d}d)_L$	$(\bar{d}d)_L$	0	0	0.0139	(D.283)
$(\bar{d}d)_L$	$(\bar{d}d)_R$	0	0	-0.0278	(D.284)
$(\bar{d}d)_L$	$(\bar{\nu}\nu)_L$	0	0	-0.0417	(D.285)
$(\bar{d}d)_L$	$(\bar{\nu}\nu)_R$	0	-0.0417	0	(D.286)
$(\bar{d}d)_L$	$(\bar{e}e)_L$	0	0	-0.0417	(D.287)
$(\bar{d}d)_L$	$(\bar{e}e)_R$	0	0.0417	-0.0833	(D.288)
$(\bar{d}d)_R$	$(\bar{d}d)_R$	0	0	0.0556	(D.289)
$(\bar{d}d)_R$	$(\bar{\nu}\nu)_L$	0	0	0.0833	(D.290)
$(\bar{d}d)_R$	$(\bar{\nu}\nu)_R$	0	0.0833	0	(D.291)
$(\bar{d}d)_R$	$(\bar{e}e)_L$	0	0	0.0833	(D.292)
$(\bar{d}d)_R$	$(\bar{e}e)_R$	0	-0.0833	0.167	(D.293)
$(\bar{\nu}\nu)_L$	$(\bar{\nu}\nu)_L$	0	0	0.125	(D.294)
$(\bar{\nu}\nu)_L$	$(\bar{\nu}\nu)_R$	0	0.125	0	(D.295)
$(\bar{\nu}\nu)_L$	$(\bar{e}e)_L$	0	0	0.125	(D.296)
$(\bar{\nu}\nu)_L$	$(\bar{e}e)_R$	0	-0.125	0.250	(D.297)
$(\bar{\nu}\nu)_R$	$(\bar{\nu}\nu)_R$	0.125	0	0	(D.298)
$(\bar{\nu}\nu)_R$	$(\bar{e}e)_L$	0	0.125	0	(D.299)
$(\bar{\nu}\nu)_R$	$(\bar{e}e)_R$	-0.125	0.250	0	(D.300)
$(\bar{e}e)_L$	$(\bar{e}e)_L$	0	0	0.125	(D.301)
$(\bar{e}e)_L$	$(\bar{e}e)_R$	0	-0.125	0.250	(D.302)
$(\bar{e}e)_R$	$(\bar{e}e)_R$	0.125	-0.500	0.500	(D.303)

Table D.19: Couplings $C^{\rm NC}_{ew.}\left(f_{1,i}, f_{2,j}\right)$ of the neutral fermion currents at the electroweak scale in the HP-T model. See text and Eq. (D.51) on page 158 for details.

$(\bar{f}_1 f_1)_C$	$(\bar{f}_2 f_2)_C$	$\frac{1}{x}$	$\frac{1}{x} s_{\hat{\phi}}^2$	$\frac{1}{x} s_{\hat{\phi}}^4$	Eqn.
$(\bar{u}u)_L$	$(\bar{u}u)_L$	0	0	0.0139	(D.304)
$(\bar{u}u)_L$	$(\bar{u}u)_R$	0	0	0.0556	(D.305)
$(\bar{u}u)_L$	$(\bar{d}d)_L$	0	0	0.0139	(D.306)
$(\bar{u}u)_L$	$(\bar{d}d)_R$	0	0	-0.0278	(D.307)
$(\bar{u}u)_L$	$(\bar{\nu}\nu)_L$	0	0	-0.0417	(D.308)
$(\bar{u}u)_L$	$(\bar{\nu}\nu)_R$	0	0	0	(D.309)
$(\bar{u}u)_L$	$(\bar{e}e)_L$	0	0	-0.0417	(D.310)
$(\bar{u}u)_L$	$(\bar{e}e)_R$	0	0	-0.0833	(D.311)
$(\bar{u}u)_R$	$(\bar{u}u)_R$	0	0	0.222	(D.312)
$(\bar{u}u)_R$	$(\bar{d}d)_L$	0	0	0.0556	(D.313)
$(\bar{u}u)_R$	$(\bar{d}d)_R$	0	0	-0.111	(D.314)
$(\bar{u}u)_R$	$(\bar{\nu}\nu)_L$	0	0	-0.167	(D.315)
$(\bar{u}u)_R$	$(\bar{\nu}\nu)_R$	0	0	0	(D.316)
$(\bar{u}u)_R$	$(\bar{e}e)_L$	0	0	-0.167	(D.317)
$(\bar{u}u)_R$	$(\bar{e}e)_R$	0	0	-0.333	(D.318)
$(\bar{d}d)_L$	$(\bar{d}d)_L$	0	0	0.0139	(D.319)
$(\bar{d}d)_L$	$(\bar{d}d)_R$	0	0	-0.0278	(D.320)
$(\bar{d}d)_L$	$(\bar{\nu}\nu)_L$	0	0	-0.0417	(D.321)
$(\bar{d}d)_L$	$(\bar{\nu}\nu)_R$	0	0	0	(D.322)
$(\bar{d}d)_L$	$(\bar{e}e)_L$	0	0	-0.0417	(D.323)
$(\bar{d}d)_L$	$(\bar{e}e)_R$	0	0	-0.0833	(D.324)
$(\bar{d}d)_R$	$(\bar{d}d)_R$	0	0	0.0556	(D.325)
$(\bar{d}d)_R$	$(\bar{\nu}\nu)_L$	0	0	0.0833	(D.326)
$(\bar{d}d)_R$	$(\bar{\nu}\nu)_R$	0	0	0	(D.327)
$(\bar{d}d)_R$	$(\bar{e}e)_L$	0	0	0.0833	(D.328)
$(\bar{d}d)_R$	$(\bar{e}e)_R$	0	0	0.167	(D.329)
$(\bar{\nu}\nu)_L$	$(\bar{\nu}\nu)_L$	0	0	0.125	(D.330)
$(\bar{\nu}\nu)_L$	$(\bar{\nu}\nu)_R$	0	0	0	(D.331)
$(\bar{\nu}\nu)_L$	$(\bar{e}e)_L$	0	0	0.125	(D.332)
$(\bar{\nu}\nu)_L$	$(\bar{e}e)_R$	0	0	0.250	(D.333)
$(\bar{\nu}\nu)_R$	$(\bar{\nu}\nu)_R$	0	0	0	(D.334)
$(\bar{\nu}\nu)_R$	$(\bar{e}e)_L$	0	0	0	(D.335)
$(\bar{\nu}\nu)_R$	$(\bar{e}e)_R$	0	0	0	(D.336)
$(\bar{e}e)_L$	$(\bar{e}e)_L$	0	0	0.125	(D.337)
$(\bar{e}e)_L$	$(\bar{e}e)_R$	0	0	0.250	(D.338)
$(\bar{e}e)_R$	$(\bar{e}e)_R$	0	0	0.500	(D.339)

Table D.20: Couplings $C_{ew.}^{\mathrm{NC}}(f_{1,i}, f_{2,j})$ of the neutral fermion currents at the electroweak scale in the FP-T model. See text and Eq. (D.51) on page 158 for details.

$(\bar{f}_1 f_1)_{L,R}$	$(\bar{f}_2 f_2)_{L,R}$	$\frac{1}{\tilde{x}}$	$\frac{1}{\tilde{x}} s^2_{\tilde{\phi}}$	$\frac{1}{\tilde{x}} s^4_{\tilde{\phi}}$	Eqn.
$(\bar{u}u)_L$	$(\bar{u}u)_L$	$\frac{1}{2}$	-1	$\frac{1}{2}$	(D.340)
$(\bar{u}u)_L$	$(\bar{u}u)_R$	0	0	0	(D.341)
$(\bar{u}u)_L$	$(\bar{d}d)_L$	$-\frac{1}{2}$	1	$-\frac{1}{2}$	(D.342)
$(\bar{u}u)_L$	$(\bar{d}d)_R$	0	0	0	(D.343)
$(\bar{u}u)_L$	$(\bar{\nu}\nu)_L$	0	$-\frac{1}{2}$	$\frac{1}{2}$	(D.344)
$(\bar{u}u)_L$	$(\bar{\nu}\nu)_R$	0	0	0	(D.345)
$(\bar{u}u)_L$	$(\bar{e}e)_L$	0	$\frac{1}{2}$	$-\frac{1}{2}$	(D.346)
$(\bar{u}u)_L$	$(\bar{e}e)_R$	0	0	0	(D.347)
$(\bar{u}u)_R$	$(\bar{u}u)_R$	0	0	0	(D.348)
$(\bar{u}u)_R$	$(\bar{d}d)_L$	0	0	0	(D.349)
$(\bar{u}u)_R$	$(\bar{d}d)_R$	0	0	0	(D.350)
$(\bar{u}u)_R$	$(\bar{\nu}\nu)_L$	0	0	0	(D.351)
$(\bar{u}u)_R$	$(\bar{\nu}\nu)_R$	0	0	0	(D.352)
$(\bar{u}u)_R$	$(\bar{e}e)_L$	0	0	0	(D.353)
$(\bar{u}u)_R$	$(\bar{e}e)_R$	0	0	0	(D.354)
$(\bar{d}d)_L$	$(\bar{d}d)_L$	$\frac{1}{2}$	-1	$\frac{1}{2}$	(D.355)
$(\bar{d}d)_L$	$(\bar{d}d)_R$	0	0	0	(D.356)
$(\bar{d}d)_L$	$(\bar{\nu}\nu)_L$	0	$\frac{1}{2}$	$-\frac{1}{2}$	(D.357)
$(\bar{d}d)_L$	$(\bar{\nu}\nu)_R$	0	0	0	(D.358)
$(\bar{d}d)_L$	$(\bar{e}e)_L$	0	$-\frac{1}{2}$	$\frac{1}{2}$	(D.359)
$(\bar{d}d)_L$	$(\bar{e}e)_R$	0	0	0	(D.360)
$(\bar{d}d)_R$	$(\bar{d}d)_R$	0	0	0	(D.361)
$(\bar{d}d)_R$	$(\bar{\nu}\nu)_L$	0	0	0	(D.362)
$(\bar{d}d)_R$	$(\bar{\nu}\nu)_R$	0	0	0	(D.363)
$(\bar{d}d)_R$	$(\bar{e}e)_L$	0	0	0	(D.364)
$(\bar{d}d)_R$	$(\bar{e}e)_R$	0	0	0	(D.365)
$(\bar{\nu}\nu)_L$	$(\bar{\nu}\nu)_L$	0	0	$\frac{1}{2}$	(D.366)
$(\bar{\nu}\nu)_L$	$(\bar{\nu}\nu)_R$	0	0	0	(D.367)
$(\bar{\nu}\nu)_L$	$(\bar{e}e)_L$	0	0	$-\frac{1}{2}$	(D.368)
$(\bar{\nu}\nu)_L$	$(\bar{e}e)_R$	0	0	0	(D.369)
$(\bar{\nu}\nu)_R$	$(\bar{\nu}\nu)_R$	0	0	0	(D.370)
$(\bar{\nu}\nu)_R$	$(\bar{e}e)_L$	0	0	0	(D.371)
$(\bar{\nu}\nu)_R$	$(\bar{e}e)_R$	0	0	0	(D.372)
$(\bar{e}e)_L$	$(\bar{e}e)_L$	0	0	$\frac{1}{2}$	(D.373)
$(\bar{e}e)_L$	$(\bar{e}e)_R$	0	0	0	(D.374)
$(\bar{e}e)_R$	$(\bar{e}e)_R$	0	0	0	(D.375)

Table D.21: Couplings $C^{\mathrm{NC}}_{ew.}(f_{1,i}, f_{2,j})$ of the neutral fermion currents at the electroweak scale in the UU-D model. See text and Eq. (D.51) on page 158 for details.

$(\bar{f}_1 f_1)_{L,R}$	$(\bar{f}_2 f_2)_{L,R}$	$\frac{1}{\tilde{x}}$	$\frac{1}{\tilde{x}} s^2_{\tilde{\phi}}$	$\frac{1}{\tilde{x}} s^4_{\tilde{\phi}}$	Eqn.
$(\bar{u}u)_L$	$(\bar{u}u)_L$	$\frac{1}{2}$	-1	$\frac{1}{2}$	(D.376)
$(\bar{u}u)_L$	$(\bar{u}u)_R$	0	0	0	(D.377)
$(\bar{u}u)_L$	$(\bar{d}d)_L$	$-\frac{1}{2}$	1	$-\frac{1}{2}$	(D.378)
$(\bar{u}u)_L$	$(\bar{d}d)_R$	0	0	0	(D.379)
$(\bar{u}u)_L$	$(\bar{\nu}\nu)_L$	$\frac{1}{2}$	-1	$\frac{1}{2}$	(D.380)
$(\bar{u}u)_L$	$(\bar{\nu}\nu)_R$	0	0	0	(D.381)
$(\bar{u}u)_L$	$(\bar{e}e)_L$	$-\frac{1}{2}$	1	$-\frac{1}{2}$	(D.382)
$(\bar{u}u)_L$	$(\bar{e}e)_R$	0	0	0	(D.383)
$(\bar{u}u)_R$	$(\bar{u}u)_R$	0	0	0	(D.384)
$(\bar{u}u)_R$	$(\bar{d}d)_L$	0	0	0	(D.385)
$(\bar{u}u)_R$	$(\bar{d}d)_R$	0	0	0	(D.386)
$(\bar{u}u)_R$	$(\bar{\nu}\nu)_L$	0	0	0	(D.387)
$(\bar{u}u)_R$	$(\bar{\nu}\nu)_R$	0	0	0	(D.388)
$(\bar{u}u)_R$	$(\bar{e}e)_L$	0	0	0	(D.389)
$(\bar{u}u)_R$	$(\bar{e}e)_R$	0	0	0	(D.390)
$(\bar{d}d)_L$	$(\bar{d}d)_L$	$\frac{1}{2}$	-1	$\frac{1}{2}$	(D.391)
$(\bar{d}d)_L$	$(\bar{d}d)_R$	0	0	0	(D.392)
$(\bar{d}d)_L$	$(\bar{\nu}\nu)_L$	$-\frac{1}{2}$	1	$-\frac{1}{2}$	(D.393)
$(\bar{d}d)_L$	$(\bar{\nu}\nu)_R$	0	0	0	(D.394)
$(\bar{d}d)_L$	$(\bar{e}e)_L$	$\frac{1}{2}$	-1	$\frac{1}{2}$	(D.395)
$(\bar{d}d)_L$	$(\bar{e}e)_R$	0	0	0	(D.396)
$(\bar{d}d)_R$	$(\bar{d}d)_R$	0	0	0	(D.397)
$(\bar{d}d)_R$	$(\bar{\nu}\nu)_L$	0	0	0	(D.398)
$(\bar{d}d)_R$	$(\bar{\nu}\nu)_R$	0	0	0	(D.399)
$(\bar{d}d)_R$	$(\bar{e}e)_L$	0	0	0	(D.400)
$(\bar{d}d)_R$	$(\bar{e}e)_R$	0	0	0	(D.401)
$(\bar{\nu}\nu)_L$	$(\bar{\nu}\nu)_L$	$\frac{1}{2}$	-1	$\frac{1}{2}$	(D.402)
$(\bar{\nu}\nu)_L$	$(\bar{\nu}\nu)_R$	0	0	0	(D.403)
$(\bar{\nu}\nu)_L$	$(\bar{e}e)_L$	$-\frac{1}{2}$	1	$-\frac{1}{2}$	(D.404)
$(\bar{\nu}\nu)_L$	$(\bar{e}e)_R$	0	0	0	(D.405)
$(\bar{\nu}\nu)_R$	$(\bar{\nu}\nu)_R$	0	0	0	(D.406)
$(\bar{\nu}\nu)_R$	$(\bar{e}e)_L$	0	0	0	(D.407)
$(\bar{\nu}\nu)_R$	$(\bar{e}e)_R$	0	0	0	(D.408)
$(\bar{e}e)_L$	$(\bar{e}e)_L$	$\frac{1}{2}$	-1	$\frac{1}{2}$	(D.409)
$(\bar{e}e)_L$	$(\bar{e}e)_R$	0	0	0	(D.410)
$(\bar{e}e)_R$	$(\bar{e}e)_R$	0	0	0	(D.411)

Table D.22: Couplings $C_{ew.}^{\mathrm{NC}}\left(f_{1,i}, f_{2,j}\right)$ of the neutral fermion currents (first two generations) at the electroweak scale in the NU-D model. See text and Eq. (D.51) on page 158 for details.

$(\bar{f}_1 f_2)_C$	$(\bar{f}_3 f_4)_C$	$\frac{1}{\tilde{x}}$ (LR-D)	$\frac{1}{\tilde{x}}$ (LP-D)	$\frac{1}{\tilde{x}}$ (HP-D)	$\frac{1}{\tilde{x}}$ (FP-D)	Eqn.
$(\bar{u}d)_L$	$(\bar{d}u)_L$	0	0	0	0	(D.413)
$(\bar{u}d)_L$	$(\bar{d}u)_R$	0	0	0	0	(D.414)
$(\bar{u}d)_L$	$(\bar{e}\nu)_L$	0	0	0	0	(D.415)
$(\bar{u}d)_L$	$(\bar{e}\nu)_R$	0	0	0	0	(D.416)
$(\bar{u}d)_R$	$(\bar{d}u)_R$	1	1	0	0	(D.417)
$(\bar{u}d)_R$	$(\bar{e}\nu)_L$	0	0	0	0	(D.418)
$(\bar{u}d)_R$	$(\bar{e}\nu)_R$	1	0	0	0	(D.419)
$(\bar{\nu}e)_L$	$(\bar{e}\nu)_L$	0	0	0	0	(D.420)
$(\bar{\nu}e)_L$	$(\bar{e}\nu)_R$	0	0	0	0	(D.421)
$(\bar{\nu}e)_R$	$(\bar{e}\nu)_R$	1	0	1	0	(D.422)

Table D.23: Couplings $C_{ew.}^{\mathrm{CC}}\left(f_{1,i}, f_{3,j}\right)$ of the charged fermion currents at the electroweak scale in the LR-D, LP-D, HP-D and FP-D model. See text and Eq. (D.412) on page 159 for details.

D.2 Couplings in $\mathscr{L}_{\mathbf{4f}}$

D.2.1 Couplings of the Neutral Fermion Currents

The effective Lagrangian $\mathscr{L}_{4f}^{\mathrm{NC}}$ that takes care of the neutral current four-fermion interactions below the electroweak scale is given as:

$$\mathscr{L}_{4f}^{\mathrm{NC}} = -\frac{1}{2\widetilde{M}_{\hat{Z}}^2}\left[J_\mu^0 J^{0,\mu} - \frac{2\delta\widetilde{M}_{\hat{Z}\hat{Z}'}^2}{\widetilde{M}_{\hat{Z}'}^2} J_\mu^0 K^{0,\mu} + \frac{\delta\widetilde{M}_{\hat{Z}\hat{Z}'}^4}{\widetilde{M}_{\hat{Z}'}^2 \widetilde{M}_{\hat{Z}}^2} J_\mu^0 J^{0,\mu}\right] - \frac{1}{2\widetilde{M}_{\hat{Z}'}^2} K_\mu^0 K^{0,\mu}$$

The coupling coefficients $C_{4f}^{\mathrm{NC}}\left(f_{1,i}, f_{2,j}\right)$ are defined such that $\mathscr{L}_{4f}^{\mathrm{NC}}$ takes the following form:

$$\mathscr{L}_{4f}^{\mathrm{NC}} \equiv -\frac{G_F}{\sqrt{2}} \sum_{f_1, f_2} \sum_{i,j} C_{4f}^{\mathrm{NC}}\left(f_{1,i}, f_{2,j}\right)\left(\bar{f}_1 f_1\right)_{i,\mu}\left(\bar{f}_2 f_2\right)_j^\mu \qquad ; i,j = L,R$$

We can write $C_{4f}^{\mathrm{NC}}\left(f_{1,i}, f_{2,j}\right)$ as the sum of the SM coupling $C_{4f,\mathrm{SM}}^{\mathrm{NC}}\left(f_{1,i}, f_{2,j}\right)$ and

$(\bar{f}_1 f_2)_C$	$(\bar{f}_3 f_4)_C$	$\frac{1}{\tilde{x}}$ (LR-T)	$\frac{1}{\tilde{x}}$ (LP-T)	$\frac{1}{\tilde{x}}$ (HP-T)	$\frac{1}{\tilde{x}}$ (FP-T)	Eqn.
$(\bar{u}d)_L$	$(d\bar{u})_L$	0	0	0	0	(D.423)
$(\bar{u}d)_L$	$(\bar{d}u)_R$	0	0	0	0	(D.424)
$(\bar{u}d)_L$	$(\bar{e}\nu)_L$	0	0	0	0	(D.425)
$(\bar{u}d)_L$	$(\bar{e}\nu)_R$	0	0	0	0	(D.426)
$(\bar{u}d)_R$	$(\bar{d}u)_R$	$\frac{1}{2}$	$\frac{1}{2}$	0	0	(D.427)
$(\bar{u}d)_R$	$(\bar{e}\nu)_L$	0	0	0	0	(D.428)
$(\bar{u}d)_R$	$(\bar{e}\nu)_R$	$\frac{1}{2}$	0	0	0	(D.429)
$(\bar{\nu}e)_L$	$(\bar{e}\nu)_L$	0	0	0	0	(D.430)
$(\bar{\nu}e)_L$	$(\bar{e}\nu)_R$	0	0	0	0	(D.431)
$(\bar{\nu}e)_R$	$(\bar{e}\nu)_R$	$\frac{1}{2}$	0	$\frac{1}{2}$	0	(D.432)

Table D.24: Couplings $C_{ew.}^{\mathrm{CC}}(f_{1,i}, f_{3,j})$ of the charged fermion currents at the electroweak scale in the LR-T, LP-T, HP-T and FP-T model. See text and Eq. (D.412) on page 159 for details.

$(\bar{f}_1 f_2)_C$	$(\bar{f}_3 f_4)_C$	$\frac{1}{\tilde{x}}$	$\frac{1}{\tilde{x}} s_{\tilde{\phi}}^2$	$\frac{1}{\tilde{x}} s_{\tilde{\phi}}^4$	Eqn.
$(\bar{u}d)_L$	$(d\bar{u})_L$	1	-2	1	(D.433)
$(\bar{u}d)_L$	$(\bar{d}u)_R$	0	0	0	(D.434)
$(\bar{u}d)_L$	$(\bar{e}\nu)_L$	0	-1	1	(D.435)
$(\bar{u}d)_L$	$(\bar{e}\nu)_R$	0	0	0	(D.436)
$(\bar{u}d)_R$	$(\bar{d}u)_R$	0	0	0	(D.437)
$(\bar{u}d)_R$	$(\bar{e}\nu)_L$	0	0	0	(D.438)
$(\bar{u}d)_R$	$(\bar{e}\nu)_R$	0	0	0	(D.439)
$(\bar{\nu}e)_L$	$(\bar{e}\nu)_L$	0	0	1	(D.440)
$(\bar{\nu}e)_L$	$(\bar{e}\nu)_R$	0	0	0	(D.441)
$(\bar{\nu}e)_R$	$(\bar{e}\nu)_R$	0	0	0	(D.442)

Table D.25: Couplings $C_{ew.}^{\mathrm{CC}}(f_{1,i}, f_{3,j})$ of the charged fermion currents at the electroweak scale in the UU-D model. See text and Eq. (D.412) on page 159 for details.

$(\bar{f}_1 f_2)_C$	$(\bar{f}_3 f_4)_C$	$\frac{1}{\tilde{x}}$	$\frac{1}{\tilde{x}} s^2_{\tilde{\phi}}$	$\frac{1}{\tilde{x}} s^4_{\tilde{\phi}}$	Eqn.
$(\bar{u}d)_L$	$(d\bar{u})_L$	1	-2	1	(D.443)
$(\bar{u}d)_L$	$(\bar{d}u)_R$	0	0	0	(D.444)
$(\bar{u}d)_L$	$(\bar{e}\nu)_L$	1	-2	1	(D.445)
$(\bar{u}d)_L$	$(\bar{e}\nu)_R$	0	0	0	(D.446)
$(\bar{u}d)_R$	$(\bar{d}u)_R$	0	0	0	(D.447)
$(\bar{u}d)_R$	$(\bar{e}\nu)_L$	0	0	0	(D.448)
$(\bar{u}d)_R$	$(\bar{e}\nu)_R$	0	0	0	(D.449)
$(\bar{\nu}e)_L$	$(\bar{e}\nu)_L$	1	-2	1	(D.450)
$(\bar{\nu}e)_L$	$(\bar{e}\nu)_R$	0	0	0	(D.451)
$(\bar{\nu}e)_R$	$(\bar{e}\nu)_R$	0	0	0	(D.452)

Table D.26: Couplings $C^{\rm CC}_{ew.}\left(f_{1,i}, f_{3,j}\right)$ of the charged fermion currents (first two generations) at the electroweak scale in the NU-D model. See text and Eq. (D.412) on page 159 for details.

various model-dependent new physics corrections that are proportional to $\frac{1}{\tilde{x}}$.

$$\begin{aligned} C^{\rm NC}_{4f}\left(f_{1,i}, f_{2,j}\right) &= C^{\rm NC}_{4f,\rm SM}\left(f_{1,i}, f_{2,j}\right) \\ &+ \frac{1}{\tilde{x}} \cdot N_1 + \frac{1}{\tilde{x}} s^2_{2\tilde{\beta}} \cdot N_2 + \frac{1}{\tilde{x}} s^2_{\tilde{\phi}} \cdot N_3 + \frac{1}{\tilde{x}} s^4_{\tilde{\phi}} \cdot N_4 \end{aligned} \tag{D.453}$$

Tabs. D.27 to D.36 list the numerical values of the coefficients N_1, N_2, N_3 and N_4 in Eq. (D.453) for all possible fermion pairs $\left(f_{1,i}, f_{2,j}\right)$ and for all considered $G(221)$ models.

D.2.2 Couplings of the Charged Fermion Currents

The effective Lagrangian $\mathscr{L}_{4f}^{\mathrm{CC}}$ that takes care of the charged current four-fermion interactions below the electroweak scale is given as:

$$\begin{aligned}\mathscr{L}_{4f}^{\mathrm{CC}} &= -\frac{1}{\widetilde{M}_{\hat{W}}^2}\left[J_\mu^+ J^{-,\mu} - \frac{\delta\widetilde{M}_{\hat{W}\hat{W}'}^2}{\widetilde{M}_{\hat{W}'}^2}\left(J_\mu^+ K^{-,\mu} + J_\mu^- K^{+,\mu}\right) + \frac{\delta\widetilde{M}_{\hat{W}\hat{W}'}^4}{\widetilde{M}_{\hat{W}'}^2\widetilde{M}_{\hat{W}}^2} J_\mu^+ J^{-,\mu}\right] \\ &\quad - \frac{1}{\widetilde{M}_{\hat{W}'}^2} K_\mu^+ K^{-,\mu}\end{aligned}$$

The coupling coefficients $C_{4f}^{\mathrm{CC}}\left(f_{1,i}, f_{3,j}\right)$ are defined such that $\mathscr{L}_{4f}^{\mathrm{CC}}$ takes the following form:

$$\mathscr{L}_{4f}^{\mathrm{CC}} \equiv -\frac{G_F}{\sqrt{2}} \sum_{f_1,f_3} \sum_{i,j} C_{4f}^{\mathrm{CC}}\left(f_{1,i}, f_{3,j}\right)\left(\bar{f}_1 f_2\right)_{i,\mu}\left(\bar{f}_3 f_4\right)_j^\mu \qquad ; i,j = L,R$$

We can write $C_{4f}^{\mathrm{CC}}\left(f_{1,i}, f_{3,j}\right)$ as the sum of the SM coupling $C_{4f,\mathrm{SM}}^{\mathrm{CC}}\left(f_{1,i}, f_{3,j}\right)$ and various model-dependent new physics corrections that are proportional to $\frac{1}{\tilde{x}}$.

$$\begin{aligned}C_{4f}^{\mathrm{CC}}\left(f_{1,i}, f_{3,j}\right) &= C_{4f,\mathrm{SM}}^{\mathrm{CC}}\left(f_{1,i}, f_{3,j}\right) \\ &\quad + \frac{1}{\tilde{x}} \cdot N_1 + \frac{1}{\tilde{x}} s_{2\tilde{\beta}}^2 \cdot N_2 + \frac{1}{\tilde{x}} s_{\tilde{\phi}}^2 \cdot N_3 + \frac{1}{\tilde{x}} s_{\tilde{\phi}}^4 \cdot N_4 \end{aligned} \qquad \text{(D.814)}$$

Tabs. D.37 to D.45 list the numerical values of the coefficients N_1, N_2, N_3 and N_4 in Eq. (D.814) for all possible fermion pairs $\left(f_{1,i}, f_{3,j}\right)$ and for all considered $G(221)$ models.

$(\bar{f}_1 f_1)_C$	$(\bar{f}_2 f_2)_C$	$C_{4f,\mathrm{SM}}^{\mathrm{NC}}$	$\frac{1}{\tilde{x}}$	$\frac{1}{\tilde{x}} s_{2\tilde{\beta}}^2$	$\frac{1}{\tilde{x}} s_{\tilde{\phi}}^2$	$\frac{1}{\tilde{x}} s_{\tilde{\phi}}^4$	Eqn.
$(\bar{u}u)_L$	$(\bar{u}u)_L$	0.237	0.546	-0.546	-1.32	0.831	(D.454)
$(\bar{u}u)_L$	$(\bar{u}u)_R$	-0.107	0.321	0.0228	-0.872	0.607	(D.455)
$(\bar{u}u)_L$	$(\bar{d}d)_L$	-0.291	-0.557	0.557	1.14	-0.527	(D.456)
$(\bar{u}u)_L$	$(\bar{d}d)_R$	0.0536	-0.333	-0.0114	0.692	-0.303	(D.457)
$(\bar{u}u)_L$	$(\bar{\nu}\nu)_L$	0.344	0.568	-0.568	-0.959	0.224	(D.458)
$(\bar{u}u)_L$	$(\bar{\nu}\nu)_R$	0	0.344	0	-0.511	0	(D.459)
$(\bar{u}u)_L$	$(\bar{e}e)_L$	-0.183	-0.534	0.534	1.50	-1.13	(D.460)
$(\bar{u}u)_L$	$(\bar{e}e)_R$	0.161	-0.310	-0.0342	1.05	-0.910	(D.461)
$(\bar{u}u)_R$	$(\bar{u}u)_R$	0.0485	0.0974	0.0911	-0.424	0.382	(D.462)
$(\bar{u}u)_R$	$(\bar{d}d)_L$	0.132	-0.445	0.0228	0.916	-0.415	(D.463)
$(\bar{u}u)_R$	$(\bar{d}d)_R$	-0.0243	-0.221	-0.0455	0.468	-0.191	(D.464)
$(\bar{u}u)_R$	$(\bar{\nu}\nu)_L$	-0.156	0.568	-0.0683	-0.959	0.224	(D.465)
$(\bar{u}u)_R$	$(\bar{\nu}\nu)_R$	0	0.344	0	-0.511	0	(D.466)
$(\bar{u}u)_R$	$(\bar{e}e)_L$	0.0830	-0.198	-0.0683	0.829	-0.798	(D.467)
$(\bar{u}u)_R$	$(\bar{e}e)_R$	-0.0728	0.0261	-0.137	0.381	-0.574	(D.468)
$(\bar{d}d)_L$	$(\bar{d}d)_L$	0.356	0.546	-0.546	-0.810	0.320	(D.469)
$(\bar{d}d)_L$	$(\bar{d}d)_R$	-0.0658	0.434	-0.0114	-0.586	0.208	(D.470)
$(\bar{d}d)_L$	$(\bar{\nu}\nu)_L$	-0.422	-0.534	0.534	0.480	-0.112	(D.471)
$(\bar{d}d)_L$	$(\bar{\nu}\nu)_R$	0	-0.422	0	0.255	0	(D.472)
$(\bar{d}d)_L$	$(\bar{e}e)_L$	0.225	0.568	-0.568	-1.47	0.735	(D.473)
$(\bar{d}d)_L$	$(\bar{e}e)_R$	-0.197	0.456	-0.0342	-1.25	0.623	(D.474)
$(\bar{d}d)_R$	$(\bar{d}d)_R$	0.0121	0.321	0.0228	-0.362	0.0956	(D.475)
$(\bar{d}d)_R$	$(\bar{\nu}\nu)_L$	0.0779	-0.534	0.0342	0.480	-0.112	(D.476)
$(\bar{d}d)_R$	$(\bar{\nu}\nu)_R$	0	-0.422	0	0.255	0	(D.477)
$(\bar{d}d)_R$	$(\bar{e}e)_L$	-0.0415	0.232	0.0342	-0.798	0.399	(D.478)
$(\bar{d}d)_R$	$(\bar{e}e)_R$	0.0364	0.120	0.0683	-0.574	0.287	(D.479)
$(\bar{\nu}\nu)_L$	$(\bar{\nu}\nu)_L$	0.500	0.500	-0.500	0	0	(D.480)
$(\bar{\nu}\nu)_L$	$(\bar{\nu}\nu)_R$	0	0.500	0	0	0	(D.481)
$(\bar{\nu}\nu)_L$	$(\bar{e}e)_L$	-0.266	-0.602	0.602	1.44	-0.336	(D.482)
$(\bar{\nu}\nu)_L$	$(\bar{e}e)_R$	0.234	-0.602	0.102	1.44	-0.336	(D.483)
$(\bar{\nu}\nu)_R$	$(\bar{\nu}\nu)_R$	0	0.500	0	0	0	(D.484)
$(\bar{\nu}\nu)_R$	$(\bar{e}e)_L$	0	-0.266	0	0.766	0	(D.485)
$(\bar{\nu}\nu)_R$	$(\bar{e}e)_R$	0	-0.266	0	0.766	0	(D.486)
$(\bar{e}e)_L$	$(\bar{e}e)_L$	0.142	0.500	-0.500	-1.53	1.53	(D.487)
$(\bar{e}e)_L$	$(\bar{e}e)_R$	-0.124	0.164	0.102	-0.860	1.20	(D.488)
$(\bar{e}e)_R$	$(\bar{e}e)_R$	0.109	-0.172	0.205	-0.188	0.860	(D.489)

Table D.27: Couplings $C_{4f}^{\mathrm{NC}}\left(f_{1,i}, f_{2,j}\right)$ of the neutral fermion currents below the electroweak scale in the LR-D model. See text and Eq. (D.453) on page 172 for details.

$(\bar{f}_1 f_1)_C$	$(\bar{f}_2 f_2)_C$	$C_{4f,\mathrm{SM}}^{\mathrm{NC}}$	$\frac{1}{\tilde{x}}$	$\frac{1}{\tilde{x}} s_{2\tilde{\beta}}^2$	$\frac{1}{\tilde{x}} s_{\tilde{\phi}}^2$	$\frac{1}{\tilde{x}} s_{\tilde{\phi}}^4$	Eqn.
$(\bar{u}u)_L$	$(\bar{u}u)_L$	0.237	0.546	-0.546	-1.32	0.831	(D.490)
$(\bar{u}u)_L$	$(\bar{u}u)_R$	-0.107	0.321	0.0228	-0.872	0.607	(D.491)
$(\bar{u}u)_L$	$(\bar{d}d)_L$	-0.291	-0.557	0.557	1.14	-0.527	(D.492)
$(\bar{u}u)_L$	$(\bar{d}d)_R$	0.0536	-0.333	-0.0114	0.692	-0.303	(D.493)
$(\bar{u}u)_L$	$(\bar{\nu}\nu)_L$	0.344	0.568	-0.568	-0.959	0.224	(D.494)
$(\bar{u}u)_L$	$(\bar{\nu}\nu)_R$	0	0	0	0	0	(D.495)
$(\bar{u}u)_L$	$(\bar{e}e)_L$	-0.183	-0.534	0.534	1.50	-1.13	(D.496)
$(\bar{u}u)_L$	$(\bar{e}e)_R$	0.161	0.0342	-0.0342	0.542	-0.910	(D.497)
$(\bar{u}u)_R$	$(\bar{u}u)_R$	0.0485	0.0974	0.0911	-0.424	0.382	(D.498)
$(\bar{u}u)_R$	$(\bar{d}d)_L$	0.132	-0.445	0.0228	0.916	-0.415	(D.499)
$(\bar{u}u)_R$	$(\bar{d}d)_R$	-0.0243	-0.221	-0.0455	0.468	-0.191	(D.500)
$(\bar{u}u)_R$	$(\bar{\nu}\nu)_L$	-0.156	0.568	-0.0683	-0.959	0.224	(D.501)
$(\bar{u}u)_R$	$(\bar{\nu}\nu)_R$	0	0	0	0	0	(D.502)
$(\bar{u}u)_R$	$(\bar{e}e)_L$	0.0830	-0.198	-0.0683	0.829	-0.798	(D.503)
$(\bar{u}u)_R$	$(\bar{e}e)_R$	-0.0728	0.370	-0.137	-0.130	-0.574	(D.504)
$(\bar{d}d)_L$	$(\bar{d}d)_L$	0.356	0.546	-0.546	-0.810	0.320	(D.505)
$(\bar{d}d)_L$	$(\bar{d}d)_R$	-0.0658	0.434	-0.0114	-0.586	0.208	(D.506)
$(\bar{d}d)_L$	$(\bar{\nu}\nu)_L$	-0.422	-0.534	0.534	0.480	-0.112	(D.507)
$(\bar{d}d)_L$	$(\bar{\nu}\nu)_R$	0	0	0	0	0	(D.508)
$(\bar{d}d)_L$	$(\bar{e}e)_L$	0.225	0.568	-0.568	-1.47	0.735	(D.509)
$(\bar{d}d)_L$	$(\bar{e}e)_R$	-0.197	0.0342	-0.0342	-0.990	0.623	(D.510)
$(\bar{d}d)_R$	$(\bar{d}d)_R$	0.0121	0.321	0.0228	-0.362	0.0956	(D.511)
$(\bar{d}d)_R$	$(\bar{\nu}\nu)_L$	0.0779	-0.534	0.0342	0.480	-0.112	(D.512)
$(\bar{d}d)_R$	$(\bar{\nu}\nu)_R$	0	0	0	0	0	(D.513)
$(\bar{d}d)_R$	$(\bar{e}e)_L$	-0.0415	0.232	0.0342	-0.798	0.399	(D.514)
$(\bar{d}d)_R$	$(\bar{e}e)_R$	0.0364	-0.302	0.0683	-0.318	0.287	(D.515)
$(\bar{\nu}\nu)_L$	$(\bar{\nu}\nu)_L$	0.500	0.500	-0.500	0	0	(D.516)
$(\bar{\nu}\nu)_L$	$(\bar{\nu}\nu)_R$	0	0	0	0	0	(D.517)
$(\bar{\nu}\nu)_L$	$(\bar{e}e)_L$	-0.266	-0.602	0.602	1.44	-0.336	(D.518)
$(\bar{\nu}\nu)_L$	$(\bar{e}e)_R$	0.234	-0.102	0.102	1.44	-0.336	(D.519)
$(\bar{\nu}\nu)_R$	$(\bar{\nu}\nu)_R$	0	0	0	0	0	(D.520)
$(\bar{\nu}\nu)_R$	$(\bar{e}e)_L$	0	0	0	0	0	(D.521)
$(\bar{\nu}\nu)_R$	$(\bar{e}e)_R$	0	0	0	0	0	(D.522)
$(\bar{e}e)_L$	$(\bar{e}e)_L$	0.142	0.500	-0.500	-1.53	1.53	(D.523)
$(\bar{e}e)_L$	$(\bar{e}e)_R$	-0.124	-0.102	0.102	-0.0941	1.20	(D.524)
$(\bar{e}e)_R$	$(\bar{e}e)_R$	0.109	-0.205	0.205	1.34	0.860	(D.525)

Table D.28: Couplings $C_{4f}^{\mathrm{NC}}(f_{1,i}, f_{2,j})$ of the neutral fermion currents below the electroweak scale in the LP-D model. See text and Eq. (D.453) on page 172 for details.

$(\bar{f}_1 f_1)_C$	$(\bar{f}_2 f_2)_C$	$C^{\rm NC}_{4f,\rm SM}$	$\frac{1}{\tilde{x}}$	$\frac{1}{\tilde{x}} s^2_{2\tilde{\beta}}$	$\frac{1}{\tilde{x}} s^2_{\tilde{\phi}}$	$\frac{1}{\tilde{x}} s^4_{\tilde{\phi}}$	Eqn.
$(\bar{u}u)_L$	$(\bar{u}u)_L$	0.237	0.546	-0.546	-1.32	0.831	(D.526)
$(\bar{u}u)_L$	$(\bar{u}u)_R$	-0.107	-0.0228	0.0228	-0.362	0.607	(D.527)
$(\bar{u}u)_L$	$(\bar{d}d)_L$	-0.291	-0.557	0.557	1.14	-0.527	(D.528)
$(\bar{u}u)_L$	$(\bar{d}d)_R$	0.0536	0.0114	-0.0114	0.181	-0.303	(D.529)
$(\bar{u}u)_L$	$(\bar{\nu}\nu)_L$	0.344	0.568	-0.568	-0.959	0.224	(D.530)
$(\bar{u}u)_L$	$(\bar{\nu}\nu)_R$	0	0.344	0	-0.511	0	(D.531)
$(\bar{u}u)_L$	$(\bar{e}e)_L$	-0.183	-0.534	0.534	1.50	-1.13	(D.532)
$(\bar{u}u)_L$	$(\bar{e}e)_R$	0.161	-0.310	-0.0342	1.05	-0.910	(D.533)
$(\bar{u}u)_R$	$(\bar{u}u)_R$	0.0485	-0.0911	0.0911	0.598	0.382	(D.534)
$(\bar{u}u)_R$	$(\bar{d}d)_L$	0.132	-0.0228	0.0228	0.660	-0.415	(D.535)
$(\bar{u}u)_R$	$(\bar{d}d)_R$	-0.0243	0.0455	-0.0455	-0.299	-0.191	(D.536)
$(\bar{u}u)_R$	$(\bar{\nu}\nu)_L$	-0.156	0.0683	-0.0683	-0.959	0.224	(D.537)
$(\bar{u}u)_R$	$(\bar{\nu}\nu)_R$	0	-0.156	0	-0.511	0	(D.538)
$(\bar{u}u)_R$	$(\bar{e}e)_L$	0.0830	0.0683	-0.0683	0.0627	-0.798	(D.539)
$(\bar{u}u)_R$	$(\bar{e}e)_R$	-0.0728	0.292	-0.137	-0.385	-0.574	(D.540)
$(\bar{d}d)_L$	$(\bar{d}d)_L$	0.356	0.546	-0.546	-0.810	0.320	(D.541)
$(\bar{d}d)_L$	$(\bar{d}d)_R$	-0.0658	0.0114	-0.0114	-0.330	0.208	(D.542)
$(\bar{d}d)_L$	$(\bar{\nu}\nu)_L$	-0.422	-0.534	0.534	0.480	-0.112	(D.543)
$(\bar{d}d)_L$	$(\bar{\nu}\nu)_R$	0	-0.422	0	0.255	0	(D.544)
$(\bar{d}d)_L$	$(\bar{e}e)_L$	0.225	0.568	-0.568	-1.47	0.735	(D.545)
$(\bar{d}d)_L$	$(\bar{e}e)_R$	-0.197	0.456	-0.0342	-1.25	0.623	(D.546)
$(\bar{d}d)_R$	$(\bar{d}d)_R$	0.0121	-0.0228	0.0228	0.149	0.0956	(D.547)
$(\bar{d}d)_R$	$(\bar{\nu}\nu)_L$	0.0779	-0.0342	0.0342	0.480	-0.112	(D.548)
$(\bar{d}d)_R$	$(\bar{\nu}\nu)_R$	0	0.0779	0	0.255	0	(D.549)
$(\bar{d}d)_R$	$(\bar{e}e)_L$	-0.0415	-0.0342	0.0342	-0.0314	0.399	(D.550)
$(\bar{d}d)_R$	$(\bar{e}e)_R$	0.0364	-0.146	0.0683	0.193	0.287	(D.551)
$(\bar{\nu}\nu)_L$	$(\bar{\nu}\nu)_L$	0.500	0.500	-0.500	0	0	(D.552)
$(\bar{\nu}\nu)_L$	$(\bar{\nu}\nu)_R$	0	0.500	0	0	0	(D.553)
$(\bar{\nu}\nu)_L$	$(\bar{e}e)_L$	-0.266	-0.602	0.602	1.44	-0.336	(D.554)
$(\bar{\nu}\nu)_L$	$(\bar{e}e)_R$	0.234	-0.602	0.102	1.44	-0.336	(D.555)
$(\bar{\nu}\nu)_R$	$(\bar{\nu}\nu)_R$	0	0.500	0	0	0	(D.556)
$(\bar{\nu}\nu)_R$	$(\bar{e}e)_L$	0	-0.266	0	0.766	0	(D.557)
$(\bar{\nu}\nu)_R$	$(\bar{e}e)_R$	0	-0.266	0	0.766	0	(D.558)
$(\bar{e}e)_L$	$(\bar{e}e)_L$	0.142	0.500	-0.500	-1.53	1.53	(D.559)
$(\bar{e}e)_L$	$(\bar{e}e)_R$	-0.124	0.164	0.102	-0.860	1.20	(D.560)
$(\bar{e}e)_R$	$(\bar{e}e)_R$	0.109	-0.172	0.205	-0.188	0.860	(D.561)

Table D.29: Couplings $C^{\rm NC}_{4f}\left(f_{1,i}, f_{2,j}\right)$ of the neutral fermion currents below the electroweak scale in the HP-D model. See text and Eq. (D.453) on page 172 for details.

$(\bar{f}_1 f_1)_C$	$(\bar{f}_2 f_2)_C$	$C^{\rm NC}_{4f,{\rm SM}}$	$\frac{1}{\tilde{x}}$	$\frac{1}{\tilde{x}} s^2_{2\tilde{\beta}}$	$\frac{1}{\tilde{x}} s^2_{\tilde{\phi}}$	$\frac{1}{\tilde{x}} s^4_{\tilde{\phi}}$	Eqn.
$(\bar{u}u)_L$	$(\bar{u}u)_L$	0.237	0.546	-0.546	-1.32	0.831	(D.562)
$(\bar{u}u)_L$	$(\bar{u}u)_R$	-0.107	-0.0228	0.0228	-0.362	0.607	(D.563)
$(\bar{u}u)_L$	$(\bar{d}d)_L$	-0.291	-0.557	0.557	1.14	-0.527	(D.564)
$(\bar{u}u)_L$	$(\bar{d}d)_R$	0.0536	0.0114	-0.0114	0.181	-0.303	(D.565)
$(\bar{u}u)_L$	$(\bar{\nu}\nu)_L$	0.344	0.568	-0.568	-0.959	0.224	(D.566)
$(\bar{u}u)_L$	$(\bar{\nu}\nu)_R$	0	0	0	0	0	(D.567)
$(\bar{u}u)_L$	$(\bar{e}e)_L$	-0.183	-0.534	0.534	1.50	-1.13	(D.568)
$(\bar{u}u)_L$	$(\bar{e}e)_R$	0.161	0.0342	-0.0342	0.542	-0.910	(D.569)
$(\bar{u}u)_R$	$(\bar{u}u)_R$	0.0485	-0.0911	0.0911	0.598	0.382	(D.570)
$(\bar{u}u)_R$	$(\bar{d}d)_L$	0.132	-0.0228	0.0228	0.660	-0.415	(D.571)
$(\bar{u}u)_R$	$(\bar{d}d)_R$	-0.0243	0.0455	-0.0455	-0.299	-0.191	(D.572)
$(\bar{u}u)_R$	$(\bar{\nu}\nu)_L$	-0.156	0.0683	-0.0683	-0.959	0.224	(D.573)
$(\bar{u}u)_R$	$(\bar{\nu}\nu)_R$	0	0	0	0	0	(D.574)
$(\bar{u}u)_R$	$(\bar{e}e)_L$	0.0830	0.0683	-0.0683	0.0627	-0.798	(D.575)
$(\bar{u}u)_R$	$(\bar{e}e)_R$	-0.0728	0.137	-0.137	-0.896	-0.574	(D.576)
$(\bar{d}d)_L$	$(\bar{d}d)_L$	0.356	0.546	-0.546	-0.810	0.320	(D.577)
$(\bar{d}d)_L$	$(\bar{d}d)_R$	-0.0658	0.0114	-0.0114	-0.330	0.208	(D.578)
$(\bar{d}d)_L$	$(\bar{\nu}\nu)_L$	-0.422	-0.534	0.534	0.480	-0.112	(D.579)
$(\bar{d}d)_L$	$(\bar{\nu}\nu)_R$	0	0	0	0	0	(D.580)
$(\bar{d}d)_L$	$(\bar{e}e)_L$	0.225	0.568	-0.568	-1.47	0.735	(D.581)
$(\bar{d}d)_L$	$(\bar{e}e)_R$	-0.197	0.0342	-0.0342	-0.990	0.623	(D.582)
$(\bar{d}d)_R$	$(\bar{d}d)_R$	0.0121	-0.0228	0.0228	0.149	0.0956	(D.583)
$(\bar{d}d)_R$	$(\bar{\nu}\nu)_L$	0.0779	-0.0342	0.0342	0.480	-0.112	(D.584)
$(\bar{d}d)_R$	$(\bar{\nu}\nu)_R$	0	0	0	0	0	(D.585)
$(\bar{d}d)_R$	$(\bar{e}e)_L$	-0.0415	-0.0342	0.0342	-0.0314	0.399	(D.586)
$(\bar{d}d)_R$	$(\bar{e}e)_R$	0.0364	-0.0683	0.0683	0.448	0.287	(D.587)
$(\bar{\nu}\nu)_L$	$(\bar{\nu}\nu)_L$	0.500	0.500	-0.500	0	0	(D.588)
$(\bar{\nu}\nu)_L$	$(\bar{\nu}\nu)_R$	0	0	0	0	0	(D.589)
$(\bar{\nu}\nu)_L$	$(\bar{e}e)_L$	-0.266	-0.602	0.602	1.44	-0.336	(D.590)
$(\bar{\nu}\nu)_L$	$(\bar{e}e)_R$	0.234	-0.102	0.102	1.44	-0.336	(D.591)
$(\bar{\nu}\nu)_R$	$(\bar{\nu}\nu)_R$	0	0	0	0	0	(D.592)
$(\bar{\nu}\nu)_R$	$(\bar{e}e)_L$	0	0	0	0	0	(D.593)
$(\bar{\nu}\nu)_R$	$(\bar{e}e)_R$	0	0	0	0	0	(D.594)
$(\bar{e}e)_L$	$(\bar{e}e)_L$	0.142	0.500	-0.500	-1.53	1.53	(D.595)
$(\bar{e}e)_L$	$(\bar{e}e)_R$	-0.124	-0.102	0.102	-0.0941	1.20	(D.596)
$(\bar{e}e)_R$	$(\bar{e}e)_R$	0.109	-0.205	0.205	1.34	0.860	(D.597)

Table D.30: Couplings $C^{\rm NC}_{4f}\left(f_{1,i}, f_{2,j}\right)$ of the neutral fermion currents below the electroweak scale in the FP-D model. See text and Eq. (D.453) on page 172 for details.

$(\bar{f}_1 f_1)_C$	$(\bar{f}_2 f_2)_C$	$C_{4f,\mathrm{SM}}^{\mathrm{NC}}$	$\frac{1}{x}$	$\frac{1}{x} s_{2\beta}^2$	$\frac{1}{x} s_\phi^2$	$\frac{1}{x} s_\phi^4$	Eqn.
$(\bar{u}u)_L$	$(\bar{u}u)_L$	0.237	0.136	-0.273	-0.330	0.208	(D.598)
$(\bar{u}u)_L$	$(\bar{u}u)_R$	-0.107	0.0804	0.0114	-0.218	0.152	(D.599)
$(\bar{u}u)_L$	$(\bar{d}d)_L$	-0.291	-0.139	0.278	0.285	-0.132	(D.600)
$(\bar{u}u)_L$	$(\bar{d}d)_R$	0.0536	-0.0832	-0.00569	0.173	-0.0758	(D.601)
$(\bar{u}u)_L$	$(\bar{\nu}\nu)_L$	0.344	0.142	-0.284	-0.240	0.0560	(D.602)
$(\bar{u}u)_L$	$(\bar{\nu}\nu)_R$	0	0.0861	0	-0.128	0	(D.603)
$(\bar{u}u)_L$	$(\bar{e}e)_L$	-0.183	-0.134	0.267	0.375	-0.283	(D.604)
$(\bar{u}u)_L$	$(\bar{e}e)_R$	0.161	-0.0775	-0.0171	0.263	-0.227	(D.605)
$(\bar{u}u)_R$	$(\bar{u}u)_R$	0.0485	0.0243	0.0455	-0.106	0.0956	(D.606)
$(\bar{u}u)_R$	$(\bar{d}d)_L$	0.132	-0.111	0.0114	0.229	-0.104	(D.607)
$(\bar{u}u)_R$	$(\bar{d}d)_R$	-0.0243	-0.0552	-0.0228	0.117	-0.0478	(D.608)
$(\bar{u}u)_R$	$(\bar{\nu}\nu)_L$	-0.156	0.142	-0.0342	-0.240	0.0560	(D.609)
$(\bar{u}u)_R$	$(\bar{\nu}\nu)_R$	0	0.0861	0	-0.128	0	(D.610)
$(\bar{u}u)_R$	$(\bar{e}e)_L$	0.0830	-0.0495	-0.0342	0.207	-0.199	(D.611)
$(\bar{u}u)_R$	$(\bar{e}e)_R$	-0.0728	0.00652	-0.0683	0.0952	-0.143	(D.612)
$(\bar{d}d)_L$	$(\bar{d}d)_L$	0.356	0.136	-0.273	-0.202	0.0799	(D.613)
$(\bar{d}d)_L$	$(\bar{d}d)_R$	-0.0658	0.108	-0.00569	-0.146	0.0519	(D.614)
$(\bar{d}d)_L$	$(\bar{\nu}\nu)_L$	-0.422	-0.134	0.267	0.120	-0.0280	(D.615)
$(\bar{d}d)_L$	$(\bar{\nu}\nu)_R$	0	-0.106	0	0.0639	0	(D.616)
$(\bar{d}d)_L$	$(\bar{e}e)_L$	0.225	0.142	-0.284	-0.367	0.184	(D.617)
$(\bar{d}d)_L$	$(\bar{e}e)_R$	-0.197	0.114	-0.0171	-0.311	0.156	(D.618)
$(\bar{d}d)_R$	$(\bar{d}d)_R$	0.0121	0.0804	0.0114	-0.0904	0.0239	(D.619)
$(\bar{d}d)_R$	$(\bar{\nu}\nu)_L$	0.0779	-0.134	0.0171	0.120	-0.0280	(D.620)
$(\bar{d}d)_R$	$(\bar{\nu}\nu)_R$	0	-0.106	0	0.0639	0	(D.621)
$(\bar{d}d)_R$	$(\bar{e}e)_L$	-0.0415	0.0580	0.0171	-0.199	0.0997	(D.622)
$(\bar{d}d)_R$	$(\bar{e}e)_R$	0.0364	0.0300	0.0342	-0.143	0.0717	(D.623)
$(\bar{\nu}\nu)_L$	$(\bar{\nu}\nu)_L$	0.500	0.125	-0.250	0	0	(D.624)
$(\bar{\nu}\nu)_L$	$(\bar{\nu}\nu)_R$	0	0.125	0	0	0	(D.625)
$(\bar{\nu}\nu)_L$	$(\bar{e}e)_L$	-0.266	-0.151	0.301	0.360	-0.0840	(D.626)
$(\bar{\nu}\nu)_L$	$(\bar{e}e)_R$	0.234	-0.151	0.0512	0.360	-0.0840	(D.627)
$(\bar{\nu}\nu)_R$	$(\bar{\nu}\nu)_R$	0	0.125	0	0	0	(D.628)
$(\bar{\nu}\nu)_R$	$(\bar{e}e)_L$	0	-0.0666	0	0.192	0	(D.629)
$(\bar{\nu}\nu)_R$	$(\bar{e}e)_R$	0	-0.0666	0	0.192	0	(D.630)
$(\bar{e}e)_L$	$(\bar{e}e)_L$	0.142	0.125	-0.250	-0.383	0.383	(D.631)
$(\bar{e}e)_L$	$(\bar{e}e)_R$	-0.124	0.0410	0.0512	-0.215	0.299	(D.632)
$(\bar{e}e)_R$	$(\bar{e}e)_R$	0.109	-0.0431	0.102	-0.0470	0.215	(D.633)

Table D.31: Couplings $C_{4f}^{\mathrm{NC}}(f_{1,i}, f_{2,j})$ of the neutral fermion currents below the electroweak scale in the LR-T model. See text and Eq. (D.453) on page 172 for details.

$(\bar{f}_1 f_1)_C$	$(\bar{f}_2 f_2)_C$	$C^{\rm NC}_{4f,{\rm SM}}$	$\frac{1}{\bar{x}}$	$\frac{1}{\bar{x}} s^2_{2\bar{\beta}}$	$\frac{1}{\bar{x}} s^2_{\bar{\phi}}$	$\frac{1}{\bar{x}} s^4_{\bar{\phi}}$	Eqn.
$(\bar{u}u)_L$	$(\bar{u}u)_L$	0.237	0.136	-0.273	-0.330	0.208	(D.634)
$(\bar{u}u)_L$	$(\bar{u}u)_R$	-0.107	0.0804	0.0114	-0.218	0.152	(D.635)
$(\bar{u}u)_L$	$(\bar{d}d)_L$	-0.291	-0.139	0.278	0.285	-0.132	(D.636)
$(\bar{u}u)_L$	$(\bar{d}d)_R$	0.0536	-0.0832	-0.00569	0.173	-0.0758	(D.637)
$(\bar{u}u)_L$	$(\bar{\nu}\nu)_L$	0.344	0.142	-0.284	-0.240	0.0560	(D.638)
$(\bar{u}u)_L$	$(\bar{\nu}\nu)_R$	0	0	0	0	0	(D.639)
$(\bar{u}u)_L$	$(\bar{e}e)_L$	-0.183	-0.134	0.267	0.375	-0.283	(D.640)
$(\bar{u}u)_L$	$(\bar{e}e)_R$	0.161	0.00854	-0.0171	0.136	-0.227	(D.641)
$(\bar{u}u)_R$	$(\bar{u}u)_R$	0.0485	0.0243	0.0455	-0.106	0.0956	(D.642)
$(\bar{u}u)_R$	$(\bar{d}d)_L$	0.132	-0.111	0.0114	0.229	-0.104	(D.643)
$(\bar{u}u)_R$	$(\bar{d}d)_R$	-0.0243	-0.0552	-0.0228	0.117	-0.0478	(D.644)
$(\bar{u}u)_R$	$(\bar{\nu}\nu)_L$	-0.156	0.142	-0.0342	-0.240	0.0560	(D.645)
$(\bar{u}u)_R$	$(\bar{\nu}\nu)_R$	0	0	0	0	0	(D.646)
$(\bar{u}u)_R$	$(\bar{e}e)_L$	0.0830	-0.0495	-0.0342	0.207	-0.199	(D.647)
$(\bar{u}u)_R$	$(\bar{e}e)_R$	-0.0728	0.0926	-0.0683	-0.0325	-0.143	(D.648)
$(\bar{d}d)_L$	$(\bar{d}d)_L$	0.356	0.136	-0.273	-0.202	0.0799	(D.649)
$(\bar{d}d)_L$	$(\bar{d}d)_R$	-0.0658	0.108	-0.00569	-0.146	0.0519	(D.650)
$(\bar{d}d)_L$	$(\bar{\nu}\nu)_L$	-0.422	-0.134	0.267	0.120	-0.0280	(D.651)
$(\bar{d}d)_L$	$(\bar{\nu}\nu)_R$	0	0	0	0	0	(D.652)
$(\bar{d}d)_L$	$(\bar{e}e)_L$	0.225	0.142	-0.284	-0.367	0.184	(D.653)
$(\bar{d}d)_L$	$(\bar{e}e)_R$	-0.197	0.00854	-0.0171	-0.248	0.156	(D.654)
$(\bar{d}d)_R$	$(\bar{d}d)_R$	0.0121	0.0804	0.0114	-0.0904	0.0239	(D.655)
$(\bar{d}d)_R$	$(\bar{\nu}\nu)_L$	0.0779	-0.134	0.0171	0.120	-0.0280	(D.656)
$(\bar{d}d)_R$	$(\bar{\nu}\nu)_R$	0	0	0	0	0	(D.657)
$(\bar{d}d)_R$	$(\bar{e}e)_L$	-0.0415	0.0580	0.0171	-0.199	0.0997	(D.658)
$(\bar{d}d)_R$	$(\bar{e}e)_R$	0.0364	-0.0755	0.0342	-0.0795	0.0717	(D.659)
$(\bar{\nu}\nu)_L$	$(\bar{\nu}\nu)_L$	0.500	0.125	-0.250	0	0	(D.660)
$(\bar{\nu}\nu)_L$	$(\bar{\nu}\nu)_R$	0	0	0	0	0	(D.661)
$(\bar{\nu}\nu)_L$	$(\bar{e}e)_L$	-0.266	-0.151	0.301	0.360	-0.0840	(D.662)
$(\bar{\nu}\nu)_L$	$(\bar{e}e)_R$	0.234	-0.0256	0.0512	0.360	-0.0840	(D.663)
$(\bar{\nu}\nu)_R$	$(\bar{\nu}\nu)_R$	0	0	0	0	0	(D.664)
$(\bar{\nu}\nu)_R$	$(\bar{e}e)_L$	0	0	0	0	0	(D.665)
$(\bar{\nu}\nu)_R$	$(\bar{e}e)_R$	0	0	0	0	0	(D.666)
$(\bar{e}e)_L$	$(\bar{e}e)_L$	0.142	0.125	-0.250	-0.383	0.383	(D.667)
$(\bar{e}e)_L$	$(\bar{e}e)_R$	-0.124	-0.0256	0.0512	-0.0235	0.299	(D.668)
$(\bar{e}e)_R$	$(\bar{e}e)_R$	0.109	-0.0512	0.102	0.336	0.215	(D.669)

Table D.32: Couplings $C^{\rm NC}_{4f}\left(f_{1,i}, f_{2,j}\right)$ of the neutral fermion currents below the electroweak scale in the LP-T model. See text and Eq. (D.453) on page 172 for details.

$(\bar{f}_1 f_1)_C$	$(\bar{f}_2 f_2)_C$	$C_{4f,\mathrm{SM}}^{\mathrm{NC}}$	$\frac{1}{\tilde{x}}$	$\frac{1}{\tilde{x}} s^2_{2\tilde{\beta}}$	$\frac{1}{\tilde{x}} s^2_{\tilde{\phi}}$	$\frac{1}{\tilde{x}} s^4_{\tilde{\phi}}$	Eqn.
$(\bar{u}u)_L$	$(\bar{u}u)_L$	0.237	0.136	-0.273	-0.330	0.208	(D.670)
$(\bar{u}u)_L$	$(\bar{u}u)_R$	-0.107	-0.00569	0.0114	-0.0904	0.152	(D.671)
$(\bar{u}u)_L$	$(\bar{d}d)_L$	-0.291	-0.139	0.278	0.285	-0.132	(D.672)
$(\bar{u}u)_L$	$(\bar{d}d)_R$	0.0536	0.00285	-0.00569	0.0452	-0.0758	(D.673)
$(\bar{u}u)_L$	$(\bar{\nu}\nu)_L$	0.344	0.142	-0.284	-0.240	0.0560	(D.674)
$(\bar{u}u)_L$	$(\bar{\nu}\nu)_R$	0	0.0861	0	-0.128	0	(D.675)
$(\bar{u}u)_L$	$(\bar{e}e)_L$	-0.183	-0.134	0.267	0.375	-0.283	(D.676)
$(\bar{u}u)_L$	$(\bar{e}e)_R$	0.161	-0.0775	-0.0171	0.263	-0.227	(D.677)
$(\bar{u}u)_R$	$(\bar{u}u)_R$	0.0485	-0.0228	0.0455	0.149	0.0956	(D.678)
$(\bar{u}u)_R$	$(\bar{d}d)_L$	0.132	-0.00569	0.0114	0.165	-0.104	(D.679)
$(\bar{u}u)_R$	$(\bar{d}d)_R$	-0.0243	0.0114	-0.0228	-0.0747	-0.0478	(D.680)
$(\bar{u}u)_R$	$(\bar{\nu}\nu)_L$	-0.156	0.0171	-0.0342	-0.240	0.0560	(D.681)
$(\bar{u}u)_R$	$(\bar{\nu}\nu)_R$	0	-0.0389	0	-0.128	0	(D.682)
$(\bar{u}u)_R$	$(\bar{e}e)_L$	0.0830	0.0171	-0.0342	0.0157	-0.199	(D.683)
$(\bar{u}u)_R$	$(\bar{e}e)_R$	-0.0728	0.0731	-0.0683	-0.0964	-0.143	(D.684)
$(\bar{d}d)_L$	$(\bar{d}d)_L$	0.356	0.136	-0.273	-0.202	0.0799	(D.685)
$(\bar{d}d)_L$	$(\bar{d}d)_R$	-0.0658	0.00285	-0.00569	-0.0825	0.0519	(D.686)
$(\bar{d}d)_L$	$(\bar{\nu}\nu)_L$	-0.422	-0.134	0.267	0.120	-0.0280	(D.687)
$(\bar{d}d)_L$	$(\bar{\nu}\nu)_R$	0	-0.106	0	0.0639	0	(D.688)
$(\bar{d}d)_L$	$(\bar{e}e)_L$	0.225	0.142	-0.284	-0.367	0.184	(D.689)
$(\bar{d}d)_L$	$(\bar{e}e)_R$	-0.197	0.114	-0.0171	-0.311	0.156	(D.690)
$(\bar{d}d)_R$	$(\bar{d}d)_R$	0.0121	-0.00569	0.0114	0.0373	0.0239	(D.691)
$(\bar{d}d)_R$	$(\bar{\nu}\nu)_L$	0.0779	-0.00854	0.0171	0.120	-0.0280	(D.692)
$(\bar{d}d)_R$	$(\bar{\nu}\nu)_R$	0	0.0195	0	0.0639	0	(D.693)
$(\bar{d}d)_R$	$(\bar{e}e)_L$	-0.0415	-0.00854	0.0171	-0.00784	0.0997	(D.694)
$(\bar{d}d)_R$	$(\bar{e}e)_R$	0.0364	-0.0366	0.0342	0.0482	0.0717	(D.695)
$(\bar{\nu}\nu)_L$	$(\bar{\nu}\nu)_L$	0.500	0.125	-0.250	0	0	(D.696)
$(\bar{\nu}\nu)_L$	$(\bar{\nu}\nu)_R$	0	0.125	0	0	0	(D.697)
$(\bar{\nu}\nu)_L$	$(\bar{e}e)_L$	-0.266	-0.151	0.301	0.360	-0.0840	(D.698)
$(\bar{\nu}\nu)_L$	$(\bar{e}e)_R$	0.234	-0.151	0.0512	0.360	-0.0840	(D.699)
$(\bar{\nu}\nu)_R$	$(\bar{\nu}\nu)_R$	0	0.125	0	0	0	(D.700)
$(\bar{\nu}\nu)_R$	$(\bar{e}e)_L$	0	-0.0666	0	0.192	0	(D.701)
$(\bar{\nu}\nu)_R$	$(\bar{e}e)_R$	0	-0.0666	0	0.192	0	(D.702)
$(\bar{e}e)_L$	$(\bar{e}e)_L$	0.142	0.125	-0.250	-0.383	0.383	(D.703)
$(\bar{e}e)_L$	$(\bar{e}e)_R$	-0.124	0.0410	0.0512	-0.215	0.299	(D.704)
$(\bar{e}e)_R$	$(\bar{e}e)_R$	0.109	-0.0431	0.102	-0.0470	0.215	(D.705)

Table D.33: Couplings $C_{4f}^{\mathrm{NC}}\left(f_{1,i}, f_{2,j}\right)$ of the neutral fermion currents below the electroweak scale in the HP-T model. See text and Eq. (D.453) on page 172 for details.

$(\bar{f}_1 f_1)_C$	$(\bar{f}_2 f_2)_C$	$C_{4f,\mathrm{SM}}^{\mathrm{NC}}$	$\frac{1}{\tilde{x}}$	$\frac{1}{\tilde{x}} s_{2\tilde{\beta}}^2$	$\frac{1}{\tilde{x}} s_{\tilde{\phi}}^2$	$\frac{1}{\tilde{x}} s_{\tilde{\phi}}^4$	Eqn.
$(\bar{u}u)_L$	$(\bar{u}u)_L$	0.237	0.136	-0.273	-0.330	0.208	(D.706)
$(\bar{u}u)_L$	$(\bar{u}u)_R$	-0.107	-0.00569	0.0114	-0.0904	0.152	(D.707)
$(\bar{u}u)_L$	$(\bar{d}d)_L$	-0.291	-0.139	0.278	0.285	-0.132	(D.708)
$(\bar{u}u)_L$	$(\bar{d}d)_R$	0.0536	0.00285	-0.00569	0.0452	-0.0758	(D.709)
$(\bar{u}u)_L$	$(\bar{\nu}\nu)_L$	0.344	0.142	-0.284	-0.240	0.0560	(D.710)
$(\bar{u}u)_L$	$(\bar{\nu}\nu)_R$	0	0	0	0	0	(D.711)
$(\bar{u}u)_L$	$(\bar{e}e)_L$	-0.183	-0.134	0.267	0.375	-0.283	(D.712)
$(\bar{u}u)_L$	$(\bar{e}e)_R$	0.161	0.00854	-0.0171	0.136	-0.227	(D.713)
$(\bar{u}u)_R$	$(\bar{u}u)_R$	0.0485	-0.0228	0.0455	0.149	0.0956	(D.714)
$(\bar{u}u)_R$	$(\bar{d}d)_L$	0.132	-0.00569	0.0114	0.165	-0.104	(D.715)
$(\bar{u}u)_R$	$(\bar{d}d)_R$	-0.0243	0.0114	-0.0228	-0.0747	-0.0478	(D.716)
$(\bar{u}u)_R$	$(\bar{\nu}\nu)_L$	-0.156	0.0171	-0.0342	-0.240	0.0560	(D.717)
$(\bar{u}u)_R$	$(\bar{\nu}\nu)_R$	0	0	0	0	0	(D.718)
$(\bar{u}u)_R$	$(\bar{e}e)_L$	0.0830	0.0171	-0.0342	0.0157	-0.199	(D.719)
$(\bar{u}u)_R$	$(\bar{e}e)_R$	-0.0728	0.0342	-0.0683	-0.224	-0.143	(D.720)
$(\bar{d}d)_L$	$(\bar{d}d)_L$	0.356	0.136	-0.273	-0.202	0.0799	(D.721)
$(\bar{d}d)_L$	$(\bar{d}d)_R$	-0.0658	0.00285	-0.00569	-0.0825	0.0519	(D.722)
$(\bar{d}d)_L$	$(\bar{\nu}\nu)_L$	-0.422	-0.134	0.267	0.120	-0.0280	(D.723)
$(\bar{d}d)_L$	$(\bar{\nu}\nu)_R$	0	0	0	0	0	(D.724)
$(\bar{d}d)_L$	$(\bar{e}e)_L$	0.225	0.142	-0.284	-0.367	0.184	(D.725)
$(\bar{d}d)_L$	$(\bar{e}e)_R$	-0.197	0.00854	-0.0171	-0.248	0.156	(D.726)
$(\bar{d}d)_R$	$(\bar{d}d)_R$	0.0121	-0.00569	0.0114	0.0373	0.0239	(D.727)
$(\bar{d}d)_R$	$(\bar{\nu}\nu)_L$	0.0779	-0.00854	0.0171	0.120	-0.0280	(D.728)
$(\bar{d}d)_R$	$(\bar{\nu}\nu)_R$	0	0	0	0	0	(D.729)
$(\bar{d}d)_R$	$(\bar{e}e)_L$	-0.0415	-0.00854	0.0171	-0.00784	0.0997	(D.730)
$(\bar{d}d)_R$	$(\bar{e}e)_R$	0.0364	-0.0171	0.0342	0.112	0.0717	(D.731)
$(\bar{\nu}\nu)_L$	$(\bar{\nu}\nu)_L$	0.500	0.125	-0.250	0	0	(D.732)
$(\bar{\nu}\nu)_L$	$(\bar{\nu}\nu)_R$	0	0	0	0	0	(D.733)
$(\bar{\nu}\nu)_L$	$(\bar{e}e)_L$	-0.266	-0.151	0.301	0.360	-0.0840	(D.734)
$(\bar{\nu}\nu)_L$	$(\bar{e}e)_R$	0.234	-0.0256	0.0512	0.360	-0.0840	(D.735)
$(\bar{\nu}\nu)_R$	$(\bar{\nu}\nu)_R$	0	0	0	0	0	(D.736)
$(\bar{\nu}\nu)_R$	$(\bar{e}e)_L$	0	0	0	0	0	(D.737)
$(\bar{\nu}\nu)_R$	$(\bar{e}e)_R$	0	0	0	0	0	(D.738)
$(\bar{e}e)_L$	$(\bar{e}e)_L$	0.142	0.125	-0.250	-0.383	0.383	(D.739)
$(\bar{e}e)_L$	$(\bar{e}e)_R$	-0.124	-0.0256	0.0512	-0.0235	0.299	(D.740)
$(\bar{e}e)_R$	$(\bar{e}e)_R$	0.109	-0.0512	0.102	0.336	0.215	(D.741)

Table D.34: Couplings $C_{4f}^{\mathrm{NC}}(f_{1,i}, f_{2,j})$ of the neutral fermion currents below the electroweak scale in the FP-T model. See text and Eq. (D.453) on page 172 for details.

$(\bar{f}_1 f_1)_C$	$(\bar{f}_2 f_2)_C$	$C_{4f,\mathrm{SM}}^{\mathrm{NC}}$	$\frac{1}{\tilde{x}}$	$\frac{1}{\tilde{x}} s_{\tilde{\phi}}^2$	$\frac{1}{\tilde{x}} s_{\tilde{\phi}}^4$	Eqn.
$(\bar{u}u)_L$	$(\bar{u}u)_L$	0.237	0.500	-0.312	0.357	(D.742)
$(\bar{u}u)_L$	$(\bar{u}u)_R$	-0.107	0	-0.156	0.133	(D.743)
$(\bar{u}u)_L$	$(\bar{d}d)_L$	-0.291	-0.500	0.234	-0.291	(D.744)
$(\bar{u}u)_L$	$(\bar{d}d)_R$	0.0536	0	0.0779	-0.0665	(D.745)
$(\bar{u}u)_L$	$(\bar{\nu}\nu)_L$	0.344	0	0	0.224	(D.746)
$(\bar{u}u)_L$	$(\bar{\nu}\nu)_R$	0	0	0	0	(D.747)
$(\bar{u}u)_L$	$(\bar{e}e)_L$	-0.183	0	0.234	-0.424	(D.748)
$(\bar{u}u)_L$	$(\bar{e}e)_R$	0.161	0	0.234	-0.199	(D.749)
$(\bar{u}u)_R$	$(\bar{u}u)_R$	0.0485	0	0	-0.0911	(D.750)
$(\bar{u}u)_R$	$(\bar{d}d)_L$	0.132	0	0.156	-0.179	(D.751)
$(\bar{u}u)_R$	$(\bar{d}d)_R$	-0.0243	0	0	0.0455	(D.752)
$(\bar{u}u)_R$	$(\bar{\nu}\nu)_L$	-0.156	0	0	0.224	(D.753)
$(\bar{u}u)_R$	$(\bar{\nu}\nu)_R$	0	0	0	0	(D.754)
$(\bar{u}u)_R$	$(\bar{e}e)_L$	0.0830	0	0	-0.0874	(D.755)
$(\bar{u}u)_R$	$(\bar{e}e)_R$	-0.0728	0	0	0.137	(D.756)
$(\bar{d}d)_L$	$(\bar{d}d)_L$	0.356	0.500	-0.156	0.201	(D.757)
$(\bar{d}d)_L$	$(\bar{d}d)_R$	-0.0658	0	-0.0779	0.0893	(D.758)
$(\bar{d}d)_L$	$(\bar{\nu}\nu)_L$	-0.422	0	0	-0.112	(D.759)
$(\bar{d}d)_L$	$(\bar{\nu}\nu)_R$	0	0	0	0	(D.760)
$(\bar{d}d)_L$	$(\bar{e}e)_L$	0.225	0	-0.234	0.380	(D.761)
$(\bar{d}d)_L$	$(\bar{e}e)_R$	-0.197	0	-0.234	0.268	(D.762)
$(\bar{d}d)_R$	$(\bar{d}d)_R$	0.0121	0	0	-0.0228	(D.763)
$(\bar{d}d)_R$	$(\bar{\nu}\nu)_L$	0.0779	0	0	-0.112	(D.764)
$(\bar{d}d)_R$	$(\bar{\nu}\nu)_R$	0	0	0	0	(D.765)
$(\bar{d}d)_R$	$(\bar{e}e)_L$	-0.0415	0	0	0.0437	(D.766)
$(\bar{d}d)_R$	$(\bar{e}e)_R$	0.0364	0	0	-0.0683	(D.767)
$(\bar{\nu}\nu)_L$	$(\bar{\nu}\nu)_L$	0.500	0	0	0	(D.768)
$(\bar{\nu}\nu)_L$	$(\bar{\nu}\nu)_R$	0	0	0	0	(D.769)
$(\bar{\nu}\nu)_L$	$(\bar{e}e)_L$	-0.266	0	0	-0.336	(D.770)
$(\bar{\nu}\nu)_L$	$(\bar{e}e)_R$	0.234	0	0	-0.336	(D.771)
$(\bar{\nu}\nu)_R$	$(\bar{\nu}\nu)_R$	0	0	0	0	(D.772)
$(\bar{\nu}\nu)_R$	$(\bar{e}e)_L$	0	0	0	0	(D.773)
$(\bar{\nu}\nu)_R$	$(\bar{e}e)_R$	0	0	0	0	(D.774)
$(\bar{e}e)_L$	$(\bar{e}e)_L$	0.142	0	0	0.467	(D.775)
$(\bar{e}e)_L$	$(\bar{e}e)_R$	-0.124	0	0	0.131	(D.776)
$(\bar{e}e)_R$	$(\bar{e}e)_R$	0.109	0	0	-0.205	(D.777)

Table D.35: Couplings $C_{4f}^{\mathrm{NC}}\left(f_{1,i}, f_{2,j}\right)$ of the neutral fermion currents below the electroweak scale in the UU-D model. See text and Eq. (D.453) on page 172 for details.

$(\bar{f}_1 f_1)_C$	$(\bar{f}_2 f_2)_C$	$C_{4f,\mathrm{SM}}^{\mathrm{NC}}$	$\frac{1}{\tilde{x}}$	$\frac{1}{\tilde{x}} s_{\tilde{\phi}}^2$	$\frac{1}{\tilde{x}} s_{\tilde{\phi}}^4$	Eqn.
$(\bar{u}u)_L$	$(\bar{u}u)_L$	0.237	0.500	-0.312	0.357	(D.778)
$(\bar{u}u)_L$	$(\bar{u}u)_R$	-0.107	0	-0.156	0.133	(D.779)
$(\bar{u}u)_L$	$(\bar{d}d)_L$	-0.291	-0.500	0.234	-0.291	(D.780)
$(\bar{u}u)_L$	$(\bar{d}d)_R$	0.0536	0	0.0779	-0.0665	(D.781)
$(\bar{u}u)_L$	$(\bar{\nu}\nu)_L$	0.344	0.500	-0.156	0.224	(D.782)
$(\bar{u}u)_L$	$(\bar{\nu}\nu)_R$	0	0	0	0	(D.783)
$(\bar{u}u)_L$	$(\bar{e}e)_L$	-0.183	-0.500	0.389	-0.424	(D.784)
$(\bar{u}u)_L$	$(\bar{e}e)_R$	0.161	0	0.234	-0.199	(D.785)
$(\bar{u}u)_R$	$(\bar{u}u)_R$	0.0485	0	0	-0.0911	(D.786)
$(\bar{u}u)_R$	$(\bar{d}d)_L$	0.132	0	0.156	-0.179	(D.787)
$(\bar{u}u)_R$	$(\bar{d}d)_R$	-0.0243	0	0	0.0455	(D.788)
$(\bar{u}u)_R$	$(\bar{\nu}\nu)_L$	-0.156	0	-0.156	0.224	(D.789)
$(\bar{u}u)_R$	$(\bar{\nu}\nu)_R$	0	0	0	0	(D.790)
$(\bar{u}u)_R$	$(\bar{e}e)_L$	0.0830	0	0.156	-0.0874	(D.791)
$(\bar{u}u)_R$	$(\bar{e}e)_R$	-0.0728	0	0	0.137	(D.792)
$(\bar{d}d)_L$	$(\bar{d}d)_L$	0.356	0.500	-0.156	0.201	(D.793)
$(\bar{d}d)_L$	$(\bar{d}d)_R$	-0.0658	0	-0.0779	0.0893	(D.794)
$(\bar{d}d)_L$	$(\bar{\nu}\nu)_L$	-0.422	-0.500	0.0779	-0.112	(D.795)
$(\bar{d}d)_L$	$(\bar{\nu}\nu)_R$	0	0	0	0	(D.796)
$(\bar{d}d)_L$	$(\bar{e}e)_L$	0.225	0.500	-0.312	0.380	(D.797)
$(\bar{d}d)_L$	$(\bar{e}e)_R$	-0.197	0	-0.234	0.268	(D.798)
$(\bar{d}d)_R$	$(\bar{d}d)_R$	0.0121	0	0	-0.0228	(D.799)
$(\bar{d}d)_R$	$(\bar{\nu}\nu)_L$	0.0779	0	0.0779	-0.112	(D.800)
$(\bar{d}d)_R$	$(\bar{\nu}\nu)_R$	0	0	0	0	(D.801)
$(\bar{d}d)_R$	$(\bar{e}e)_L$	-0.0415	0	-0.0779	0.0437	(D.802)
$(\bar{d}d)_R$	$(\bar{e}e)_R$	0.0364	0	0	-0.0683	(D.803)
$(\bar{\nu}\nu)_L$	$(\bar{\nu}\nu)_L$	0.500	0.500	0	0	(D.804)
$(\bar{\nu}\nu)_L$	$(\bar{\nu}\nu)_R$	0	0	0	0	(D.805)
$(\bar{\nu}\nu)_L$	$(\bar{e}e)_L$	-0.266	-0.500	0.234	-0.336	(D.806)
$(\bar{\nu}\nu)_L$	$(\bar{e}e)_R$	0.234	0	0.234	-0.336	(D.807)
$(\bar{\nu}\nu)_R$	$(\bar{\nu}\nu)_R$	0	0	0	0	(D.808)
$(\bar{\nu}\nu)_R$	$(\bar{e}e)_L$	0	0	0	0	(D.809)
$(\bar{\nu}\nu)_R$	$(\bar{e}e)_R$	0	0	0	0	(D.810)
$(\bar{e}e)_L$	$(\bar{e}e)_L$	0.142	0.500	-0.467	0.467	(D.811)
$(\bar{e}e)_L$	$(\bar{e}e)_R$	-0.124	0	-0.234	0.131	(D.812)
$(\bar{e}e)_R$	$(\bar{e}e)_R$	0.109	0	0	-0.205	(D.813)

Table D.36: Couplings $C_{4f}^{\mathrm{NC}}\left(f_{1,i}, f_{2,j}\right)$ of the neutral fermion currents (first two generations) below the electroweak scale in the NU-D model. See text and Eq. (D.453) on page 172 for details.

$(\bar{f}_1 f_2)_C$	$(\bar{f}_3 f_4)_C$	$C_{4f,\mathrm{SM}}^{\mathrm{CC}}$	$\frac{1}{\tilde{x}}$	$\frac{1}{\tilde{x}} s_{2\tilde{\beta}}$	Eqn.
$(\bar{u}d)_L$	$(du)_L$	1	0	0	(D.815)
$(\bar{u}d)_L$	$(\bar{d}u)_R$	0	0	1	(D.816)
$(\bar{u}d)_L$	$(\bar{e}\nu)_L$	1	0	0	(D.817)
$(\bar{u}d)_L$	$(\bar{e}\nu)_R$	0	0	1	(D.818)
$(\bar{u}d)_R$	$(\bar{d}u)_R$	0	1	0	(D.819)
$(\bar{u}d)_R$	$(\bar{e}\nu)_L$	0	0	1	(D.820)
$(\bar{u}d)_R$	$(\bar{e}\nu)_R$	0	1	0	(D.821)
$(\bar{\nu}e)_L$	$(\bar{e}\nu)_L$	1	0	0	(D.822)
$(\bar{\nu}e)_L$	$(\bar{e}\nu)_R$	0	0	1	(D.823)
$(\bar{\nu}e)_R$	$(\bar{e}\nu)_R$	0	1	0	(D.824)

Table D.37: Couplings $C_{4f}^{\mathrm{CC}}\left(f_{1,i}, f_{3,j}\right)$ of the charged fermion currents below the electroweak scale in the LR-D model. See text and Eq. (D.814) on page 173 for details.

$(\bar{f}_1 f_2)_C$	$(\bar{f}_3 f_4)_C$	$C_{4f,\mathrm{SM}}^{\mathrm{CC}}$	$\frac{1}{\tilde{x}}$	$\frac{1}{\tilde{x}} s_{2\tilde{\beta}}$	Eqn.
$(\bar{u}d)_L$	$(du)_L$	1	0	0	(D.825)
$(\bar{u}d)_L$	$(\bar{d}u)_R$	0	0	1	(D.826)
$(\bar{u}d)_L$	$(\bar{e}\nu)_L$	1	0	0	(D.827)
$(\bar{u}d)_L$	$(\bar{e}\nu)_R$	0	0	0	(D.828)
$(\bar{u}d)_R$	$(\bar{d}u)_R$	0	1	0	(D.829)
$(\bar{u}d)_R$	$(\bar{e}\nu)_L$	0	0	1	(D.830)
$(\bar{u}d)_R$	$(\bar{e}\nu)_R$	0	0	0	(D.831)
$(\bar{\nu}e)_L$	$(\bar{e}\nu)_L$	1	0	0	(D.832)
$(\bar{\nu}e)_L$	$(\bar{e}\nu)_R$	0	0	0	(D.833)
$(\bar{\nu}e)_R$	$(\bar{e}\nu)_R$	0	0	0	(D.834)

Table D.38: Couplings $C_{4f}^{\mathrm{CC}}\left(f_{1,i}, f_{3,j}\right)$ of the charged fermion currents below the electroweak scale in the LP-D model. See text and Eq. (D.814) on page 173 for details.

$(\bar{f}_1 f_2)_C$	$(\bar{f}_3 f_4)_C$	$C^{\rm CC}_{4f,{\rm SM}}$	$\frac{1}{\tilde{x}}$	$\frac{1}{\tilde{x}} s_{2\tilde{\beta}}$	Eqn.
$(\bar{u}d)_L$	$(d\bar{u})_L$	1	0	0	(D.835)
$(\bar{u}d)_L$	$(\bar{d}u)_R$	0	0	0	(D.836)
$(\bar{u}d)_L$	$(\bar{e}\nu)_L$	1	0	0	(D.837)
$(\bar{u}d)_L$	$(\bar{e}\nu)_R$	0	0	1	(D.838)
$(\bar{u}d)_R$	$(\bar{d}u)_R$	0	0	0	(D.839)
$(\bar{u}d)_R$	$(\bar{e}\nu)_L$	0	0	0	(D.840)
$(\bar{u}d)_R$	$(\bar{e}\nu)_R$	0	0	0	(D.841)
$(\bar{\nu}e)_L$	$(\bar{e}\nu)_L$	1	0	0	(D.842)
$(\bar{\nu}e)_L$	$(\bar{e}\nu)_R$	0	0	1	(D.843)
$(\bar{\nu}e)_R$	$(\bar{e}\nu)_R$	0	1	0	(D.844)

Table D.39: Couplings $C^{\rm CC}_{4f}\left(f_{1,i}, f_{3,j}\right)$ of the charged fermion currents below the electroweak scale in the HP-D model. See text and Eq. (D.814) on page 173 for details.

$(\bar{f}_1 f_2)_C$	$(\bar{f}_3 f_4)_C$	$C^{\rm CC}_{4f,{\rm SM}}$	$\frac{1}{\tilde{x}}$	$\frac{1}{\tilde{x}} s_{2\tilde{\beta}}$	Eqn.
$(\bar{u}d)_L$	$(d\bar{u})_L$	1	0	0	(D.845)
$(\bar{u}d)_L$	$(\bar{d}u)_R$	0	0	0	(D.846)
$(\bar{u}d)_L$	$(\bar{e}\nu)_L$	1	0	0	(D.847)
$(\bar{u}d)_L$	$(\bar{e}\nu)_R$	0	0	0	(D.848)
$(\bar{u}d)_R$	$(\bar{d}u)_R$	0	0	0	(D.849)
$(\bar{u}d)_R$	$(\bar{e}\nu)_L$	0	0	0	(D.850)
$(\bar{u}d)_R$	$(\bar{e}\nu)_R$	0	0	0	(D.851)
$(\bar{\nu}e)_L$	$(\bar{e}\nu)_L$	1	0	0	(D.852)
$(\bar{\nu}e)_L$	$(\bar{e}\nu)_R$	0	0	0	(D.853)
$(\bar{\nu}e)_R$	$(\bar{e}\nu)_R$	0	0	0	(D.854)

Table D.40: Couplings $C^{\rm CC}_{4f}\left(f_{1,i}, f_{3,j}\right)$ of the charged fermion currents below the electroweak scale in the FP-D model. See text and Eq. (D.814) on page 173 for details.

$C(\bar{f}_1 f_2)_C$	$C(\bar{f}_3 f_4)_C$	$C_{4f,\mathrm{SM}}^{\mathrm{CC}}$	$\frac{1}{\tilde{x}}$	$\frac{1}{\tilde{x}} s_{2\tilde{\beta}}$	Eqn.
$(\bar{u}d)_L$	$(d\bar{u})_L$	1	0	0	(D.855)
$(\bar{u}d)_L$	$(\bar{d}u)_R$	0	0	$\frac{1}{2}$	(D.856)
$(\bar{u}d)_L$	$(\bar{e}\nu)_L$	1	0	0	(D.857)
$(\bar{u}d)_L$	$(\bar{e}\nu)_R$	0	0	$\frac{1}{2}$	(D.858)
$(\bar{u}d)_R$	$(\bar{d}u)_R$	0	$\frac{1}{2}$	0	(D.859)
$(\bar{u}d)_R$	$(\bar{e}\nu)_L$	0	0	$\frac{1}{2}$	(D.860)
$(\bar{u}d)_R$	$(\bar{e}\nu)_R$	0	$\frac{1}{2}$	0	(D.861)
$(\bar{\nu}e)_L$	$(\bar{e}\nu)_L$	1	0	0	(D.862)
$(\bar{\nu}e)_L$	$(\bar{e}\nu)_R$	0	0	$\frac{1}{2}$	(D.863)
$(\bar{\nu}e)_R$	$(\bar{e}\nu)_R$	0	$\frac{1}{2}$	0	(D.864)

Table D.41: Couplings $C_{4f}^{\mathrm{CC}}\left(f_{1,i}, f_{3,j}\right)$ of the charged fermion currents below the electroweak scale in the LR-T model. See text and Eq. (D.814) on page 173 for details.

$C(\bar{f}_1 f_2)_C$	$C(\bar{f}_3 f_4)_C$	$C_{4f,\mathrm{SM}}^{\mathrm{CC}}$	$\frac{1}{\tilde{x}}$	$\frac{1}{\tilde{x}} s_{2\tilde{\beta}}$	Eqn.
$(\bar{u}d)_L$	$(d\bar{u})_L$	1	0	0	(D.865)
$(\bar{u}d)_L$	$(\bar{d}u)_R$	0	0	$\frac{1}{2}$	(D.866)
$(\bar{u}d)_L$	$(\bar{e}\nu)_L$	1	0	0	(D.867)
$(\bar{u}d)_L$	$(\bar{e}\nu)_R$	0	0	0	(D.868)
$(\bar{u}d)_R$	$(\bar{d}u)_R$	0	$\frac{1}{2}$	0	(D.869)
$(\bar{u}d)_R$	$(\bar{e}\nu)_L$	0	0	$\frac{1}{2}$	(D.870)
$(\bar{u}d)_R$	$(\bar{e}\nu)_R$	0	0	0	(D.871)
$(\bar{\nu}e)_L$	$(\bar{e}\nu)_L$	1	0	0	(D.872)
$(\bar{\nu}e)_L$	$(\bar{e}\nu)_R$	0	0	0	(D.873)
$(\bar{\nu}e)_R$	$(\bar{e}\nu)_R$	0	0	0	(D.874)

Table D.42: Couplings $C_{4f}^{\mathrm{CC}}\left(f_{1,i}, f_{3,j}\right)$ of the charged fermion currents below the electroweak scale in the LP-T model. See text and Eq. (D.814) on page 173 for details.

$C(\bar{f}_1 f_2)_C$	$C(\bar{f}_3 f_4)_C$	$C^{\rm CC}_{4f,{\rm SM}}$	$\frac{1}{\tilde{x}}$	$\frac{1}{\tilde{x}} s_{2\tilde{\beta}}$	Eqn.
$(\bar{u}d)_L$	$(\bar{d}u)_L$	1	0	0	(D.875)
$(\bar{u}d)_L$	$(\bar{d}u)_R$	0	0	0	(D.876)
$(\bar{u}d)_L$	$(\bar{e}\nu)_L$	1	0	0	(D.877)
$(\bar{u}d)_L$	$(\bar{e}\nu)_R$	0	0	$\frac{1}{2}$	(D.878)
$(\bar{u}d)_R$	$(\bar{d}u)_R$	0	0	0	(D.879)
$(\bar{u}d)_R$	$(\bar{e}\nu)_L$	0	0	0	(D.880)
$(\bar{u}d)_R$	$(\bar{e}\nu)_R$	0	0	0	(D.881)
$(\bar{\nu}e)_L$	$(\bar{e}\nu)_L$	1	0	0	(D.882)
$(\bar{\nu}e)_L$	$(\bar{e}\nu)_R$	0	0	$\frac{1}{2}$	(D.883)
$(\bar{\nu}e)_R$	$(\bar{e}\nu)_R$	0	$\frac{1}{2}$	0	(D.884)

Table D.43: Couplings $C^{\rm CC}_{4f}\left(f_{1,i}, f_{3,j}\right)$ of the charged fermion currents below the electroweak scale in the HP-T model. See text and Eq. (D.814) on page 173 for details.

$C(\bar{f}_1 f_2)_C$	$C(\bar{f}_3 f_4)_C$	$C^{\rm CC}_{4f,{\rm SM}}$	$\frac{1}{\tilde{x}}$	$\frac{1}{\tilde{x}} s_{2\tilde{\beta}}$	Eqn.
$(\bar{u}d)_L$	$(\bar{d}u)_L$	1	0	0	(D.885)
$(\bar{u}d)_L$	$(\bar{d}u)_R$	0	0	0	(D.886)
$(\bar{u}d)_L$	$(\bar{e}\nu)_L$	1	0	0	(D.887)
$(\bar{u}d)_L$	$(\bar{e}\nu)_R$	0	0	0	(D.888)
$(\bar{u}d)_R$	$(\bar{d}u)_R$	0	0	0	(D.889)
$(\bar{u}d)_R$	$(\bar{e}\nu)_L$	0	0	0	(D.890)
$(\bar{u}d)_R$	$(\bar{e}\nu)_R$	0	0	0	(D.891)
$(\bar{\nu}e)_L$	$(\bar{e}\nu)_L$	1	0	0	(D.892)
$(\bar{\nu}e)_L$	$(\bar{e}\nu)_R$	0	0	0	(D.893)
$(\bar{\nu}e)_R$	$(\bar{e}\nu)_R$	0	0	0	(D.894)

Table D.44: Couplings $C^{\rm CC}_{4f}\left(f_{1,i}, f_{3,j}\right)$ of the charged fermion currents below the electroweak scale in the FP-T model. See text and Eq. (D.814) on page 173 for details.

$(\bar{f}_1 f_2)_C$	$(\bar{f}_3 f_4)_C$	$C_{4f,\mathrm{SM}}^{\mathrm{CC}}$	$\frac{1}{\tilde{x}}$ (UU-D)	$\frac{1}{\tilde{x}}$ (NU-D)	Eqn.
$(\bar{u}d)_L$	$(d\bar{u})_L$	1	1	1	(D.895)
$(\bar{u}d)_L$	$(\bar{d}u)_R$	0	0	0	(D.896)
$(\bar{u}d)_L$	$(\bar{e}\nu)_L$	1	0	1	(D.897)
$(\bar{u}d)_L$	$(\bar{e}\nu)_R$	0	0	0	(D.898)
$(\bar{u}d)_R$	$(\bar{d}u)_R$	0	0	0	(D.899)
$(\bar{u}d)_R$	$(\bar{e}\nu)_L$	0	0	0	(D.900)
$(\bar{u}d)_R$	$(\bar{e}\nu)_R$	0	0	0	(D.901)
$(\bar{\nu}e)_L$	$(\bar{e}\nu)_L$	1	0	1	(D.902)
$(\bar{\nu}e)_L$	$(\bar{e}\nu)_R$	0	0	0	(D.903)
$(\bar{\nu}e)_R$	$(\bar{e}\nu)_R$	0	0	0	(D.904)

Table D.45: Couplings $C_{4f}^{\mathrm{CC}}\left(f_{1,i}, f_{3,j}\right)$ of the charged fermion currents below the electroweak scale in the UU-D and NU-D model. The results for the NU-D model apply to the first two fermion generations. See text and Eq. (D.814) on page 173 for details.

BIBLIOGRAPHY

[1] M. B. Popovic, arXiv:hep-ph/0204345.

[2] T. Appelquist and M. S. Chanowitz, Phys. Rev. Lett. **59**, 2405 (1987) [Erratum-ibid. **60**, 1589 (1988)].

[3] T. G. Rizzo, arXiv:hep-ph/0610104.

[4] R. N. Mohapatra and J. C. Pati, Phys. Rev. D **11**, 2558 (1975).

[5] R. N. Mohapatra and J. C. Pati, Phys. Rev. D **11**, 566 (1975).

[6] R. N. Mohapatra and G. Senjanovic, Phys. Rev. D **23**, 165 (1981).

[7] R. S. Chivukula, B. Coleppa, S. Di Chiara, E. H. Simmons, H. J. He, M. Kurachi and M. Tanabashi, Phys. Rev. D **74**, 075011 (2006) [arXiv:hep-ph/0607124].

[8] V. D. Barger, W. Y. Keung and E. Ma, Phys. Rev. D **22**, 727 (1980).

[9] V. D. Barger, W. Y. Keung and E. Ma, Phys. Rev. Lett. **44**, 1169 (1980).

[10] H. Georgi, E. E. Jenkins and E. H. Simmons, Phys. Rev. Lett. **62**, 2789 (1989) [Erratum-ibid. **63**, 1540 (1989)].

[11] H. Georgi, E. E. Jenkins and E. H. Simmons, Nucl. Phys. B **331**, 541 (1990).

[12] X. Li and E. Ma, Phys. Rev. Lett. **47**, 1788 (1981).

[13] J. Polak and M. Zralek, Phys. Rev. D **46**, 3871 (1992).

[14] J. Polak and M. Zralek, Nucl. Phys. B **363**, 385 (1991).

[15] J. Chay, K. Y. Lee and S. h. Nam, Phys. Rev. D **61**, 035002 (2000) [arXiv:hep-ph/9809298].

[16] A. Donini, F. Feruglio, J. Matias and F. Zwirner, Nucl. Phys. B **507**, 51 (1997) [arXiv:hep-ph/9705450].

[17] R. S. Chivukula, E. H. Simmons and J. Terning, Phys. Lett. B **346**, 284 (1995) [arXiv:hep-ph/9412309].

[18] J. Erler, arXiv:hep-ph/0005084.

[19] C. P. Burgess, S. Godfrey, H. Konig, D. London and I. Maksymyk, Phys. Rev. D **49**, 6115 (1994) [arXiv:hep-ph/9312291].

[20] C. Amsler *et al.* [Particle Data Group], Phys. Lett. B **667**, 1 (2008).

[21] J. Erler Private communication.

[22] D. Zeppenfeld and K. m. Cheung, arXiv:hep-ph/9810277.

[23] K. S. McFarland *et al.* [CCFR Collaboration and The E744 Collaboration and The E770 Collaborati], Eur. Phys. J. C **1**, 509 (1998) [arXiv:hep-ex/9701010].

[24] P. Vilain *et al.* [CHARM-II Collaboration], Phys. Lett. B **364**, 121 (1995).

[25] C. S. Wu, E. Ambler, R. W. Hayward, D. D. Hoppes and R. P. Hudson, Phys. Rev. **105**, 1413 (1957).

[26] P. L. Anthony *et al.* [SLAC E158 Collaboration], Phys. Rev. Lett. **95**, 081601 (2005) [arXiv:hep-ex/0504049].

[27] R. D. Young, R. D. Carlini, A. W. Thomas and J. Roche, Phys. Rev. Lett. **99**, 122003 (2007) [arXiv:0704.2618 [hep-ph]].

[28] F. James and M. Roos, Comput. Phys. Commun. **10**, 343 (1975).

[29] K. Hagiwara, R. D. Peccei, D. Zeppenfeld and K. Hikasa, Nucl. Phys. B **282**, 253 (1987).

[30] S. Schael *et al.* [ALEPH Collaboration], Phys. Lett. B **614**, 7 (2005).

[31] Z. Xu, D. H. Zhang and L. Chang, Nucl. Phys. B **291**, 392 (1987).

[32] W. T. H. Van Oers [Qweak Collaboration], Nucl. Phys. A **790**, 81 (2007).

[33] D. Mack [e2cPV Collaboration], "Outlook of an Improved Measurement of Parity Violation in Moller Scattering at Jlab," Talk at PAVI06, Milos Island, Greece (2006).

[34] B. W. Lee, C. Quigg and H. B. Thacker, Phys. Rev. Lett. **38**, 883 (1977).

[35] B. W. Lee, C. Quigg and H. B. Thacker, Phys. Rev. D **16**, 1519 (1977).

[36] M. S. Chanowitz and M. K. Gaillard, Nucl. Phys. B **261**, 379 (1985).

[37] C. P. Yuan and T. C. Yuan, Phys. Rev. D **44**, 3603 (1991).